Vol 11 • No. 1 • April 2017

ISSN : 0976 - 1330

Journal of GEOMATICS

INDIAN SOCIETY OF GEOMATICS

Journal of Geomatics

(A publication of the Indian Society of Geomatics)

Editorial Board

Journal of Geomatics Vol. 11 No. 1 April 2017

Indian Society of Geomatics
Executive Council 2017 – 2020

Secretary: (address for correspondence)
6202, SAC Bopal Campus, Ahmedabad – 380058, India
Email : *secretary@isgindia.org; sasharma@sac.isro.gov.in*

Journal of Geomatics

(A Publication of the Indian Society of Geomatics)

Vol. 11 No. 1 Research Articles April 2017

Published biannually by the Secretary, Indian Society of Geomatics on behalf of the Society

ISG Website : www.isgindia.org

Journal of Geomatics Vol 11 No. 1 April 2017

Horizontal coordinate transformation using artificial neural network technology- A case study of Ghana geodetic reference network

Bernard Kumi-Boateng[1] and Yao Yevenyo Ziggah[1, 2]
[1]Department of Geomatic Engineering, University of Mines and Technology, Tarkwa-Ghana
[2]Department of Surveying and Mapping, China University of Geosciences, Wuhan-P. R. China
Email: kumi@umat.edu.gh, yyziggah@umat.edu.gh

(Received: Feb 24, 2016; in final form: Mar 08, 2017)

Abstract: Transformation of coordinates between different geodetic datums has been a common practice within the geospatial profession. Relating different geodetic datums mostly involves the use of conformal transformation techniques which could produce results that are not very often satisfactory for certain geodetic, surveying and mapping purposes. This has been attributed to the inability of the conformal models to absorb more of the heterogeneous and local character of deformations existing within the local geodetic networks. In light of this, most researchers have resorted to Artificial Neural Network (ANN) as a plausible alternative technology for coordinate transformation. Although the ANN technique has been applied successfully, the method is yet to be adopted and tested within the Ghana geodetic reference network. In view of this, the present study applied the Radial Basis Function Neural Network (RBFNN) to transform plane coordinates between the two classical geodetic networks namely, Accra datum and Leigon datum which is used in Ghana for its surveying and mapping activities. The RBFNN results obtained were compared with the four-parameter and six-parameter transformation models. It was noticed that the RBFNN could produce more reliable and accurate results and thus is more applicable in modelling distortions existing in the local geodetic networks more effectively than the traditional techniques (six-parameter and four-parameter).

Keywords: Radial basis function neural network, Four-parameter model, Six-parameter model, Artificial neural network

1. Introduction

Coordinate transformation is a common problem faced by the geospatial practitioners. Its significance is to enable transformation of coordinate from a separate survey into a common system thereby integrating data from different sources on to the same reference surface. One of the most common examples of these reference surfaces is the geometric reference ellipsoid. This ellipsoid serves as the horizontal datum for two or three-dimensional positions obtained via Global Positioning System (GPS) and control survey methods such as triangulation, trilateration, resection (Schofield, 2001) and many others for both developed and developing countries such as Ghana.

Currently, there are two reference ellipsoids that are being utilized by the geospatial professionals in Ghana. These are the War Office 1926 ellipsoid built on the Accra datum 1920 and the Clark 1880 (modified) ellipsoid built on the Leigon datum1977. Issues have been raised in Ghana about the implementation of these two datums for survey and mapping purposes. For instance, it was pointed out by Ayer and Fosu (2008) that the discrepancies between War Office and Clark 1880 (modified) ellipsoid is about 26 m which does not meet the requirements of ± 0.9114 m stipulated by the Survey and Mapping Division of Lands Commission in Ghana. The large error value could be attributed to the different geometric parameters of the two local reference ellipsoids. This has therefore necessitated the need to have an integrated approach to solve the issue of discrepancies between the War Office1926 and Clark 1880 ellipsoid in Ghana. One of the proposed ways is to determine coordinate transformation parameters between the two local ellipsoids namely, War Office1926 and Clark 1880 (modified). However, conformal coordinate transformation models which have mostly been frequently used could not produce satisfactory results (Grgic et al., 2015). Most researchers have attributed this limitation to the heterogeneous nature of local geodetic networks contributed by the methods used for its establishment (Tierra et al., 2008).

In order to correct for such defects in the conformal models, artificial intelligence method such as Artificial Neural Network (ANN) has been resorted to by several researchers in recent times. For instance, the Radial Basis Function Neural Network (RBFNN) has been widely used and compared to other transformation models such as the 3-parameter, standard Molodensky, Abridged Molodensky, Bursa-Wolf, 2D conformal model, 2D Affine, Molodensky-Badekas and many others (Tierra et al., 2008; Tierra et al., 2009; Gullu et al., 2011; Gullu 2010). Likewise, the Backpropagation Neural Network (BPNN) has also been tested in coordinate transformation (Tierra and Romero, 2014; Mihalache, 2012; Turgut, 2010; Yilmaz and Gullu, 2011; Zaletnyik, 2004; Lin and Wang, 2006). In addition, an investigation into a genetic based method for directly transforming 2D coordinates has also been studied (Chih-Hung et al., 2008). Furthermore, a preliminary study on the concept of the recurrent cascade neural networks and the Neuro-Fuzzy Neural Network (NFNN) based on the Takagi-Sugeno-Kang system for coordinate transformation has also been explored (Gil and Mrowczynska, 2012). The conclusions drawn from the various studies indicate that

the artificial intelligence methods are dominant over the traditional transformation techniques and thus could serve as a better alternative approach for coordinate transformation.

Whereas the artificial intelligence methods have been gainfully applied, literature covered pertaining to this study revealed that, in Ghana, only the three-dimension (3D) similarity transformation models have been utilized to transform from global (WGS84) datum to local datums (Accra and Leigon). The most commonly used 3D coordinate transformation methods in Ghana are the conformal similarity models of Bursa-wolf, Molodensky-Badekas, Abridged Molodensky, Veis model, 3D affine model and 3D projective model (Ayer, 2008; Ayer and Fosu, 2008; Dzidefo, 2011; Kotzev, 2013; Ziggah et al., 2013 a and b). Thus, no research work has been done to establish transformation parameters between War Office 1926 and Clark 1880 ellipsoidal datums used in Ghana. This is because Ayer and Fosu (2008) only showed the differences between the local ellipsoids with no parameters determined to unify the two geodetic datums. This implies that determining parameters to assimilate War Office 1926 and Clark 1880 ellipsoids data has not yet been fully investigated. In addition, the recent artificial neural network technology is yet to be adopted.

Therefore, this study focuses on Ghana as a case of application for its national geodetic network and proposes artificial neural network as a viable approach for integrating data from War Office 1926 to Clark 1880 (modified) ellipsoid and vice versa.

2. Study area and data source

The study area is Ghana located in West Africa. It is bordered on the North by Burkina Faso, Ivory Coast to the West, Togo to the East and Gulf of Guinea to the South. Ghana uses two horizontal datums known as the Accra and Leigon datum for its geodetic activities. The reference surface of the Accra datum is the War Office 1926 ellipsoid suggested by the British War Office, with semi-major axis a = 6378299.99899832 m, semi minor axis b = 6356751.68824042 m, flattening f = 1/296 (Ayer, 2008; Ayer and Fosu, 2008). On the other hand, Leigon datum has the Clark 1880 (modified) ellipsoid as its reference surface, with semi-major axis a = 6378249.145 m, semi minor axis b = 6356514.870 m, flattening f = 1/293.465006079115. The plane coordinates are estimated on the Transverse Mercator projection with central meridian at longitude 1° W (Mugnier, 2000; Poku-Gyamfi and Hein, 2006). It is important to note that, the coordinate system used to indicate positions of features on all survey maps in Ghana is the projected grid coordinates of Easting and Northing derived from the Transverse Mercator projection.

In this study, secondary data of 27 common plane coordinate points in Easting and Northing in both Accra datum and Leigon datum were obtained from the Survey and Mapping Division of Lands Commission in Ghana. These acquired co-located points are the historical triangulation positions that were used as the realisation of the War Office 1926 and Clark 1880 (modified) reference systems. Records from the Ghana Survey and Mapping Division indicate that these historical triangulation points used in this study covers the mountainous southern regions of Ghana and thus were established on hilly terrain (Kotzev, 2013). These 27 historical triangulation points provided covers the area of the on-going GNSS national geodetic reference network establishment under the Land Administration Project (LAP) sponsored by the World Bank (Kotzev, 2013). One of the objectives for the LAP is to establish GNSS geodetic reference network to enhance the use of Global Navigation Satellite System (GNSS) for land related positioning undertakings such as geotechnical investigations, traffic and transportation, meteorology, survey and mapping, timing, engineering and many others in Ghana (Wonnacot, 2007; Poku-Gyamfi and Schueler, 2008). Furthermore, the LAP tend to achieve the proposed unification of all national reference frames for all African countries under the African Reference Frame into a single continental reference system based on the International Terrestrial Reference System (ITRS). The southern section where these historical triangulation points are situated has been termed the golden triangle. Figure 1 shows the data distribution of the historical points in the golden triangle.

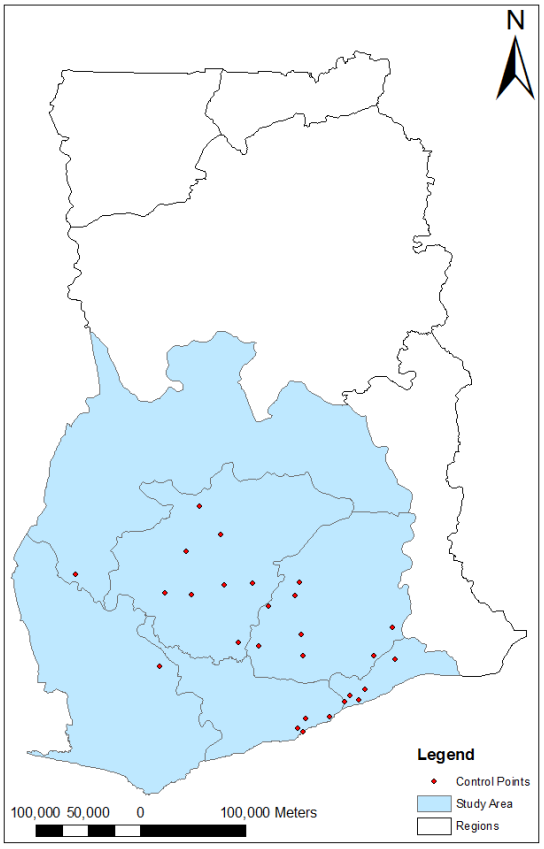

Figure 1: Study area showing geographic data distribution

3. Methods

3.1 Four-parameter similarity model

The four-parameter similarity model is composed of two translations of the coordinate origin, one scale factor and one rotation parameter. This model was applied in this study to determine parameters suitable to transform coordinates from War Office 1926 ellipsoid to Clark 1880 (modified) ellipsoid and vice versa. It is stated by Ghilani (2010) that the four parameter model is mostly suitable when converting separate surveys into a common reference coordinate system. Moreover, Deakin (2006) also emphasised that the model preserves shape and angles after transformation and hence is a useful tool for mapping activities. The four-parameter similarity model relates two rectangular coordinate systems expressed in Equation 1 (Ghilani, 2010) as

$$\begin{aligned} ax - by + c &= X \\ bx + ay + d &= Y \end{aligned} \quad (1)$$

Applying the least squares method, Eq. 1 could be represented in matrix form (Eq. 2) as

$$V + BX = L \quad (2)$$

where V is the residual, B is the designed matrix, L is the observation vector matrix and X is the vector of the unknown parameters to be determined.

Hence, expressing Eq. 1 in the form of Eq. 2 gives Eq. 3 expressed as

$$\begin{bmatrix} x & -y & 1 & 0 \\ y & x & 0 & 1 \end{bmatrix} \begin{bmatrix} a \\ b \\ c \\ d \end{bmatrix} + \begin{bmatrix} V_x \\ V_y \end{bmatrix} = \begin{bmatrix} X \\ Y \end{bmatrix} \quad (3)$$

where

$B = \begin{bmatrix} x & -y & 1 & 0 \\ y & x & 0 & 1 \end{bmatrix}$ is the design matrix;

$X = \begin{bmatrix} a \\ b \\ c \\ d \end{bmatrix}$ is the vector of the unknown transformation parameters to be determined;

$V = \begin{bmatrix} V_x \\ V_y \end{bmatrix}$ is the residual; and $L = \begin{bmatrix} X \\ Y \end{bmatrix}$ is the observation vector respectively.

3.2 Six-parameter transformation model

The six-parameter transformation model consists of two translations of the origin, two different scale factors; one in the x direction and the other in the y direction. Also there is a rotation about the origin, plus a small non-orthogonality correction between the x and y axes (Ghilani, 2010). This model was also used in this study to calculate parameters suitable to transform coordinates from War Office 1926 ellipsoid to Clark 1880 (modified) ellipsoid and vice versa.

The observation equations for the six-parameter transformation are given in Eq. 4 (Ghilani, 2010)

$$\begin{aligned} ax + by + c &= X \\ dx + ey + f &= Y \end{aligned} . \quad (4)$$

Equation 4 when expressed in the matrix form (Eq. 2) is given by Eq. 5 as

$$\begin{bmatrix} x & y & 1 & 0 & 0 & 0 \\ 0 & 0 & 0 & x & y & 1 \end{bmatrix} \begin{bmatrix} a \\ b \\ c \\ d \\ e \\ f \end{bmatrix} = \begin{bmatrix} X \\ Y \end{bmatrix} + \begin{bmatrix} V_x \\ V_y \end{bmatrix} \quad (5)$$

where:

$B = \begin{bmatrix} x & y & 1 & 0 & 0 & 0 \\ 0 & 0 & 0 & x & y & 1 \end{bmatrix}$,

$L = \begin{bmatrix} X \\ Y \end{bmatrix}$, $V = \begin{bmatrix} V_x \\ V_y \end{bmatrix}$

and $X = \begin{bmatrix} a \\ b \\ c \\ d \\ e \\ f \end{bmatrix}$ respectively.

3.3 Radial Basis Function Neural Network (RBFNN)

The RBFNN is a three layered topology namely, input, hidden and output layer that are completely linked together in a feed forward manner. The input layer receives the input data information while the output layer produces the final computed results. The layer that does not have direct access to the external world is known as the hidden layers. Figure 2 shows the RBFNN architecture with inputs (X_d), radial basis function (φ_N), weight (W_N) and output (y) respectively.

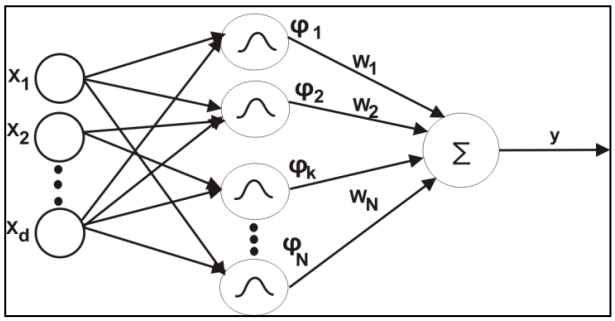

Figure 2: Radial basis function neural network

In the hidden layer chamber, the input layer data is received by means of unweighted connections. The data is then transformed by means of a non-linear activation function with each neuron estimating a Euclidean norm that shows the distance between the input to the network and the position of the neuron called the centre. This is then inserted into a radial basis activation function which calculates and outputs the activation of the neuron (Deyfrus, 2005). The present study applied the Gaussian activation function (Gurney, 2005) expressed in Eq. 6 as

$$a_j = \varphi_j(X) = \exp\left[-\frac{\|X-\mu_i\|^2}{2\sigma_j^2}\right] \qquad (6)$$

where X is the input vector, μ_i is the centre of the Gaussian function and σ_j is the spread parameter of the Gaussian function bells and $\|\ \|$ is the Euclidean norm. The output layer contains the linear function and uses the weighted sum of the hidden layer as propagation function expressed in Eq. 7 (Tierra et al., 2008) as

$$Y_k = \sum_{j=1}^{p} W_{jk}\, a_j + b_0 . \qquad (7)$$

Here, each W_{jk} is the output weight that matches to the association between a hidden node and an output node while b_0 is the bias that has a unit weight and p denotes the number of hidden neurons. Equation 7 could be achieved by the RBFNN through learning. Hence, in this study, the supervised learning paradigm was used to establish the input-output mapping functions. Thus, in a supervised application a set of data samples called training for which the corresponding desired outputs are known is fed into the network. It is important to note that the training can be characterized as a non-linear optimization problem where the network parameters are to be solved (Barsi, 2001) such that the estimated outputs from the RBFNN will be in good agreement with the target data.

The error e_k in the output of a neuron k is defined as the deviation of the desired value d_k from the

computed value Y_k in the first step (Haykin, 1999). This is expressed (Eq. 8) by

$$e_k = d_k - Y_k . \qquad (8)$$

The training process continues until the network error reaches an acceptable value.

4. Accuracy assessment

In order to compare the results attained by the RBFNN model with the six-parameter and four-parameter models, the residuals computed between the desired plane coordinates and the transformed plane coordinates based on the test data set was used. The performance indicators utilized include the Mean Squared Error (MSE), Mean Bias Error (MBE), Mean Absolute Error (MAE), Horizontal Position Error (HE), Mean Horizontal Position Error (MHE) and Standard Deviation (SD). The mathematical expression for the various performance indices are given by Eq. 9 to 14 respectively.

$$MSE = \frac{1}{n}\sum_{i=1}^{n}(O_i - P_i)^2 ; \qquad (9)$$

$$MBE = \frac{1}{n}\sum_{i=1}^{n}(O_i - P_i) ; \qquad (10)$$

$$MAE = \frac{1}{N}\sum_{i=1}^{N}|O_i - P_i| ; \qquad (11)$$

$$HE = \sqrt{(E_2 - E_1)^2 + (N_2 - N_1)^2} ; \qquad (12)$$

$$MHE = \frac{1}{n}\sum_{i=1}^{n} HE_i ; \qquad (13)$$

$$SD = \sqrt{\frac{1}{n-1}\sum_{i=1}^{n}(e_i - \bar{e})^2} ; \qquad (14)$$

where n is the total number of test examples presented to the learning algorithm; O and P are the measured and predicted plane coordinates from the various procedures; e represents the deviations between the measured and predicted plane coordinates; and $\bar{e}$ is the mean of the deviations.

5. Test results

The 27 common points (Figure 3) coordinate in Accra datum and Leigon datum for the Ghana national geodetic reference network was divided into reference data set and testing data set. Twenty points were selected as the reference points (P_1, P_2, … P_{20}) while the testing data set consisted of 7 points (T_1, T_2, … , T_7). In this study, the chosen reference coordinates were used to determine the transformation parameters based on the four and six-parameter models as well as the RBFNN training process in the ANN approach. The test data served as an independent check on the performance of the afore mentioned techniques with the test results presented in the following sections.

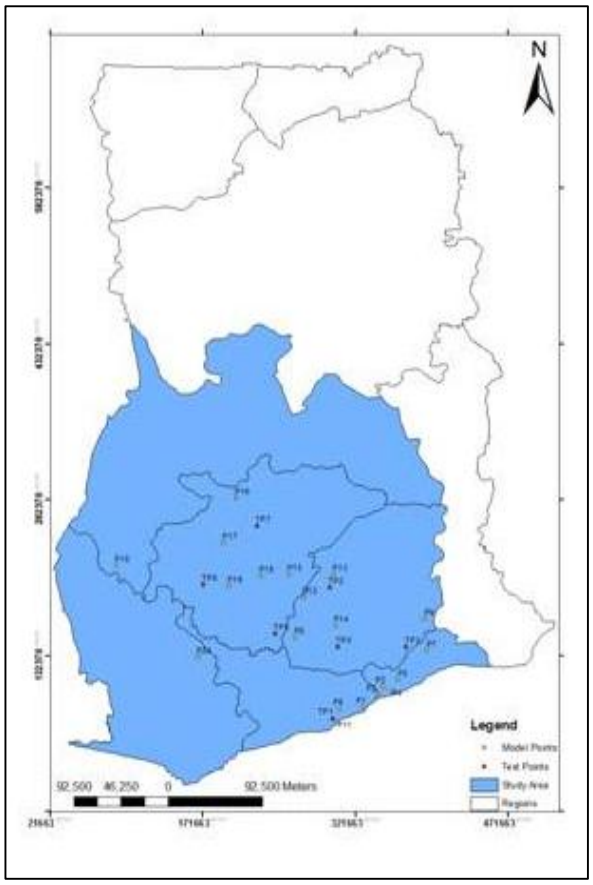

Figure 3: Area of interest showing the training and testing data distribution

5.1. Coordinate transformation from Leigon datum to Accra datum

Transformation parameters with their standard deviation (SD) values determined based on the six and four-parameter models for transforming coordinates from Leigon datum to Accra datum are presented in Tables 1 and 2, respectively. In the ANN approach of the RBFNN, plane coordinates of the points in Leigon datum denoted as (E_{clark}, N_{clark}) were used as the input layer neurons while (E_{war}, N_{war}) in Accra datum were used as the output layer neurons. The MSE was then used as the criterion to determine the optimum RBFNN structure during the training process. After several trials, the optimum structure of the RBFNN for transforming coordinates from Leigon datum to Accra datum was [2-20-2]. Thus, two inputs (E_{clark}, N_{clark}) with twenty hidden neurons and two outputs (E_{war}, N_{war}).

Table 1: Six parameter model

Parameters	Values	Standard Deviation
A	0.99999	3.20E-06
B	-1.13E-05	4.23E-06
C	2.22345	1.417531
D	1.75E-05	3.20E-06
E	1.00001	4.23E-06
F	0.50298	1.417531

Table 2: Four parameter model

Parameters	Values	Standard Deviation
S	1.000001	2.06E-06
R	1.27E-05	2.06E-06
ΔX	2.080065	0.692668
ΔY	2.98E+00	0.693

Table 3 shows how much the estimated plane coordinates by the six-parameter, four-parameter and RBFNN deviate from the existing plane coordinates. The HE, mean error and SD values for each test coordinate are also presented. As indicated earlier at the study area and data source section, these historical triangulation points cover the mountainous southern section of Ghana and thus were established on hilly terrain. Hence, the analyses presented henceforth should be viewed as a way of assessing the applicability of the RBFNN, four-parameter and six-parameter models for transforming 2D national coordinates between the Accra and Leigon datums based on hilly terrain data.

Table 3: Deviation of transformed test coordinates from observed coordinates

Test Point	SIX PARAMETER			FOUR PARAMETER			RBFNN		
	ΔE(m)	ΔN(m)	HE (m)	ΔE(m)	ΔN(m)	HE (m)	ΔE(m)	ΔN(m)	HE (m)
T1	-0.14795	1.39339	1.40122	-0.29524	0.85961	0.90890	-0.32905	0.01167	0.32926
T2	0.638301	0.62816	0.89555	0.67542	1.00285	1.20909	-0.06739	0.32282	0.32978
T3	0.464141	-1.33447	1.41289	0.32020	-1.02109	1.07012	0.13081	-0.13691	0.18936
T4	0.32133	0.07592	0.33018	0.36458	-0.13244	0.38789	0.38690	-0.26637	0.46973
T5	0.601158	0.48968	0.77536	0.54608	0.48550	0.73070	-0.08138	0.34873	0.35810
T6	-1.51539	0.33729	1.55247	-1.31129	0.14019	1.31877	-0.40711	0.71348	0.82145
T7	-0.22456	0.81286	0.84331	-0.01026	1.27667	1.27672	0.59942	-0.48508	0.77111
Mean Error	**0.01958**	**0.34326**	**1.03014**	**0.04136**	**0.37304**	**0.98603**	**0.03317**	**0.07262**	**0.46697**
SD	**0.75868**	**0.84776**	**0.44063**	**0.68125**	**0.78697**	**0.33689**	**0.36597**	**0.41294**	**0.23975**

The deviations (ΔE, ΔN) (Table 3) known as errors indicate the variation between the transformed plane coordinates and the measured plane coordinates relative to the ideal zero error value. Analysis of Table 3 indicates that the RBFNN predicted outcomes in both Eastings and Northings are in good agreement with the measured plane coordinates compared with the six and four-parameter models. In order to ascertain the practicality of the transformed plane coordinates from both methods, their horizontal positional accuracies were assessed. This was done by estimating the amount of HE from the transformed plane coordinates.

Figure 4 shows the HE for the results obtained by the six-parameter model, four-parameter model and RBFNN. Based on visual observation of Figure 4 and Table 3, it can be seen that, the six-parameter, four-parameter and RBFNN methods predicts the horizontal errors with a minimum uncertainty in the order of approximately 0.33 m, 0.39 m and 0.19 m respectively. On the other hand, the maximum horizontal displacement of about 1.55 m, 1.32 m and 0.8 m were known for the six-parameter, four-parameter and RBFNN.

The reason for improvement in the horizontal positional accuracies attained by the RBFNN might possibly be that the distortions existing in both datums established by conventional surveying techniques have been modelled and more absorbed by the RBFNN model compared with the four-parameter and six-parameter models. Hence, the inference to be made here is that the influence of the local geodetic network distortions on the coordinate transformation results has been minimized by the RBFNN model thereby improving the transformation accuracy.

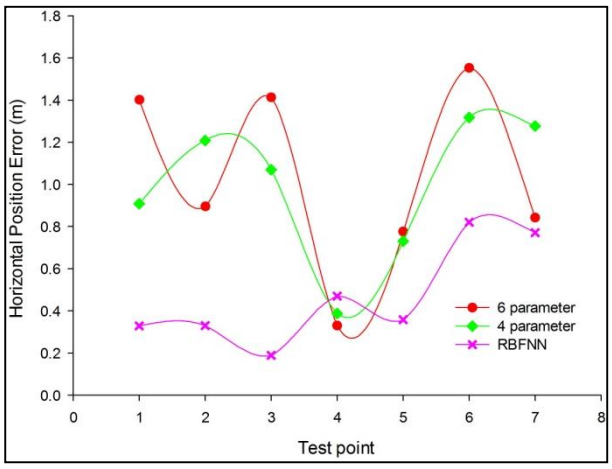

Figure 4: Horizontal displacement of test coordinates

In addition, Table 4 presents the extent at which the four and six-parameter models HE values deviate from the RBFNN values. This was estimated by subtracting the individual HE of the test points attained by the four and six-parameter models from the RBFNN results. The objective here is to further ascertain the efficiency of applying the ANN approach of RBFNN compared with the other two methods.

Table 4: Difference in the horizontal positional accuracy between the traditional techniques and RBFNN

Test Point	Six parameter (m)	Four parameter (m)
T1	1.07196	0.57964
T2	0.56577	0.87931
T3	1.22353	0.88076
T4	-0.13955	-0.08184
T5	0.41726	0.3726
T6	0.73102	0.49732
T7	0.0722	0.50561

With reference to Table 4, it can be seen that the four and six-parameter HE values deviated from the RBFNN results on a higher level. This implies that the traditional techniques could not absorb more of the distortions within the two local geodetic networks as compared to the RBFNN. However, a close inspection of Table 4 and Figure 3 shows that only the test point T4 HE value for the six-parameter and four-parameter model was approximately 0.14 m and 0.08 m better than the RBFNN model transformed value. This could be due to the inability of the RBFNN model to absorb more of the distortion in the T4 contributing to the calculated HE value of T4 being a little higher. This is because HE is highly dependent on the horizontal position coordinates for its estimation. This further confirms the assertion made by Featherstone (1997) that mathematical transformation models cannot completely account for the distortions in local geodetic network and thus geocentric datum adoption should be the preferred choice. Nonetheless, overall, in the present study the RBFNN gave more reasonable and applicable transformed values than the six and four-parameter models. Hence, the RBFNN results could be used as an interim solution until the adoption of a geocentric datum in Ghana.

In Table 5, a summary of the total error attained when the three methods were applied for transforming coordinates from Leigon to Accra datum is presented. It can be observed from Table 5 that there is a significant improvement in the results for the RBFNN in all the Performance Criteria Indices (PCI) utilized as compared with the other two techniques. The inference made in line with the maximum and minimum values (Table 5) is that the RBFNN model predicted outputs differed by not more than 0.82 m whereas 1.55 m and 1.32 m was realized by the six-parameter and four-parameter models. The SD values (Tables 3 and 5) estimated show a practical expression for the precision of the transformed test coordinates. Analysis of Tables 3 and 5 show that the RBFNN had the least SD values which further indicate the limit of the error bound by which every value within the transformed test dataset varies from the most probable value.

Table 5: Total error of the coordinate differences with the three methods

PCI	Six parameter (m)	Four parameter (m)	RBFNN (m)
Max Error	1.5525	1.3188	0.8215
Min Error	0.3302	0.3879	0.1894
MHE	1.0301	0.9860	0.4670
SD	0.4406	0.3369	0.2397

Furthermore, two statistical indicators namely, MSE and MAE were also used to ascertain the quality of the transformation results produced by the three methods. The closer these statistical indices are to zero the better the prediction capabilities of the method. With reference to Table 6, it was uncovered that the MSE and MAE values obtained for RBFNN is considerably less compared to the six-parameter and four-parameter models. The obtained results (Table 6) portray the closeness of the models fit to the measured test coordinates. On the basis of the results (Table 6), it can be seen that the RBFNN transformed plane coordinates are in better agreement with the measured coordinates compared with the six and four-parameter models. Thus, signifying the extent at which the RBFNN model could perform against an independent test data.

Table 6: Model performance statistics

Model	Coordinate difference	PCI	
		MSE (m)	MAE (m)
6 parameter	**ΔE**	0.49374	0.55898
	ΔN	0.73386	0.72454
4 parameter	**ΔE**	0.39952	0.5033
	ΔN	0.67001	0.70262
RBFNN	**ΔE**	0.1159	0.28601
	ΔN	0.15143	0.32664

Moreover, to have a better idea of how well the determined parameters for the traditional techniques and the optimum RBFNN model will generalize with large unseen plane coordinates data, the whole dataset (27 common points) were used as a test data in the already determined six-parameter model, four-parameter model and optimum RBFNN model.

Figure 5 displays the horizontal errors when the whole data was used to test the determined six-parameter, four-parameter and the optimum RBFNN model. This evidently shows that within the Ghana national geodetic reference network the ANN technique of RBFNN could serve as a plausible alternative technology to be applied for plane coordinate transformation from Leigon datum to Accra datum. This claim is further confirmed by the total error attained by each method as shown in Table 7.

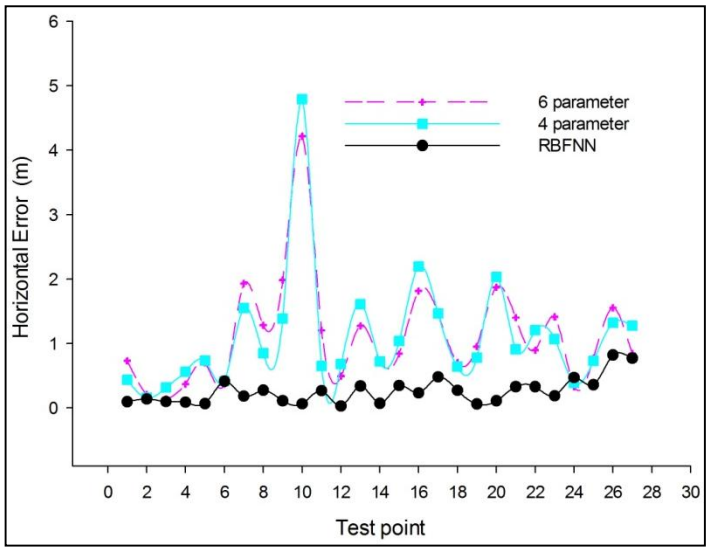

Figure 5: Horizontal displacement of the whole data

Table 7: Total Error of the coordinate differences for the whole data

PCI	Six parameter	Four parameter	RBFNN
Max Error	4.2158	4.7913	0.8215
Min Error	0.1369	0.1577	0.0283
MHE	1.1294	1.1082	0.2600
SD	0.8206	0.8961	0.2042

5.2 Coordinate transformation from Accra datum to Leigon datum

The derived parameters for transforming data from Accra datum to Leigon datum with their associated standard deviations using six-parameter and four-parameter transformation models are presented in Tables 8 and 9 respectively. In the RBFNN training, plane coordinates of the points in Accra datum denoted as (E_{war}, N_{war}) were used as the input layer neurons while (E_{clark}, N_{clark}) in Leigon datum were used as the output layer neurons. The MSE was used as the optimality criterion to aid in the selection of the best RBFNN structure during the training process. The optimum RBFNN structure for carrying out the transformation was [2-18-2]. That is, two inputs (E_{war}, N_{war}) with eighteen hidden neurons and two outputs (E_{clark}, N_{clark}).

Table 8: Six parameter model

Parameters	Values	SD
a	1.00000042	3.20E-06
b	1.13E-05	4.23E-06
c	-2.2234323	1.41753
d	-1.75E-05	3.20E-06
e	0.99999	4.23E-06
f	-0.50284	1.41753

Table 9: Four parameter model

Parameters	Values	SD
S	0.99999	2.06E-06
R	-1.27E-05	2.06E-06
ΔX	-2.08003	0.69267
ΔY	-2.98E+00	0.69267

Table 10 presents the extent at which the six-parameter, four-parameter and RBFNN transformed coordinates deviate from the measured plane coordinates.

Judging from the outcomes in Table 10, it can be stated that the RBFNN model is superior to the six-parameter and four-parameter models. This is because the RBFNN was able to produce more satisfactory transformed coordinates in both Eastings and Northings based on (ΔE, ΔN) as compared with the six and four-parameter models results. Again, taking into account the HE values (Table 10), it can obviously be concluded that the transformed test coordinates rendered by the RBFNN are closer to the desired testing target outputs after the testing data (untrained) were introduced to the neural network. This assertion can also be gathered from Figure 6 where the

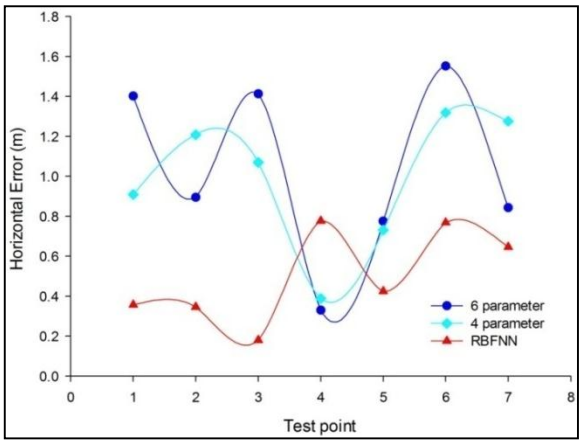

Figure 6: Horizontal displacement of test coordinates

RBFNN showed better generalization to the test data than the six-parameter and four-parameter models. This is because the RBFNN model achieved a maximum horizontal uncertainty of 0.78 m compared to1.55 m and 1.32 m obtained by the six-parameter and four-parameter models.

Table 10: Deviation of transformed test coordinates from measured coordinates

Test Point	6 parameter			4 parameter			RBFNN		
	ΔE(m)	ΔN(m)	HE (m)	ΔE(m)	ΔN(m)	HE (m)	ΔE(m)	ΔN(m)	HE (m)
T1	0.14794	-1.39341	1.40124	0.29524	-0.85963	0.90892	0.33354	0.12541	0.35634
T2	-0.63831	-0.62812	0.89553	-0.67543	-1.00283	1.20908	0.07168	-0.33876	0.34626
T3	-0.46411	1.33447	1.41288	-0.32017	1.02109	1.07011	-0.15019	-0.09838	0.17954
T4	-0.32133	-0.07592	0.33018	-0.36459	0.13244	0.38790	-0.37632	0.67953	0.77678
T5	-0.60116	-0.48967	0.77535	-0.54608	-0.48550	0.73069	0.08081	-0.41617	0.42395
T6	1.51537	-0.33731	1.55245	1.31127	-0.14020	1.31874	0.41666	-0.64543	0.76824
T7	0.22454	-0.81282	0.84326	0.01023	-1.27665	1.27669	-0.60426	0.23030	0.64666
Mean	**-0.01958**	**-0.34326**	**1.03013**	**-0.04136**	**-0.37304**	**0.98602**	**-0.03258**	**-0.06621**	**0.49968**
SD	**0.75867**	**0.84776**	**0.44063**	**0.68124**	**0.78697**	**0.33687**	**0.36932**	**0.44983**	**0.23196**

Furthermore, Table 11 presents the how much the HE values attained by the four and six-parameter models deviate from the RBFNN HE values.

Table 11: Deviation in the horizontal positional accuracy between the traditional techniques and RBFNN

Test Point	six parameter (m)	four parameter (m)
T1	1.0449	0.55258
T2	0.54927	0.86282
T3	1.23334	0.86057
T4	-0.4466	-0.3889
T5	0.3514	0.30674
T6	0.78421	0.5505
T7	0.1966	0.63003

From Table 11, it can be observed that the magnitude by which the four and six-parameter models HE values deviate from the RBFNN results are very high. This signifies that if the RBFNN is applied to transform plane coordinates within the study area, better horizontal position accuracy could be achieved as compared to the four and six-parameter models. Similar phenomenon for the test point T4 estimated HE values by the six and four-parameters being better than RBFNN when transforming coordinates from Leigon to Accra datum were also observed in transforming Accra datum to Leigon datum. However, in comparison, the RBFNN produced more accurate transformed values than the six and four-parameter models.

The estimated total errors in transforming coordinates from Leigon to Accra datum are presented in Table 12. It can be seen from the analysis of the maximum and

minimum values given inTable12 that the RBFNN model transformed coordinates differ from the measured coordinates by approximately not more than 0.78 m compared with 1.55 m and 1.32 m given by the six-parameter and four-parameter models. The MHE also indicates that the RBFNN is superior over the six-parameter and four parameter models.

Table 12: Total error of the coordinate differences with the three methods

PCI	six parameter	Four parameter	RBFNN
Max Error	1.5525	1.3187	0.7768
Min Error	0.3302	0.3879	0.1795
MHE	1.0301	0.9860	0.4997
SD	0.4406	0.3369	0.2320

The results presented in Table 13 shows that RBFNN transformed the plane coordinates with a better accuracy than the six-parameter and four-parameter methods in terms of MSE and MAE. These results (Table 13) show how closely the transformed coordinate are related to the observed coordinates.

Table 13: Model performance assessment

Model	Coordinate difference	PCI	
		MSE (m)	MAE (m)
6 parameter	ΔE	0.49373	0.55897
	ΔN	0.73385	0.72453
4 parameter	ΔE	0.3995	0.50329
	ΔN	0.6700	0.70262
RBFNN	ΔE	0.11798	0.29049
	ΔN	0.17782	0.3620

Besides, to check the generalization capability of the determined six-parameter, four-parameter and the optimum RBFNN models the whole dataset was used as the testing data. On the basis of Figure 6, the horizontal error values obtained signify the extent that the horizontal transformed coordinates produced by the RBFNN, six-parameter and four parameter models deviate from the measured plane coordinates. It also shows the positional accuracy of the transformed data in horizontal terms to the measured data. In comparison, the RBFNN yielded a better horizontal positional accuracy than the six-parameter and four-parameter as illustrated in Figure7.

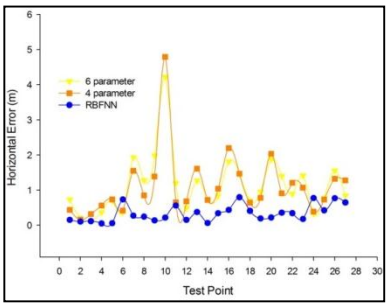

Figure 7: Horizontal displacement of the whole data

Table 14 shows that in the case of plane coordinate transformation the RBFNN is superior to the six-parameter and four-parameter transformation models. Besides, it indicates that there is improvement of 100% in the MHE and the SD.

Table 14: Total error of the coordinate differences for the whole data

PCI	6 parameter	4 parameter	RBFNN
Max Error	4.2158	4.7913	0.7981
Min Error	0.1369	0.1577	0.0507
MHE	1.1294	1.1082	0.3389
SD	0.8206	0.8961	0.2362

6. Conclusion

Coordinate transformation is necessary in developing countries like Ghana where the local geodetic networks applied for surveying and mapping purposes are non-geocentric and highly heterogeneous in nature. This study applied for the first time the artificial neural network technology of radial basis function to transform coordinates from the two classical geodetic reference networks namely, Accra and Leigon datum in Ghana. The results obtained by using the six-parameter and four parameter transformation models confirm the existence of heterogeneity in the classical geodetic networks of Ghana. Therefore, the transformation parameters determined could not model and absorb the distortions in the coordinates between the Accra and Leigon datum. However, the application of the radial basis function neural network showed improvement in absorbing and compensating for the deformations in the classical geodetic networks in a more effective way. The conclusion to be drawn here is that, in the case of plane coordinate transformation, the artificial neural network technology could be exploited as viable alternative tool to the traditional transformation techniques applied in the present study.

Acknowledgement

The authors would like to thank the Ghana Survey and Mapping Division of Lands Commission for providing us with the necessary data set and information. We are also grateful to the anonymous reviewers for their helpful comments.

References

Ayer, J. (2008). Transformation models and procedures for framework integration of Ghana geodetic network. The Ghana Surveyor, 1(2), 52-58.

Ayer, J. and C. Fosu (2008). Map coordinates referencing and the use of GPS datasets in Ghana. Journal of Science and Technology, 28 (1), 116-127.

Barsi, A. (2001). Performing coordinate transformation by artificial neural network. AVN, 4, 134-137.

Chih-Hung, W., Hung-Ju, C., and Wei-Han, S. (2008). Direct Transformation of Coordinates for Global Positioning Using the Techniques of Genetic Programming and Symbolic Regression. Engineering Applications in Artificial Intelligence, 21, 1347-1359.

Deakin, R.E. (2006). A note on the Bursa-Wolf and Molodensky-Badekas transformations. School of Mathematical and Geospatial Sciences, RMIT University, 1-21.

Deyfrus, G. (2005). Neural networks: Methodology and applications. Springer –Verlag, Berlin, Germany.

Dzidefo, A. (2011). Determination of transformation parameters between the World Geodetic System 1984 and the Ghana Geodetic Network. Masters Thesis, Department of Civil and Geomatic Engineering, KNUST, Kumasi, Ghana.

Featherstone, W.E. (1997). A comparison of existing co-ordinate transformation models and parameters in Australia. Cartography, 26 (1), 13-26.

Ghilani, C. (2010). Adjustment computations: Spatial data analysis. John Wiley and Sons Inc., New York, 464-470.

Gil, J. and M. Mrowczynska (2012). Methods of artificial intelligence used for transforming a system of coordinates. Geod. List, 4, 321-336.

Grgic, M., M. Varga and T. Basic (2015). Empirical research of interpolation methods in distortion modelling for the coordinate transformation between local and global geodetic datums. Journal of Surveying Engineering, 10.1061/(ASCE)SU.1943-5428.0000154, 05015004.

Gullu, M. (2010). Coordinate transformation by radial basis function neural network. Scientific Research and Essays, 5 (20), 3141-3146.

Gullu, M., M. Yilmaz, I. Yilmaz and B. Turgut (2011). Datum transformation by artificial neural networks for geographic information systems applications. International Symposium on Environmental Protection and Planning: Geographic Information Systems (GIS) and Remote Sensing (RS) Applications (ISEPP), Izmir-Turkey, 13-19.

Gurney, K. (2005). An introduction to neural networks, Taylor and Francis, London.

Haykin, S. (1999). Neural networks: A comprehensive Foundation, second ed. Prentice Hall, New Jersey, 842p.

Kotzev, V. (2013). Consultancy service for the selection of a new projection system for Ghana. Draft Final Reports, World Bank Second Land Administration Project (LAP-2), Ghana.

Lin, L.S. and Y.J. Wang (2006). A study on cadastral coordinate transformation using artificial neural network. Proceedings of the 27th Asian Conference on Remote Sensing, Ulaanbaatar, Mongolia.

Mugnier, J.C. (2000). OGP-coordinate conversions and transformations including formulae. COLUMN, Grids and Datums. The Republic of Ghana. Photogrammetric Engineering and Remote Sensing, 695-697.

Mihalache, R.M. (2012). Coordinate transformation for integrating map information in the new geocentric European system using artificial neural networks. GeoCAD, 1-9.

Poku-Gyamfi, Y. and W.G. Hein (2006). Framework for the establishment of a nationwide network of Global Navigation Satellite System (GNSS) - A cost effective tool for land development in Ghana. 5th FIG Conference on Promoting Land Administration and Good Governance, Workshop – AFREF I, Accra, Ghana, 1-13.

Poku-Gyamfi, Y. and T. Schueler (2008). Renewal of Ghana's geodetic reference network. 13thFIG Symposium on Deformation Measurement and Analysis, 4th IAG Symposium on Geodesy for Geotechnical and Structural Engineering, LNEC, LISBON, 2008, 1-9

Schofield, W. (2001). Engineering surveying: Theory and examination problems for students. Butterworth-Heinemann, 5th Ed., Linacre House, Jordan Hill, Oxford OX2 8DP, UK.

Tierra, A., R. Dalazoana and S. De Freitas (2008). Using an artificial neural network to improve the transformation of coordinates between classical geodetic reference frames. Computers & Geosciences, 34, 181-189.

Tierra, A.R., S.R.C. De Freitas and P.M. Guevara (2009). Using an artificial neural network to transformation of coordinates from PSAD56 to SIRGAS95. Geodetic Reference Frames International Association of Geodesy Symposia, Springer 134, 173-178.

Tierra, A. and R. Romero (2014). Planes Coordinates Transformation between PSAD56 to SIRGAS using a Multilayer Artificial Neural Network. Geodesy and Cartography, 63 (2), 199-209.

Turgut, B. (2010). A back-propagation artificial neural network approach for three-dimensional coordinate transformation. Scientific Research and Essays, 5 (21), 3330-3335.

Wonnacott, R. (2007). A progress report on the AFREF project and its potential to support development in Africa. Space Geodesy Workshop, Matjiesfontein, 13-14 November.

Yilmaz, I. and M. Gullu (2011). Georeferencing of historical maps using back propagation artificial neural network. Society of Experimental Mechanics, 1-5.

Zaletnyik, P. (2004). Coordinate transformation with neural networks and with polynomials in Hungary.

International Symposium on Modern Technologies, Education and Professional Practice in Geodesy and Related Fields, Sofia, Bulgaria, 471-479.

Ziggah, Y.Y., H. Youjian, C.A. Odutola and D.L. Fan (2013a). Determination of GPS coordinate transformation parameters of geodetic data between reference datums - A case study of Ghana geodetic reference network. International Journal of Engineering Sciences and Research Technology, 2 (4), 2277-9655.

Ziggah, Y.Y., H. Youjian, C.A. Odutola and T.T. Nguyen, (2013b). Accuracy assessment of centroid computation methods in precise GPS coordinates transformation parameters determination - A case study, Ghana. European Scientific Journal, 9 (15), 1857-7431.

ISG Website
(http://www.isgindia.org)

The web site of Indian Society of Geomatics contains all pertinent information about ISG and its activities. The latest announcements can be found on homepage itself. "About ISG" link gives information about the constitution of ISG and its role in Geomatics, both the technology and its applications in the Indian context. The site also furnishes information about the members in different categories, like – Patron Members, Sustaining Members, Life Members and Annual Members. One can download Membership form from this section or through the Downloads link. The website also has full information about the Executive Council Meetings' Agenda of past and present along with Executive Agenda and Minutes. The details of local Chapters' office bearers are also provided. The Annual General-body Meeting (AGM) Agenda, their minutes for particular year can also be seen in the "AGM" section. The list of Events organized by the society can be found through the "Events" link.

Visit ISG Website
http://www.isgindia.org

Website related queries, suggestions and feedback to improve the website can be sent to the webmaster by e-mail:

info@isgindia.org
or
g_rajendra@sac.isro.gov.in

Journal of Geomatics Vol 11 No. 1 April 2017

Automated snow data processing tool for Natural Resource Data Base (NRDB)

Rajendra N Gaikwad, Shweta Mishra and Pushpalata Shah
Space Applications Centre, Ahmedabad
Email: g_rajendra@sac.isro.gov.in

(Received: Jan 03, 2017; in final form: Mar 28, 2017)

Abstract: Geographic Information System (GIS) tool was developed within ArcGIS for automation of snow data processing. This utility was developed using Visual Basic for Applications (VBA) language based on Arc Objects technology offered by the Environmental Systems Research Institute (ESRI). Tool provides an integrated solution for snow data processing which involve tasks i.e. raster to vector conversion, projection transformation, clipping operation and attribute addition. Datasets contain snow information about 33 basins of Himalayan regions. Further, non-spatial information was added to finally generated vector layers like basin name, code etc. These vector layers were organized in Natural Resources Database (NRDB) and available as OGC (Open Geospatial Consortium) compliant WMS (Web Map Service) service through NNRMS (National Natural Resources Management System) portal (www.nnrms.gov.in).

Keywords: Snow, ArcObjects, VBA, GIS, ArcGIS, WMS, NRDB, NNRMS

1. Introduction

India has a unique geographical location and is endowed with abundant natural resources. It comprises of rivers, fertile soil, forests, mineral deposits, mountains etc. To meet the increasing demand of food and fuel, optimal utilization of natural resources is required. To achieve this, the Department of Space, Government of India has initiated a programme titled National Natural Resources Repository (NRR) for creating and maintaining a systematic archive of all the digital spatial database of thematic and base maps generated using remote sensing data and promote / encourage its usage. The NRR programme consists of three elements, namely (i) data generation, (ii) database organization, and (iii) spatial data services. Data generation is being addressed through Natural Resources Census (NRC) project, database organization through Natural Resources Data Base (NRDB), and spatial data services through NNRMS portal which houses the GIS repository of natural resources for entire country in a secured environment (Anon., 2005). NNRMS supports optimal utilization of country's natural resources by providing systematic inventory of natural resources available using remote sensing data in conjunction with conventional data / techniques. Under NNRMS (www.nnrms.gov.in), the NRDB was established as a repository of all thematic data sets generated within ISRO-DOS. NRDB is collection of data sets on natural resources including the datasets collected over past several years under NNRMS. Access to these databases can be done through NNRMS portal. NRDB repository is regularly updated with new spatial data, especially for the projects like Monitoring snow and glaciers, wetland, NRC. Updation requires several stages of processes starting from metadata generation, database organization to map generation. This paper addresses the development of methodology for automatic processing and organizing snow data in NRDB on regular basis.

2. Study area and data

Himalayan region falls in to different geographical locations which belong to states of Jammu and Kashmir, Himachal Pradesh, Uttarakhand, Arunachal Pradesh and Sikkim. Himalayas possess one of the largest resources of snow and ice outside the polar regions. There are increasing concerns by scientific community that global warming caused by increase in concentration of greenhouse gases in atmosphere can cause dramatic impact on the snow melt runoff in the river systems. Sensitivity of snow and glaciers to variations in temperature makes them a key indicator of climate change. In order to study climate change, inventory of snow cover is required.

Under project Snow and Glacier Studies, snow cover monitoring was done (every 5 days and 10 days) by Space Applications Centre (SAC) along with 13 concerned Central / State government Departments and Academic Institutes during year 2008 to 2014 of Himalayan region covering Indus, Ganga and Brahmaputra river basins using IRS (Resourcesat 1 and 2) AWiFS data (SAC, 2016).

Snow cover data of Himalayan region with respect to different basins was generated as classified images for the months from October to June. This data is generated in raster format representing snow and no snow, respectively. In this study, six basins of Ganga, Brahmaputra, Indus, Chenab, Satluj and Tista and 33 sub-basins was taken up for snow cover monitoring (SAC 2016). The list of study sub-basins is given in Table 1.

Table 1: List of study sub-basins

Sr. No.	Sub-basin	Sr. No.	Sub-basin
1	Alaknanda	18	Parbati
2	Astor	19	Pin
3	Baspa	20	Rangit
4	Beas	21	Ravi
5	Bhaga	22	Shasgan
6	Bhagirathi	23	Shigar
7	Bhut	24	Shigo
8	chandra	25	Shyok
9	Dibang	26	Spiti
10	Dras	27	Subansiri
11	Gilgit	28	Suru
12	Hanza	29	Tawang
13	Jhelum	30	Tista
14	Jiwa	31	Warwan
15	Kisanganga	32	Yamuna
16	Miyar	33	Zaskar
17	Nubra		

Snow cover datasets (every 10 days) from year 2008 to 2014 in raster format were provided to NRDB for organization into geo database and serving the data as OGC (Open Geospatial Consortium) compliant Web Map Service (WMS). Data was required to be processed and organized as per NNRMS standards before database insertion (Anon. 2005). Tasks associated with processing i.e. raster to vector conversion, projection transformation, clipping for state wise separation and inserting feature attributes for large volume of data was tedious, repetitive, and time consuming. So the objective was to convert manual processing of snow cover data into automatic one.

Converting the classified snow cover raster images to vector format and projection transformation were the primary objectives. Additionally, clipping of the data as per respective basin and adding attribute along with respective attribute values i.e. names, area, code were also required so as to put the snow cover mapping layers into the pre-defined geo database of NRDB.

3. Conceptualization and methodology

Before development of automated snow data processing tool for NRDB, sample snow dataset was taken and processed manually using ArcGIS to develop methodology and required product generation. Initially, the user interface in ArcGIS used to identify objects, properties, and methods to be integrated in code. Then to convert manual process to automatic, ArcObjects library was examined and studied. ArcObjects is the development environment of the desktop ArcGIS applications and it is used to customize and extend ArcGIS using the embedded Visual Basic for Applications (VBA). VBA is COM (Component Object Model) compliant and is supported by the ArcObjects technology of ESRI, which are available in higher software versions of ArcGIS (at http://www.esri.com). ArcObjects can actually mitigate the amount of repetitive work, streamline the workflow and even produce functionalities that are not easily available in ArcGIS (Wunderlich, 2009; Chang Kang-Tsung, 2008). ArcObjects includes APIs (Application Programming Interface) that support the built-in functionalities like reprojection and other raster and vector operations (Xu and Gao, 2008). The steps involved in processing data are shown in figure 1. During the initial phase of development, semi-automated process was prepared to accomplish the requirement. Subsequently it was converted into the fully automated tool.

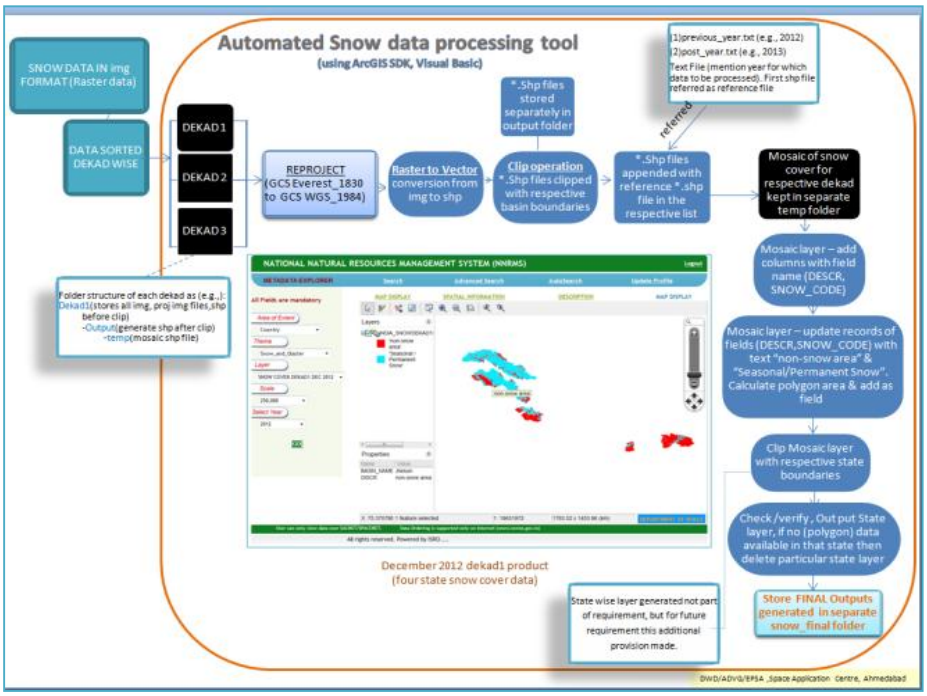

Figure 1: Steps for processing data

First step in the processing was the projection of raster file. Initially, snow raster datasets submitted to NRDB were in GCS Everest-1830 (also called Indian Datum). All data in NRDB organized is in geographic projection. According to NNRMS standards for GIS database, the recommended system is Geographic Coordinates. This is to allow flexibility for seamlessness and also for providing outputs in any desired Map projection of choice of user (Anon., 2005). So, module for automatic reprojection of raster datasets was developed in VBA using ArcObjects library (Song et al., 2013). Next step in automated process was to perform clipping operation with respective basin boundaries. A separate clip function is referred using ARCGIS SDK library. After clipping operation, first shape file of respective basin is taken as reference file and rest of the shape files were appended accordingly, this work was carried out by using append function provided in ArcObjects library. Next process was the attribute insertion into mosaic/appended file, it is carried out using additional function of add field in the library. After field insertion, all attributes information gets added against the code generated during raster to vector conversion. Using area calculation method, Respective polygon area was calculated and added to attribute table of the shape file generated. Algorithm has been developed in such a way that final product generated from mosaic after clipping will be checked for the existence of the unnecessary polygons. During processing name of respective polygon is added with basin name of the area it belongs.

These generated vector layers were organized in NRDB and available as OGC compliant WMS service through NNRMS portal. NNRMS is WebGIS based portal which disseminates natural resources datasets archived from various national projects as WMS Service. AutoDesk software is used for publishing all snow layers as WMS Service which can be displayed in a browser application i.e. NNRMS. The WMS defines the interface for accessing geospatial data uniformly from remote servers in a standard format, such as Portable Network Graphics (PNG) and Graphics Interchange Format (GIF), through HTTP (Mishra and Sharma, 2016).

4. Results and discussion

Following outputs shown in Figures describe the product generated using automated tool and snow layers as WMS Service in NNRMS portal. Figure 2 shows raster classified image of snow data for Alaknanada basin for the year 2012 of the first dekad of month December.

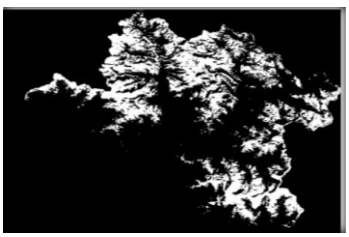

Figure 2: Snow cover area of Alaknanda basin

Figure 3 shows the shape file of Alaknanda basin utilized for clipping operation.

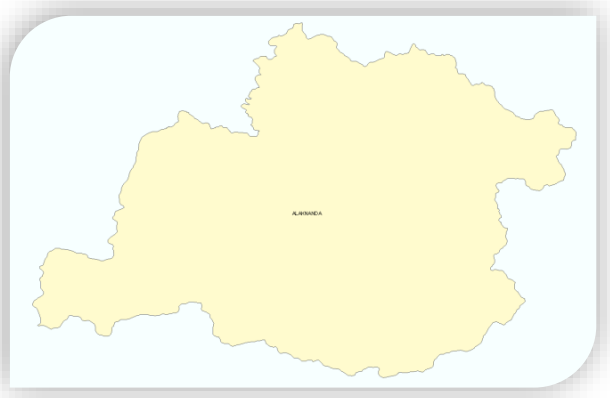

Figure 3: Shapefile of Alaknanda basin

Figure 4 (a) shows the final output layer generated for first dekad of December along with its attributes table as shown in Figure 4 (b), showing added columns i.e. “BASIN NAME”, “SNOW_CODE, DISCR (description)” and “F_AREA (area)”.

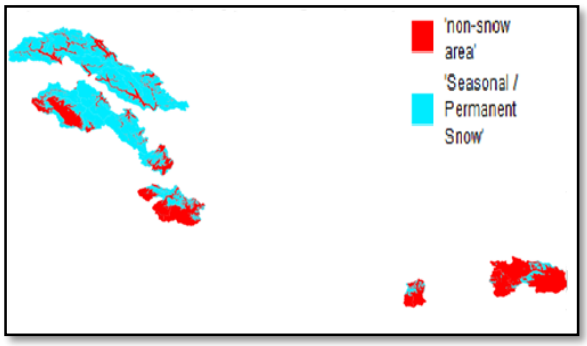

Attributes of INDIA_SNOWDEKAD1DEC2505CM2012

FID	Shape *	ID	GRIDCODE	BASIN_NAME	SNOW_CODE	DISCR	F_AREA
0	Polygon	13	10	Alaknanda	1	non-snow area	0
1	Polygon	17	10	Alaknanda	1	non-snow area	0.000002
2	Polygon	18	10	Alaknanda	1	non-snow area	0.000001
3	Polygon	27	10	Alaknanda	1	non-snow area	0
4	Polygon	28	10	Alaknanda	1	non-snow area	0
5	Polygon	29	10	Alaknanda	1	non-snow area	0.000003
6	Polygon	30	10	Alaknanda	1	non-snow area	0.000002
7	Polygon	31	10	Alaknanda	1	non-snow area	0.000006
8	Polygon	33	10	Alaknanda	1	non-snow area	0.000001
9	Polygon	35	10	Alaknanda	1	non-snow area	0.000001
10	Polygon	36	10	Alaknanda	1	non-snow area	0.000009
11	Polygon	37	10	Alaknanda	1	non-snow area	0.000001
12	Polygon	38	10	Alaknanda	1	non-snow area	0.00001
13	Polygon	39	10	Alaknanda	1	non-snow area	0
14	Polygon	41	10	Alaknanda	1	non-snow area	0.000006
15	Polygon	44	10	Alaknanda	1	non-snow area	0.000002
16	Polygon	46	10	Alaknanda	1	non-snow area	0.000001
17	Polygon	47	10	Alaknanda	1	non-snow area	0.000001
18	Polygon	48	10	Alaknanda	1	non-snow area	0
19	Polygon	49	10	Alaknanda	1	non-snow area	0
20	Polygon	51	10	Alaknanda	1	non-snow area	0.000001
21	Polygon	52	10	Alaknanda	1	non-snow area	0.000005

Record: 1 Show: All Selected Records (0 out of 64256

Figure 4: (a) Vector layer as WMS Service; and (b) Attribute table of vector layer in ArcGIS

As described in the methodology a separate state wise vector layers showing availability of snow were also generated using state boundary vector layer. Indian State Boundary layer used for generating state wise layers are

already available in NRDB have been generated under National GIS (NATGIS) project. Figure-5 to 9 shows screen shots of generated snow cover WMS Service using automated tool for the Indian states of Jammu& Kashmir, Uttarakhand, Himachal Pradesh, Arunachal Pradesh and Sikkim.

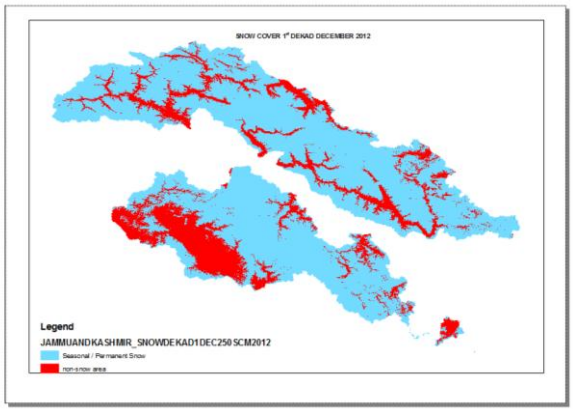

Figure 5: Snow cover WMS of Jammu & Kashmir

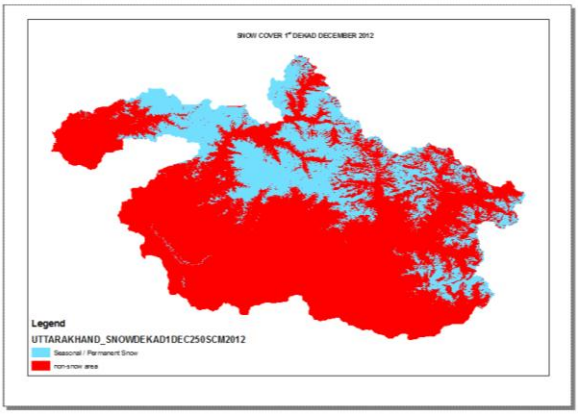

Figure 6: Snow cover WMS of Uttarakhand

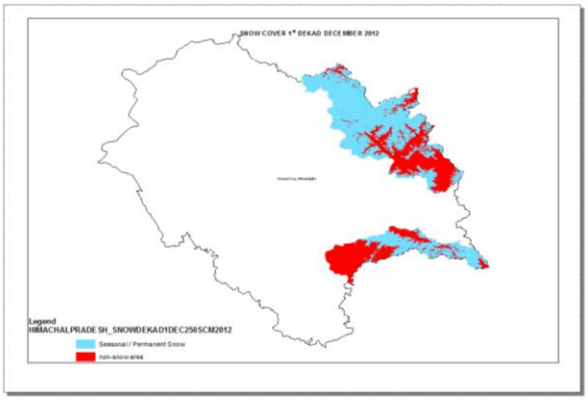

Figure 7: Snow cover WMS of Himachal Pradesh

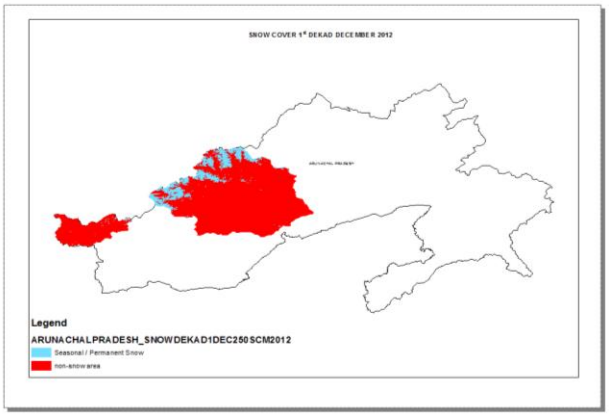

Figure 8: Snow cover WMS of Arunachal Pradesh

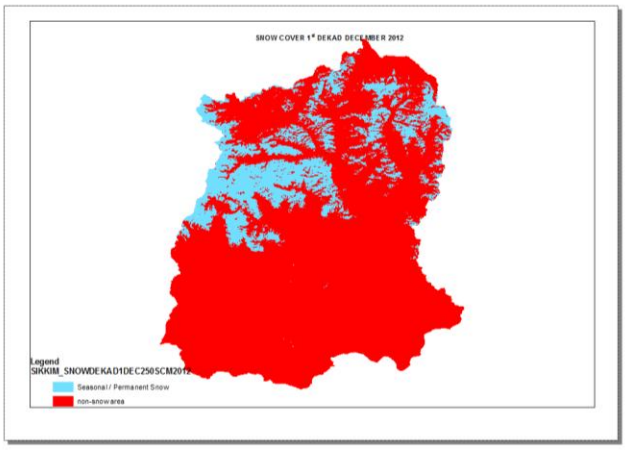

Figure 9: Snow cover WMS of Sikkim

The combined snow product is published as WMS and disseminated in NNRMS portal as shown in Figure 10. Related metadata generated is shown in Figure 11 (a) and (b).

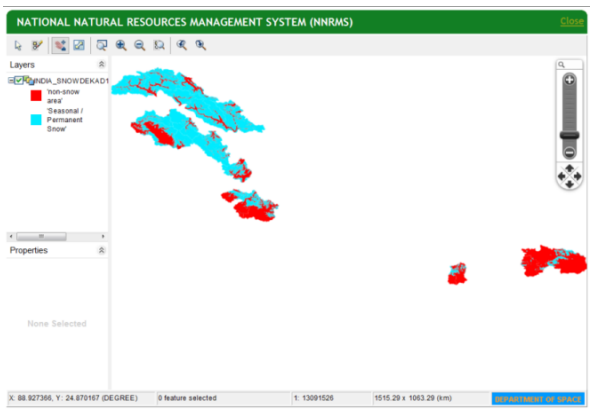

Figure 10: Snow cover WMS service of all basins in NNRMS Portal

Figure 11: (a) Spatial information of combined snow cover layer in English and Hindi respectively; and (b) Description of combined snow cover layer English and Hindi respectively

5. Conclusion

The development of automated snow data processing tool fastens the processing of voluminous spatial datasets like snow cover. It saves time and avoids processing errors if performed manually. This developed automated tool fulfils all requirements for generation of vector layers to be organized into Natural Resources Data Base according to its predefined standards. This also endorses the use of advanced computer assisted technology applied to the management of natural resources i.e. snow. Any novice user can process the snow data using this tool without having any detail knowledge of GIS. The VBA programming language and the ArcObjects used for developing this tool are an emerging technology in GIS based applications. The flexibility of the tool for further modification and updation is an added advantage with developed one.

Acknowledgements

The authors would like to thank Shri Tapan Misra, Director, Space Applications Centre, Dr. Raj Kumar, Deputy Director and Shri Shashikant A. Sharma, Group Head for providing all required infrastructure and encouragement to conduct this work. We also express our thanks to Shri B.P. Rathod, Scientist, Dr. A S Rajawat and Dr. I M Bahuguna for fruitful discussions. We also thank Shri Prateek Mathur and Shri Purnesh Jani for providing development support.

References

Anonymous (2005). A national standard for EO images, thematic and cartographic maps, GIS databases and spatial inputs. http://www.nnrms.gov.in/download/ NnrmsStandardsDoc.pdf

Mishra, S. and N. Sharma (2016). WebGIS based decision support system for disseminating nowcast based alerts: OpenGIS Approach. Global Journal of Computer Science and Technology, 2016, Vol. 16 Issue 7, Online ISSN: 0975-4172.

http:// www.esri.com

http://www.nnrms.gov.in

SAC (2016). Monitoring snow and glaciers of Himalayan region. Space Applications Centre, ISRO, Ahmedabad, India, 413 pages, ISBN: 978 – 93 – 82760 – 24 – 5.

Song, X., S. Qiu, L. Du, X. Liu and J. Chen (2013). Arable land quality assessment system development and its application based on ArcGIS engine. Journal of software, Vol. 8, No.2, February 201, 320-326.

Wunderlich, A.L. (2009). Improving ArcGIS workflow: Automation using Visual Basic for Applications (VBA), Digital Mapping Techniques, 2009 Workshop Proceedings, 21-26.

Xu, H. and P. Gao (2008). Custom image processing capabilities in ARCGIS. The International Archives of the Photogrammetry, Remote Sensing and Spatial Information Sciences. Vol. XXXVII. Part B4. Beijing 2008, 263-266

Journal of Geomatics Vol 11 No.1 April 2017

Suitable land assessment for urban expansion around Shimla, Himachal Pradesh (India) – MCE approach

Shashi Shekhar
Himachal Pradesh State Pollution Control Board, Shimla
E mail: shashi_ptn@yahoo.com

(Received: Feb 11, 2016; in final form: Mar 10, 2017)

Abstract: The present study aims to identify suitable zones for future urban expansion and development of new satellite township around Shimla using Geographic Information System (GIS) and Multi Criteria Evaluation (MCE). Shimla being located in the high altitude zone, several factors play important roles in guiding the urban development pattern and its form. There are several physiographic and natural limiting factors, which need to be taken into consideration while identifying suitable sites. The study aims to identify suitable sites and plots of above 100 ha by taking into consideration natural factors prevailing in seven surrounding tehsils of Shimla and Solan districts. While assessing suitable lands, different thematic layers were taken into account for GIS based multi-criteria evaluation such as elevation, slope, aspect, land use/cover, geomorphology, lithology, soil texture, lineaments, drainage network, road network and geology. Produced suitability map is intended to help in the selection of suitable sites/lands for development of future satellite township.

Keywords: Geographical Information System (GIS), Multi Criteria Evaluation (MCE), Weighted overlay analysis, Landsat, Thematic layers, Urban expansion

1. Introduction

Land-use suitability mapping and analysis is one of the most useful applications of GIS for spatial planning and management (Collins et al., 2001; Malczewski, 2004). Previously, various methods of spatial analysis for land use are commonly used in the suitability assessment studies. The problem of land use suitability assessment has often been tackled using multi-criteria decision analysis (MCDA) since 1980s (Antoine et al., 1997; Collins et al., 2001; Kiker et al., 2005; Sharifi et al., 2006; Kunwar et al., 2010). Cheng et al. (2003) have reported an integrated MCDA linear programming approach to support selection of an optimal landfill site. To create visualized suitability map for users and decision makers, the integration of MCDA and GIS has been widely promoted for solving spatial problems in urban assessment and planning (Phua and Minowa, 2005; Joerin et al., 2001). The land-use suitability problem involves evaluation and classification of the areal units according to their suitability for a particular activity. This has been very useful in evaluating suitable plots for sustainable urban expansion. It is necessary to explore suitable lands for future urban expansion quantitatively and objectively to provide a reliable basis for improving the persuasiveness of the effective decision-making. The rapid development of remote sensing technology and gradual maturing of GIS technology applications provide the foundation for such analysis. These advanced technologies are recognized worldwide as valuable technologies in environmental applications and are very useful in monitoring the environmental changes due to human activity (Gao and Skillcorn, 1995; Migul-Ayanz and Biging, 1997; Riaza et al., 1998; Yeh and Li, 1998). Some of the medium coarse resolution satellite data such as Landsat based MSS, TM, ETM+, OLI-TIR and IRS based LISS-III in public domain do offer basic inputs to the researchers to conduct such independent studies aimed at planning for better/suitable urban environment.

Shimla has been experiencing massive urban expansion for last two decades. It is also observed that sub-urban areas experienced more consolidation and expansion during last two decades. During these years, the city has been attracting lots of tourists from within and outside country by virtue of its England like climate and disturbance in its neighboring state i.e. Jammu and Kashmir. Moreover, the city has been recipient of major share of its migration from all parts of the state by virtue of its multi-functional role with respect to administration, commerce and tourism.

All these led to unprecedented expansion of the city in all direction and also in areas, which were otherwise not suitable for further human habitation growth. Age-old barriers for urban expansion of Shimla such as high slope, north aspect and dense vegetation cover started crumbling down and development is taking place on otherwise marginal sites.

With the unprecedented growth of concrete structure, the city has turned into concrete jungle and road network is choked with burgeoning personalized vehicles all around. There is not a single stretch of road where parking of vehicle is not observed. Consequently not a single day goes without traffic jam in the city. With the advent of rainy season, loose strata also give in to the massive development pressure on high slope in the form of landslides/landslips, which is also a regular occurrence of the city now. All above activities have continuous impact on the sentitive land uses of Shimla. Such impacts might lead to a series of complexities toward environment and land resources development

(Huang and Xia 2001) It is in this context, it is being felt that there is a need to decentralize some of the basic functions of the city or identify satellite township to ease the growing pressure of Shimla.

2. Study area

While identifying suitable lands for urban expansion, it is desired that suitable lands should not be far away from the current city, at the same time it has limited dependence on the old city. Therefore, all the tehsils surrounding the city have been selected for the study. Of all, five tehsils, are from Shimla district and two from neighbouring Solan district. Total population and their population density as per Census of India 2011 are given below.

Table 1: Tehsils in study area

Sr. No.	Tehsils	District	Population as per Census of India 2011	Population density (calculated from map area)
1	Shimla (R)	Shimla	84,382	257
2	Shimla (U)	Shimla	1,69,578	2828
3	Theog	Shimla	84,684	180
4	Junga	Shimla	13,398	129
5	Kandaghat	Solan	40,529	176
6	Arki	Solan	56,908	151
7	Sunni	Shimla	35,379	132
Total population			**4,84,858**	**264**

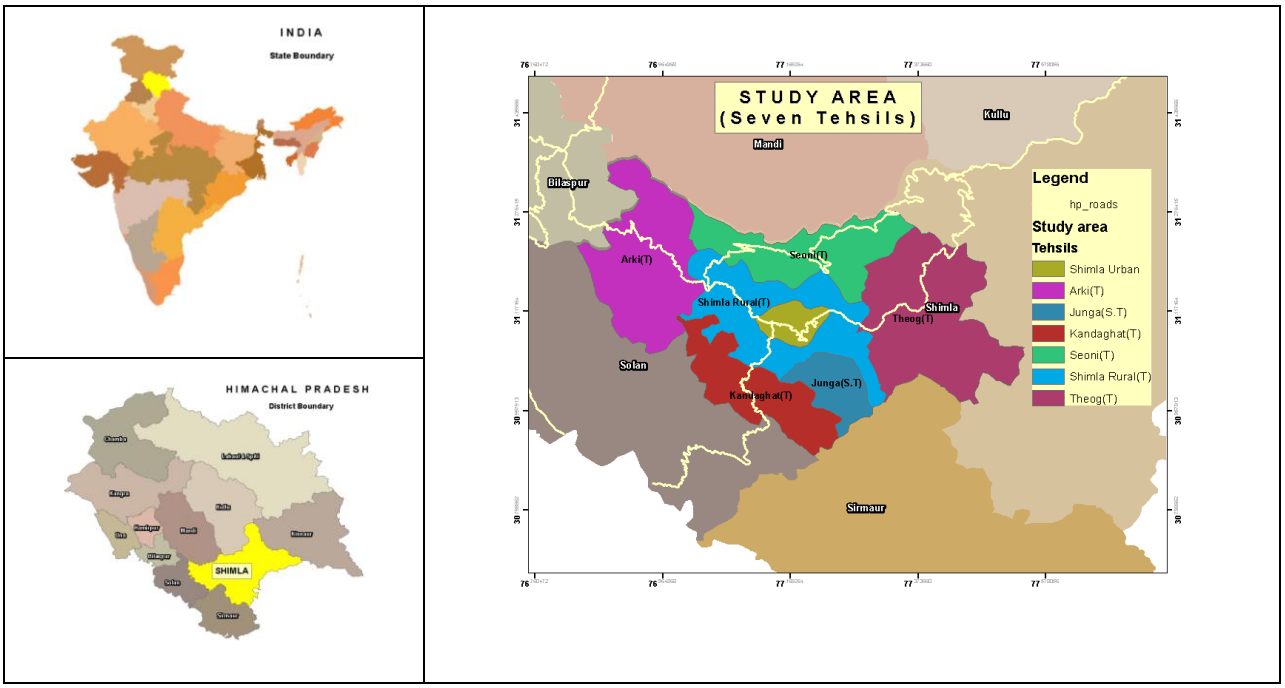

Figure 1: The study area

3. Emerging need

There has been an emerging need to look for suitable lands to decentralize some of the functions of the city with the objective to decongest the crowded city and identify satellite town to act as counter magnet to ease the growing pressure of the city and check Shimla bound migration. As it is observed from Table 1, except Shimla Urban & Rural tehsils, the tehsils have population density of less than 200 persons per km^2. This also offers some space for further urban expansion in such areas. However, Himachal Pradesh being a mountainous state, it has many constraints with respect to topography, sensitive environmental resources such as vegetation cover, high slopes, aspects, numerous cultural heritage and complex geological formations etc.

Any decentralization activity must consider these aspects for identifying suitable areas/sites for urban development around Shimla. In addition, there is a need to identify areas which need conservation; protection by

virtue of its environmental sensitivity and no development is permitted on such restricted lands.

4. Data used and methodology

There is no dearth of geospatial data/image of coarse or moderate resolution of multi-spectral bands (MS) of 30 meters and 24 meters from Landsat-7 ETM+ and IRS LISS-III respectively. The biggest source of such imagery of high temporal resolution available from the Landsat program helps the researchers to undertake time-series analysis. The IRS series LISS-III is also in public domain now with spatial resolution of 24 meters. Other thematic data have been collected from numerous sources such as Survey of India (toposheets), Bhuvan India, Census of India, Department of Forests and more importantly from open source. Some old spatial data collected by the author have also been updated through the help of Google Earth and OpenStreetMap.

Table 2: Different data layers / maps and sources

Sr. No.	Data layer / maps	Source	
1.	Base map	Topographical Maps of Survey of India (1:50,000) and ArcGIS 10 base map and Bhuvan portal.	
2.	Urban extent and land use mapping	Remote Sensing Data	
		LANDSAT-7 ETM+ (30 m) & PAN (15 m)	22nd October 2011
		Google Earth	
		OpenStreetMap	
3.	Elevation map	ASTER –DEM (30 m)	Version 2 released (October 17, 2011).
	Slope map	Derived from DEM	
	Aspect map	Derived from DEM	
4.	Land use/land cover map	Land use and land cover map has been prepared digitally by using Unsupervised Classification method in ERDAS IMAGINE 9.2 with limited field check and Google Earth maps.	
5.	Geological map	Geological Map has been obtained from Geological Survey of India portal and also available in various reports.	
6.	Geomorphological map	Lithology& geomorphological map have been prepared using Survey of India Toposheets (1:50,000) and remote sensing imagery and State Environment Report, Govt. of Himachal Pradesh.	
7.	Demographic map and tehsil map	Census of India, 2011	
8.	Forest density map	Forest Survey of India, Department of Forests, GoHP and Landsat ETM+ satellite data.	
9.	Road network	Public Works Department, Govt. of HP & Google Earth.	
10.	Soil texture	National Bureau of Soil Survey and Land Use Planning, Nagpur prepared Atlas in collaboration with Department of Agriculture, Govt. of Himachal Pradesh (Scale:1:2,50,000).	
11.	Location map	OpenStreetMap	

4.1 GIS based Multi Criteria Evaluation (MCE) Suitability analysis in GIS environment is a GIS-based process used to determine the appropriateness of a given area for a particular use. The basic premise of GIS suitability analysis is that each aspect of the landscape has intrinsic characteristics that are either suitable or unsuitable for the activities being planned. Suitability is determined through systematic, multi-factor analysis of the different aspects of the terrain.

The present study is based on land resource data collected from various sources (Table 2), which have been weighted overlaid together using a common measurement scale and weights were provided according to its importance. The same has been implemented through ArcGIS 10 and ERDAS Imagine 9.2.

4.2 Weighted overlay and modelling of criteria Different thematic layers, which were taken into account for multi criteria evaluation using Weighted Overlay tool by incorporating thematic areas are soil texture, slope, aspect, elevation, land use/cover, geomorphology, lithology, lineaments, drainage network, road network and geology. The Weighted Overlay tool (ArcGIS 10) applies one of the most commonly used approaches for overlay analysis to solve multi-criteria problems such as site selection and suitability models. As with all overlay analysis, in weighted overlay analysis, one must define the problem, break the model into sub-models and identify the input

layers. Since the input criteria layers were in different numbering systems with different ranges, to combine them in a single analysis, each cell for each criterion has been reclassified into a common preference scale such as 1 to 10 (or 1 to 5 etc), with 10 being the most favorable. An assigned preference on the common scale implies the phenomenon's preference for the criterion.

For example, in a simple housing suitability model, you may have three input criteria: slope, aspect, and distance to roads. The slopes are reclassed on a 1 to 10 scale with the flatter being less costly: therefore, they are the most favorable and are assigned the higher values. As the slopes become steeper, they are assigned decreasing values, with the steepest slopes being assigned weight 1. Same is applied for aspect and other layers as well, with the more favorable aspects, in this case the more southerly, being assigned the higher values. The same reclassification process is applied to the distance to roads criterion. The locations closer to the roads are more favorable since they are less costly to build on because they have easier access to power and require shorter driveways. A location assigned a suitability value of 5 on the reclassed slope layer will be twice as costly to build on as a slope assigned a value of 10. A location assigned a suitability of 5 on the reclassed slope layer will have the same cost as a 5 assigned on the reclassed distance to roads layer. (http://desktop.arcgis.com/en/arcmap/10.3/tools/spatial-analyst-toolbox/how-weighted-overlay-works.htm)

Based on the criteria and weightage as mentioned in Annexure-I, suitability map is produced. Landuse, being the central criteria, had maximum weight followed by slope and aspect, which is so important in the case of hill town like Shimla. Nearness to road gives additional advantage to urban growth (ribbon development is a natural occurrence in hill areas) in addition to assigning weights to distance to Municipal Corporation Shimla limit, elevation, geomorphological features geological formation and silt texture.

4.3 Modelling workflows of thematic layers

ModelBuilder application of ArcGIS has been used to create, edit and manage models for the current study. Models are basically workflows that string together sequences of geoprocessing tools, feeding the output of one tool into another tool as input. ModelBuilder can also be thought of as a visual programming language for building workflows. The follwing three models were applied to reach the final suitable plot identification for the study (figure 2).

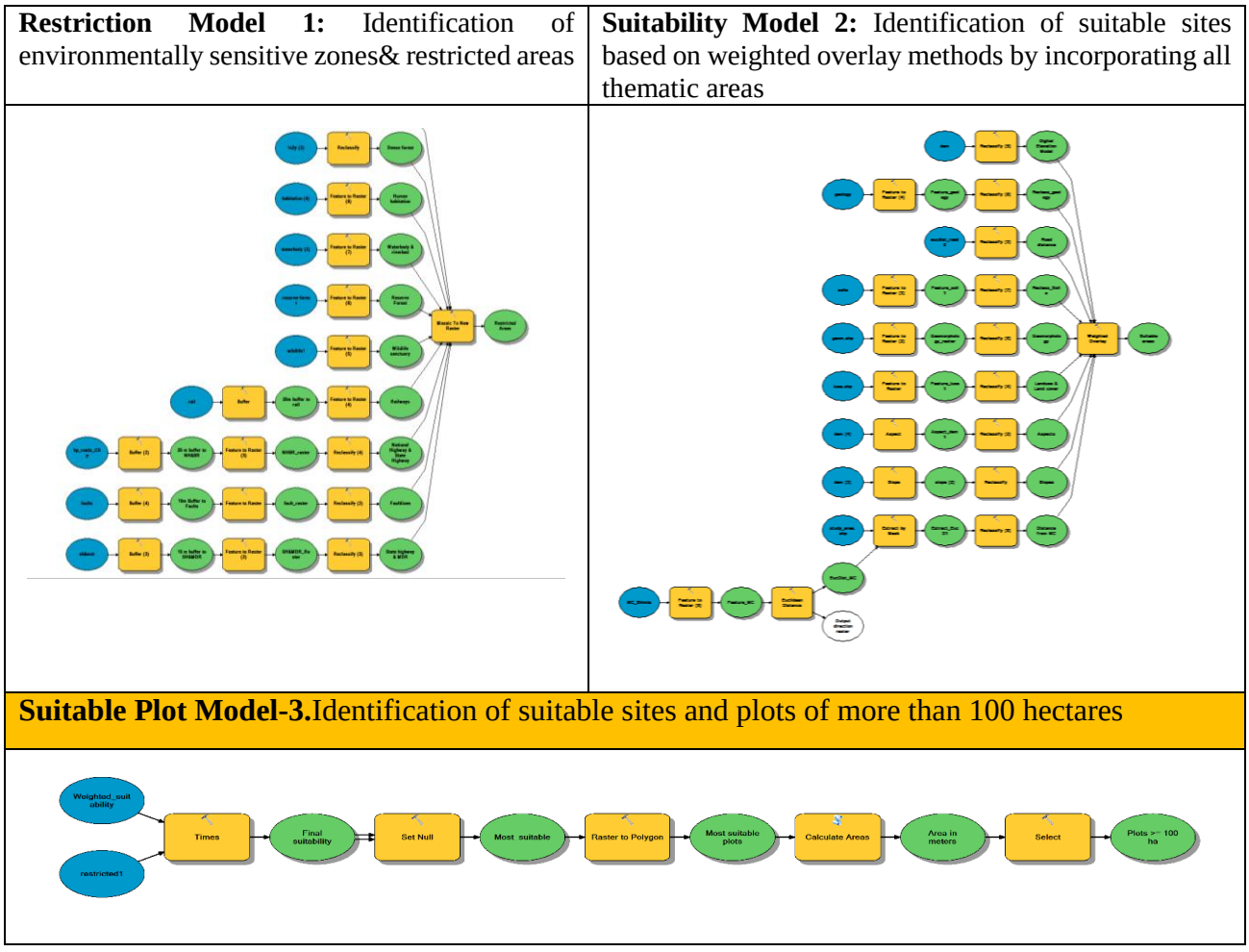

Figure 2: Modelling workflows

4.4 Identifiation of environmentally sensitive areas and restricted areas

In such assessment, it is also imperative to consider the natural limiting factor, ecologically sensitive factor, ecological protection factor for safeguarding fragile natural resources of hill ecology. Table 3 indicates such areas which have been identified under the restricted zone as no development zone for human habitation growth.

4.5 Thematic mapping

The thematic layers (Figure 3) were prepared based on data and maps collected from multiple sources as mentioned earlier and reclassified as per the weights assigned in the weighted overlay analysis as per Annexure 1. The lower slope obviously shall have lower risk of hazard and weighted as per Geological Survey of India guidelines

Table 3: Environmentally sensitive zones or restricted area

Restricted area	Restricted/buffer in meters
Wildlife sanctuaries	Restricted
Reserve forest	Restricted
Water channel/pond area/river bed	Restricted
Very Dense Forest	Restricted
Dense Forest	Restricted
Cantonment Board & airport	Restricted
Existing Urban and Rural settlements	Restricted
Railway buffer	20 m buffer restriction
Buffer to NH & border roads	20 m buffer restriction
Buffer to SH & MDR	10 m buffer restriction
Lithology fault	10 m buffer restriction

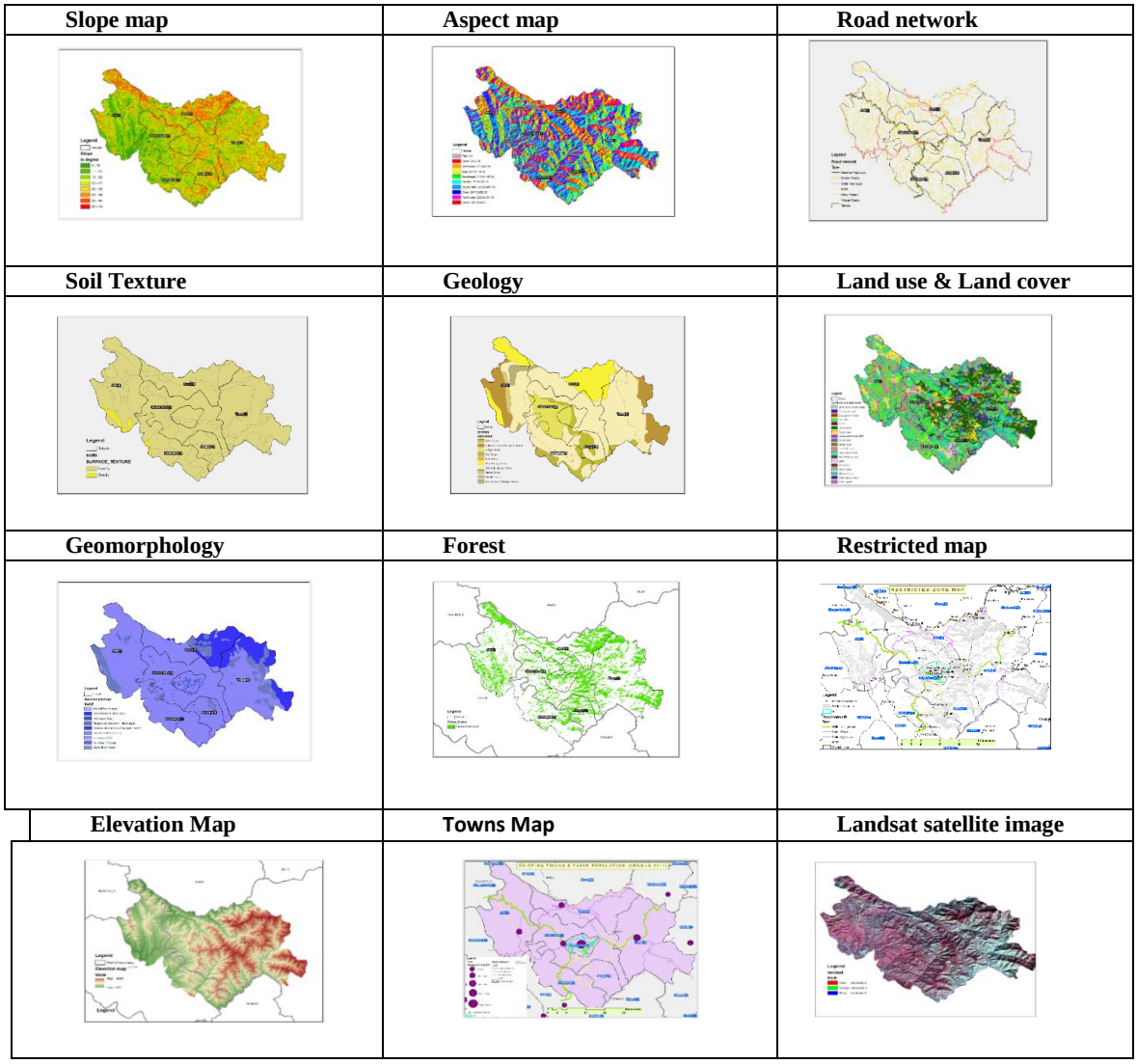

Figure 3: Thematic layers used in the study

4.6 Suitability assessment analysis:

The following criteria have been identified and their thematic maps prepared for the current study along with their assigned weights for suitability analysis as per the breakup indicated in table 4. Higher weights have been assigned to dominating criteria such as land-use/land-cover, slope, aspect, nearness to road as they are very important in guiding spatial pattern of urban development in Himachal Pradesh.

Table 4: Weights assigned to thematic layers

Criteria	Assigned Weights
Landuse	20
Slope	20
Aspect	20
Nearness to roads	15
Distance from Shimla	12
Elevation	6
Geomorphology	3
Soil Texture	2
Geology	2
Total weights	**100**

5. Results and discussion

The final suitability map indicates that about 42 percent of total geographical area (TGA) of the study area is suitable for urban expansion (Figure 5), while about 34 percent is medium suitable, 9% highly suitable and less than 1 percent most suitable. However, plot size of above 100 ha constitutes of about 10.7 percent of total suitable lands (Figure 4), which is spread across all parts of the study area, which indicates there is scope for small sized satellite towns all around. Final large plots have appeared mostly along State Highways and Major District Roads (MDR) falling in most tehsils of study area.

Table 5: Suitable lands

Suitable lands	Area (ha)	Percent area of TGA of study area
TGA of study area	183727	
Medium Suitable	61553.07	33.50
High Suitable	15471.81	8.42
Most Suitable	126.54	0.07
Total suitable lands	**77151.42**	**41.99**

As far as spatial pattern is concerned, suitable plots are fairly distributed among all tehsils. This pattern shall help in identification of specialized satellite township to ease the pressure on Shimla. Site plans can accordingly be formulated out of the suitable patches for further distribution of lands for the purpose of residential, industrial, commercial and recreational activities as per the UDPFI Guidelines of Institute of Town Planners (India) accordingly. Development of above identified suitable lands will be less susceptible to natural disaster and will not have any adverse impact on ecology and environment of the study area.

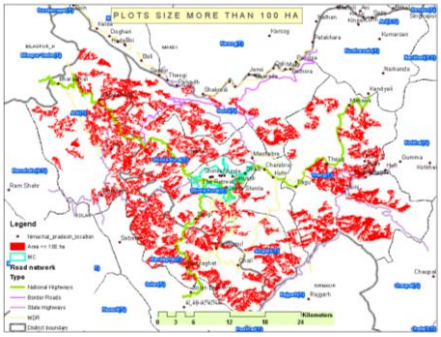

Figure 4: Large plots (over 100 ha) in suitable areas

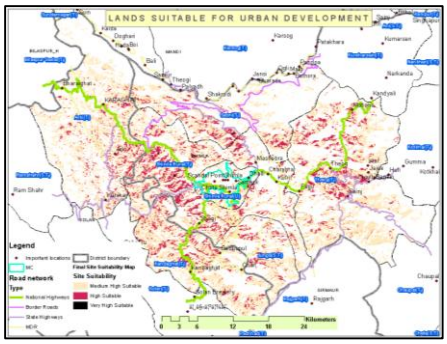

Figure 5: Site suitable for urban expansion

However, most of all, planning any urban expansion or satellite town is going to be an important craft. Respecting the natural limiting factors and judiciously planning on suitable lands is very important for hill town. It is pertinent to mention that a city has several types of land uses, some are highly used and some are sensitive and used as protection area. Therefore, planning of land uses around the suitable land plots are of paramount importance. Some sensitive land uses may be developed, protected, rehabilitated and restored, while some lands of waste nature with moderate and low slope, with southern aspect, solid geological foundation with no geological fault make an ideal location for urban development/expansion in hills. Thus putting a particular piece of land for a particular use is the essence of spatial planning for hill terrain. Hence identifying suitability through the use of available GIS/RS tool is the pre-requisite for sustainable urban expansion.

Furthermore, it would also be appropriate to develop specialized satellite township in different parts of the study area such as horticultural produce based township, which may be located towards Theog in order to market and further value addition of apple production, while

other suitable lands may be developed for different specialized township based on the specialized function/character of the region. In addition, several villages have been detected in the areas identified in the suitable zones. These settlements can be strengthened further with appropriate functions/facilities so as to act as catalyst for positive change for its surrounding. Furthermore, it will check Shimla bound migration and ease the growing pressure of Shimla. These urban settlements will also act as marketplace for their hinterland in the long run.

Use of high resolution satellite data coupled with primary/field surveys, integrating them into work of planning activities is of utmost importance. Application of highest resolution satellite data shall completely refine the output of the study, which is mere an indication. The present paper is only a modest attempt to explore the broad opportunities that these geospatial tools offer us, to plan for a better future. Recommendations made for future studies is to improve the efficacy and objectivity of local land use evaluation to support the land use suitability assessment and avoid the subjectivity. As for the accuracy of the real-world case study, the criteria selection and the weight assignment should be widely and deeply discussed and researched.

6. Conclusion

For a sustainable land use plan, land use planning approach requires high resolution satellite data, its seamless integration, multi-disciplinary analysis and need faster or more precise information to the planners and decision makers. This stands very important in view of the topographic complexity of hill town in general and Shimla in particular. Use of high resolution satellite data coupled with primary/field surveys, integrating them into work of planning activities is of utmost importance. The present paper is only a modest attempt to explore the broad opportunities that these geospatial tools offer us, to plan for a better future.

Acknowledgement

The author acknowledges the assistance rendered by Shri Vishal Pathak, Urban Planning Specialist, Shimla in making this paper possible. The idea/position adopted in the paper is independent of the institutional affiliation of the author.

References

Antonie, J., G. Fischer and M. Makowski (1997). Multiple criteria land use analysis. Applied Mathematics and Computation. Vol.85, 195-215.

Cheng, S., C.W. Chan and G.H. Huang (2003). An integrated multi-criteria decision analysis and inexact mixed integer linear programming approach for solid waste management. Eng Appl Artif. Intel.,16(5): 543–554.

Collins, M.G., F.R. Steiner and M.J. Rushman (2001). Landuse suitability analysis in the United States: Historical development and promising technological achievements. Environ. Manage. 28 (5), 611–621.

Gao, J. and D. Skillcorn (1998). Capability of SPOT XS data in producing detailed land cover maps at the urban-rural periphery. International Journal of Remote Sensing, 19(15): 2877–2891.

Joerin, F., M. Thériault and A. Musy (2001). Using GIS and outranking multicriteria analysis for land-use suitability assessment. Int. J. Geogr. Inf. Sci.,15(2):153–174.

Kunwar, P., T. Kachhwaha, A. Kuma, A.K. Agrawal, A. Singh, N. Mendiratta (2010). Use of high-resolution IKONOS data and GIS technique for transformation of landuse / landcover for sustainable development. Curr Sci., 98(2): 204–212.

Kiker, G.A., T.S. Bridges, A. Varghese, P.T. Seager and I. Linkov (2005). Application of multicriteria decision analysis in environmental decision making. Integr. Environ. Assess Manag., 1(2): 95-108.

Malczewski, J. (2004). GIS-based land-use suitability analysis: A critical overview. Progr. Plann. 62 (1), 3–65.

Miguel-Ayanz, J.S. and S. Biging (1997). Comparison of single-stage and multi-stage classification approaches for cover type mapping with TM and SPOT data. Remote Sensing of Environment, 59, (1), 92-104

Phua, M. and M. Minowa (2005) A GIS-based multi-criteria decision making approach to forest conservation planning at a landscape scale: A case study in the Kinabalu area, Sabah, Malaysia. Land Scape Urban Plan 71(2):207–222.

Riaza, A., M.L. Martinez-Torres, R. Ramon-Lluch, J. Alonso and P. Heras (1998). Evolution of equatorial vegetation communities mapped using Thematic Mapper images through a geographical information system (Guinea, Equatorial Africa). International Journal of Remote Sensing 19: 43 - 54.

Sharifi, M.A., L. Boerboom, K.B. Shamsudin and Loga Veeramuthu (2006). Spatial multiple criteria decision analysis in integrated planning for public transport and land use development study in Klang valley, Malaysia. ISPRS Technical Commission II Symposium, Vienna, 12 – 14 July 2006, 85 – 91.

Yeh, A.G. and X. Li (1998). Sustainable land development model for rapid growth area using GIS. International Journal Geographical Information Science 12: 169 - 189.

Annexure 1: Sub-criteria and their assigned weights

Sr.No	1. Land use and Land cover	Weight	Slope in degree	2. Slope Stability	Weight
1	Barren Rocky/Stony waste	9	0^0-15^0	Most stable for urban use	5
2	Crop Land in Forest	3	15^0-30^0	May be utilized for urban development	4
3	Degraded	10	30^0-45^0	Small sized construction where there are in sites rock exposure	3
4	Dense forest	1	45^0-60^0	Should not be normally used without exceptionally sound protective measures.	2
5	Gullied/Ravenouse Land	5	More than 60^0	Should not be used	1
6	Kharif+Rabi	4	**Sr. No.**	**4. Aspect in degree**	**Weight**
7	Land with scrub	5	1	Flat (-1)	10
8	Land without scrub	6	2	North (0-22.5)	1
9	Mixed Built-up land	0	3	Northeast (22.5-67.5)	4
10	Open forest	5	4	East (67.5-112.5)	6
11	Perennial	0	5	Southeast (112.5-157.5)	8
12	Sandy Area	3	6	South (157.5-202.5)	9
13	Scrub Forest	7	7	Southwest (202.5-247.5)	7
14	Habitation	0	8	West (247.5-292.5)	5
15	Water body	0	9	Northwest (292.5-337.5)	3
Sr. No	**3. *Nearness to roads (m)**	**Weight**	10	North (337.5-360)	2
1	0 – 83	5	**Sr. No.**	**5. *Distance from Shimla (m)**	**Weight**
2	83- 193	4	1	523 – 1193	5
3	193- 332	3	2	1193 – 1442	4
4	332- 553	2	3	1442 – 1703	3
5	553- 3514	1	4	1703 – 2012	2
Sr. No	**6. *Elevation in meters**	**Weight**	5	2012 – 3055	1
1	2012 – 3055	5	**Sr. No**	**1. Geomorphology**	**Weight**
2	1703 – 2012	4	1	Alluvial fan Younger	3
3	1442 – 1703	3	2	Denudational Hills (Large)	9
4	1193 – 1442	2	3	Habitation Mask	0
5	523 – 1193	1	4	Ridge type Structural Hills (Large)	8
Sr. No.	**2. Geology**	**Weight**	5	Shallow alluvial plain (Younger/ Lower)	7
1	Balini Group	2	6	Structural Hills (Large)	10
2	Dalhausie-Mandi-KarsogGranitoid	7	7	Terraces – Older	6
3	Jutogh Group	10	8	Terraces – Younger	5
4	Krol Group	6	9	Water Body Mask	0
5	Kullu Group	8	**Sr. No.**	**3. Soil Texture**	**Weight**
6	Shali&Largi Group	1	1	Loamy	5
7	Shimla &Jaunsur Group	9	2	Sandy	2
8	Sirmur Group	5			
9	Siwalik Group	2			
10	Sundarnagar& Rampur Group	3			

**Quantile method of ArcGIS 10 classification applied*– Each class contains an equal number of features. A quantile classification is well suited to linearly distributed data. Quantile assigns the same number of data values to each class. There are no empty classes or classes with too few or too many values.

Journal of Geomatics Vol 11 No. 1 April 2017

Delineation of ground water potential zone in Sweta sub-watershed using remote sensing and GIS in parts of Perambalur district of Southern India

A. Muthamilselvan
Centre for Remote Sensing, Bharathidasan University, Trichy
Email: thamil_ak@yahoo.co.in

(Received: Jan 19, 2016; in final form: Jan 04, 2017)

Abstract: Perambalur district has been declared as one of the over exploited regions in Tamil Nadu by the Central Groundwater Board. Therefore, it is very important to delineate potential for groundwater development and management. Perambalur district is partially and ephemerally drained by Sweta sub-watershed which extends over an area of 730 km^2. The study area exhibits dendritic and sub dendritic drainage patterns with maximum of 6th order drainage. In the present study, groundwater potential zones have been delineated with the help of Remote Sensing (RS) and Geographic Information System (GIS) techniques. In this study, a standard weight and rank method is adopted to identify groundwater potential zone using integration of RS and GIS techniques. The parameters considered for identifying the groundwater potential zone are geology, geomorphology, slope, drainage density, lineament density and land use / land cover which are generated using the satellite data and survey of India (SOI) toposheets at the scale of 1:50000. They are then integrated based on rank and weightage method in GIS platform and classified into five categories such as very poor, poor, moderate, good and excellent. Rank and weightage has been assigned based on the interpreter's prior knowledge. The integrated analysis showed that about 41% of the area falls in the category of excellent and good; rest are in other categories. This groundwater potential information will be useful for effective identification of suitable locations for extraction of groundwater for drinking and agricultural purpose.

Keywords: Groundwater, Remote sensing, GIS

1. Introduction

Perambalur district in Tamil Nadu faces severe water scarcity since last decade in all sectors, especially in domestic and agricultural. It is mainly due low annual rain fall, monsoon failure and over exploitation of ground water. Water is an important constituent of all forms of life and is required in sufficient quantity and quality to meet the ever increasing demand for various sectors. Exploitation of groundwater in uncontrolled manner led to decrease in groundwater potential, lowering of groundwater level and deterioration in groundwater quality. It is therefore necessary to develop sustainable groundwater management scheme for proper utilization of this natural resource, which in turn requires delineation of groundwater potential zones. Remote sensing (RS) is one of the best tools for delineating groundwater potential zone because of it facilitates identifying and demarcating various parameters that may serve either as direct or indirect indicators for groundwater availability. Geographic Information System (GIS) is being used for various purposes such as feasibility study of recharge sites, finding contaminated sites etc. The main objective of the present study is to locate the favourable groundwater zone using weight and rank method with the help RS and GIS.

Many geoscientists and hydrogeologists like Murthy (2000), Naga Rajani et al. (2006), Preed Kumar (2009), Nagaraju et al., (2011) and Waiker and Nilawar (2014) have used RS and GIS techniques for groundwater exploration and identification of artificial recharge sites. Ravi and Mishra (1993), Jaiswal et al. (2003), Jothiprakash et al. (2003), Prasad et al. (2008), Chowdhury et al. (2009) have utilised RS and GIS techniques to delineate groundwater potential zones. GIS has also been considered for multi-criteria analysis in resource evaluation. Boutt et al. (2001) and Elkadi et al. (1994) have carried out groundwater modelling through the application of GIS. In the present study Landsat satellite data acquired on March 2013 has been used for preparation of various thematic maps such as base, drainage, geology, lineament, geomorphology, drainage-density and land use/land cover. Aster DEM has been used for slope calculations.

2. Study area

The study area lies between 78°30'- 11°32' and 78°58'-11°15' of Perambalur district, Indian state of Tamil Nadu and is situated about 60 km from Tiruchirappalli in southern direction. Study area covers about 730 km^2, which comprises of numerous villages and drought prone areas of Perambalur district. The entire area is drained by a small stream Sweta, which flows west to east. The basin is characterized by poor soil cover, erratic rainfall and lack of soil moisture for most part of the year (Fig. 1). Frequent drought coupled with over exploitation results in decline in groundwater levels. In order to manage and develop sustainable development, it is essential to delineate the groundwater potential zones in this watershed.

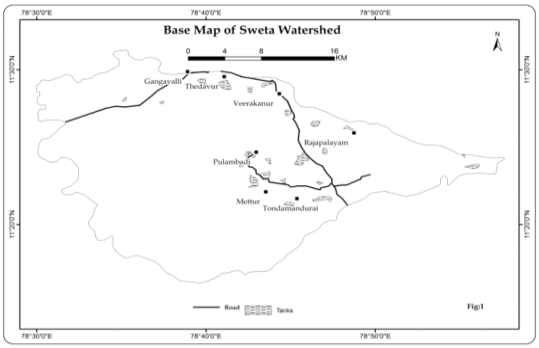

Figure 1: Base map of Sweta watershed

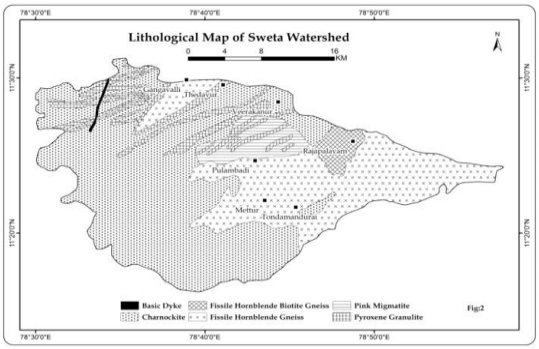

Figure 2: Lithology map of Sweta watershed

3. Methodology

There are six important indicators namely, (i) Geology, (ii) slope, (iii) geomorphology, (iv) land use / cover, (v) drainage and (vi) lineament for groundwater prospects. Preparation of maps for these themes (except slope) based on image characteristics such as tone, texture, shape, colour and association are standardised. Slope is derived from ASTER DEM 30m resolution (www.jspacesystems.or.jp /ersdac/ GDEM/E/2.html). Thematic maps of the study area were prepared.

To get wholistic view of the above mentioned indicators, overlay analysis is required. Assignment of rank to an individual class was based on influence of these themes as reported in literature (Krishnamurthty et al., 1996; Saraf and Chowdhary, 1998). Rank and weight based thematic layers were integrated through GIS to find out the resultant groundwater potential zones. Overlay analysis was carried out from the derived multi thematic layers in a GIS environment. ARCGIS software was used for the same.

4. Result and discussion

4.1 Geology

The study area comprises Archaean to late Proterozoic rocks which include Pyroxene granulite, Migmatite, fissile Hornblende gneiss, fissile Hornblende biotite gneiss, Charnockite and intrusive basic dyke. Western part of the hill exposes massive charnockite whereas the eastern part of plain area is covered by fissile hornblende gneiss rocks. Youngest litho unit observed in this area is basic dyke which is trending NNE-SSW direction (Fig. 2). The trend of the dyke is akin to the Attur – Gangavalli shear zone. Lithological distribution in the study area is given in table 1. Charnockite is the major rock type exposed in the study area covered over an area of 398.78 km^2(54.57%) followed by fissile hornblende gneiss about 219.02 km^{2}and rest of the rock types covered small portion of the study area.

Table 1: Area coverage for lithological units

Sr. No	Description of Lithology	Area (km^2)	Area (%)
1	Fissile Hornblende Biotite Gneiss	19.33	2.65
2	Fissile Hornblende Gneiss	219.02	29.97
3	Pink Migmatite	34.26	4.69
4	Pyroxene Granulite	57.71	7.90
5	Charnockite	398.78	54.57
6	Basic Dyke	1.62	0.22

4.2 Slope

The slope is one of the important factors for controlling the residence time of runoff water and thereby the infiltration of groundwater into the subsurface of any terrain. Hence, it is also one of the indicators for the suitability for groundwater prospect. Surface runoff is slow where the slope is gentle and also allows more time for rain water to percolate which leads to more infiltration. Slope of the area varies from 0 to 58.45 degree which is derived from ASTER DEM 30m resolution (www.jspacesystems.or.jp /ersdac/ GDEM/E/2.html) and is shown in figure 3. The slope of the area is classified into five classes based on the method given by Patil and Mohite(2014).

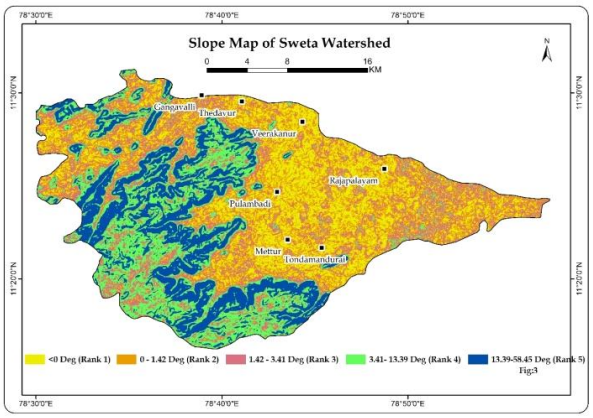

Figure 3: Slope map of Sweta watershed

4.3 Geomorphology

Geomorphological units are very important for the identification and characterization of various landforms and structural features in the study area for groundwater development and management activities. Geomorphologic units are delineated based on image characteristics such as tone, texture, shape, colour and association of features. Structural hills and Inselbergs are observed on western part of the study area, which mostly act as runoff zones due to their sloping topography. This results in poor potential for groundwater occurrence and recharge. Shallow pediments, which have considerable slope with less thickness of sediments indicate moderate occurrences of groundwater. Valleys are low lying depressions formed longitudinally along the streams or amongst the ridge portions, which show excellent potential for groundwater occurrence and recharge. Colluvial fills also have high potentiality of groundwater (Fig. 4). By extraction of various classes of geomorphology, a thematic map for geomorphology is generated (Fig. 4). The ranks and weight were assigned to the individual landform, according to their respective influence of groundwater occurrence, holding and recharge, as given in table 2. In the study area, structural hill covered over an area of 246.42 km^{2}followed by shallow pediment 189.02 km^2, colluvial fill 117.97 km^2, valley fill etc.

Table 2: Area coverage for geomorphological units

Sr. No.	Geomorphological Units	Area (km^2)	Area (%)
1	Colluvial Fill	117.97	16.23
2	Valley Fill	104.28	14.34
3	Plateau Dissected	58.49	8.05
4	Bajada	10.90	1.50
5	Shallow Pediment	189.02	26.00
6	Structural Hill	246.42	33.89
7	Inselberg	4.16	0.57

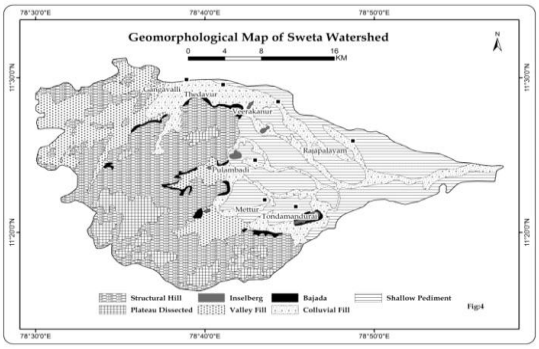

Figure 4: Geomorphological map of Sweta watershed

4.4 Landuse / landcover

Baseline information about occurrences of surface and groundwater can be directly or indirectly obtained using landuse / landcover information of that particular area. RS and GIS tools play a vital role in mapping of land use / land cover pattern of any terrain (Fig. 5). The effect of land use / land cover is manifested either by reducing runoff and facilitating, or by trapping water on their leaf. Land use / land cover distribution in percentage as well as in km^2 is listed in table 3. Majority of the study area is crop land covered over an area of 395.77 km^2, followed by forest area, fallow land etc.

Table 3: Area coverage for land use /land cover units

Sr. No.	Categories	Area (km^2)	Area (%)
1	Crop Land	395.77	54.12
2	Plantation	4.59	0.63
3	Salt Affected Land	8.39	1.15
4	City/Town	1.09	0.15
5	Barren Rock	8.59	1.18
6	Land with Scrub	16.88	2.31
7	Forest	237.75	32.51
8	Tanks	7.98	1.09
9	Gullied/Ravenous Land	7.84	1.07
10	Fallow Land	42.45	5.80

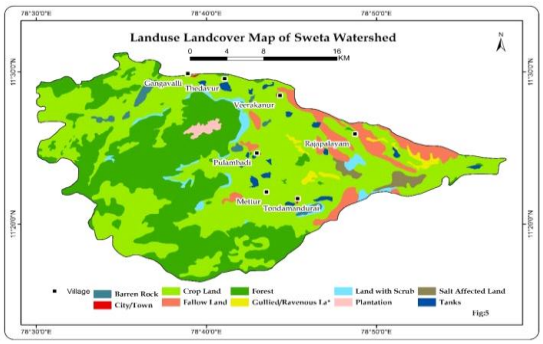

Figure 5: Land use/ land cover map of Sweta watershed

4.5 Drainage

The drainage of the study area shows dendritic to sub dendritic pattern, the drainage is highly dense in hilly region with steep slope noticed on the western part. Moderate to low density observed is on eastern side part where the slope is gentle. Seasonal streams are noticed in this area which are flowing from west to east towards the Sweta river (Fig. 6). By extraction of drainage density features, a thematic map is generated. It is classified into five zones according to their respective drainage density as shown in figure 7.

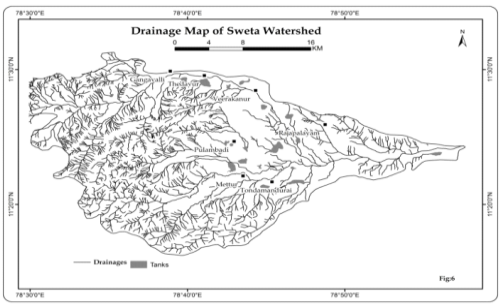

Figure 6: Drainage map of Sweta watershed

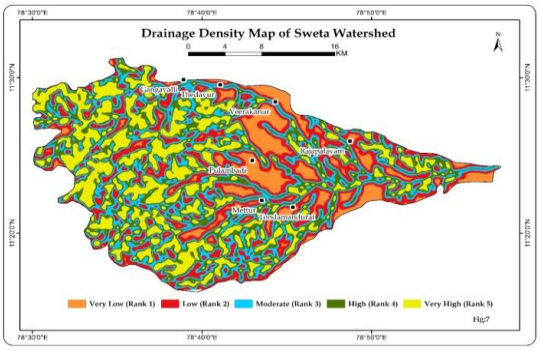

Figure 7: Drainage density map of Sweta watershed

4.6 Lineament

Lineaments are the surface manifestation of subsurface weakness or structural displacement and deformations. It represents deep seated faults, fractures and joints sets, drainage lines and different litho-contacts. In hard rock terrains, lineaments are represented by areas and zones of faulting and fracturing which results in increased secondary porosity and permeability. Lineaments are linear and curvilinear feature that are significant for groundwater, mineral and metal explorations and exploitations. Lineament map (Fig. 8) is prepared from satellite imagery and the lineament density is derived from the lineament map (Fig. 9). High density zone represents the maximum intersection of lineaments and favourable zone for any kind of mineral and groundwater exploration activities. The lineament analysis provides important information on subsurface fractures that may control the movement and storage of groundwater.

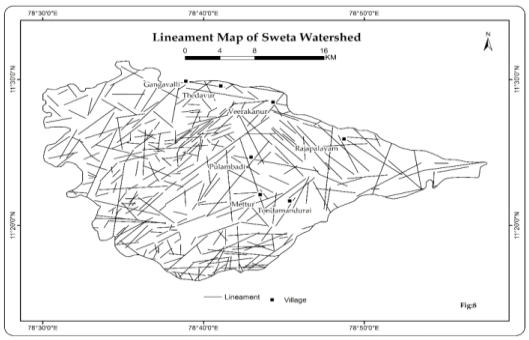

Figure 8: Lineament map of Sweta watershed

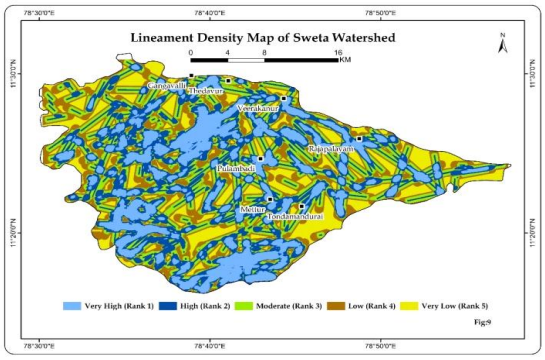

Figure 9: Lineament density map of Sweta watershed

4.7 Assigning of rank and weights

Overlay analysis has been carried out from the available multi thematic layers with the help of assignment of rank to the individual class and assigning weights to the individual features by considering their influence over the occurrence and movement of ground water. The weights and rank have been taken considering the work carried out by researchers such as Krishnamurthty et al. (1996) and Saraf and Chowdhary(1998). In this method, all the thematic layers were converted into raster format. Rank and weight based thematic layers were integrated through GIS to find out the groundwater potential zones. The ARCGIS software has been used for preparation of thematic maps, integration analysis /overlay analysis in GIS environment. The rank and weight assigned for the features are given in table 4.

Table 4: Ranks and weights of parameters for groundwater recharge potential zones

Parameter	Classes	GW Prospect	Wt %	Rank
Geomorphology	Colluvial Fill	Very Good	20	1
	Valley Fill	Very Good		1
	Plateau Dissected	Good		2
	Bajada	Good		2
	Shallow Pediment	Moderate		3
	Structural Hill	Poor		4
	Inselberg	Very Poor		5
	< 0	Very good		1
Slope	0 - 1.42	Good	25	2
	1.43 - 3.41	Moderate		3
	3.42 - 13.49	Poor		4
	13.40 - 58.45	Very Poor		5
	<0.00	Very Good		1
Drainage Density	0 - 1.02	Good	5	2
	1.02 - 2.01	Moderate		3
	2.01 - 3.09	Poor		4
	3.09 - 7.66	Very Poor		5
	<0.00	Very Good		1
Lineament Density	0 - 0.94	Good	20	2
	0.94 - 1.26	Moderate		3
	1.26 - 2.10	Poor		4
	2.10-5.83	Very Poor		5
	Crop Land	Very Good		1
Land use Land cover	Plantations	Good	25	2
	Tanks	Good		2
	Forest	Moderate		3
	Fallow Land	Moderate		3
	Gullied/Ravenous Land	Moderate		3
	Land with Scrub	Poor		4
	Salt affected Land	Poor		4
	Barren Rock	Very Poor		5
	City/Town	Very Poor		5
	Fissile Horn. Bio- Gneiss	Very Good		1
Lithology	Fissile Horn. Gneiss	Good	5	2
	Charnockite	Moderate		3
	Pyroxene Granulite	Poor		4
	Pink Migmatite	Poor		4
	Basic Dyke	Very Poor		5

4.8 Discussion

The present study has resulted in identifying various groundwater potential zones based on geologic, geomorphic and hydrologic parameters such as geomorphology, lithology, slope, land use / land cover, drainage density and lineament density. During the weighted overlay analysis, the ranks have been given for each individual parameter of each thematic map and the weight is assigned according to the influence of the different parameters. The weights and rank have been taken by considering researchers' knowledge about the area (Krishnamurthty et al., 1996; Saraf and Chowdhary, 1998). Based on these analysis, groundwater potential zones were demarcated. This map has been categorized into five classes such as very poor, poor, moderate, good and excellent. The detail of the area covered is given in table 5. In this study, it is observed that the good and excellent area covers almost 41% of the study area (Fig. 10).

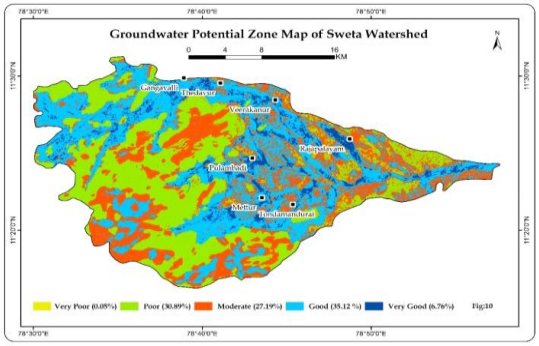

Figure 10: Groundwater potential zone map

Table 5: Area distribution for groundwater potential zones

Sr.No	Potential Zones	Area (km^2)	Area (%)
1	Very Poor	0.33	0.05
2	Poor	225.98	30.89
3	Moderate	198.96	27.19
4	Good	256.91	35.12
5	Excellent	49.44	6.76

The groundwater potential zone categories good and moderate are falling in the plain area of Gangavalli, Thedavur, Veerakanur, Rajapalayam, Pulambadi, Mettur and Thondamandurai. Most of these areas are coming under the over exploitation block of Vepanthattai in Perambalur district. Therefore, the state and central groundwater board can concentrate on these resulted zone of good and moderate categories for drilling new bore wells. In addition, along the Gangavalli shear zone also groundwater potential zones were delineated. Hence, this area can be considered for future drilling programme for groundwater exploration. However, resolution of satellite imagery and its geometric correction procedure, ASTER DEM data resolution are having some limitations in this approach that should be considered before proceeding to drilling activity.

5. Conclusion

The present study carried out for groundwater exploration has brought to light few important zones for ground water extraction for drinking as well as irrigation purpose. The study area is a hard rock terrain, therefore the availability of groundwater is mainly based on the structural porosity and permeability. The integrated groundwater potential zone map for the study area is categorized into five qualitative classes which are very poor, poor, moderate, good and excellent. Most of the good and excellent areas are located in the NW of Attur - Gangavalli shear zones and Eastern part where most of the excellent parts fall all along the colluvial fills. Among 730 km^2, 306 km^2 falls under the good and excellent categories.

Acknowledgement

I express my sincere thanks to HOD and Faculty members of Centre for Remote Sensing, Bharathidasan University, Tiruchirappalli for their support.

References

Boutt, D.F., D.W. Hyndman, B.C. Pijanowski and D.T. Long (2001). Identifying potential land use-derived solute sources to stream base flow using ground water models and GIS. Groundwater, 39(1): 24–34.

Chowdhury, A., M.K. Jha, B.C. Mal and V.M. Chowdary (2009). Delineation of groundwater prospect zones using remote sensing and geographical information system techniques: A case study. Proceedings of the International Conference WEES - 2009, New Delhi, Conducted by NIH, (1): 1975–1981.

Nagaraju, D. C. Papanna, S. Iddalingamurthy, Lakshmamma, Mohammad Subhan lone, P.C. Nagesh, G. Mahadevaswamy and Krishna Rao (2011). Identification of groundwater potential zones through remote sensing and GIS techniques in Kollegal taluk, Chamarajnagar district, Karnataka, India. International Journal of Earth Sciences and Engineering, Vol. 04, No. 04, 651-658.

Elkadi, A.I., A.A. Oloufa, A.A. Eltahan and H.U. Malik (1994). Use of a geographic information system in site specific groundwater modelling. Groundwater, 32(4), 617–625.

Jaiswal, R.K., S. Mukherjee, J. Krishnamurthy and R. Saxena (2003). Role of remote sensing and GIS techniques for generation of groundwater prospect zones towards rural development–An approach. International Journal of Remote Sensing, 24(5): 993–1008.

Jothiprakash, V., G. Marimuthu, R. Muralidharan and N. Senthil Kumar (2003). Delineation of potential zones for the artificial recharge using geographical information system. Journal of the Indian Society of Remote Sensing, 31(1): 37–47.

Patil, S.G. and N.M. Mohite (2014). Identification of groundwater recharge potential zones for a watershed using remote sensing and GIS. International Journal of Geomatics and Geosciences, 4 (3), 485 – 498.

Pradeep Kumar, G.N., (2009). Demarcation of groundwater prospect zones through RS and GIS techniques in a basin. Indian Geotechnical Society (IGC), 819 - 822.

Saraf, A. and P.R. Choudhary (1998). Integrated remote sensing and GIS for ground water exploration and identification of artificial recharge site. Int. J. RemoteSensing 19, 1825–1841.

Krishnamurthy, J., K.N. Venkatesan, V.Jayaraman and M. Manivel (1996). Anapproach to demarcate groundwater potential zones through remote sensing and geographic information system. Int. Journal of Remote Sensing 17, 1867-1884.

Waikar, M.L. and A.P. Nilawar (2014). Identification of groundwater potential zone using remote sensing and GIS technique. International Journal of Innovative Research in Science, Vol. 3, Issue 5, 12163-12174.

Journal of Geomatics Vol 11 No. 1 April 2017

RS and GIS based integrated study on hydrogeomorphic unit wise ground water quality evaluation for Nalgonda district, Telangana state

Aswini Kumar Das, Prathapani Prakash, Gade Kumar and N. Ramudu
Telangana State Remote Sensing Applications Centre(TRAC), Ameerpet, Hyderabad, 500038, India
Email:aswini.das81@gmail.com,prakashmhbd@gmail.com

(Received: Jul 20, 2016; in final form: Mar 16, 2017)

Abstract: Groundwater is the main source of water for domestic, agriculture and industrial uses especially in water scarce semi-arid regions. About 85% of rural and nearly 30% of the urban population depend on ground water for drinking and accounts for nearly 65% of the total irrigation potential in the country. The availability of ground water is dependent on many factors like geological history of the area, geomorphology, rainfall, geological structures that are controlled through the earth's history, porosity and permeability of soil or rock formations, depth of weathering and nature of weathered material etc. The quality of ground water deteriorates when there is overdraft of water for agriculture and industrial uses. The phreatic aquifer which was in use two decades ago, is not existing any more in major part of the study area and the water is being drawn from deeper aquifers beyond phreatic aquifers. As the ground water is the main source, states are being guided to prepare watershed wise Sustainability plans for all over-exploited blocks in the country for taking up groundwater recharge and water harvesting structures by converging different schemes of MNREGS, NRDWP etc. This will improve the condition of ground water in space and time. An integrated remote sensing and GIS study is taken up for Nalgonda district for studying the hydrogeomorphic unit wise ground water quality variation and its impact by using other collateral data like soils, land use, command area, ground water exploitation, rainfall etc.

Keywords: Ground water quality, Hydrogeomorphology, GIS, Remote sensing, Sustainability, Drinking water, Health, Water harvesting

1. Introduction

Nalgonda district, spread over a geographical area of 14,210 km^2 and with a population of 34,88,809 as per 2011 census, is chronically drought affected. Out of the total net area irrigated, about 36% is from surface water and 64% from ground water sources. This clearly indicates the stress on ground water in the district.

The objective of the work is to study hydrogeomorphology or ground water prospects unit wise ground water quality evaluation in relation to various parameters affecting it, like lithology, geologic structure, Land use and land cover, soils, rainfall and slope to know their relationship with one another. While rainfall is the source of recharge, geomorphology plays a vital role in controlling distribution of precipitation, runoff and infiltration contributing to recharge. Sustainability of ground water dictates that its extraction should be at a rate which does not exceed annual recharge and does not lead to ground water mining.

2. Study area

The Nalgonda district lies in between 16° 25' and 17° 50' North Latitudes and 78° 40' and 80° 05' East Longitudes covering the Survey of India toposheet Nos. 56 K, L, O, and P. It is bounded on the north by Medak and Warangal districts; on the south by Andhra Pradesh state and partly with Mahabubnagar district; on the east by Khammam and Andhra Pradesh states; on the west by Mahabubnagar district and partly by Ranga Reddy district (Figure 1) respectively.

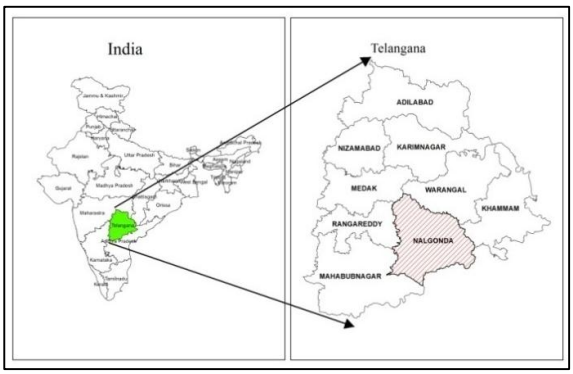

Figure 1: Location map of the study area

2.1 Physiography of the study area

Physiographically, the terrain, except for a small portion in the south, is a gently undulating country with hummocky hills, rocky knobs, denudational hills, ridges and inselbergs. The southern part of the district along the northern bank of Krishna river is a plateau. Based on photo-geological studies the terrain can be classified in to four major geomorphic units, viz, Denudational hills, dissected pediments, pediplains and valley fills. The mean elevation of the terrain is 150 m above mean sea level and general slope is towards southeast. The general drainage pattern in the granitic country is coarse dendritic to sub-dendritic, whereas in the lime stone dominant sediments, a trellis to radial pattern is found. Major rivers include Krishna, Dindi, Peddavagu, Musi, Aler, Hallia, Kongal and Paleru, which form a part of Krishna river basin.

2.2 Geology andhydrogeology of the study area

The district forms a part of the stable Indian Peninsular Shield consisting of older Metamorphics, Peninsular Gneissic Complex (PGC), Dharwar Supergroup, Cuddapah Supergroup and Kurnool group of rocks. The Archaean crystalline rocks, which occupy 90% of the district, comprise granites, gneisses, schists and intrusives. The hornblende schists and amphibolites (Older Metamorphics) which are the oldest rocks occur as rafts, enclaves and discontinuous linear bands, within the Peninsular Gneissic Complex. The PGC occupies a major part of the district and comprises migmatites, granites, granodiorite, tonalite-trondhjemite suite of rocks and hornblende-biotite schists. The PGC and Dharwar rocks are intruded by younger granites, basic dykes and quartz-pegmatite veins.

In the southern part of the district along the northern bank of the Krishna river rocks of Archaean PGC are unconformably overlain by sedimentary rocks, constituting the Cuddapah Supergroup in the district is predominantly made up of arenaceous and argillaceous sediments respectively, represented by quarzite and shale of Cumbum Formation (Nallamalai Group) and SrisailamQuarzite. The Kurnool Group of rocks comprises calcareous (chemical precipitates) sediments and quartzite. These consolidated meta-sedimentary rocks of Cuddapah and Kurnool system comprising limestones, quartzites and shales occupy 9% in the southern part of the district.

The unconsolidated deposits comprising alluvial sands,clay occur as isolated and narrow patches along the major rivers and streams occupying around 1% of the area.

2.3 Soils

The soils of the district are mostly consisting of Red soil. Among the red soils 47% is Loamy soil, which has a very low moisture retaining capacity, and the rest is chalka soil, forming 44%. The fertile black cotton soil forms only 9% and occurs on the banks of Krishna and in isolated patches. Black soils of significant areal extent are found in the southeastern part of the district of where limestone formation occurs. Alkaline soil occurs as limited minor patches in the central part of the district. Alluvial soils occur along Alair, Musi and Kargal river valleys.

2.4 Land use

As per the Land use classification on 1:10,000 scale prepared by using high resolution (Cartosat–1 Pan + LISS-IV Mx) orthorectified satellite imagery (2013-2014), out of total geographical area of the district, agriculture land is 10,038 km^2 (71%); waste lands is 1,929 km^2 (14%); forest area is 706 km^2 (5%); water body is 1,006 km^2 (7%); built up land is 531 km^2 (4%) respectively.

3. Groundwater development: A spatiotemporal analysis

Groundwater is an invisible resource and the laws governing its storage, movement and exploitation are distinct from those of surface water.

3.1 Estimates of groundwater in Telangana

Based on Groundwater resource Estimation Committee report (GEC 2011), the annual replenishable ground water resource is 15.09 bcm of which the net ground water availability after deducting for natural discharge during non-monsoon season is 13.67 bcm. The annual ground water draft for irrigation, domestic and industrial uses combined is 7.5 bcm. The stage of ground water development in the state is 55% which is falling in safe category. Out of 447 mandals in the state, 343 mandals are falling in safe category, 55 mandals in semi-critical, 8 mandals in critical and 41 mandals in over exploitation category.

3.2 Estimates of groundwater in Nalgonda

Based on Groundwater Resource Estimation Committee (GEC-97) report 2010-11, the annual replenishable ground water resource is 2.11 bcm of which the net ground water availability after deducting for natural discharge during non-monsoon season is 1.91 bcm. The annual ground water draft for irrigation, domestic and industrial uses combined is 1.14 bcm. The stage of ground water development in the district is 59% which is falling in safe category. There are 47 mandals in safe category, 10 mandals in semi-critical, 1 mandal in critical namely Chandurmandal, and 1 mandal in over exploitation category namely Munugodemandal.

3.3 Why is water quality an issue?

In India about 73% waste water generated from different sources is being left out to rivers, canals, tanks or in to the Ground without proper treatment for which the ground as well as surface waters are at threat qualitatively. Water quality monitoring should be taken up regularly for taking up preventive measures in advance so that there may not be any health problems.

4. Methodology

The ground water quality data pertaining to Nalgonda district during the period from 2012-14 is collected for pre and post monsoon seasons separatelyfrom line department (Rural Water Supply & Sanitation Department, Govt. of Telangana). The drinking water sources are essentially Bore wells / Hand pumps with depth ranges varying from 30-90 metres. It consists of the ground water quality data pertaining to 9 elements pertaining to (1) Total Dissolved Solids (TDS), (2) Total Hardness (TH), (3) Fluoride (F), (4) Total Alkalinity (TA), (5) Chloride (Cl) & (6) pH. The legacy Ground water prospects maps prepared under Rajiv Gandhi National Drinking Water Mission (NRSA, 2007; NRSA, 2013) are used for correlation with respect to quality.

Contamination spread of element-wise distribution from a single element to 9 elements are plotted against to each habitation for pre and post monsoon seasons separately and its spatial distribution is studied using satellite remote sensing techniques (IRS P-6 LISS III, 2012-13) and with respect to other collateral data as mentioned below:

1. Geology
2. Geomorphology
3. Hydrogeomorphology
4. Groundwater Exploitation (GEC) report
5. Forest layer
6. Irrigation command area map
7. Rainfall data
8. Land use land cover
9. Soils

5. Results and discussion

5.1 Groundwater prospects

The occurrence and spatial distribution of ground water is not uniform throughout the district and it is dependent on different aspects like porosity and permeability of underlying rock / soil formations, structural fabrics, distribution of water bodies and slope etc. Due to erratic rainfall there is tremendous stress on ground water for meeting the agriculture needs in the district and consequently many of the existing wells are getting dried-up due to depletion of water table as the natural recharge is not sufficient. Ultimately this leads to water quality problems for the elements like Fluoride, Total Hardness, and Total Dissolved Solids etc day by day.

Satellite data provides cost and time effective information on different variables like hydrogeological properties of geological materials, distribution of water bodies, and history of regional structures etc that govern the availability and movement of ground water by integrated study of different factors and evaluating the ground water condition of an area. By using the IRS-1C/1D, LISS-III satellite data the ground water prospects maps are prepared under Rajiv Gandhi National Drinking Water Mission (RGNDWM) project (NRSA, 2007; NRSA, 2011). The hydrogeomorphic units are derived by integrating lithology and land forms layers.

The following (Table 1) are the different hydrogeomorphic units depicted based on integrated satellite remote sensing study in the study area:

Table 1: Hydrogeomorphic units

Geomorphic Unit	Area (km^2)	Percentage
Hills	724	5
Pediment	1070	8
Pediplain Shallow (PPS)	6868	48
Pediplain Moderate (PPM)	3510	25
Plateau	837	6
Valley	215	2
Alluvium / Flood Plain	75	1
Waterbody	911	6
Total	**14210**	

5.2 Groundwater quality study in pre-monsoon season

The following is the status of element-wise number of sources potable and or contaminated during the pre monsoon season (Table 2).

Table 2: Status of sources in pre-monsoon season

Total sources quality tested	19,407	-
All elements potable	10,001	51.53%
At least one element quality affected source	9,406	48.47%

The following is the list of number of elements contaminated with respect to total number of sources affected during pre-monsoon season (Table 3andFigure 2):

Table 3: Status of percentage of elements contamination

Sl No	Element(s) contaminated	Total sources quality affected, nos	% of quality affected to total sources in Nalgonda dist.
1	1	5,933	30.57 %
2	2	1,952	10.06 %
3	3	943	4.86 %
4	4	448	2.31 %
5	5	115	0.59 %
6	6	12	0.06 %
7	7	3	0.02 %

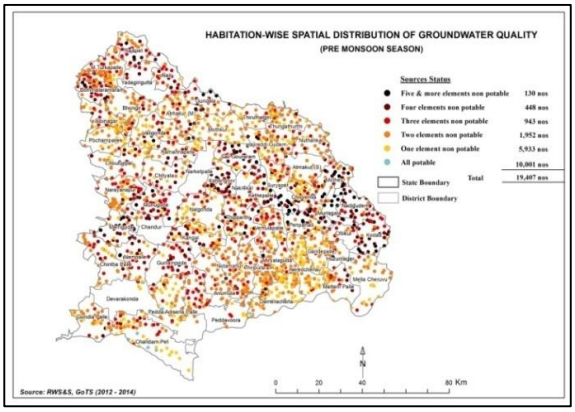

Figure 2: Element wise ground water quality during pre monsoon season

The following table shows the major contaminated elements out of total quality tested sources in Nalgonda district (Table 4).

Table 4: Status of percentage of major elements

Only Fluoride contaminated	14.32 %
Only Iron contaminated	9.07 %
Only TDS contaminated	5.24 %
TDS & TA contaminated	3.32 %
TDS, TH, TA contaminated	2.71 %
TDS & F contaminated	2.51 %
F & Fe contaminated	2.10 %
No3 contaminated	1.36 %
TDS & Iron contaminated	0.80 %
Other elements combinations of contamination	0.63 %
All potable sources	57.94 %

5.3 Groundwater quality study in post-monsoon season

The following is the status of element-wise number of sources potable and or contaminated during the post monsoon season (Table 5).

Table 5: Status of sources in post-monsoon season

Total sources quality tested	19,408	-
All elements potable	10,247	52.80 %
At least one element qualityaffected source	9,161	47.20 %

The following is the list of number of elements contaminated with respect to total number of sources affected during post-monsoon season (Table 6andFigure 3):

Table 6: Status of percentage of elements contamination

Sl No	Element(s) contaminated	Total sources quality affected, nos	% of quality affected to total sources in Nalgonda dist.
1	1	5,930	30.55 %
2	2	1,849	9.53 %
3	3	895	4.61 %
4	4	386	1.99 %
5	5	87	0.45 %
6	6	12	0.06 %
7	7	2	0.01 %

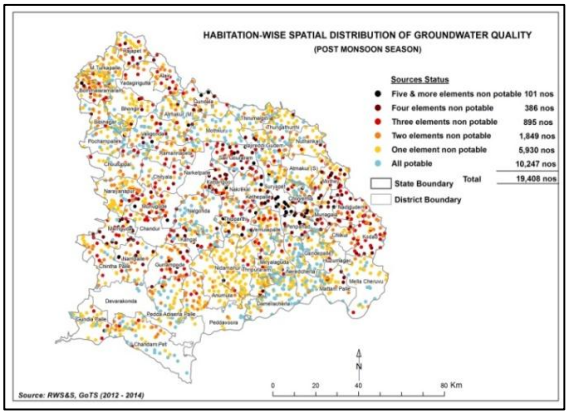

Figure 3: Element wise ground water quality during post monsoon season

The following table shows the major contaminated elements out of total quality tested sources in Nalgonda District (Table 7):

Table 7: Status of major contaminated elements

Only Fluoride contaminated	14.34 %
Only Iron contaminated	9.08 %
Only TH contaminated	4.94 %
TH & TA contaminated	3.29 %
TDS, TH, TA contaminated	2.64 %
F &Fe contaminated	2.07 %
No3 contaminated	1.80 %
TDS, TA, F contaminated	1.22 %
TH & Iron contaminated	1.09 %
TH & F contaminated	0.98 %
Other elements combination contamination	0.56 %
All potable sources	57.99 %

5.4 Groundwater quality vs groundwater prospects during pre and post monsoon seasons

Hydrogeomorphic unit wise ground water quality variation is studied using satellite remote sensing techniques. It is observed that the major ground water quality problem exists in granitic terrain as compared to Meta-sedimentary rocks.

It is observed that majority of the area is contaminated with at least 2 or 3 elements from a combination of F, TDS, TH, TA, Fe, No3. The Fluoride contamination exists predominantly in older Metamorphics, Dharwar Supergroup and Peninsular Gneissic Complex (PGC) except Grey Hornblende Granite rock formations, whereas, it is minimal in Meta-sedimentary formations belonging to Cuddapah Supergroup and Kurnool Group of rocks. In command areas underlain by Grey Hornblende Granite, the contamination is observed with at least 2 elements from a combination of TDS, TH, Fe, or No3 only. The density of fluoride affected sources is very less in Grey Hornblende Granite as compared to other rock formations like Grey / alkali feldspar Granite, Leuco Granite, Grey biotite granite gneiss etc. The Majority of Chloride contamination (in command as well as no-command areas) is dominated in the areas underlain by Grey / alkali feldspar Granite.

Major geomorphic unit wise quality variation is studied in conjunction with other ancillary data. It has been observed that in plain areas, as compared with shallow (PPS) and moderate (PPM) weathered zones, percentage of contaminated sources is 55% in PPM areas whereas in that of PPS it was 45% only. There is major contamination for a combination of one or two elements from F, Fe, TDS/TH in plain areas. In pediment zones 43% sources are contaminated of which the majority of sources are affected with one or two elements from F, Fe, TDS/TH. In plateau areas (meta-sedimentary rocks), 29% sources are quality affected of which the majority of the sources are contaminated with at least one element from TDS/TH or Fe only. In Valleys portions 49% of the sources are contaminated primarily one or two elements combination from F, Fe, TDS/TH. In Alluvium areas 45% sources are contaminated for which the majority of the sources are at least one or two elements from a combination of F, TDS/TH. In post monsoon season, the TH contamination is more as compared to TDS. It is observed that longer residence time in aquifers with fractured fluoride rich rocks increases fluoride levels in the groundwater.

5.5 Groundwater quality vs rainfall

The mandal wise average normal rainfall for the past 21 years is calculated based on the data collected from the Directorate of Economics and Statistics for studying quality problem with respect to rainfall. It is found that the rainfall is inversely related to ground water quality i.e. in high rainfall areas there will be less quality problem is there. It is observed that in low rainfall areas (Below 652 mm), there is contamination of 59% of sources for at least one element whereas in 653-802 mm rainfall areas the percentage of quality affected sources is 47% and it is 45% in 803-953 mm rainfall areas. This clearly indicates that rainfall is also one of the contributing factors for water quality.

5.6 Waterconservation and artificial recharge

For ground water conservation and artificial recharge, number of structures have been constructed since 1995 by District Water Management Agency (DWMA) in a big way in the district under DPAP, IWDP, RIDF, APRLP, EAS, NEERU MEERU and other programmes in the non- command area. About 3,684 Hactares land is brought under irrigation facility up to 2012-13under different watershed programmes in the district. During 2011-15, about 5,847 water harvesting structures like Recharge of dried up open wells, farm pond, percolation tank, dugout pond, Gabion WHS, sub surface dykes, check dam, recharge of dried up bore wells, recharge pit etc., are taken up.

The rain water harvesting structures sites must be selected scientifically on watershed basis especially in non-command areas on war foot basis for the benefit of farmers/people as well as for drinking water purpose, as most of the water is being used for agriculture and industrial needs. As per the hydro-geomorphic study in the area, most suitable recharge structure is percolation tanks / check dams. In addition, gully controls and bunding may be taken up where considerable gradient and length of slope is available. For those who take up roof top harvesting structures in urban and rural areas should be given incentives for enhancing groundwater recharge.

5.7 Groundwater quality: Causes, implications and mitigation measures

Out of a total of 19,408 sources quality tested; about 4,208 sources (22%) have been affected with fluoride during pre and post monsoon seasons. Fluoride is the major element contaminated in the district. The district is witnessing the dental as well as skeletal Fluorosis and is a renowned place in the world.

Fluoride is one of the important micronutrient in humans which is required for strong teeth and bones. Fluoride concentration of at least 0.6 mg/l is required for human consumption as it will help to have stronger teeth and bones. BIS (Bureau of Indian Standards) (1992) has prescribed the range of fluoride from 0.6 to 1.0 mg/l in drinking water as suitable for human consumption and has set the maximum permissible limit of fluoride in drinking water to be up to 1.5 mg/l. Drinking groundwater with fluoride concentration above 1.50 mg/l is the main cause of fluorosis in the area. The other possible sources of intake of fluoride apart from drinking water are through food, beverages and dental products like tooth paste.

As the district is falling in semi-arid tract, due to which the intake of ground water is more as compared to other non-tropical areas. This is also causing to increase the fluorosis problem. Phosphate containing fertilisers add up to the fluoride content in soil and

groundwater (Motalane and Strydom, 2004; Farooqi et al., 2007). Intake of fluoride higher than the optimum level is the main reason for dental and skeletal fluorosis. The health outcome by consuming fluoride at different concentration was given by Dissanayake (1991) i.e. when fluoride concentration in drinking water is below 0.5 mg/l it causes dental carries; fluoride between 0.5 to 1.5 mg/l results in optimum dental health; 1.5 to 4 mg/l causes dental fluorosis; 4to 10 mg/l induces dental and skeletal fluorosis while fluoride above 10 mg/l results in crippling fluorosis. However, fluorosis results not only due to the presence of high concentration fluoride in drinking water but also depend on other sources such as the dietary habits which enhance the incidence of fluorosis. The malnutrition adds to fluorosis. If sufficient dietary food is taken, there are chances of less effect on fluorosis.

Exposure to very high fluoride over a prolonged period of time results in acute to chronic skeletal fluorosis. It was stated in 1993 that crippling skeletal fluorosis might occur in people who have ingested 10 to 20 mg of fluoride per day for over 10 to 20 years (National Research Council, 1993). The district has high fluoride due to the inherent fluoride rich granitic rocks. The granitic crocks in Nalgonda district contain fluoride from 325 to 3200 mg/kg with a mean of 1440 mg/kg as compared to the world average fluoride concentration of 810 mg/kg (Wedepohl, 1969).

When the fluoride rich water is used for agriculture purpose, the fluoride is entering in to the food grains indirectly and when these food grains are consumed, the concentration of fluoride is getting added to fluoride rich drinking water.

To mitigate the fluoride problem, one should shift to safe ground water sources available nearby or use the defluoridated and safe drinking water with changing dietary habits like to avoid use of fluoride rich foods like black rock salt, canned fruit juices / other domestic market products etc. Avoid use of fluoride rich dental products or drugs. Use food which is rich in Calcium, Vitami C, Anti-Oxidants etc.

High TDS in ground waters causes Gastrointestinal irritation and may damage the kidneys in human beings.

Iron although having Aesthetic taste and is an essential for human health [Heamoglobin Synthesis], but its excess is stored in Spleen, Liver, Bone marrow & causes Haemochromatosis.

Nitrate if beyond 45mg/l in drinking water, methaemoglobinamia takes place and may be indicative of pollution

The most common problem associated with ground water after Fluoride and TDS is hardness, caused by an abundance of calcium or magnesium ions. Hard water causes no health problems, but it may cause soap curds to form on pipes and other plumbing fixtures.

6. Discussion

Various hydro-geomorphic units are classified as high, medium low and poor zones of groundwater. Groundwater development is more promising in the alluvial plains, which are associated with thick alluvium and weathered material due to high porosity and permeability which are limited in the area. Shallow (< 10m) and moderate (10-20m) weathered pediplains are distributed in majority of the area and they can be classified as medium to good favourable zones of groundwater. Dissected pediment zone with poor weathering and rugged appearance is a poor zone of groundwater. The geomorphological units like residual hills and linear ridges acts as runoff zones. Other observations are as follows:

- Overall water quality of the study area was found unsatisfactory for drinking purposes. Pollution of the groundwater due to geogenic and anthropogenic factors often render the groundwater unsuitable as consumption of such water can lead to various health-related complications.

- The occurrence and quality of groundwater in an area is largely controlled by rainfall and the characteristics of the terrain features like landforms, geology, soil, drainage, topography. The information provided in the groundwater prospect zones helps in identifying areas suitable for artificial recharge to ensure sustainable groundwater draft.

- The intake of fluoride above the permissible limit in drinking water is the major reason for both dental and skeletal Fluorosis diseases in part of the study area.

- For fluoride mitigation preventive measures like taking safe drinking water with sufficient dietary food needs to be encouraged.

- Health education with focus on fluoride toxicity and the need to avoid fluoride consumption to be encouraged to each and every citizen.

- Training for local government functionaries, NGOs, voluntary organizations engaged in watershed development activity are to be trained in scientific techniques in the selection of sites, design of structures, etc. for construction of rainwater harvesting and artificial recharge structures.

- Conjunctive use of groundwater and surface water are to be encouraged for irrigation purpose to enhance yield potential and at the same time improving the water quality in non-command areas and minimizing the water logging threat in command areas.

- Mass awareness programmes need to be conducted on regular basis in the rural areas to educate the farmers regarding the water management like water saving methods or to use less water consuming crops like maize, jowar etc and to update their knowledge.

7. Conclusions

The utility of remote sensing and GIS technique helps in delineating groundwater prospects zones as well as to relate its association with ground water quality. It is observed that the percentage of contaminated sources is more in high yielding hydrogeomorphic units as compared to less yielding hydrogeomorphic units in non-command area as it is wholly dependent on ground waters for all its uses. From the study the following conclusions can be made:

- As the non-command area is extensive, there is tremendous pressure on ground water for agriculture and industrial uses which results in pollution of ground water resources and in future these limited resources will not be able to meet the water demand qualitatively and quantitatively. Therefore, it is imperative to make the fruitful long term planning like transfer of perennial river water to the area to conserve these resources and utilize it in systematic way for the maximum benefit of society.

- Groundwater conservation and artificial recharge structures are needed to be taken up watershed wise on war footing, on scientific lines, for enhancing the groundwater storage so as to make the existing bore wells sustainable.

- Scientific mapping of resources needs to be taken for preventing quality problem with remedial measures. It is important to look for holistic and people-centred approaches for water management.

Acknowledgments

Authors would like to thank to Telangana State Remote Sensing Applications Centre (TRAC) for providing support and encouragement to carry out the study. Authors are also thankful to the reviewers for critically going through the manuscript and giving valuable suggestions for the improvement of manuscript.

References

BIS (1992). Bureau of Indian Standards. Indian standard for drinking water ISO 10500.

Dissanayake, C.B. (1991). The fluoride problem in the ground water of Sri Lanka - Environmental management and health. International Journal of Environmental Studies, 38(2), 137-155.

Farooqi, A., H. Masuda, M. Kusakabe, M. Naseem and N. Firdous (2007). Distribution of highly arsenic and fluoride contaminated groundwater from east Punjab, Pakistan and the controlling role of anthropogenic pollutants in the natural hydrological cycle. Geochemical Journal, 41, 213-234.

GEC (2011). Groundwater resource Estimation Committee report. Dynamic Ground Water Resources of Andhra Pradesh, 2008-09 (Vol I & II), December 2011

Motalane, M.P. and C.A. Strydom (2004). Potential groundwater contamination by fluoride from two South African phosphogypsums. Water SA, 30 (4), 465-468.

NRSA (2007), Groundwater prospects mapping using remote sensing techniques and geographic information system under Rajiv Gandhi national drinking water mission (RGNDWM). Technical manual, National Remote Sensing Agency, Department of Space, Government of India (2007).

NRSA (2013). Groundwater quality mapping for Rajiv Gandhi National Drinking Water Mission (RGNDWM) - Methodology manual. National Remote Sensing Agency, Department of Space, Government of India (2013).

Wedepohl, K.H. (Ed.) (1969). Handbook of geochemistry. vol. II/1.Springler-Verlag, Berlin, 9C1-B9O3

Journal of Geomatics Vol 11 No. 1 April 2017

3D model reconstruction from aerial ortho-imagery and LiDAR data

ElSonbaty Loutfia, Hamed Mahmoud, Ali Amr and Salah Mahmoud
Faculty of Engineering Shoubra, Benha University, Cairo, Egypt
Email: loutfia_karam2001@hotmail.com, prof.mahmoudhamed@yahoo.com, amrhali@feng.bu.edu.eg, engmod2000@yahoo.com

(Received: Jul 13, 2016; in final form: Feb 15, 2017)

Abstract: Three dimensional (3D) city model is an interesting research topic in the last decade. This is because achieving rapid, automatic and accurate extraction of a realistic model for the large urban area is still a challenge. Consequently, increasing the efficiency of 3D city modeling is required. The objective of this research is to develop a simple and efficient semi-automatic approach to generate a 3D city model for urban area using the fusion of LiDAR data and ortho-rectified imagery. These data sources provide efficiency for 3D building extraction. This approach uses both LiDAR and imagery data to delineate building outlines, based on fuzzy c-means clustering (FCM) algorithm. The third dimension is obtained automatically from the normalized digital surface model (nDSM) using spatial analyst tool. The 3D model is then generated using the multi-Faceted patch. The accuracy assessment for both height and building outlines is conducted referring to the ground truth and by means of visual inspection and different quantitative statistics. The results showed that the proposed approach can successfully detect different types of buildings from simple rectangle to circular shape and LOD2 (level of detail) is formed by including the roof structures in the model.

Keywords: 3D city model, LiDAR, Ortho-rectified aerial imagery, Data fusion, FCM, nDSM

1. Introduction

The way of representing earth has changed with the fast growth of technologies. Two-dimensional (2D) maps have turned from the traditional paper-based to digital forms and from planar 2D to a three-dimensional (3D) representation of objects. Among different cartographic products, 3D city models have shown to be valuable for several applications such as urban planning and management, flood simulation, land monitoring, mobile telecommunication, 3D visualization, solar radiation potential assessment, etc. (Tack et al., 2012).

With the fast advancement of spatial and spectral data acquisition systems in recent years, numerous approaches for generating 3D city model from various types of data such as high-resolution aerial images, airborne LiDAR data, terrestrial laser scanning, digital surface derives from stereo and multi-stereo matching and heterogeneous data sources have been presented (Partovi et al., 2013). In this regard, LiDAR and photogrammetry are receiving major attention due to their complementary characteristics and potential.

Nowadays, the algorithms that have been used for automatic extraction and visualization of 3D building archive various level of progress. However, extracting building boundary from LiDAR only is still challenging task where the horizontal spacing of the sample points is scattered. Therefore the need for supplementary data such as digital maps, high-resolution satellite imagery and ortho-imagery is necessary (Park et al., 2011). Different trials are carried out to generate 3D city model.

Ruijin (2004) reconstructed 3D building models from aerial imagery and LiDAR data. They used stereo aerial photographs to improve the geometric accuracy of the building model. Complex buildings are reconstructed using the polyhedral building model in a data-driven oriented method. The proposed methodology has some limitations caused by the data used. For example, two individual buildings might be detected as one building if they are very close to each other. On the other hand, the algorithm may fail in ordering roof polygons in the correct sequence. Another type of limitation is from the modeling process itself. In this work, it is assumed that all buildings have rectangular footprints. Thus, non-rectangular footprints will be forced to have rectangular shapes.

Hongjian and Shiqiang (2006) presented a 3D building reconstruction approach based on aerial images and LiDAR data. First, an edge detecting algorithm combing Laplacian edge sharpening with the threshold segmentation was developed and employed to detect the edges and lines on the images. Then, a method using bi-direction projection histogram was used to determine the corner points of building and extract the contour of the building by searching and matching gradually. The four corners of the building can be extracted by combining the two directions according to the direction of the histogram. The heights of the building were calculated according to the Laser points within the building boundary. Because of the limitation of using the bi-direction histogram and the method to obtain the height of the roofs, the proposed method seems to be only suitable for buildings with rectangular shapes and flat roofs. It is very hard to apply it for complex building reconstruction.

Langue (2007) developed an object-oriented based method for 3D building extraction by integrating LiDAR data and aerial imagery. The object-oriented building model for 3D building extraction is developed by integrating data collection and construction methods, geometry and topology, semantics and properties as well

as data storage and management of 3D buildings into one model.

Arefi et al. (2008) proposed an automatic approach for reconstructing models in three levels of details. The building outlines are detected by classification of non-ground objects and building outlines are approximated by hierarchical filtering of minimum boundary rectangles (MBR) and RANSAC-based straight line fitting algorithm. Jarvis (2008) outlined the integration of photogrammetric and LiDAR data, within GIS, for the accurate reconstruction of a 3D realistic urban model in a semi-automated procedure.

Kada and McKindle (2009) developed an approach for automatic reconstruction of 3D building models from LiDAR data and existing ground plans by assembling building blocks from a library of parameterized standard shapes. This approach based on an algorithm to decompose the building shape into sets of nonintersecting cells, and for each cell, the roof top is reconstructed by checking the normal direction of digital surface model (DSM). Sirmacek et al. (2012) extracted 3D block models using an object-oriented approach based on data fusion from LiDAR and very high resolution (VHR) optical imageries.

Kwak (2013) developed a framework for fully-automated building model generation by integrating data-driven and model-driven methods as well as exploiting the advantages of images and LiDAR datasets. The major limitation is that it can model only the types of buildings which decompose into rectangles.

The main goal of this research is to outline a semi-automatic method for reconstructing 3D city model in a third level of details from both LiDAR data and ortho-aerial imagery. The proposed work was accomplished using a combination of the following software sets: 1) Erdas Imagine 9.2 for data preprocessing, and 2) a set of programs generated by the authors in Matlab environment for the rest of the work.

2. Study area and data sources

The area is a part of the university of New South Wales Campus, Sydney, Australia. It is largely urban area containing residential buildings, large campus buildings, a network of main roads as well as minor road, trees, and green areas. The multispectral imagery was captured by film camera on June 2005 at 1:6000 scale. The film was scanned in red, green and blue colour bands with 15 µm pixel size (GSD of 0.096m) and radiometric resolution of 16-bit. On the other hand, LiDAR data were acquired over the study area on April 2005 and provided in ASCII format (easting, northing, heights, intensity and returns for first and last pulses). The LiDAR system used was the Optech ALTM 1225. Figures 1 and 2 show the multispectral imagery and the produced image from the LiDAR points respectively. The characteristics of aerial image and LiDAR data are provided in tables 1 and 2 respectively.

Table 1: Characteristics of image datasets

bands	*Cell size (m)*	*Camera*	*Look Angle*	
			along track	across track
RGB	0.096	LMK1000	±30º	±30º

Table 2: Characteristics of LiDAR datasets

Spacing/across track	1.15m
Spacing/along track	1.15m
Vertical accuracy	0.10m
Horizontal accuracy	0.5m
Density	1 Point/m2
Wavelength	1.047µm
Altitude	1100m
Swath width	800m

Figure 1: Ortho-rectified image of the test area

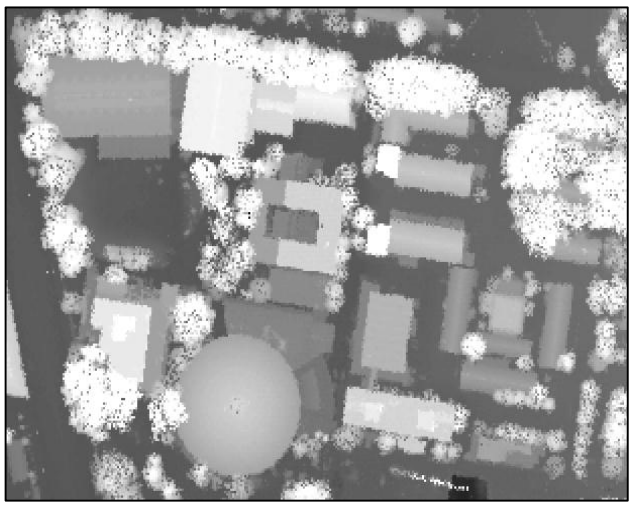

Figure 2: Digital Surface Model (DSM) generated from the original LiDAR pointcloud

3. Methodology

This study proposes a semi-automatic method for generating 3D city model by integrating single aerial imagery and LiDAR data. This method is composed of five key steps. The five main procedures are discussed in the following sections. Figure 3 summarizes the workflow for the proposed techniques.

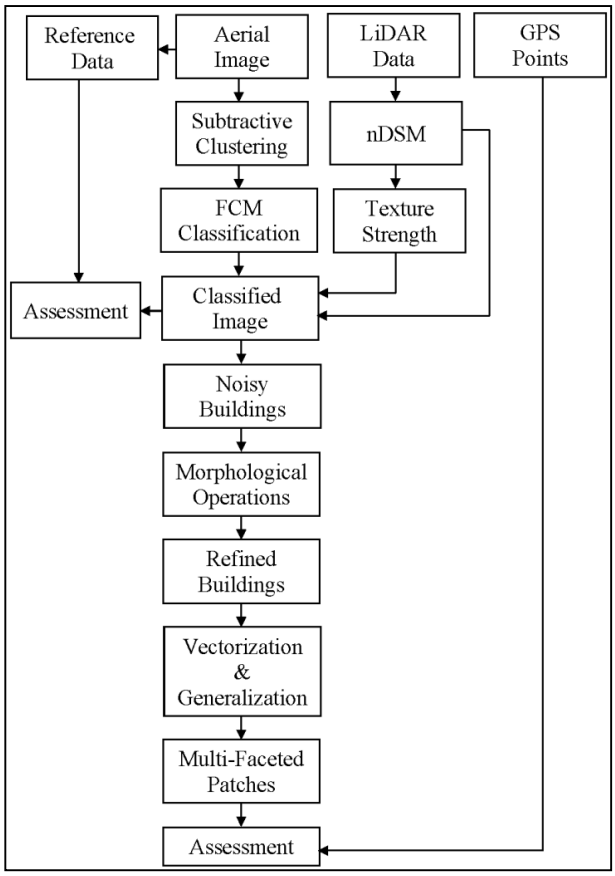

Figure 3: Ortho-rectified image of the test area

3.1. Data preparation

3.1.1 Image and LiDAR data co-registration: Image registration is the method of bringing different datasets into a single coordinate system. After multiple datasets acquired by different sensors having the same coordinate system it still requires some kind of additional pixel-to-pixel matching in order to ensure higher reliability in data fusion techniques. This kind of matching is known as image co-registration (Fikri, 2012).

The orthorectified image (already orthorectified by AAMHatch with a RMSE of 0.41m) is registered to the LiDAR intensity image using the projective transformation in ERDAS 9.2 environment. The Root Mean Square (RMS) error from the modeling process was 0.098m. Following the projective transformation, the image was resampled to 30cm x 30cm pixel size to match the resolution of the LiDAR data. The bilinear interpolation was used for resampling, which results in a better quality image and requires less processing time.

3.1.2 Generation of the nDSM: The nDSM represents the absolute heights, of non-ground objects such as buildings and trees, above the ground. First, the DSM was generated from both the first and the last echoes. The DSM was then filtered to generate a digital terrain model (DTM) as shown in figure 4. In this case, the Tilted Surface Method (Salah, 2010) was used. In order to compensate for the difference in resolution between image and LiDAR data, DSM and DTM grids were interpolated to 30cm interval. Then, nDSM was generated. Finally, a height threshold of 3m was applied to nDSM to eliminating other objects such as cars as shown in Figure 5.

Figure 4: Digital Terrain Model (DTM) generated using the simple tilted plane filtering method

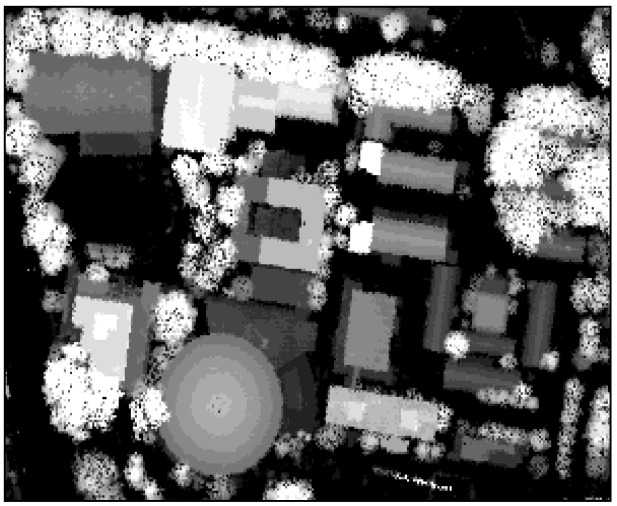

Figure 5: nDSM of the test area

3.1.3 Texture strength: Texture strength is based on a statistical analysis of the gray level gradients $\nabla g(r,c)$, which are the first derivative of the gray level function *g(r, c)*. The framework of the polymorphic texture strength based on the Förstner operator (Förstner and Gülch, 1987) has been applied. The gray level gradient $\nabla g(r,c)$ can be computed from Equation 1:

$$\nabla g(r,c)=\begin{bmatrix}\nabla g_r(r,c)\\ \nabla g_c(r,c)\end{bmatrix}=\frac{1}{2}.\begin{bmatrix}g(r+1,c)-g(r-1,c)\\ g(r,c+1)-g(r,c-1)\end{bmatrix} \quad (1)$$

From the gray level gradients $\nabla g(r,c)$ of small windows, 3 x 3 pixels, a measure W for texture strength is calculated as the average squared norm of the gray level gradients normalized by $\sigma_{n'}^2$ as shown in Equation 2:

$$W = L * \| \frac{1}{\sigma_{n'}^2} \cdot \nabla g(r,c) \|^2 = L * (\frac{\Delta g_r^2 + \Delta g_c^2}{\sigma_{n'}^2}) = L * (\frac{\Delta g_r^2 + \Delta g_c^2}{k \cdot \sigma_n^2}) \quad (2)$$

with L being a linear low pass filter, Gaussian filter with $\sigma = 0.71$, k equals the squared sum of components of the convolution kernel. Thus, $k=0.5^2+0.5^2=0.5$. The noise variance σ_n^2 is equal to the square of the norm of the gray level grad $\| \nabla g(r,c) \|^2$. W is high in image windows containing large gray level differences.

For texture strength calculation, a window of 3 x 3 pixels is placed over the top left 3 x 3 block in the image and then the texture is calculated for all pixel values within that window. The texture value is then written to the central pixel of that window in a new raster layer. Then the window "moves" over one pixel and the process is repeated until all the pixels in the image have served as central pixels - except the ones around the outside. These edge pixels were filled in with the nearest texture calculation. Finally and since most texture calculations are not integers, images were linearly scaled to the full range for 8-bit data (0-255) as shown in figure 6.

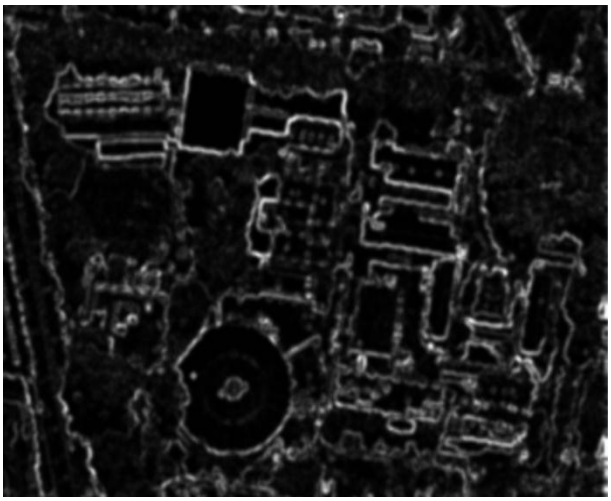

Figure 6: Texture strength of the nDSM

3.1.4 Reference data: In order to evaluate the accuracy of the classifications, reference data were captured by digitizing buildings, trees, roads and ground in the ortho-photo as shown in figure 7. During this process, adjacent buildings that were joined but obviously separated were digitized as individual buildings; otherwise, they were digitized as one polygon. Roofs were first digitized and then shifted so that at least one point of the polygon coincided with the corresponding point on the ground. This is to overcome the horizontal layover problem of tall objects such as buildings.

Figure 7: Reference data

3.2. Image classification

3.2.1 Fuzzy C-Means clustering (FCM): A cluster can be defined as a group of pixels that are more similar to each other than to members of other clusters. In most of the clustering approaches, the distance measure used is the Euclidean distance. Thus, the distance measure is an important means by which the research can influence the outcome of clustering (Velmurugan and Santhanam, 2011).

Clustering can be divided into two main approaches: hard clustering and the other one is fuzzy clustering (Moertini, 2002). In hard clustering, data is partitioning into a specified number of mutually exclusive subsets (Babuska, 2001). In hard clustering method, the boundary between clusters is fully defined. However in many real cases, the boundaries between clusters cannot be clearly defined, where some patterns may belong to more than one cluster. In such cases, the fuzzy clustering method provides better results (Moertini, 2002). FCM is the most representative fuzzy clustering algorithms since it is suitable for tasks dealing with overlapping clustering.

In FCM, each data point belongs to a cluster to some degree that is specified by a membership grade (Bora and Gupta, 2014). This technique was introduced in 1973 and first reported in 1974 and subsequently improved in 1981 (Suganya and Shanthi, 2012). It provides a method of how to group data points that populate some multidimensional space into a specific number of different clusters. In Fuzzy clustering methods, the objects could belong to several clusters simultaneously with different degrees of membership, between 0 and 1 indicating their partial membership (Babuska, 2001).

This gives the flexibility to express that data points can belong to more than one cluster (Bora and Gupta, 2014). The clustering algorithm is performed with an iterative optimization of minimizing a fuzzy objective function (J_m) defined as Equation (3).

$$J_m = \sum_{i=1}^{c} \sum_{k=1}^{n} (\mu_{ik})^m d^2(x_k, V_i) \quad (3)$$

where
n = number of pixels
c = number of clusters
μ_{ik}= membership value of i^{th} cluster of k^{th} pixel
m = fuzziness for each fuzzy membership.
x_k= vector of k^{th} pixel
V_i= center vector of i^{th} cluster
$d^2(x_k,V_i)$ = Euclidean distance between $x_k$and V_i

The membership (μ_{ik}) can be estimated from the distance between k^{th} pixel and center of i^{th} cluster as follows:

$$\begin{cases} 0 \le \mu_{ik} \le 1 & \text{for all} i,k \\ \sum_{i=1}^{c} \mu_{ik} = 1 & \text{for all} k \\ 0 < \sum_{k=1}^{n} \mu_{ik} < n & \text{for all} i \end{cases} \quad (4)$$

The center of cluster (V_i) could be calculated by equations (5) and the membership value (μ^{ik}) could be calculated by equations (6) as follow.

$$V_i = \frac{\sum_{k=1}^{n}(\mu_{ik})^m x_k}{\sum_{k=1}^{n}(\mu_{ik})^m}, 1 \le i \le c \quad (5)$$

$$\mu_{ik} = \left[\sum_{j=1}^{c}\left(\frac{d(x_k,V_i)}{d(x_k,V_j)}\right)^{\frac{2}{m-1}}\right]^{-1}, 1 \le i \le c, 1 \le k \le n \quad (6)$$

J_m can be minimized by iteration through equations (5) and (6). The first step of the iteration is to initialize the following parameters: a fixed *c*, a fuzziness parameter (*m*), a threshold of convergence *ε*, and an initial center for each cluster, then computing μ_{ik} and V_i using Equations (5) and (6) respectively. The iteration is stop when the change in V_i between two iterations is smaller than *ε.* At last, each pixel is classified into a combination of memberships of clusters.

Several parameters must be specified before using the FCM algorithm which include: the number of clusters, *c*, the 'fuzziness' exponent, *m*, the termination tolerance, *ε*, and the norm-inducing matrix, A. Moreover, the fuzzy partition matrix, U, must be initialized (Babuska, 2001).

3.2.2 Subtractive clustering: Fuzzy C-Means algorithm requires the analyst to pre-specify the number of cluster centers and their initial locations. The quality of the results depends strongly on the number of cluster centers and their initial locations. Chiu (1994) proposed an effective algorithm, called the subtractive clustering, for estimating the number and initial location of cluster centers. By using this method, the computation is simply proportional to the number of data points and independent of the dimension problem as shown in equation 7 (Moertini, 2002). For a problem of *c* clusters and *m* data points, the required number of calculations is:

$$\mathrm{N}= \underset{1^{st}cluster}{m^2} + \underset{remainder clusters}{(c-1)m} \quad (7)$$

Consider a group of *n* data points $\{x_1,x_2,...,x_n\}$, where, x_i is a vector in the feature space. Assume that the feature space is normalized so that all data are bounded by a unit hypercube. As well, consider each data point as a potential cluster center and define a measure of the point to serve as a cluster center. The potential of x_i denoted as P_i is given in equation 8.

$$\sum_{j=1}^{n} exp\left(-\frac{\|x_i - x_j\|^2}{(r_a/2)^2}\right) \quad (8)$$

Where r_a is a positive constant defining a neighbourhood radius || || denotes the Euclidean distance. A data point that has many neighbouring data points will have a higher potential value and the points outside will have little influence on its potential. The first cluster center c1 is chosen as the point with the highest potential. The potential of c1 is referred to as PotVal (c1). The potential of each data point xi is then revised as follows:

$$P_i = P_i - PotVal(c_i)exp\left(-\frac{\|X_i - c_i\|^2}{\left(\frac{r_b}{2}\right)^2}\right) \quad (9)$$

To avoid obtaining closely spaced cluster centers, rb is usually set to 1.5 ra. The data points near the first cluster center will greatly reduce their potential and will unlikely be selected as the next center. From equation 9 the potential of all data points will be reduced, after that the point with the highest potential is selected as the second center. After the kth cluster center c_k is determined, the potential is revised as follows:

$$P_i = P_i - PotVal(c_k)exp\left(-\frac{\|X_i - c_k\|^2}{\left(\frac{r_b}{2}\right)^2}\right) \quad (10)$$

where
c_k = the location of the k^{th} cluster center
PotVal (c_k) = potential value.

The process proceeds until the stopping criterion is reached. From the clustering process, two conclusions can be drawn: 1) a point with relatively high potential has more chance to be selected as center than less potential point; 2) Cluster centers are selected only from the data points even if the actual cluster centers are in the dataset or not. (Chen et al., 2008). The Strengths of the subtractive clustering are:1) reduces the time complexity; and 2) results are fixed and has no random cluster value. On the other hand, accuracy is less and cautious about choosing the neighbour radius (Leela et al., 2014).

3.3. Post-processing

3.3.1 Morphologic operations: Morphologic operations have been applied to separate objects in the image from the background. The basic operations of binary morphology are: erosion, dilation, opening, and closing. A dilation operation enlarges a region, while erosion makes it smaller. An opening operation (erosion followed by

dilation) can get rid of small portions of the region that jut out from the boundary into the background region. A closing operation (dilation followed by erosion) can close up internal holes in a region and eliminate bays along the boundary (Shapiro and Stockman, 2011).

For clarity, the small buildings were merged into larger ones or deleted according to a 1m distance and 30m^2 area thresholds. A certain building was retained if it was larger than 30m^2 and/or adjacent to another building by a distance less than 1m. The area threshold represents the expected minimum building size, while the distance threshold was set to 1m to fill in any holes or gaps produced by the classification process. Building borders were then cleaned by removing regions that were smaller than 5 pixels in size and that were connected to the building border. Cleaning thresholds less than 5 pixels may leave the original buildings uncleaned, while thresholds larger than 5 pixels may remove parts of the original buildings. The results are the detected buildings without holes or any noisy features.

3.3.2 Vectorization and generalization: In order to extract building boundaries, the smoothed binary image is converted from raster to vector format. After that, the obtained boundaries need more processing to overcome the problem of irregularities and to adjust the rectangularity of the polygons. One of the most common used generalization algorithms is The Ramer–Douglas–Peucker algorithm (RDP). This algorithm reduces the number of points in a curve that is approximated by a series of points. The first form of the algorithm was suggested in 1972 and then modified by Douglas and Peucker (1973).

This approach automatically marks the first and last points to be kept, and then it finds the furthest point from the line segment between the first and last points as end points. If the vertex is closer than the tolerance (ε) to the line segment then any points not currently marked to be kept can be discarded without the simplified curve being worse than ε. If the vertex that is furthest away from the line segment is greater than ε from the approximation then that point must be kept. The algorithm recursively calls itself with the first point and the worst point and then with the worst point and the last point (which includes marking the worst point being marked as kept). When the recursion is completed a new output curve can be generated consisting of all (and only) those points that have been marked as kept (Douglas and Peucker, 1973).

3.4. Three dimensional model construction

For the construction of the three dimensional model, Multi-Faceted Patches are used. In this regard, x, *y*, and *z* coordinate of the faces of a given building are specified as matrix. MATLAB draws one face per column, producing a single patch with multiple faces as shown in figure 9(The MathWorks, 2015).

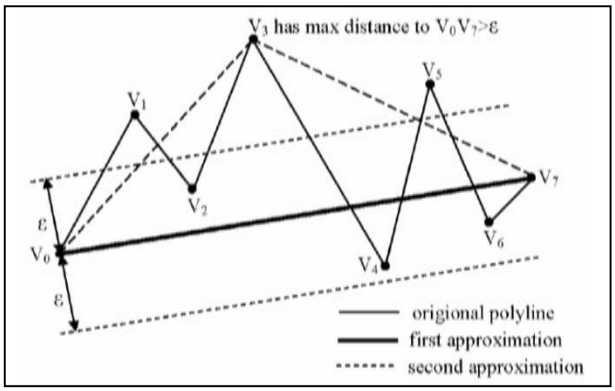

Figure 8: Smoothing a line segment with the Douglas–Peucker algorithm (Douglas and Peucker, 1973).

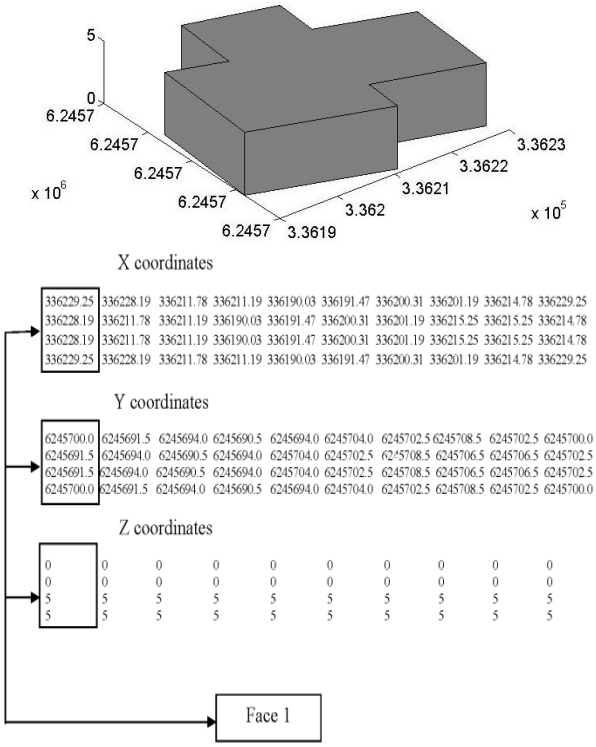

Figure 9: The concept of multi-faceted patches

4. Analysis and results

To initialize FCM algorithm, the parameters are set to the following values: the total number of clusters *c* is initialized as 13 (as obtained by the subtractive clustering), the maximum number of iteration as 100, the exponent for μ_{ik} as 2.0 and a minimum improvement ε of 1e^{-6}. The clustering process terminates when the maximum number of iterations is reached, or when the objective function improvement between two consecutive iterations is less than the minimum amount of improvement specified. Figure 10 shows the FCM output.

The obtained overall classification accuracy was 87.84%, while the per-class accuracies were 83.51%, 89.06%, 82.83% and 92.33% for buildings, trees, roads and grass respectively.

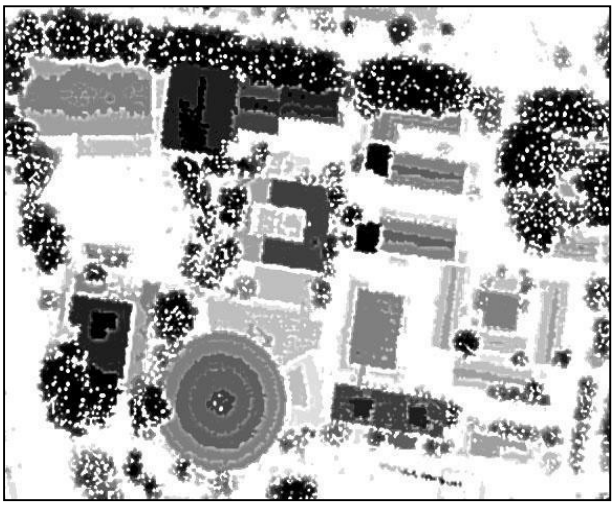

Figure 10: Classified image using fuzzy c-means clustering

In order to extract buildings from the classified image, the classified image was compared with the nDSM and texture strength images. Digital values of the classified image are converted to 1 (background) if it corresponds to 0 in the nDSM and/or higher value (over 0.5) in the texture strength image. Otherwise, the pixel value is kept as it is. The result is a building image with noisy features as shown in figure 11.

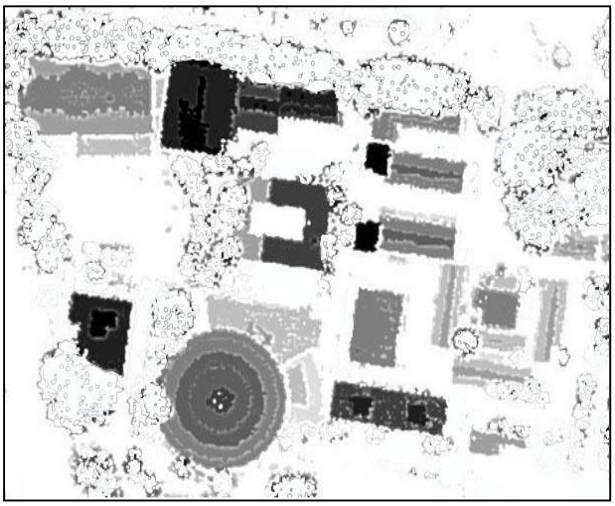

Figure 11: Classified image using fuzzy c-means clustering

Morphologic operations were then applied to merge small buildings into larger ones and fill in holes according to the specified 1m distance and 30m^2 area thresholds. Building borders were then cleaned according to the specified 5 pixels threshold. The result was an image that represents the detected buildings with a considerable lower degree of noisy features as shown in Figure 12.

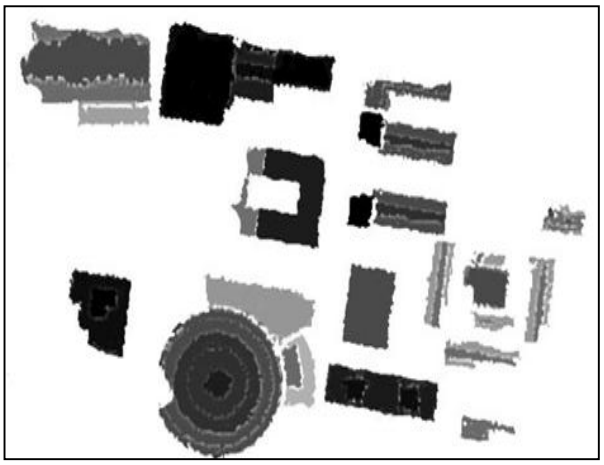

Figure 12: The final detected buildings

The smoothed image is then converted from raster to vector format to extract building boundaries. The Ramer–Douglas–Peucker algorithm (RDP) was used to overcome the problems of irregularities and adjust the rectangularity of the polygons. The tolerance was initially specified equal to the pixel size of the data. If the output still contains too much detail, then the tolerance can be doubled and so on. Similarly, if the output lines do not have enough detail, the tolerance can be halved. Figure 13 shows the extracted buildings before and after the simplification and adjustment of the rectangularity.

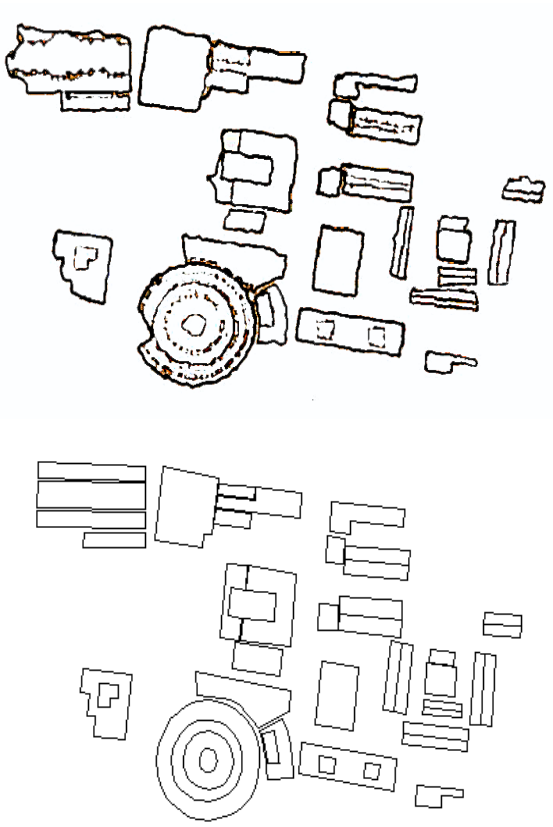

Figure 13: Buildings map before and after adjusting the rectangularity

In order to construct 3D model, two main items must exist: building outlines, and height information. In the proposed

methodology and to determine the heights of the buildings, a set of random sample points (constrained by building footprints) are generated at the corners of each building as shown in figure 14. The result is a feature class containing groups of points. Elevation information extracted from elevation surface can be added to each point as an attribute. The MATLAB code is then used to construct the 3D model as shown in figure 15.

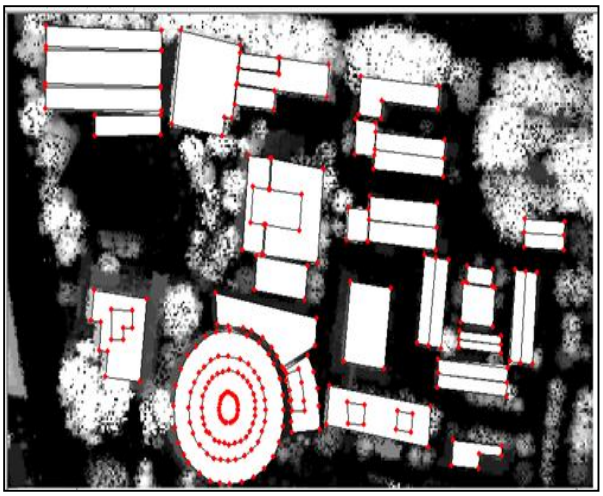

Figure 14: Generation of a set of random sample points (constrained by building footprints)

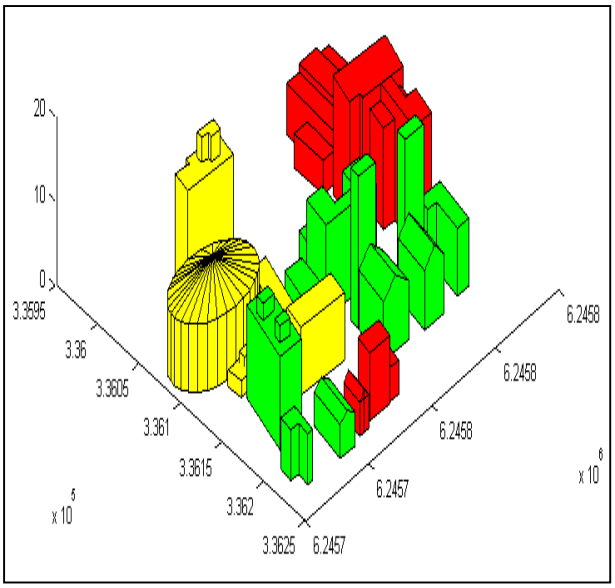

Figure 15: buildings extracted from the study area

In order to evaluate the planimetric accuracy of the resulted vector map, three GCPs were determined by field surveys. The GCPs were selected to be evenly distributed throughout the study area as shown in Figure 16, and a comparison was carried out between GPS observations and the extracted building data coordinates with a RMSE of 0.51m as shown in Table 3. The vertical accuracy of the constructed 3D building model is within 15- 20 cm which matches with a vertical accuracy of LiDAR.

Figure 16: Distribution of the GPS control points

Table 3: The accuracy estimate of the building vectorization process

Point	Δ_E (GPS – map)	Δ_N (GPS – map)	$\sqrt{\Delta E^2 + \Delta N^2}$
1	0.47	-0.46	0.6576
2	0.14	-0.03	0.1431
3	0.32	0.74	0.8062
Mean	0.31	0.41	
RMS	0.51		

5. Conclusion and future work

This paper discusses the fusion of LiDAR and aerial ortho-rectified imagery data for the construction of 3D city models. In the proposed approach data classification was carried out with an overall accuracy of almost 83.51%. The horizontal accuracy of building outlines reached 0.51 m, while vertical accuracy ranged between 15- 20 cm. As a future step and in order to maximize the benefits of the proposed method, the authors aim at increasing the degree of automation and level of details. Due to the limitation of LiDAR data on hand, current work has been done with only one data set. In the future it is planned to process more and larger test areas in order to confirm the results found so far.

Acknowledgements

The Authors wish to acknowledge AAMHatch for the provision of the UNSW dataset.

References

Arefi, H., J. Engels, M. Hahn and H. Mayer (2008). Levels of detail in 3D building reconstruction from LIDAR data. International Archives of the Photogrammetry, Remote Sensing and Spatial Information Sciences. 37, 485–490

Babuska, R. (2001). Fuzzy and neural control - DISC course lecture notes. Faculty of Information Technology and Systems, Delft University of Technology, Delft, the Netherlands.

Bora, D. and A. Gupta (2014). A comparative study between fuzzy clustering algorithm and hard clustering algorithm. International Journal of Computer Trends and Technology (IJCTT) – Vol 10, No. 2, 108 – 113.

Chen, J., Z. Qin, Z. and J. Jia (2008). A weighted mean subtractive clustering algorithm. Information Technology Journal 7(2), 356-360.

Chiu, S. (1994). Fuzzy model identification based on cluster estimation. Rockwell Science Center Thousand Oaks, California, 91360.

Douglas, D. and T. Peucker (1973). Algorithms for the reduction of the number of points required to represent a digitized line or its caricature. The Canadian Cartographer 10(2), 112–122.

Fikri, A. (2012). A methodology for processing raw LiDAR data to support urban flood modeling framework. Ph.D. Dissertation, Institute for Water Education, Delft University of Technology.

Förstner, W. and E. Gülch (1987). A fast operator for detection and precise location of distinct points, corners and centres of circular features. In Proceedings of the ISPRS Intercommission Workshop on Fast Processing of Photogrammetric Data, 2–4 June 1987, Interlaken, Switzerland, 281–305.

Hongjian, Y. and Z. Shiqiang (2006). 3D building reconstruction from aerial CCD image and sparse laser sample data. Optics and Lasers in Engineering 44(6): 555-566

Jarvis, A. (2008). Integration of photogrammetric and LiDAR data for accurate reconstruction and visualization of urban environments. MSc. Dissertation, Department of Geomatics Engineering, University of Calgary.

Kada, M. and L. McKinley (2009). 3D building reconstruction from LiDAR based on a cell decomposition approach. International Archives of the Photogrammetry, Remote Sensing and Spatial Information Sciences, 38, 47–52.

Kwak, E. (2013) Automatic 3D building model generation by integrating LiDAR and aerial images using a hybrid approach. Ph.D. Dissertation, Department of Geometrics Engineering, University of Calgary.

Langue, W. (2007) Object-oriented model based 3D building extraction using airborne laser scanning points and aerial imagery. M.Sc. Dissertation, Institute of Geo-Information Science and Earth Observation, ITC.

Leela, V., K. Sakthi priya and R. Manikandan (2014). Comparative study of clustering techniques in Iris data sets. World Applied Science Journal, 29, 24-29.

Moertini, V.S. (2002). Introduction to five data clustering algorithms. Integral, Vol 7, No 2, 87 – 96.

Park, H., M. Salah and S. Lim (2011). Accuracy of 3Dmodels derived from aerial laser scanning and aerial ortho-imagery. Surveying Review, 43, 320, 109-122.

Partovi, T., H. Arafi, T. Kraub and P. Reinartz (2013). Automatic model selection of 3D reconstruction of buildings from satellite imagery. International Archives of Photogrammetry, Remote Sensing and Spatial Information Sciences. Volume XL-1/W2. Tehran, Iran.

Ruijin, Ma. (2004). Building model reconstruction from LiDAR data and aerial photographs. PhD thesis, The Ohio State University.

Salah, M. (2010). Towards automatic feature extraction from high resolution digital imagery and LiDAR data for GIS applications. Ph.D. Dissertation, Department of Surveying Engineering, University of Benha.

Shapiro, L. and G. Stockman (2011). Computer vision. Prentice Hall, New Jersey.

Sirmacek, B., H. Taubenboeck and P. Reinartz (2012). A novel 3D city modelling approach for satellite stereo data using 3D active shape models on DSMS. International Archives of the Photogrammetry, Remote Sensing and Spatial Information Sciences, Volume XXXIX-B3, 2012-XXIIi ISPRS Congress, Melbourne, Australia.

Suganya, R. and R. Shanthi (2012). Fuzzy C- means algorithm- A review. International Journal of Scientific and Research Publications, 2(11), November 2012 Edition, ISSN 2250-3153.

Tack, F., G. Buyuksalih and R. Goossens (2012). 3D building reconstruction based on given ground plan information and surface models extracted from spaceborne imagery. ISPRS Journal of Photogrammetry and Remote Sensing, vol (67), 52-64.

The MathWorks (2015). 3-D visualization. The MathWorks, Inc. http://www.mathworks.com/help/pdf_doc/matlab/visualize.pdf

Velmurugan, T. and T. Santhanam (2011). A comparative analysis between k-medoids and fuzzy C-means clustering algorithms for statistically distributed data points. Journal of Theoretical and Applied Information Technology, Vol 27 No 1, 19 – 30.

Journal of Geomatics Vol 11 No. 1 April 2017

Route and optimal location analysis of egg supplychain using geo-spatial technology

M. Krishnaveni, Sandeep Kumar Patakamuri and A. Rajeswari
Centre for Water Resources, Anna University, Chennai, India- 600 025
Email: mkveni@annauniv.edu, sandeep.patakamuri@gmail.com, raje_kesavan@yahoo.co.in

(Received: Jun 07, 2016; in final form: Mar 20, 2017)

Abstract: Supply chain of eggs is marred with inefficiencies starting from field level, till it reaches the customers. Present work concentrates on bringing down the cost of delivery of eggs from collection centres to the distribution centres by incorporating geospatial technologies in identifying optimal route rather than following vehicle driver's own discretion. Data pertaining to eggs handled per day, travel routes, travel time and fuel expenses etc., are collected by conducting on-field questionnaire survey. GPS survey was conducted to collect the spatial information of collection centres and distribution centres. The study results in identifying three optimal routes and also to identify four suitable sites for establishing new distribution centres. The optimal route identified in the study reduces the travelling distance by approximately 40km per day and thereby reducing fuel consumption.

Keywords: Location Based Services (LBS), Network analysis, Resource optimization, Routing, GIS

1. Introduction

Supply chain management is an integrated approach which synchronizes a series of processes involved in business management starting from raw material procurement to product delivery and customer feedback collection (Oliver and Webber, 1982; Hewitt, 1994; Brimer, 1995; Cooper, 1997; Pirim et al., 2014). In present world scenario, members of the supply chain compete as an integral part of supply chain links rather than as individual entities (Min and Zhou, 2002; Arshinder et al., 2011). Sustainability of any business depends on strategically well designed supply chain management by incorporating all the members of supply chain at different levels (Gardner and Cooper, 2003; Carter and Easton, 2011). Supply chain management has the potential to stimulate intra national and cross boundary marketing (Roekel et al., 2002).

Transportation and storage of goods are important components of supply chain management. Optimization of resources is possible by incorporating spatial information in resource management and planning (Koo et al., 1985; McKenzie et al., 1999; Wilson et al., 2004; Kumar and Agrawal, 2011).With the recent advancements in the field of Geographical Information Systems (GIS), it is possible to incorporate path constrains taking into consideration of the distances traversed by actual vehicle routes (Keenan, 2008).

Fresh eggs, irrespective of the farms where they are produced, would have almost same quality and taste. In a competitive market, profitability could be achieved by lowering the transportation costs, reducing breakages and timely transportation (Chakraborty, 2011). GIS has the ability to optimize the travel routes there by saving time and fuel resources. In agriculture sector, there are enormous challenges to incorporate spatial decision making in supply chain management (Opara, 2003; Ruteri and Xu, 2009; Gemesi, 2010). By suitable selection of spatial data along with some other ancillary data helps in identifying suitable locations for establishing new facilities (Melo et al., 2009; Zhang et al., 2011) or to find optimal routes for transportation of goods from one location to the other in a distribution network, till it reaches the end customer (Ljungberg and Gebresenbet, 2004; Sambrani and Subhas, 2009; Gebresenbet et al., 2011; Bosona and Gebresenbet, 2013).

Present study identified the reasons for inefficacy in the current practices and tried to bring down the cost incurred in delivery of eggs from collection centres to distribution centres and also to identify the suitable location for establishing new distribution centres. An estimated 25% of Green House Gas Emissions (GHGs) are attributed to transport sector. Out of this 75% of the emissions are resulting from road transport (Chapman, 2007; IPCC, 2007; Määttä-Juntunen et al., 2011).

2. Study area and data description

Out of more than three crore eggs produced in Tamilnadu state of India, Chennai alone consumes approximately 50 lakh eggs per day (Hindu, 2012). South Chennai region is considered in the present study to understand the existing supply chain practices and to identify optimal transport routes to enable high profitability with minimal damages. The interesting fact in the supply chain of eggs in the study area is the ubiquitous presence of eggs. But the complex network of supply chain behind this presence is often overlooked. The geographical extent to the south of Adyar river is considered as South Chennai. It consists of four zones namely Alandur, Adayar, Perungudi and Sholiganallur which comprises of 45 wards with an area of 143 square kilometres. All the distribution centres in the study area receive eggs from two collection centres, one in Triplicane and the other in Perungulathur. Collection centre in Perungulathur covers only three distribution centres and hence it is not considered in this analysis. Location map of the study area is shown in the Figure 1.

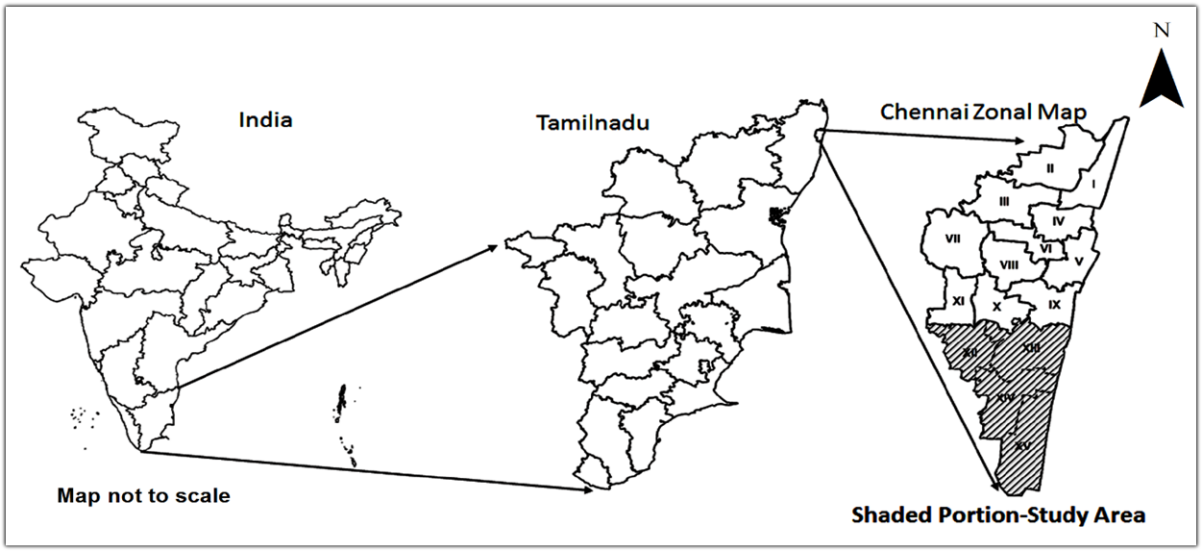

Figure 1: Location map of the study area

3. Materials and methods

Present study involves primary data collection from field visits using hand held GPS to obtain the spatial information of egg distribution centres. Data pertaining to current management practices like the volume of eggs handled per day, travel routes followed by the drivers, time of travel, fuel expenses etc., are collected by conducting user interviews. Secondary data on road network layer was obtained from Open Street Maps and refined as per the requirements of the study. Land use and ward maps were collected from various governmental sources. Incorporating these parameters assists in spatial decision making. Figure 2 shows the detailed flow chart of the methodology followed in the present research.

There are a large number of methods available in generating optimal routes. Network analysis has the ability to handle real world constraints in solving vehicle routing problems. The information collected from the drivers and the distribution centres indicated that the route followed by the drivers are clearly based on their own discretion which caused high fuel expenses (Goodchild, 2000; Bender et al., 2001; Martin et al., 2001; Papinski and Scott, 2011).

Road network layer is downloaded from open street maps data and clipped to the extent of South Chennai and used in network analysis. Road network data base is generated from ArcCatalog menu by modeling the turns, connectivity, elevation, cost metrics, network restriction and driving directions. Distribution centre layer is generated using the GPS points collected from field visit. South Chennai ward map is generated by digitizing Chennai wards map obtained from Corporation of Chennai. All the maps are generated at a uniform scale of 1:75,000 and added to ArcMap environment to proceed with route analysis.

Three optimal routes were requested to be generated from collection centre to the distribution centres as identified from the field interview conducted at collection centre. The Network Analyst window present in the Network Analyst toolbarenables input of network parameters like origin, destination, point barriers, line barriers and polygon barriers and the network restrictions like speed limits, one-way roads etc. The distance travelled, time consumed, serviceable area, closest facility, origin-destination cost matrices, Vehicle Routing Problems etc., were provided to the network analysis which were used in generating optimal path. The optimum routes are generated in a way to cover all the distribution centre while travelling lesser distances in a short span of time. This will ensure fuel savings and improved profitability.

In the second stage, suitable sites for establishing new distribution centres are identified by using the data on egg demand in an area and the handling capability of the existing distribution centres. GIS has the capability to identify the optimal site identification, making use of a well-defined criteria passed during spatial decision making (Ma et al., 2005; Kar and Hodgson, 2008; Irizarry et al., 2013; Hiremath et al., 2013).

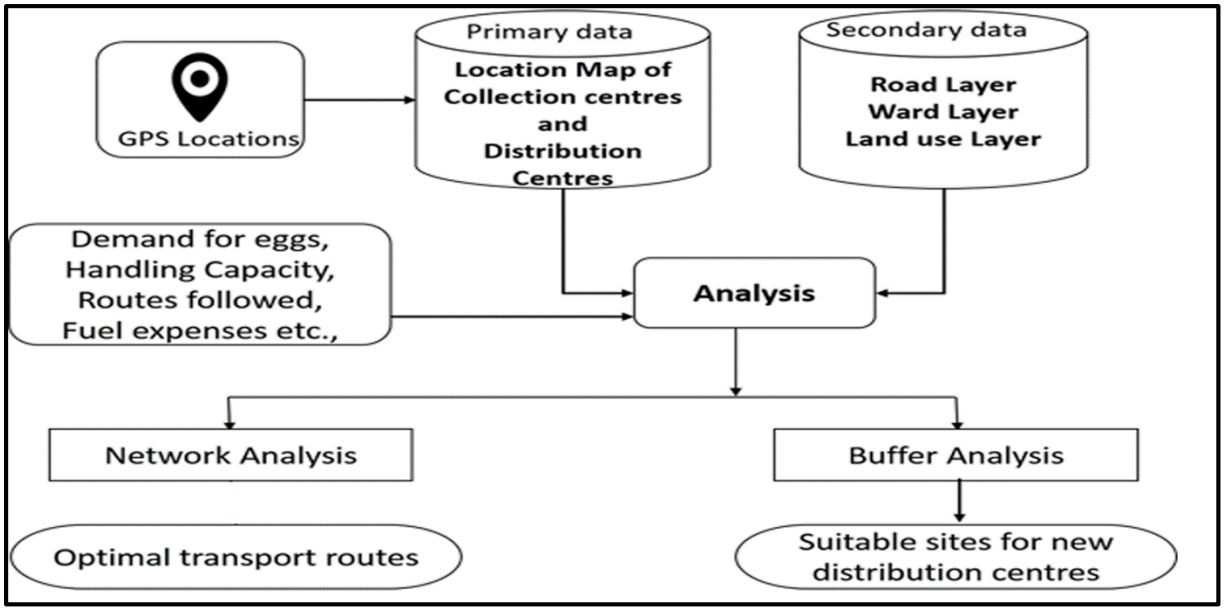

Figure 2: Methodology flow-chart for route and optimal location analysis of egg supply chain

4. Results and discussions

Route optimization for egg distribution aims at minimizing the cost of travel involved in transporting from one location to another either in terms of the number of trips required or total distance travelled or through a combination of these two factors. Identifying the existing path taken and the distance travelled by the drivers was a difficult task as thedrivers were allowed to take different routes at different times of the day. This made the comparison of the data a challenging task. Nevertheless, enormous efforts were taken to obtain the information from the drivers pertainingtotheroutestheyfollow and distance and time estimations were made.

All the spatial layers and relevant network constrain parameters required to run the network analysis were provided to the network analyst and three routes were generated that cover all the distribution centres at a reduced travel distance in a short time period. The paths optimized for transportation of eggs is depicted in Figure 3.

Without the optimal path selection, the drivers were estimated to be travelling approximately 150 km. This distance could be reduced to 110 km per day (about 27 %) by following optimal path. This leads to a phenomenal savings in terms of fuel expenses.

From the interviews with distributors, the operational convenience is found to be about 750 metres for any given distribution centre. Hence buffers zones are created around the distribution centre with a circular radius of 750metres as shown in Figure 4.

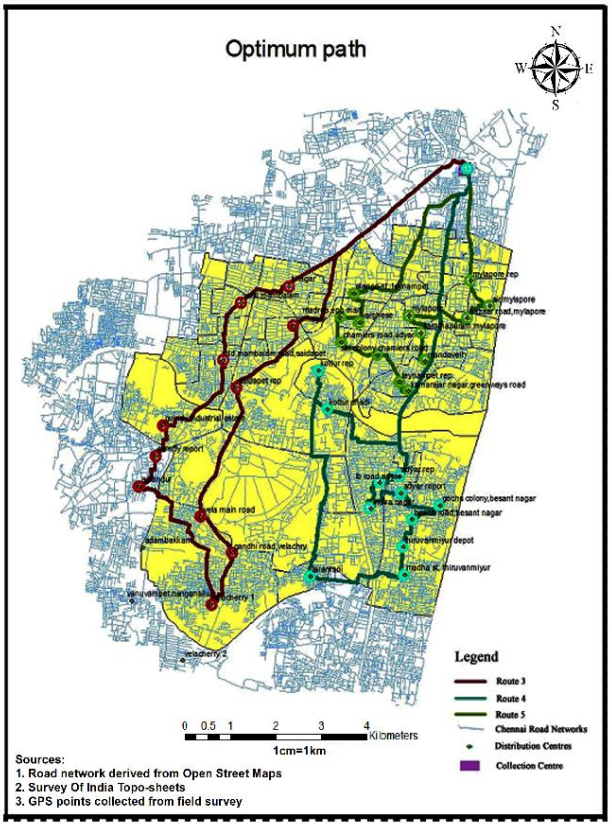

Figure 3: Map showing shortest path for transportation of eggs

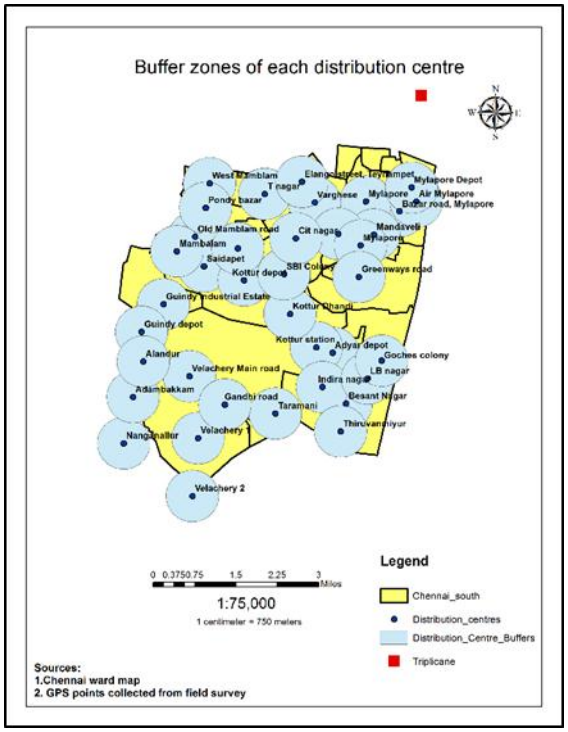

Figure 4: Map showing distribution centres and their operational convenience (750m buffer)

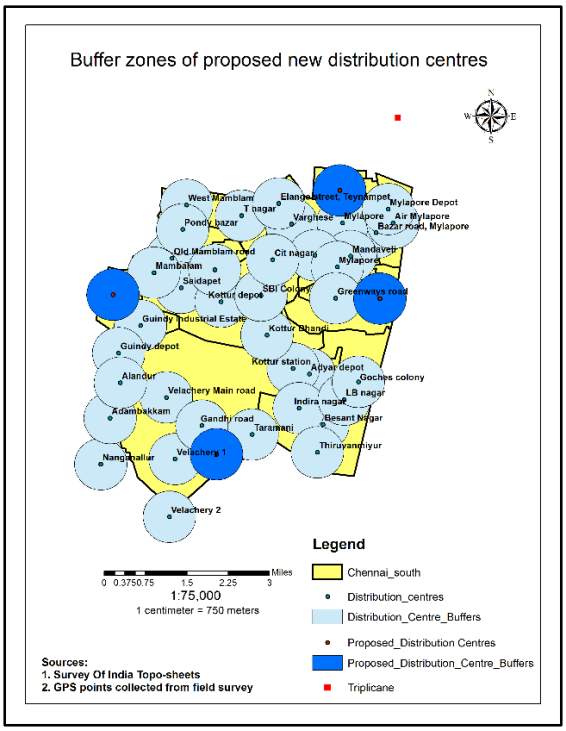

Figure 5: Map showing proposed distribution centres and their operational convenience (750m buffer)

From the buffer analysis, it is found that there were regions in the study area which are not covered by any of the existing distribution centres but eggs were supplied from surrounding distribution centres. And some regions are found to be served by more than one distribution centre.

The viability for setting up a new egg distribution centre has been decided based on the demand in the region and the minimum handling capacity of existing distribution centres. From the statistics collected from distribution centres (Appendix A), it has been decided that any region with a demand of 8000 eggs per day is ideal for setting up a new distribution center. The rationale behind this idea is based on the assumption that it is the minimum Return on Investment (ROI) that people in this business consider worthy.

The study identified four sites to establish new distribution centres as depicted in Figure 5. All these distribution centre, if operate with mutual collaboration, will improve the efficiency of egg distribution.

In South Chennai, six distribution centres are being served by the collection centre at Perangulathur location. Irregularities are observed during field observations ranging from lack of record keeping to lack of control over delivery routes. Most of the data required were either inaccurate or not available and in worst case scenario, distributors were not willing to part with the data. Due diligence was paid to rectify errors and to ensure the data quality. It is recommended to educate the distributors and retailers of the importance in keeping record of the sales and business transactions.

Egg shell breakages are directly proportional to transportation and handling activities. Transportation and handling activities start at the farm level and continue till it reaches the consumers. Since the study is concerned only with transportation from collection centres to distribution centres and limited to the southern parts of Chennai, amount of breakages in the earlier part were unknown. Hence, establishing relationship between breakages and transportation was not possible. However, the officials at the National Egg Coordination Committee pointed out that the breakages might get reduced to 6-8% from the 8-10%.

In some of the regions, density of distribution centres is very high and the operational area overlap in such regions. It is found that traders operate on their own discretion which culminates in inefficient practices. And some of the distribution centres found to be operating on larger geographical area. It is proposed to establish new distribution centre in the areas with high demand for eggs and lesser distribution density. It is suggested that all the distributors and traders operate with proper understanding and collaboration among them in order to improve profits and conserve resources. This study is easily reproducible at various geographical locations and will help in saving resources and will aid in sustainable business development.

5. Conclusion

The study identified three optimal routes for supplying eggs in south Chennai. It is suggested to add four new distribution centres. The optimal route identified in the study reduces the travelling distance by approximately 40km per day (about 27 %) and thereby reducing fuel consumption.

Acknowledgements

Authors would like to thank undergraduate students of our centre for their efforts in collecting field data and involvement in this work. We are thankful to all the distributors and vehicle drivers for their valuable time and information in successful completion of this project.

References

Arshinder, K., A. Kanda andS.G. Deshmukh (2011). Supply chain coordination under uncertainty. Vol 115. doi:10.1007/978-3-642-19257-9.

Bender, T., H. Hennes, K. Kalcsisc,M.T. Melo andS. Nickel (2001). Location software and interface with GIS and supply chain management. Facil Locat Appl Theory, vol 23(23), 233-274.

Bosona, T. and G. Gebresenbet (2013). Food traceability as an integral part of logistics in food and agricultural supply chain. Food Control. 33(1), 32-48.

Brimer, R.C. (1995). Logistics networking. Logist Inf Manag. 8(4), 8-11. doi:10.1108/09576059510091850.

Carter, C.R. and P.L.Easton (2011). Sustainable supply chain management: Evolution and future directions. Int J Phys Distrib Logist Manag. 41(1), 46-62. doi:10.1108/09600031111101420.

Chakraborty, S. (2011). An exploratory study of important aspects of egg market in Kolkata. SAMVAD-Res J Symbiosis Inst Bus Manag. III(September), 13-34.

Chapman, L. (2007). Transport and climate change: a review. J Transp Geogr. 15(5), 354-367.

Cooper, M. (1997). Supply chain management: More than a new name for logistics. Supply Chain Manag An International Journal, 5(4), 206-213. doi:10.1108/09574099710805556.
ESRI. ArcGIS.(2007). Network Analyst - Parte III.

Gardner, J.T. and M.C.Cooper (2003). Strategic supply chain mapping approaches. J Bus Logist, 24(2), 37-64. doi:10.1002/j.2158-1592.2003.tb00045.x.

Gebresenbet, G., I. Nordmark, T. Bosona and D. Ljungberg (2011). Potential for optimised food deliveries in and around Uppsala city, Sweden. J. Transp. Geogr., vol 19(6), 1456-1464.

Gemesi, H.G. (2010). Food Traceability information modeling and data exchange and GIS based farm traceability model design and application. Available http://lib.dr.iastate.edu/etd/11597/.

Goodchild, M.F. (2000). GIS and transportation: Status and challenges. Geoinformatica, vol 4(2), 127-139. doi:10.1023/A:1009867905167.

Hewitt, F. (1994). Supply chain redesign. Int J Logist Manag., 5(2), 1-10. doi:10.1108/09574099410805162.

Hiremath, D.B., N.R. Patil andA. Dasgupta (2013) Geospatial technique for potato cold storage allocation. J Geomatics. vol7(1), 13-17.

IPCC. (2007)IPCC Fourth Assessment Report (AR4). Vol 1. Available http://www.ipcc.ch/publications_and_data/publications_ipcc_fourth_assessment_report_wg2_report_impacts_adaptation_and_vulnerability.

Irizarry, J., E.P. Karan andF. Jalaei (2013). Integrating BIM and GIS to improve the visual monitoring of construction supply chain management. Autom Constr., 241-254.

Kar, B. andM.E. Hodgson (2008). A GIS-based model to determine site suitability of emergency evacuation shelters. Trans GIS. vol 12(2), 227-248.

Keenan, P. (2008). Modelling vehicle routing in GIS. Oper. Res., (3), 201-218.

Koo, W.W., S.R. Thompson andD.W. Larson (1985). Alternative transportation rate and cost structures: A linear programming model. In: Transportation Models for Agricultural Products, 125-153.

Kumar, S., and S. Agrawal (2011) GIS as a decision support for supply chain management. Geospatial World Forum, 253.

Ljungberg, D. andG. Gebresenbet (2004). Mapping out the potential for coordinated goods distribution in city centres: The case of Uppsala. Int J Transp Manag. vol 2(3-4), 161-172.

Ma, J., N.R. Scott,S.D. DeGloria and A.J. Lembo (2005). Siting analysis of farm-based centralized anaerobic digester systems for distributed generation using GIS. Biomass and Bioenergy. vol 28(6), 591-600.

Määttä-Juntunen, H., H. Antikainen,O. Kotavaara andJ. Rusanen. (2011). Using GIS tools to estimate CO2 emissions related to the accessibility of large retail stores in the Oulu region, Finland. J Transp Geogr. vol 19(2), 346-354.

Martin, A.M, P.M.O. Owende, N.M. Holden, S.M. Ward andM.J. O'Mahony (2001). Designation of timber extraction routes in a GIS using road maintenance cost data. For Prod J, vol 51(10), 32.

McKenzie, A.M., P.E. Laferney, E. Wail and H.D. Otwell (1999). An economic evaluation of optimal intermodal soybean flows in Arkansas with projected effects of the North American free trade agreement. University of Arkansas, NTL/TIRS report, Accession Number: 00763754, Available https://ntl.bts.gov/lib/9000/9700/9794/FR1491.pdf

Melo, M.T.,S. Nicke and F.Saldanha-da-Gama,(2009). Facility location and supply chain management - A review. Eur. Journal Oper, Res., vol 196(2), 401-412.

Min, H. and G.Zhou (2002). Supply chain modeling: Past, present and future. Comput Ind Eng., 43(1-2), 231-249. doi:10.1016/S0360-8352(02)00066-9.

Oliver, R.K. andM.D. Webber (1982). Supply-chain management: Logistics catches up with strategy. Outlook, 5(1), 42-47.

Opara, L.U. (2003). Traceability in agriculture and food supply chain: A review of basic concepts, technological implications, and future prospects. J Food Agric Environ., vol 1(1) 101-106. Available http://www.world-food.net.

Papinski, D. andD.M. Scott (2011). A GIS-based toolkit for route choice analysis. J Transp Geogr. vol 19(3), 434-442.

Pirim, H., U. Al-Turki and B.S.Yilba (2014).Supply chain management and optimization in manufacturing. Springer.

Roekel, J., Van, S. Willems,M. Dave and W.U.Boselie (2002).Agri-supply chain to stimulate cross-border trade in developing countries and emerging economies. Available www.infodev.org/en/Document.923.pdf.

Ruteri, J.M. and Q.Xu,(2009). Supply chain management and challenges facing the food industry sector in Tanzania. Int. J. Bussiness Manag., vol 4(12), 70-80.

Sambrani, V.N. andM.S. Subhas (2009). Routing analysis in Supply Chain Management (SCM)–A manager's perspective. Geospatial world forum.

The Hindu. (Daily Newspaper). Chennai consumes 55 lakh eggs every day. http://www.thehindu.com/news/cities/chennai/chennai-consumes-55-lakh-eggs-every-day/article2995772.ece. Published August 9, 2012. Accessed October 10, 2014.

Wilson, W.W., D.C.E. Carlson,and B.L. Dahl (2004). Logistics and supply chain strategies in grain exporting. Agribusiness, 20(4), 449-464. doi:10.1002/agr.20026.

Zhang, F, D.M. Johnson and J.W.Sutherland,(2011). A GIS-based method for identifying the optimal location for a facility to convert forest biomass to biofuel. Biomass and Bioenergy, vol 35(9), 3951-3961.

Journal of Geomatics Vol 11 No. 1 April 2017

Spatio-temporal dynamics of mines in Singrauli, India: An analysis using geospatial technology

Firoz Ahmad and Laxmi Goparaju
Vindhyan Ecology and Natural History Foundation, Mirzapur, Uttar Pradesh, India
Mirzapur-231001, Uttar Pradesh, India
Email:goparajulaxmi@yahoo.com

(Received: Feb 03, 2017; in final form: Feb 24, 2017)

Abstract: Forests are at present facing threat because of various reasons. One such reason is the blooming of mining industry. It has many adverse impacts on the forest environment, water resources and wildlife habitat. Evaluation of such impacts time to time and controlling the negative aspects to promote sustainable living would benefit the nation and the people.The present study is an attempt to evaluate the spatial and temporal expansion of mines near Singrauli district (Uttar Pradesh and Madhya Pradesh border) since 1976. Amidst the dry tropical forests, the mines are prevalent since 1980s and are now a threat to the health of these forests. Satellite remote sensing data have the potential to observe large areas at regular intervals. Further, in GIS domain, area statistics can be computed which help in quantifying the actual loss or gain in various LULC classes. The temporal datasets for the present case were from Landsat (1976, 2002, 2010 and 2015). After the image processing and classification, the expansion of mines and transformation of various LULC classes were observed. The loss of forests and conversion to other land use was analyzed between different time periods. It was observed that the annual increase in mines area is 4.25 times higher when compared with the period (2010-2015) to (1976-2002). Continuous losses in the annual forest cover was due to increase in the mining area between the study periods (1976-2015) was observed.

Keywords: Geographic Information System (GIS); Land Use Land Cover (LULC), Mining, Remote sensing data, Satellite imagery

1. Introduction

Natural resources like oils, minerals, water, forests and fertile land have been the backbone of human existence by providing the necessities of life such as food, fodder, medicines and fuel. Over the years, they have been exploited immensely for economic gains. Increasing population and the quest for power has led to extraction of minerals, especially coal, to meet the ever increasing demand. Mining and its related activities in forested region are responsible for a change in the land use/ land cover (LULC) and have a profound effect on the forest ecosystems (Greenpeace, 2011).

India is a country which has large reserves of minerals. It is the third largest producer of coal (565.6 MT) and has the fifth largest coal reserves (of 301.6BT) in the world (Energy statistics 2016). The Government of India has facilitated and favored the mining sector by increasing the lease period. The enforcement of the MMDR [Mines and Mineral (Development and Regulation) bill, 2015] has given an opportunity to dig more and for longer time periods. In light of these mining dominated environment, it is necessary to monitor the status of the forests and water bodies in proximity to such areas.

There are many states in India which harbor rich mineral deposits within their forest cover. One of them is the Singrauli area situated at the border of Uttar Pradesh (near Sonebhadra district) and Madhya Pradesh (Sidhi and Surguja districts) and is known as the energy capital of India with rich reserves of coal. It is the largest industrial area of the South east Asia. The presence of GovindBallabh Pant Sagar (which came into existence in 1960s) in the vicinity has facilitated the establishment of many thermal power plants. Some of them are like National Thermal Power Plant in 1977, National Coalfields Limited in 1986, Singrauli Super Thermal Power Plant in 1982 and Vindhyachal STP in 1987 (Pandey, 2005). Some of the coal blocks are Jayant, Chilkadand, Dudhichua, Basi and JogiChaura.

By the year 2009, Singrauli was declared as one of the critically polluted areas in an analysis conducted by Central Pollution Control Board and MoEF in collaboration with IIT, Delhi. It ranked ninth among the list of 14 critically polluted areas with an index of 81.79 (CPCB, 2009). As a result, a temporary moratorium was imposed in January, 2010, when no new mining lease was sanctioned and expansion was halted. The ban was lifted in July, 2011. The “no –go” areas did not allow mining within its premises while the “go” areas were permitted after 2009. The expansion of mines and leases sanctioned to upcoming mines was more prevalent after 2008-2009 and a rapid expansion of mines is observed in between 2010-2015. The new mines are finding place in the Moher basin on the left side of the present existing blocks. As analysed by Singh (2014), it was seen that mining area was lowest in 2000 between the study periods analysed by him (1991-2011).

It has also decimated the growth of the tropical dry deciduous forests and has been singled out as an Eco sensitive zone (Singh et al., 2003). Further, this region is characterized by hot summers, erratic and scanty

rainfall and moisture stress conditions. Deforestation, conversion of forest to agricultural farmlands and subsequently losing it to urbanization has become the norm of the dry tropical deciduous forests. Thus the fragile ecosystem is now on the verge of desertification (Singh et al., 1991). The mines operating in Singrauli are open cast mines (Chopra, 2011).

Spatio-temporal analysis of LULC patterns are required to understand the impacts of minig activities on the environment. In this endeavour, satellite remote sensing provides the suitable data which can be processed and interpreted in a precise manner. The availability of satellite data at various resolutions and time period helps to study the situation at various spatial scales and time periods.

Singrauli has been the focal point for research by many enthusiasts. Areendran et al. (2013) have analysed LULC changes using multidate satellite data. Changes were quantified using landscape metrics and using Markov transition matrix.They noted that dense forests decreased from 1978 to 2010. In another study by Khan and Javed (2012), a comparative analysis of LULC was done for 2001 and 2010 using post classification comparison. The study concluded that before industrialization and mining, this area was covered with tropical dry deciduous forests. Forest has been destroyed to make way for infrastructure establishment and various industries.

Changing landscape patterns were analysed by Viswakarma et al. (2016) in Singrauli using Landsat data of 1991, 2000 and 2014. They noted that the rate of deforestation is more from 2000-2014 than 1991-2000. The mines have increased rapidly in between 2000-2014 and many forest patches have either disappeared or got converted to other land use. In all these studies it was observed that progress of mining activities has caused forest loss and much transformation in LULC patterns. Towards this, the present study focusses on the impact of mining on the forests and LULC pattern using satellite remote sensing data and GIS. It analysed the spatio - temporal changes related to mines and its expansion over the years 1976, 2002, 2010 and 2015 along with simultaneous forest loss.

2. Study area

The study area is located at the border of the two states that is Uttar Pradesh and Madhya Pradesh. It extends between latitude $24^0 00' 31.39'' N$ to $24^0 16' 14.98'' N$ and longitude $82^0 27' 58.05'' E$ to $82^0 50' 19.16'' E$. (figure 1). The Sonbhadra and Mirzapur districts of Uttar Pradesh form the eastern and the northern boundary. The topography is distinctly characterized by undulating terrain with altitude ranging from 243m to 640m above mean sea level. The climate of this region is mainly tropical to semi-arid. It is marked by three distinct seasons in a year. The summer season begins in March/April till June, the rainy season is from July to September and winter season is from October to February/March. The mean annual maximum and minimum temperatures are 37°C and 20°C, respectively. The soils in the study area vary from loamy sand to clay. Alluvium soil exists in the plain areas; colour varies from red to yellow.

3. Materials and methods

3.1 Data acquisition and preprocessing

The required Landsat satellite imagery of years 1976, 2002, 2010 and 2015 were downloaded from the USGS Earth explorer database and the specifications are given in table 1. The scenario before the start of mining activity and after can be studied in these years.

All the datasets belong to the December month, when the vegetation is in good condition. Tropical dry deciduous forest has a characteristic phenology marked by leaf fall during the dry season. Each dataset was found to be cloud free and was radiometrically and geometrically corrected. The image processing and interpretation for delineation of mining area and other LULC classes was performed in ERDAS Imagine software. The generated maps were studied and analyzed to detect the expansion of mines temporally and spatially. The detailed methodology is given through a schematic flowchart (Figure 2).

Table 1: Details of the satellite data acquired

Years	Satellite	Sensor	Spatial resolution	Dates
1976	Landsat	MSS	60 meter	22/12/1976
2002	Landsat	ETM+	30 meter	21/12/2002
2010	Landsat	TM	30 meter	03/12/2010
2015	Landsat	OLI	30 meter	01/12/2015

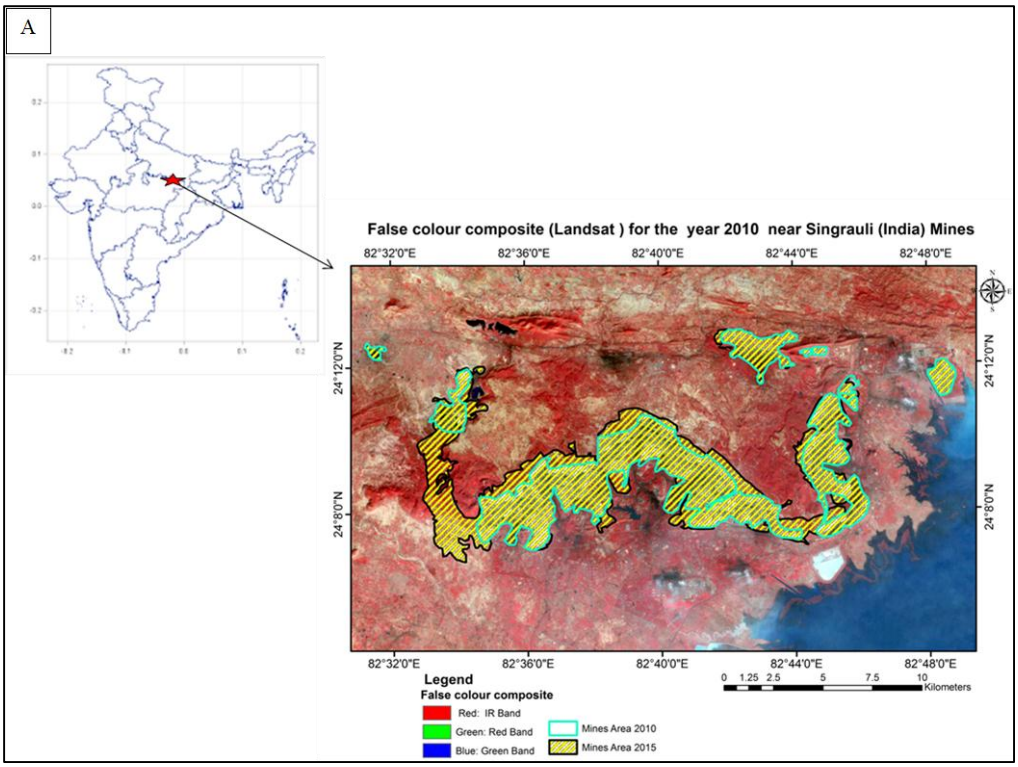

Figure 1: A) Map of India; B) FCC showing the location of Singrauli coal fields and overlay of mines boundary for the year 2010 and 2015

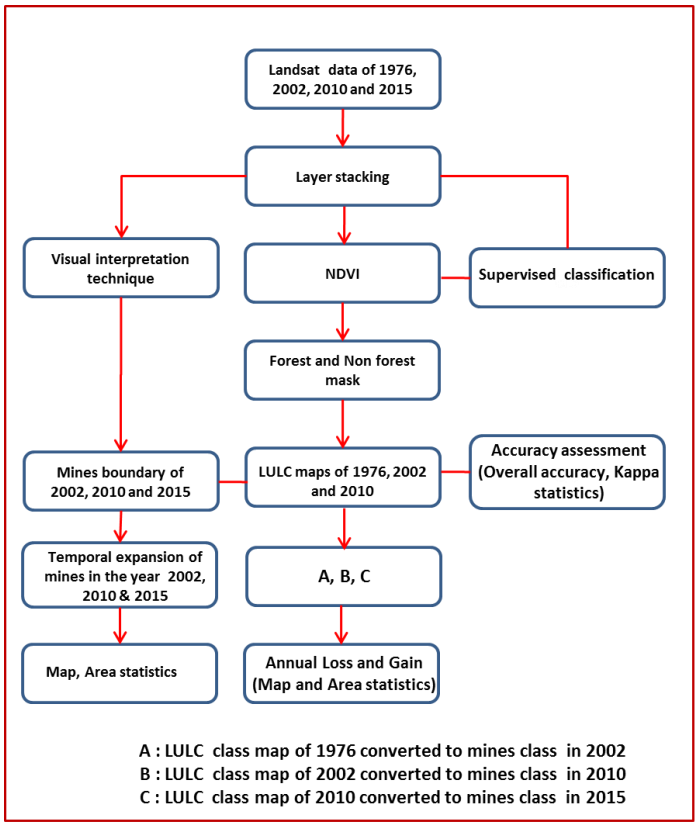

Figure 2: Schematic flowchart for analyzing the expansion of mines

3.2 Image processing and classification

Each of the satellite images was first enhanced to increase its visual interpretability. The boundary of the mines was visually interpreted on the false colour composite (FCC) and extracted from each of the datasets of time periods 2002, 2010, 2015. In the year 1976, no such mining area was visible as the mines were not established by that time. To explain the contribution of each year in expansion, it has been elaborated briefly below.

2015 mining area= 2002 mining area +(expansion from 2002-2010) mining area +(expansion from 2010-2015) mining area
2010 mining area = 2002 mining area +(expansion from 2002-2010) mining area
2002 mining area = zero (no mines was visible in 1976 Image) + (expansion from 1976-2002) mining area.

The individual shape file of the boundary of mines for 2002, 2010 and 2015 were brought in ArcGIS and integrated for generating the shape file of mines expansion between the period 1976-2002, 2002-2010 and 2010-2015.

The Landsat imagery for the year 2015 was not classified but only used to generate the boundary of mines visually because the objective of our study was to see the mines expansion till the year 2015.
For the datasets of 1976, 2002 and 2010, Normalized Difference Vegetation Index (NDVI) was executed to delineate vegetation. Further, by visual interpretation, the derived vegetation was utilized to generate two masks viz forest and non-forest.

The supervised classification technique (maximum likelihood) was performed on each data set to delineate different LULC classes viz., dense forest, open forest, water, other class. The training sets were given (9-10) for each class distributed uniformly throughout the image. Non forest mask was used to extract the other vegetation class. Finally all the LULC classes were integrated in model maker of ERDAS Imagine to obtain a single classified dataset. A brief description of each class is given in the table 2.

Accuracy assessment was executed for each classified dataset1976, 2002 and 2010 years for evaluating the quality of classification. Random sampling points were generated for various classes of the classified dataset. Confirmation was based on ground truth. Other ancillary and literature sources also assisted in confirming that the classified data matched with the ground truth. The generated shape file of mines expansion for the period of 1976-2002, 2002-2010 and 2010-2015 was used to subset classified output from 1976, 2002 and 2010 respectively for further analysis.

Table 2: Description of various LULC class

LULC class	Description
Dense forest	Canopy > 40%
Open forest	Canopy 10-40%
Water	Reservoirs, ponds, dam, lakes, water logged area
Others class	Areas with no vegetation cover, Waste land, Barren land, fallow, settlement and Uncultivated agricultural lands
Other vegetation	Vegetation outside the forest boundary such as trees, gardens, parks and playgrounds, grassland, agricultural lands and crop fields

The statistics for the mining area for the years 2002, 2010 and 2015 were generated and its annual expansion was calculated. Temporal change of LULC with respect to preceding time frame due to mining in 2002, 2010 and 2015 was examined. Subset of the classified LULC output of mines expansion for the period of 1976-2002, 2002-2010 and 2010-2015 was used to generate area statistics. Further, changing patterns of LULC class categories during period 1976-2002, 2002-2010 and 2010-2015 were evaluated.

4. Results

LULC maps for four study time periods were prepared. Changing patterns of LULC class categories during period 1976-2002, 2002-2010 and 2010-2015 were evaluated (see figure 3). The results are presented,

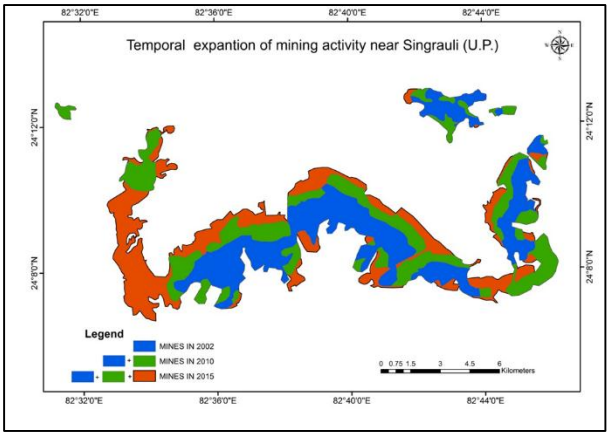

Figure 3: Temporal expansion of mines

4.1 Classification accuracy assessment

No image classification is complete until an assessment of accuracy has been performed. The overall accuracy and the Kappa statistic were also calculated and tabulated on the classified output (Table 3).

Table 3: Overall accuracy and Kappa statistic for LULC analysis

Years	% Overall Accuracy	Kappa statistic
1976	92	0.89
2002	94	0.91
2010	92	0.88

4.2 Spatial and temporal expansion of mining activity

The mining area for years 2002, 2010 and 2015 were 3515.4, 6433.92 and 9305.46 ha, respectively. Annual increase in mining area was found to be 135.2ha, 364.8ha and 574.3 ha during the period 1976-2002, 2002-2010 and 2010-2015, respectively. It was observed that the annual increase in mines area during 2010-2015 was 4.25 times higher compared with 1976-2002.

4.3 Temporal analysis (Change detection)

As the mines got established many activities related to it evolved. This resulted in changing the LULC. The boundary of mines as delineated in the present case when overlaid over the preceding classified data clarifies visually which all classes were converted at the expense of mines (Figures 4, 5 and 6). During the period 1976 -2002, it was observed that all the four LULC classes of the year were converted to one class that is mines for the year 2002 (Figure 4). The loss of dense forest, open forest, other vegetation and other class during this period were 1234.44, 930.96, 90.72 and 1259.28 ha respectively (see figure 7). The annual loss in dense forest, open forest were 47.48, 35.8 ha respectively (see figure 8).

During the period 2002 – 2010, it was noted that the loss of dense forest, open forest, other vegetation, other class and water during this period were 466.2, 369.72, 419.67, 1662.48 and 0.45 ha respectively (see figure 7). The annual loss in dense forest, open forest were 58.28, 46.22 ha respectively (see figure 8).

During the period 2010 – 2015, it is seen that the loss of dense forest, open forest, other vegetation, other class and water during this period were 526.41, 520.38, 163.98,1660.59 and 0.18ha respectively (refer figure 7). The annual loss in dense forest, open forest was 105.28, 104.08 ha respectively (refer figure 8).

From the above results, it is clear that the trend of the annual forest loss is increasing gradually due to mining activity over the whole study period (1976-2015). The annual gain in the mining area also shows an increasing trend.

5. Discussion

The coal reserves are abundant in the dry tropical forests of this region. The presence of Rihand reservoir made this place quiet suitable for locating thermal power plants as they require a continuous supply of water and coal to generate electricity. Within few years, mines as well as thermal power plants got established and later expanded during 1976 - 2000. By this time, they started polluting the air and water resources which occurred concurrently with the loss of forest cover. After the year 2000, more rapid increase in the number of mines was noticed. Around the year 2006, five super thermal power plants, namely DainikBhaskar, Essar, Hindalco, Jaypee and Reliance were set up under the private-public partnership. After 2010, it is seen that the new mines have paved way through the Moher basin. The forest land was diverted to facilitate them and more such diversions are expected in the coming days (Chakravartty, 2011). So, Singrauli hosts about 10 thermal power plants with aggregate capacity of 13,200 MW and 14 coal mines with potential production of 83 million tonnes per annum (Junega, 2012).

The Singrauli district was once dominated by tropical dry deciduous forests before the advent of mines. The forests were dense and formed a part of the Vindhyan mountain ranges (Munshi, 2013; Khan and Javed, 2012). They provided habitat to a number of wild animals. The commercially important tree species found were Acacia catechu, Diospyrosmelanoxylon and Dendrocalamusstrictus. Other economically important tree species are Anogeissuslatifolia, Butea monosperma, Bassialatifolia, Lagerstroemia parviflora, Terminalia bellirica, Boswelliaserrata, Holarrhenaantidysenterica (Singh, 2007). These were a source of livelihood to the people of this area. Due to anthropogenic pressure like mining, agriculture expansion, illegal logging etc., the dry tropical forests are being converted to open secondary forests or savannahs and native tree species fail to establish further (Singh et al., 1991; Sagar and Singh, 2004). Further, Singh (2012) conducted a study to record the plant species growing on mine spoil in Singrauli coal fields. He noticed that the flora was dominated by members of family Poaceae, Fabacea and Asteracea. Only three native tree species like Butea monosperma , Acacia catechu and Zizyphus were found.

Plantation activity was undertaken by some private companies towards the south of the present study area. Mainly *Eucalyptus* species were planted. Some of the activities were undertaken by Northern Coalfields Limited in a programme called “Green Gold”, NTPC undertook plantation programme in the townships and colonies. Monoculture plantations have yielded less significant results as native tree species failed to establish themselves in the changed environment.

Besides, the air and water in the surroundings is highly polluted with traces of Mercury, arsenic and fluoride. Water is contaminated with mercury and so is fish, which is now not worth consuming. People are suffering various ailments. Now, Singrauli is also known as "India's Minimata" and "A coal curse" (Junega, 2012).

Mining is not a natural phenomenon; it depends upon the number of leases commissioned by the Government. Many companies flout the norms and do not maintain standard emission rates. Such impacts should be monitored at regular intervals and negative impacts should be mitigated urgently. Accordingly, laws and policy decisions should be taken.

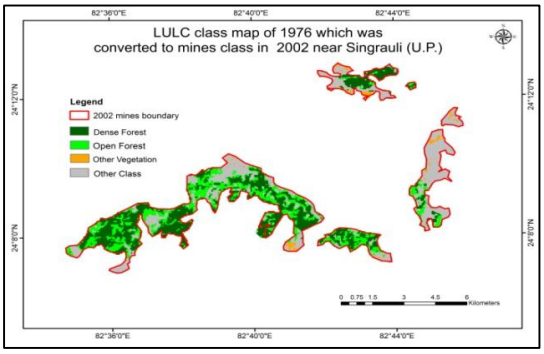

Figure 4: Temporal expansion of mines (1976-2002)

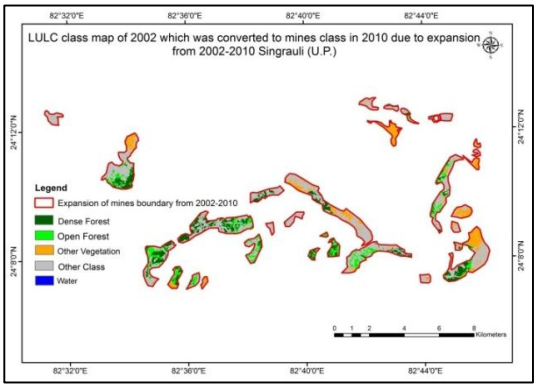

Figure 5: The expansion of mines (2002-2010)

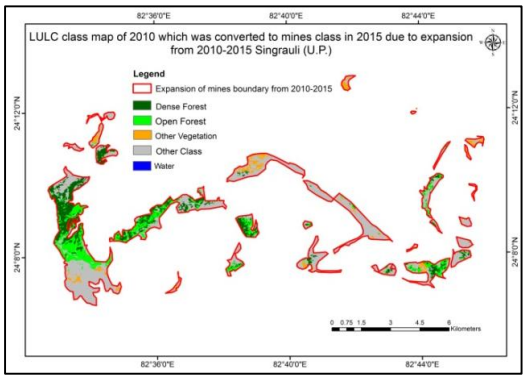

Figure 6: The expansion of mines (2010-2015)

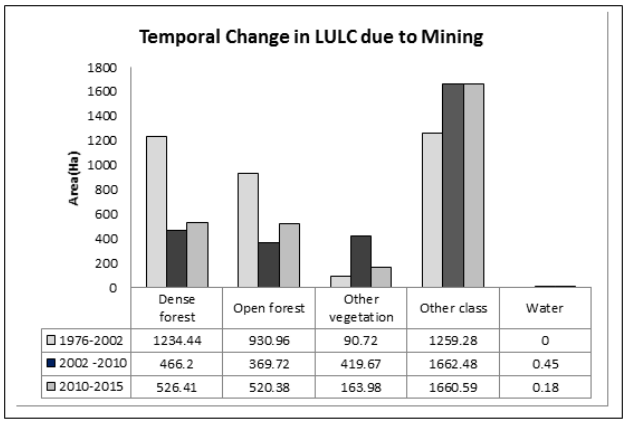

	Dense forest	Open forest	Other vegetation	Other class	Water
1976-2002	1234.44	930.96	90.72	1259.28	0
2002 -2010	466.2	369.72	419.67	1662.48	0.45
2010-2015	526.41	520.38	163.98	1660.59	0.18

Figure 7: Graph to represent temporal change in LULC due to mining

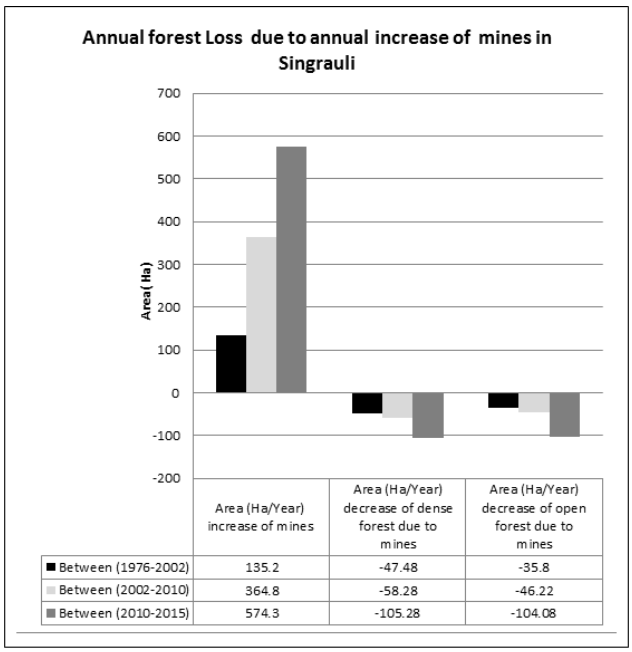

	Area (Ha/Year) increase of mines	Area (Ha/Year) decrease of dense forest due to mines	Area (Ha/Year) decrease of open forest due to mines
Between (1976-2002)	135.2	-47.48	-35.8
Between (2002-2010)	364.8	-58.28	-46.22
Between (2010-2015)	574.3	-105.28	-104.08

Figure 8: Graphical representation of annual forest loss

6. Conclusion

The study emphasizes that the satellite remote sensing data can be succesfully utilized for studying the spatial and temporal changes in LULC with respect to the mining activities. It is very helpful in monitoring at regular intervals such that the adverse impacts be identified and further appropriate steps should be taken to mitigate them. Such data is useful for staekeholders who operate the mines as well as forest officials to assist them in decision making such that they ensure that sustainability of forest ecosystems and healthy environment is maintained.

Acknowledgement

The authors are grateful to the USGS for free download of Landsat data. We express our gratitude to anonymous reviewers for their suggestions to improve the manuscript.

References

Areendran, G., P. Rao, K, Raj, S. Mazumdar and K. Puri (2013). Land use/land cover change dynamics analysis in mining areas of Singrauli district in Madhya Pradesh, India. Tropical Ecology, 54(2), 239-250.

Chakravartty, A. (2011). More forest diversions likely in Singrauli. Down to Earth. http://www.downtoearth.org.in/news/more-forest-diversions-likely-in-singrauli-34055 (accessed on 24 Feb. 2017).

Chopra, N. (2011). Land use/ land cover information at various levels from different scales of remote sensing data of Southern part of Sonbhadra district, U.P. International Journal of Geomatics and Geosciences, vol 2, No.1, 336-348.

CPCB (2009). http://www.cpcb.nic.in/upload/NewItems/NewItem_152_Final-Book_2.pdf (Accessed on 21.03. 2017).

Energy Statistics, (2016). 23 rd issue. Central Statistics Office, Ministry of Statistics and Programme implementation, GOI, New Delhi.

Greenpeace (2011). Singrauli: The coal curse - A fact finding report on the impact of coal mining on the people and environment of Singrauli. Greenpeace India Society.

http://www.greenpeace.org/india/Global/India/report/Fact-finding-report-Singrauli-Report.pdf (Accessed on 21.03. 2017).

Junega, S. (2012). India's Minamata. Down to Earth. http://www.downtoearth.org.in/coverage/indias-minamata-39334 (accessed on 24 Feb. 2017).

Khan, I. and A. Javed (2012). Spatio-temporal land cover dynamics in open cast coal mine area of Singrauli, M.P. Indian Journal of Geographic Information System, 4, 521-529.

Munshi, A. (2013). Sasan ultra mega power project Singrauli, Madhya Pradesh. Prepared by Bank Information Center Trust In association with SrijanLokhitSamiti.

Pandey, R.K. (2005). Assessing the overall environmental impacts of Vindhyachal super thermal power project at Singrauli. Enviromedia 24: 871-874.

Sagar R. and J.S. Singh (2004). Local plant species depletion in a tropical dry deciduous forest of northern India. Environ Conserv 3:55–62.

Singh, J.S., K.P. Singh and M. Agrawal (1991). Environmental degradation of the Obra–Renukoot–Singrauli area, India and its impact on natural and derived ecosystems. The Environmentalist 11:171–180.

Singh, A. (2012). Pioneer flora on naturally revegetated coal mine spoil in a dry tropical environment. Bulletin of Environment, Pharmacology and Life Sciences. 1: 3: 72 – 73.

Singh, N.P. (2014). Application of remote sensing satellite data in coal exploration & mining. UIM 2014. CMPDI.- (http://sac.gov.in/nisar/NISAR%20Science%20Workshop_Presentations_2015/CMPDI.pdf. (accessed on 24 Feb. 2017).

Singh, R.K., B.P. Shukla and R.C. Tripathi (2003). Environmental status of problem area –Singrauli. In: V.P.Singh and R.N.Yadav (eds.) Environmental Pollution, Allied Publishers,New Delhi, 151-164.

Viswakarma, C.S., S. Thakur, P.K. Rai, V. Kamal and S. Mukherjee (2016). Changing land trajectories: A case study from India using a remote sensing based approach. European Journal of Geography, 7(2), 61-71.

Journal of Geomatics Vol 11 No. 1 April 2017

Morphometric analysis in Koldari watershed of Buldhana district (MS), India using geoinformatics techniques

Kanak Moharir[1], Chaitanya Pande[2], Abhay M. Varade[3] and Rajeshwari Pande[1]
[1]Department of Geoinformatics, ShriShivaji College, Akola
[2]All India Coordinated Research Centre for Dryland Agriculture Centre, Akola
[3]P. G. Department of Geology, RTM Nagpur University, Nagpur, MS, India
Email: kanak.moharir1@gmail.com

(Received: Jul 11, 2016; in final form: Apr 06, 2017)

Abstract: This current study, an attempt is made to study the morphometric characteristics of Koldari watershed of Buldhana district, Maharashtra, India by using geo-informatics techniques and Carto satellite DEM data at 30m spatial resolution. Morphometric analysis is carried out for watershed boundary, flow accumulation, stream number, stream ordering and stream length. The watershed boundary was delineated from digital elevation model data. The total length of all stream segments under stream order I to IV in the watershed is 61.56 km2. The area of Koldari watershed is 22.28 km2. This study is very useful for planning of rain water harvesting structures and watershed management.

Keywords: Morphometric analysis, DEM, Remote sensing, GIS

1. Introduction

In India, the population is continuously increasing land and water resources are decreasing. Watersheds are natural hydrological entities that cover a specific aerial expanse of land surface from which the rainfall runoff flows to a defined drain, channel, stream or river at any particular point (Anon., 1990). Soil and water conservation are key issues in watershed management in India. In developing countries, watershed projects focus on three objectives. Namely, (i) to conserve and strengthen the natural resource base; (ii) to make natural resource based activities like agriculture more productive and (iii) to support rural livelihood to alleviate poverty.

Watersheds are natural hydrological entities that cover a specific aerial expanse of land surface from which the rainfall runoff flows to a defined drain, channel, stream or river at any particular point. Watersheds have been classified into different categories based on area viz., micro watershed (5 to 10 km2), mini watershed (10 to 30 km2), sub watershed (30 to 50 km2) (Anon. 1995). Watersheds can be delineated by several methods. One used extensively is manually delineation based on the contour information depicted on topographic maps. Even with the advent of GIS technology, this method is still prevalent. With the availability of digital topographic maps, digital techniques are possible. The watershed features should be derived and made available for its use in watershed planning and management, estimating upland erosion and evaluating the impacts of human activities on the quality and quantity of the streams. Geographical Information System (GIS), with its ability to gather spatial data from different sources into an integrated environment, has emerged as an important tool for delineation of watersheds. GIS provides a consistent method for watershed delineation using contours derived from digital elevation models (DEM's). GIS has unique features to relate to the point, liner and areal features in terms of the topology as well as connectivity (Murali Krishna, 2006).

Morphometry is the measurement and analysis of the configuration of the earth's surface, shape and dimension of its landforms (Agarwal, 1998). The morphometric analysis involves measurement of linear aspects of the watershed and slope contribution. The morphometric characteristics of a watershed are helpful in synthesizing hydrological behavior (Pandey et. al., 2004). The watershed morphometric characteristics have been studied by many scientists using conventional (Horton, 1945; Smith, 1950; Strahler, 1957; Dhinwa, 1982) and remote sensing and GIS methods (Biswas et al., 1999; Khadri and Moharir, 2013; Narendra and Rao, 2006; Rudraiah et al., 2008). In the present study, stream number, order, length, Rho coefficient and bifurcation ratio are derived and tabulated on the basis of linear properties of drainage channels using GIS based on drainage lines as represented over the topographical maps (scale 1:50,000).

2. Study area and data used

Koldari watershed is situated in Buldhana district, Maharashtra and located between 20°15′ 59" N and 76° 42'30'' E, 77° 39'00''E and 20°21′00" N longitude and covers an area of 22.28 km2 (Fig. 1). The study area is covered in Survey of India toposheet (55D/11) on 1:50,000 scale. Survey of India toposheet (55D/11) on 1:50,000 scale and CartoSAT-1 DEM (30m) have been used in this study to extract watershed boundary, drainage network and analysis of morphometric parameters.

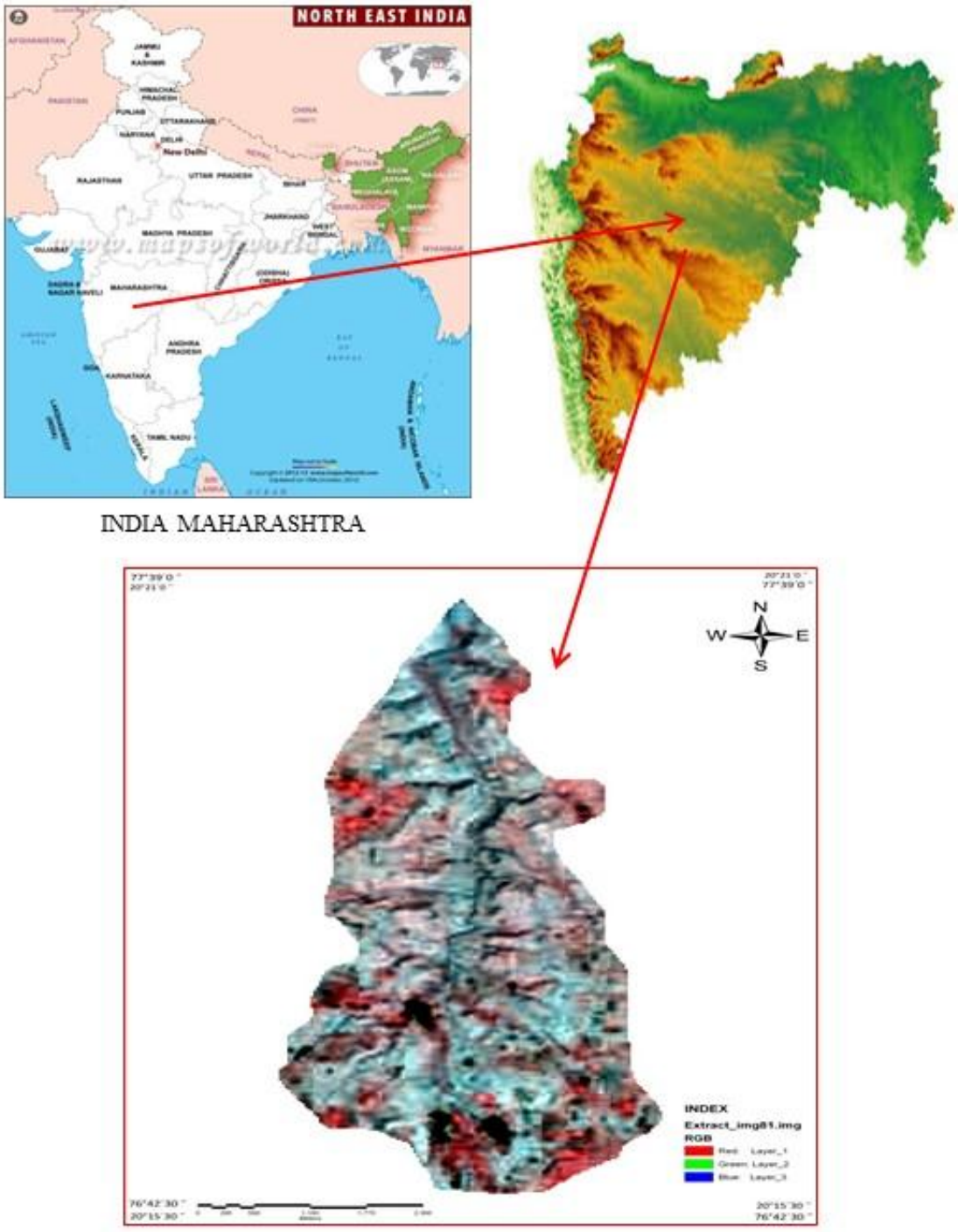

Figure 1: Location map of study area

3. Methodology

There are two major components of the methodology namely, extraction of drainage network from DEM data and morphometric analysis.

3.1 Extraction of drainage network from DEM data

The extraction of the drainage network of the study area is carried out using Cartosat data (March 15, 2015) based DEM with a 30m*30m grid cell size. which was downloaded from Bhuvan site (www.nrsc.gov.in). Hydrology tool under Spatial Analyst Tools in ArcGIS-10.1 software are used to extract drainage channels, and other parameters. The automated method for delineating streams followed a series of steps i.e. DEM, watershed and stream order (fig. 2).

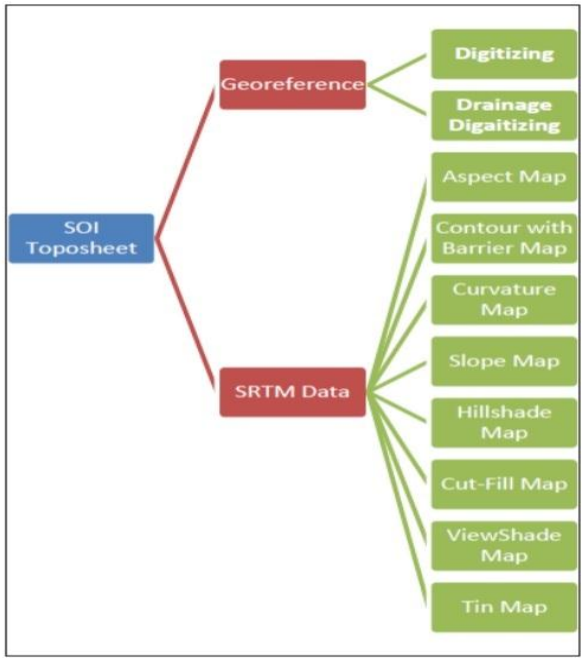

Figure 2: Flowchart of the methodology

3.2 Morphometric analysis

The present study integrated the use of remote sensing and GIS techniques in morphometric analysis. Morphometric indicators such as Stream Order (Su), Stream Number (Nu), Bifurcation Ratio (Rb), Weighted Mean Bifurcation Ratio (Rbwm), Stream Length (Lu), Ratio of stream length and stream order, Stream Length Ratio (Lur), Stream Length used in the ratio (Lur-r), Weighted Mean Stream Length ratio (Luwm) are calculated from the Cartosat DEM derived drainage network (fig. 3)

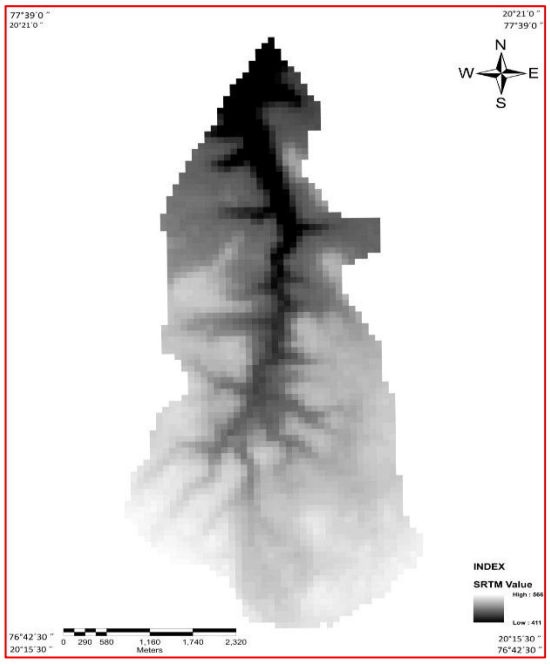

Figure 3: Digital Elevation Model (DEM) map of Koldari watershed

4. Results and discussion

4.1 Stream Order (Su)

Stream ordering is the first step of quantitative analysis. In this research, stream order of Koldari watershed is carried out by using Arc GIS10.1 software. It is observed that first order stream has maximum frequency followed by second order, third order and fourth order respectively as shown in (Table 2). It is also noticed that there is a decrease in stream frequency as the stream order increases (Fig. 4).

4.2 Stream Number (Nu)

When two channel of different order join then the higher order is maintained. Stream number is derived by using Arc GIS10.1. Total 106 streams are identified of which 73 are of first order, 28 of second order, 4 of third order and 1 of fourth order as is shown in table 2 and 1. Higher order of stream indicates lesser permeability and infiltration in the watershed (Strahler, 1964). In this watershed area, dendritic type of drainage patterns is observed which indicates homogeneity in texture and lack of structural control.

4.3 Bifurcation Ratio (Rb)

The bifurcation ratio is the ratio of the number of the stream segments of given order 'Nu' to the number of streams in the next higher order (Nu+1),

Rb =Nu/Nu+1

where, Nu =Total no. of stream segments of order 'u'; Nu + 1= Number of stream segments of the next higher order.

The bifurcation ratio is a dimensionless property. It was found that range of bifurcation ratio vary from 2.6 to 7.0 (table 2). The higher values of Rb indicates strong structural control on the drainage pattern, while the lower values indicative of watershed that are not affect by structural disturbances. The lower values of Rb are characteristics of the watersheds, which have suffered less structural disturbances and the drainage pattern has not been distorted because of the structural disturbances. The highest Rb (7.0) is found between 4th order in Kolderi watershed which indicates corresponding highest overland flow and discharge due to hilly metamorphic formation associated with high slope configuration. Also the higher values of Rb indicate strong structural control in the drainage pattern whereas the lower value indicates that the Kolderi watershed is less affected by structural disturbances. The lowest Rb is found between 2nd orders in Kolderi watershed which indicates corresponding lower overland flow and discharge moderate slope configuration. The bifurcation ratio of different stream number and mean bifurcation ratio are shown (Table 1 and 2).

4.4 Weighted Mean Bifurcation Ratio (Rbwm)

Weighted mean bifurcation ratio in the M/s. Weighted mean bifurcation ratio obtained by multiplying the bifurcation ratio for each successive pair of orders by the total numbers of streams involved in the ratio and taking the mean of the sum of these values. It has been

observed that the mean bifurcation ratio is 4.53 of the Kolderi watershed Maharashtra. The values of the weighted mean bifurcation ratio have been found to be very close to the mean value of bifurcation ratio in Kolderi watershed (Table 2).

4.5 Stream Length (Lu)

The total length of the 1st order streams is highest, that is, respectively. Generally, the higher the order, the longer the length of stream is noticed in the nature. Longer length of stream is advantageous over the shorter length, in that the former collects water from wider area and greater option for construction of a bund along the length. Lower stream lengths are likely to have lower runoff. Longer lengths of streams are generally indicative of flatter gradient. Generally, the total length of stream segments is maximum in first order stream and decreases as stream order increase (Table 1).

4.6 Ratio of stream length and stream order

Stream length and stream order ratio for different stream order has been calculated for Kolderi watershed. Highest value for Lu/Su has been found in the 1st stream order whereas lowest Lu/Su has been found in the 4th stream order (Table 1 and 3).

4.7 Stream Length Ratio (Lur)

Stream Length Ratio is defined as the ratio of the mean (Lu) of segments of order (So) to mean length of segments of the next lower order (Lu-1).

RL = Lsm/Lsm-1

Lsm =Mean stream length of a given order and

Lsm-1 = Mean stream length of next lower order.

After calculating the stream length ratio it has been absorbed that stream length ration has been changed from one order to another (Table 1). Change of stream length ratio from one order to another order indicating there late youth stage of geomorphic development (Singh and Singh, 1997). The variation in stream length ratio might be due to change in slope and topography.

4.8 Stream Length used in the ratio (Lur-r)

Stream Length used in the ratio (Lur-r) is defined as the Sum of first order Stream Length and second order Stream Length. Lur-r value is calculated for all stream length which is shown in table 1.

4.9 Weighted Mean Stream Length ratio (Luwm)

Weighted Mean Stream Length ratio obtained by summation of Stream Length Ratio multiplied by Stream Length used in the ratio divided by Stream Length used in the ratio shown in table 1 and 3.

Luwm = Lur*Lur-r/Lur-r

Figure 4: Stream order map of study area

Table 1: Morphometric Parameters of Kolderi watershed

Sr. No.	Morphometric Parameter	Formula	Reference	Results
A	**Drainage Network**			
1	Stream Order (S_u)	Hierarchical Rank	Strahler (1952a)	1 to 4
2	1st Order Stream (S_{uf})	Suf = N1	Strahler (1952b)	73.00
3	Stream Number (N_u)	$Nu = N_1+N_2+ \ldots N_n$	Horton (1945)	106.00
4	Stream Length (L_u) mts	$Lu = L_1+L_2 \ldots L_n$	Strahler (1964)	616.44
5	Stream Length Ratio (L_{ur})	see Table 3	Strahler (1964)	8.45
6	Mean Stream Length Ratio (L_{urm})	see Table 3	Horton (1945)	2.81
7	Weighted Mean Stream Length Ratio (L_{uwm})	see Table 3	Horton (1945)	2.059
8	Bifurcation Ratio (R_b)	see Table2	Strahler (1964)	4.53-13.6
9	Mean Bifurcation Ratio (R_{bm})	see Table 2	Strahler (1964)	4.53
10	Weighted Mean Bifurcation Ratio (R_b)	see Table 2	Strahler (1953)	3.67
11	Main Channel Length (C_1) Km.	GIS Software Analysis		11.192
12	Valley Length (VI) km	GIS Software Analysis		9.31
13	Basin Length (L_b) km	GIS Software Analysis	Schumm(1956)	9.31
14	Basin Perimeter (P)km	GIS Software Analysis	Schumm(1956)	23.05
15	Basin Area (A) km^2			22.28

Table 2: Stream order, stream number and bifurcation ratio's in Kolderi watershed

S_u	N_u	R_b	N_{u-r}	R_b*N_{u-r}	R_{bwm}
I	73	---	---	---	3.67
II	28	2.60	101	262.6	
III	4	7	32	224	
IV	1	4	5	20	
Total	106	13.6	138	506.6	
Mean		4.53			

Su: Stream order, Nu: Number of streams, Rb: Bifurcation ratios, Rbm: Mean bifurcation ratio*,
Nu-r: Number of stream used in the ratio, Rbwm: Weighted mean bifurcation ratios.

Table 3: Stream length and stream length ratios in Kolderi watershed

S_u	L_u	L_u/S_u	Lur	L_{ur-r}	$L_{ur}*L_{ur-r}$	L_{uwm}
I	401.24	5.49	---	---	---	0.40
II	95.85	3.42	0.23	497.09	114.33	
III	86.98	21.74	0.90	182.83	164.54	
IV	32.37	32.37	0.37	119.35	44.15	
Total	616.44	63.02	1.5	799.2	323.02	
Mean	154.11		0.5			

S_u: Stream order, L_u: Stream length, L_{ur}: Stream length ratio, L_{urm}: Mean stream length ratio*, L_{ur-r}: Stream length used in the ratio, L_{uwm}: Weighted mean stream length ratio.

4.10 Discussion

This analysis has revealed that the total number and length of stream segments is higher in first order streams and decreases as the stream order increases. The bifurcation ratio (R_b) between different successive orders varies revealing the geostructural control. From this study it can be concluded that the higher values of R_b in Kolderi watershed shows strong structural control, while the lower values indicate that watershed are not affected by structural disturbances. The lower values of R_b are characteristics of the watersheds, which have suffered less structural disturbances and the drainage pattern has not been distorted because of the structural disturbances.

Thus, it can be perceived that morphometric analysis provides a better understanding for the status of land form and their processes, stream management and evolution of groundwater potential zone mapping for watershed development planning and their management in water-deficient areas. The created data may be used for various future soil and water conservation projects Kolderi watershed management like groundwater surveys by locating the zones of higher secondary porosity through drainage density data. Such studies are very useful for planning of rain water harvesting structures and watershed management.

5. Conclusion

Morphometric parameters of watershed were calculated from Cartosat DEM and their influence on landforms was studied through GIS based analysis. This study reveals that morphometric analysis based on GIS technique is a very useful and adequate tool for conducting geo-hydrological studies.

References:

Anonymous (1995). Integrated mission for sustainable development. Technical Guidelines, NRSC, Hydearabad.

Agarwal, C.S. (1998). Study of drainage pattern through aerial data in Naugarh area of Varanasi district, U.P. Journal of Indian Society of Remote Sensing, 26, 169-175.

Biswas, S., S. Sudhakar and V.R. Desai (1999). Prioritization of sub-watersheds based on morphometric analysis of drainage basin, district Midnapore West Bengal. Journal Indian Society Remote sensing 27(3): 155-166.

Dhinwa, P.S., (1982). Geomorphology and human settlements in the Berach basin, Rajasthan. Unpublished Ph.D. Thesis.

Horton, R.E. (1945). Erosional development of streams and their drainage basins. Bulletin of the Geological Society of America, 56, 275-370.

Khadri, S.F.R. and Kanak Moharir (2013). Detailed morphometric analysis of Man river basin in Akola and Buldhana districts of Maharashtra, India using Cartosat-1 (DEM) data and GIS techniques. International Journal of Scientific & Engineering Research, Volume 4, Issue 11, 832-854.

Murali Krishna, I.V. (2006). Spatial information technology for water resources management. Proc. of National workshop on Watershed management and impact of Environmental changes on Water resources (WMEC) JNTUCEH, JNT.

Narendra, K. and K.N. Rao (2006). Morphometry of the Mehadrigedda watershed, Visakhapatnam district, Andhra Pradesh using GIS and Resourcesat data. J. Indian Soc. Remote Sensing, 34(2), 101-110.

Pandey, A., V.M. Chowdhary and B.C. Mal (2004). Morphological analysis and watershed management using GIS. J. of Hydrology, 27(3), 71-84.

Rudraiah, M., S. Govindaiah and S.S. Vittala (2008). Morphometry using remote sensing and GIS techniques in the sub-basins of kagna river basin. Journal of the Indian Society of Remote Sensing, December 2008, Volume 36, Issue 4, 351–360

Singh, S. and M.C. Singh (1997). Morphometric analysis of Kanhar river basin, National Geographical Journal of lndia, 43(1), 31-43.

Smith, G.H. (1950). The morphometry of Ohio: The average slope of the land (abstract). Annals of the Association of American Geographers, 29, 94.

Strahler, A.N. (1952a). Dynamic basis of geomorphology. Bulletin of the Geological Society of America, 63, 923-938.

Strahler, A.N. (1952b). Hypsometric analysis of erosional topography. Bulletin of the Geological Society of America, 63, 1117-42.

Strahler, A.N. (1957). Quantitative analysis of watershed geomorphology. Transactions-American Geophysical Union, 38, 913-920.

Strahler, A.N. (1964). Quantitative geomorphology of drainage basin and channel network. Handbook of Applied Hydrology, 39-76.

Journal of Geomatics Vol 11 No. 1 April 2017

Application of remote sensing and GIS for groundwater potential zones identification in Bata river basin, Himachal Pradesh, India

K.V. Suryabhagavan
School of Earth Sciences, Addis Ababa University, Addis Ababa, Ethiopia
Email: drsuryabhagavan@gmail.com

(Received: Dec 28, 2016; in final form: Mar 12, 2017)

Abstract: Groundwater is not uniformly distributed all over and is limited in hard rock terrains. A case study was made to find out the groundwater potential zones in Bata river basin, in Himachal Pradesh, India. Thematic maps of geology, geomorphology, soil, land-use/land-cover and drainage were prepared for 288 km^2 study area. Digital Elevation Model (DEM) was generated from 20 m interval contour lines to obtain the slope of the study area. Ground water potential zones were obtained by overlaying all thematic maps in terms of the weighted index overlay method. Ranking was given for each individual parameter of each of the thematic maps and weights were assigned according to the influence such as land-use/land-cover (8%), slope (5%), geomorphology (6%), fault buffer (5%), aspect map (5%), lineament buffer (5%), drainage buffer (7%) and geology (7%) in terms of very poor, poor, moderate to good, good and very good within the study area. The GIS method output results were validated by conducting field survey by randomly selecting wells in different villages using GPS instruments. Coordinates of each of the well locations were obtained and plotted in the data base. The spatial variation of the potential zones indicates that groundwater occurrence is controlled by structures, landforms and slope.

Keywords: Open potential, GIS, Index overlay method, Remote sensing

1. Introduction

Ground water is one of the most important natural resources on which the survival and progress of mankind depends to a great extent. It is a renewable resource. In view of its wide distribution, low level of contamination and availability in the reach of the consumer, ground water development gets priority for meeting the ever-growing demand of water for domestic, agricultural and industrial purposes (Murthy, 2000; Sener et al., 2005; Ibrahim-Bathis and Ahmed, 2016). It is a critical resource in many parts of the world, especially in the arid and semiarid drought prone regions. It sets limits on the agricultural development *via-a-vis* the density of population and standard of living that can be sustained. In India, more than eighty percent of the population lives in villages. The overall development of the country would be meaningful only when the rural living conditions are improved (Dey and Naithani, 1988). In this context, ground water development is vital for rural upliftment. Though the replinishible groundwater resources in India is estimated to be around 42.3 million hectare meters (mhm) per year, at present only about 13.5 mhm is being exploited. This clearly shows that there is major scope for further ground water development. Ground water development does not require major investment, planning and government machinery. To meet the basic needs of rural population for portable water, national drinking water technology mission has been taken up using remote sensing technology for finding water sources. In India, 65% of the total geographical area is covered by hard rock formations with low porosity (less than 5%), and very low permeability (10^{-1} to 10^{-5} m/day) (Saraf and Choudhury, 1998). Therefore, efficient management and planning of groundwater is of utmost importance. Remote sensing provides multi-spectral, multi-temporal and multi-sensor data of the earth's surface (Krishnamurthy and Srinivas, 1995; Choudhury, 1999; Singh and Prakash., 2002; NRSA, 2008; Avtar et al., 2010; Chowdhury et al., 2010; Rashid et al., 2011; Ibrahim-Bathis and Ahmed, 2016). One of the avdvantages of using remote sensing and GIS for hydrological investigations and monitoring is its ability to generate information in spatial and temporal domin, which is very crucial for successful predication and validation (Burrough, 1986; Dar et al., 2010; Senthil Kumar and Shankar, 2014). Remote sensing is providing useful base-line information in conjunction with ground water truths on soils, land use, vegetation, surface and ground water, geology, landforms, topography and settlements in the regional prospectives. During the present investigation, ground water potential zones were studied in Bata river basin in Himachal Pradesh, India by integrating various thematic maps in GIS environment.

2. Materials and methodology

2.1 Study area

The Bata river basin, lying between latitude 30° 25′ 3.33″–30° 35′ 13.71″N and longitude 77° 22′ 34.75″–77° 39′ 42.31″E is spread over about 288 km^2 in the district of Srimaur in Himachal Pradesh (Fig. 1). It is bounded by the sinuous and meandering grip in the north-east by the Yamuna. The catchment is roughly elliptical in shape. The maximum east-west and north-south datum lengths are 36.4 km. The climate is sub-humid sub-tropical in lower part of the tract lying in Siwaliks and wet temperate in the upper part in central Himalaya. The region has distinct seasons of summer (April-June), monsoon (July-September), autumn

(October-November) and winter (December-March). Summer variation is very high; temperatures go up to about 42ºC in the lower Siwaliks, but it is around 25ºC in the upper part. The Bata river is characterized by highly dissected Siwalik hills merging into the valley on either side of the Bata river. The valley extension of Dun valley is called Kiarda dun. About 95 per cent of area falls under low hills of altitude <1,000 m. Half of the area is under moderately steeply sloping lands. Geomorphologically, the area can be divided into hills, piedmonts, terraces, flood plain and channel bars. A greater part of the Bata river lying in the middle Himalaya and Siwaliks is hilly with deep and narrow valleys separated by spurs and ridges. The altitude of the tract varies from 400 m at the mouth of Bata river at Sidhpurwala, northern ridge Baila (1020 m asl) and in south above Kolar (665 m asl). Large part of the study area falls under a variety of vegetation types with tropical and sub-tropical sal, khair and sissoo in Dun and lower Siwaliks, chir in the middle and upper Siwaliks and kail, deodar and oaks in the central Himalayan part. There is a good mixture of broad-leaved species in all the vegetation zones. Some part of the study area comes under the shrubland. Barren lands are also observed in some parts of the study area.

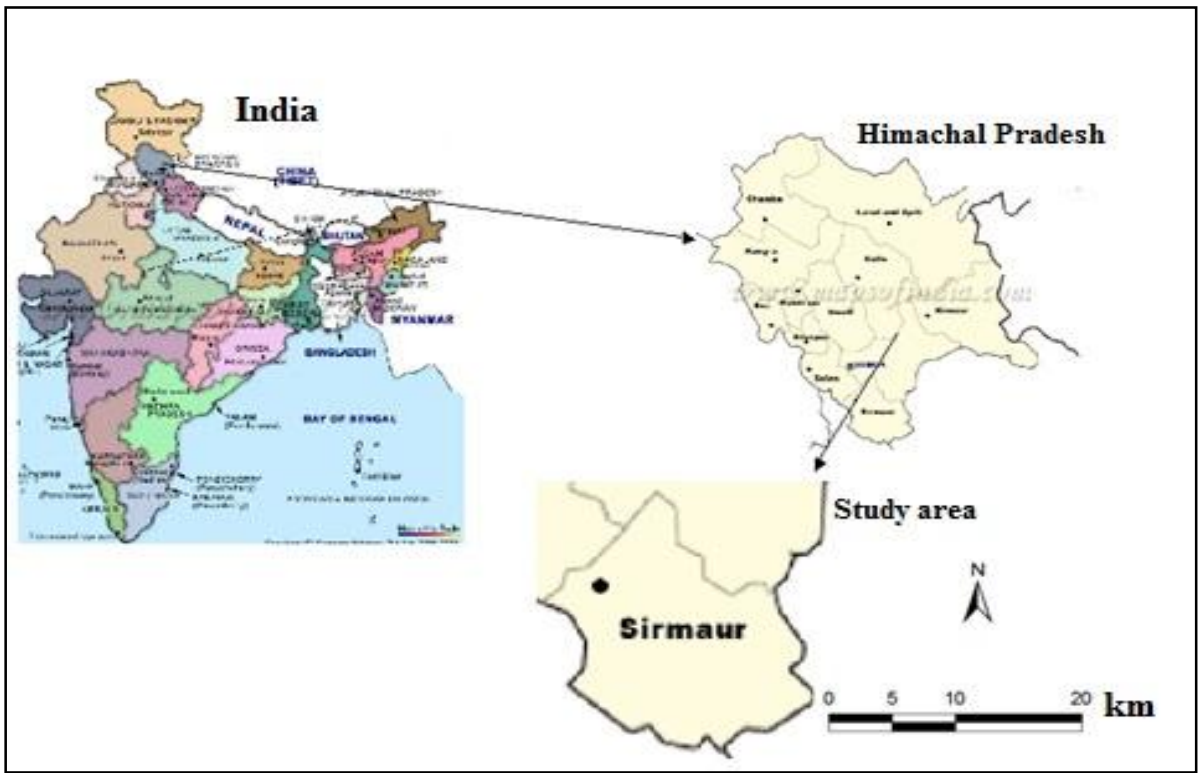

Figure 1: Location map of the study area

2.2 Method

2.2.1 Data acquisition and software: Topographical base of Bata River Basin area: The Survey of India (SOI) toposheets no. 53F/6, 53F/7, 53F/10 and 53F/11 on 1:50.000 scales formed the source of data for the study. The image data was a product of Indian Remote Sensing (IRS) 1D LISS III of December 2016 with spatial resolution of 23.5 m and the image has four bands and PAN data 5.8 m were merged using principal component analysis. Tube well data, dug well data, rainfall data of various locations in and around the Bata river were collected from the government offices. SOI toposheets and visual analysis of satellite data in conjunction with the available ancillary data were used as reference maps for the preparation of thematic maps. Considering seven factors *viz*., land-use/land-cover, slope, geology, geomorphology, fault buffer, lineament buffer and drainage buffer maps weightages were assigned to each of these factors according to their relative importance. These attributes were used to create database in ArcGIS and the groundwater potential map was derived. The flowchart (Fig. 2) shows the sequential steps involved in this study.

Software used: The GIS software used for digitization and overlay analysis in the present study area were the ArcGIS®10 software and ERDAS Imagine®2013. These were used for geo-referencing, creation of attributes table and digitization of the collected maps. ArcGIS®10 is vector based package and it is capable of accessing spatial data base, analysis and produce outputs for the present study.

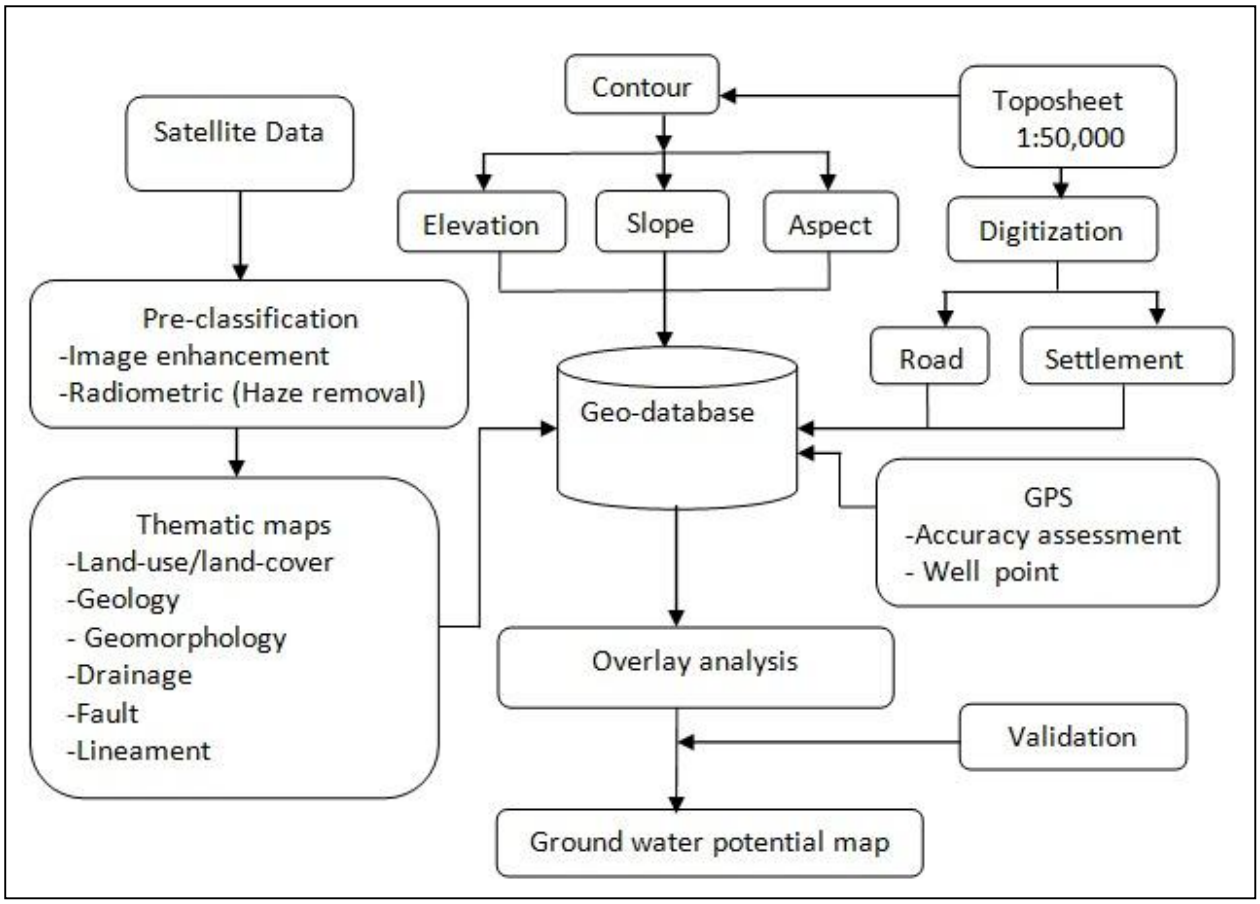

Figure 2: Methodology flow chart of the present study

2.2.2 Field data collection: A pre-field interpretation map was prepared and the bore well points were verified by ground truth. Ground truth information was collected by GPS survey. Recent satellite data were used during the field survey and the current land use classes and the field data of wells location points were collected. Geomorphic provinces and hydrological characters of various units were recorded. Major lineaments/faults affecting the area and mass movement activities were also studied during prefield interpretation. Visual interpretation of above satellite data of the study area was required for comparative study of geology, structure, geomorphology, hydrology, land-cover and land-use. Data were transfered on base map in order to prepare the overlays of geology, geomorphology, land use derived from imagery. Geotraverses were planned for the selected field check to finalize the pre-field map. The GPS points were downloaded and overlaid on the imagery and used for refinement of the pre-field interpretated land-use/land-cover and ground water potential map.

2.2.3 Index overlay method: Index overlay method was applied where maps were analysed together in a weighted combination. In this simplest type of weighted model, input maps are binary and each map carries a single weight factor (Saaty, 1980). However, multiclass maps are used, each class of every map is given a different rating score. In case the map classes occurring on each output map are assigned different score, as well as the map receiving different weights. It is convenient to define the score in attribute table for each input map. The average score can be defined as:

$$S = \sum S_{ij} W_i / \sum W_i$$

i = 1 to n (no. of thematic layers)
j = 1 to m (no. of classes in theme)

where S is the weighted score for this study area object (polygon, pixel), Wi is the weight of the input map, and S ij is the rating score for the j^{th} class of the i^{th} map. The value of j depending upon the class actually occurring at the current location. Each map must be associated with a list of scores, one per map class. Class scores can be put into an attribute table with an editor, for access by the modeling procedure. The attribute table can be modified without changing the procedure. If the score for some classes are set to negative value, area where such a class occurs are automatically set to class 0 (zero) in the output map.

2.2.4 Integration of thematic layers: In order to integrate various thematic maps, a rating was developed for the integration of these thematic maps. A numerical rating system ranging from 1 to 9 were assigned to various classes of individual themes, based on degree of influence of individual categories on ground water regime of the region (Table 1). All the thematic maps were assigned a "weightage factor, called equal weightage integration method" aimed at reducing subjectivity in rating of coding, completely from the analysis (Dinesh Kumar et al., 2007; Preeja et al., 2011).

Ground water potential zones were obtained by overlaying all thematic maps' output in raster format and classified in to user-defined classes, showing different ground water prospective area based on the selected parameter in ArcGIS®10 software.

Table 1: Rank and weightage of different parameters for groundwater potential zones

Parameter	Classes	Individual weights	Total Weight
Land-use	River bed Scrubland Degraded Forest Dense Forest Exposed Rock Water Standing Crop Fallow land	6 2 5 6 1 9 8 7	25
Slope (°)	$0\text{-}15^0$ $15\text{-}30^0$ $30\text{-}45^0$ $45\text{-}60^0$ $60\text{-}90^0$	8 7 5 4 1	15
Geomorphology	Structural hill Subdued hill Upper Piedmont River Terrace Middle Piedmont River bed	2 3 3 8 4 9	25
Fault	100 200 300	2 2 3	5
Lineament buffer (km/km2)	25 50 75	2 2 3	5
Drainage (km/km2)	5 8 12 16 20	2 3 5 6 7	10
Lithology	Lower Siwalik Upper Siwalik Alluvium Doon Gravel Subathu Dagshi formation Mandhali formation	3 3 8 5 2 2 4	10

3. Results and discussion

3.1 Lithology

In the present study, seven types of lithological characteristics were considerd to understand the distribution and occurrence of ground water (Table 1). The lithological map of the study area is shown in (Fig. 3). The upper Siwalik are exposed in the southern part of the basin and are overlaid by the Nahans (lower Siwalik) along the Markanda thrust. The pre-tertiary limestones, (Sataun formation) wherever exposed, occur as discontinuous outcrops along the fringe of Nahan thrust separating them with lower Siwaliks. The main boundary thrust demarcates the boundary between Siwalik and the older rocks and marks the boundary between the Nahan (lower Siwaliks) and the pre-Nahan (Sabathu and /or Sataun formation), (NRSA, 1999).

3.1.1 Upper Siwaliks: This formation is encountered in the southern part of Bata catchment separating its boundary with Haryana. It is composed of grey, soft friable sandstone with clay bands. These are interbedded with conglomerates (Dey and Naitnani, 1988). The upper Siwaliks are exposed in the south along the Bata and Markanda rivers and deposit more dissected topography in the area. The formation consist of coarse classic deposits such as boulder conglomerate, grit, sand and earthy clays. It generally starts with pebbles horizon at the base grading upward into thick. Some part of the band alternating with conglomerates is soft sand stone and in the upper part there are clays with same sandstone. The boulders and pebbles are ill sorted and composition is heterogeneous and they are of all shapes, sub rounded to rounded and sub angular. They are mostly formed of quartzite, schist, chert phyllite slates and granite gneisses. The upper Siwaliks are expressed in road section of Puruwala and Kolar.

3.1.2 Lower Siwaliks: The lowermost part of Siwalik formation has fine to medium grained relatively matured sediments with calcareous cementing material (Devi and Wankhede, 1995). These sediments are said to be from the rising mountains in the north and were laid down in alluvial plains of a series of rivers or a single river system named as "Indo-Brahma" river. In the Bata basin, Nahans are northerly dipping in general amounting to 20°-30°. Nahans in the area succeeded upwards by the older Subathu rocks. It is made up of alternating beds of sandstone and clay. The sandstone is micaceous and light gray in colour. It is mainly formed along both the sides of ridge dividing Giri catchment with Bata river.

3.1.3 Middle Siwaliks: These rocks are exposed in the northern part of Bata catchment overlaying the lower Siwalik along the ridge dividing Bata with Giri river. It consists of hard grey sandstone with small potion of orange clay and subordinate shale.

3.1.4 Alluvium: The central regions parallel to the NW-SE flowing Bata river and planking its sides are mostly covered with recent alluvium. It contains lenticular beds of sand and gravels.

3.1.5 Subathus: Subathu is named after the town Subathus of the Simla hills, which consists of thick succession of green, grey and red shales intercalated with thin lenticular bands of sandstone and impure limestone (Jugran, 2003). The red shale often contains gypseans, carbonaceous and pyretic layer. These rocks are exposed in the central part of the area just after Baila towards Birla village, extending upto the northwestern tip.

3.1.6 Dagshi formation: It consists of massive, very hard grey and purplish brown quartezitic sandstone, intercalated with seams of red clay. It covers major

portion of Sarahan and Narg ranges and small part occurs in the study area.

3.1.7 Mandhhali: Mandhali of the study area marked plane of structural discordace exits as a distinct linear feature between lower Siwalik and Pretertiary rock. Stromatolitic (algal shape) structure is the charctaristics feature of this rock unit. It occupies northern part just up of the lower Siwalik of the study area associated with green slate, phyllite and black shale and extend to further eastward across Yamuna river. Quartzite, carboniferous material is also found here. Strain in the rock indicates slikenside nature. This is the older rock. While carrying out detailed geological study the limestone belt of pre-Tertiary in the Bata basin marked plane of structural discordance exists as a distinct linear feature between Nahanas (lower Siwaliks) to its south and the older Tertiaries (Subathu) to its north. The carbnate rocks of the Basantpur formations extends in time to lower Palaeozoic, and there is no fossil records to support. The limestone is massive, thinly bedded, white grey in colour and are seen on road sections of Grinagar-Baila.

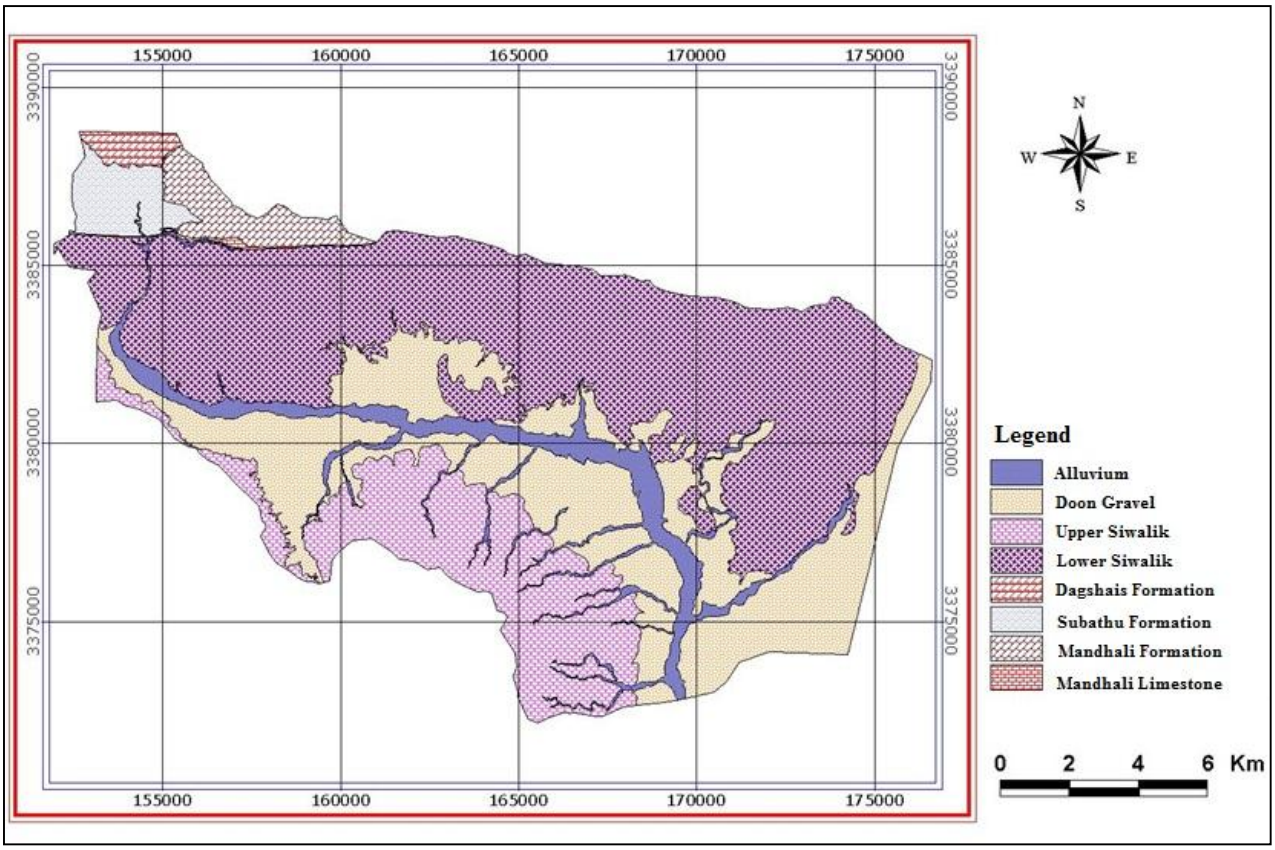

Figure 3: Lithology map

3.2 Geomorphology

It is well known fact that the geomorphological characteristics of an area affect its response to a considerable extent of groundwater occurrence (Nossin, 1971; Thomas et al., 2009). Thus, linking of geomorphological parameters with hydrological characteristics of a basin provides a simple way to understand their hydrological behavior (El-Gammal et al., 2013). The geomorphological characteristics were divided into six major groups. The geomorphological features such as river bed, river terrace, middle piedmont, upper piedmont, structural hills, subdued hills are the good sources of groundwater of the study area (Fig. 4). The alluvial plain of the Bata basin cover an area of 75.0 km^2, which is 27.55 percent of the total area of the Bata basin. The younger alluvium of the alluvial plain of the Bata basin covers only 17.1 km^2 area, which is 6.28 percent of the total basin. The older plains, which extend in an area of 57.9 km^2 or 21.27 percent of the total Bata basin, are in fact, relics of older flood plain. The piedmont zone of the Bata basin covers 133.3 km^2 area or 48.97% of the total area of the Bata basin. The upper piedmont zone or the denudational slopes cover an area of 41.4 km^2 or 15.21% of the total area, where as the middle piedmont zone or the fan-plain cover an area of 52.5 km^2 or 19.29% of the total area. The denudational sub-dued hills are found almost in all the three sections of the piedmont zone. These are mainly the highly eroded hills in the lower and upper Siwalik. Older and younger fan terraces are the most important landform found in the lower piedmont zone or fan-plain area of the Bata basin. The denudo-structuralhills of Bata basin cover an area of 63.9 km^2 or 23.48% of the total area of the basin. The ranks are given to geomorphological units considering their contribution to groundwater infiltration.

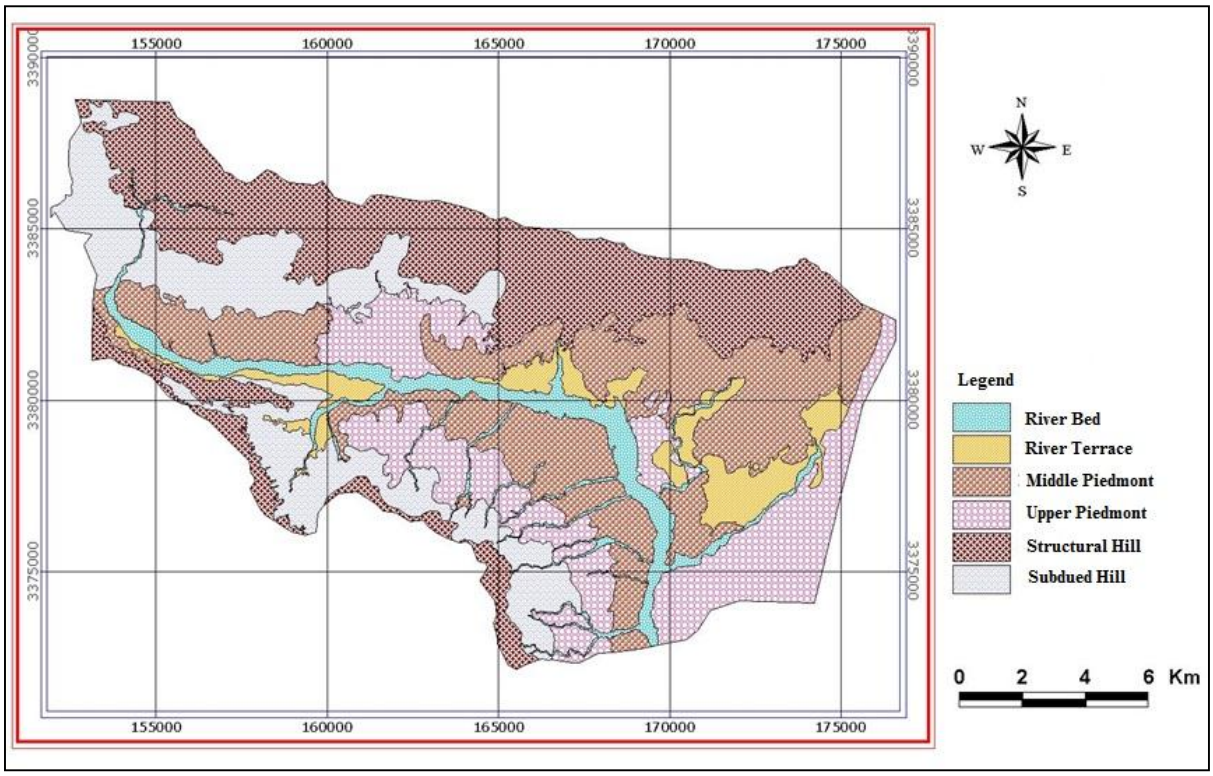

Figure 4: Geomorphological map

3.3 Slope

Slope of a surface refers to change in height across a region of surface. Slope is an important factor as it affects land stability. The slope of the study area ranged from 0º–>90º (Fig. 5) Steep slope was found mainly in North-south part of the province. In the central part the area has flat topography. Mostly, the hilly terrains are having steep slope. Slope steepness/gradient is important because it influences groundwater recharge (IMSD, 1995; Rokade et al., 2007). Flat areas are capable of holding the rainfall and facilitate groundwater replenishment in contrast to steep areas which instigate runoff. Low slope indicates the presence of high groundwater potential zones, high slope shows the presence of poor groundwater potential zones, as water drains rapidly off the surface.

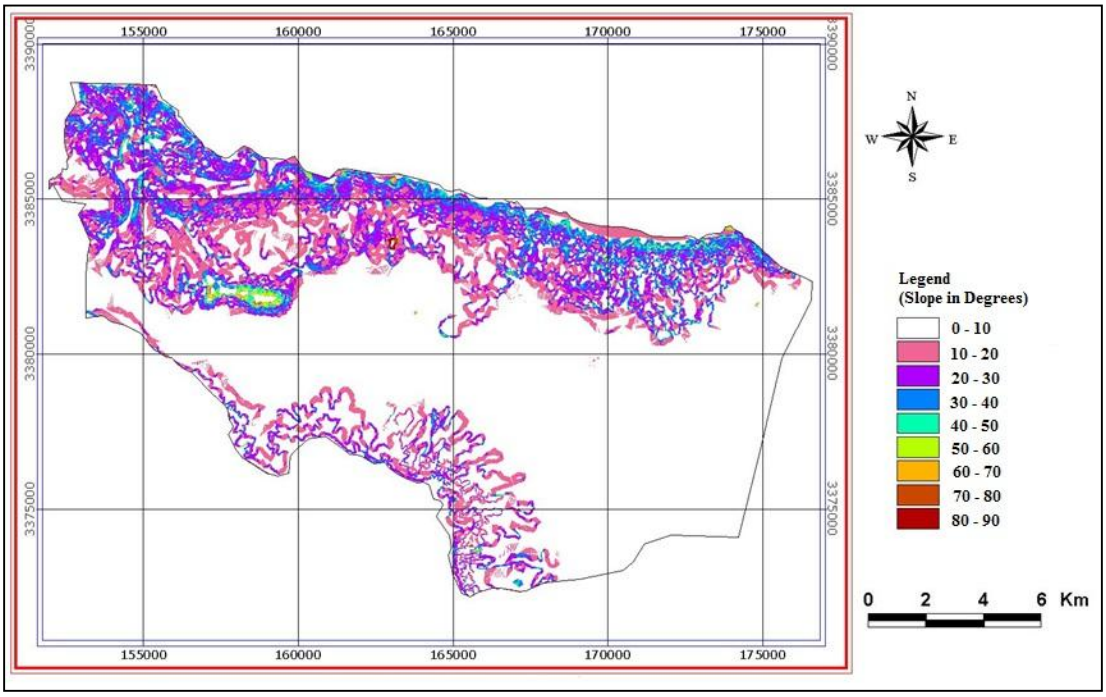

Figure 5: Slope map

3.4 Drainage density

Another input to evaluate the recharge property can be realized by detailed morphometric analysis of the drainage network. Drainage pattern of any terrain reflects the characteristics of surface as well as subsurface formations. In areas where the number of streams is more in a unit area, the largest proportion of the water coming from precipitation goes to runoff (Tribe, 1991; Shaban et al., 2006; Sreedevi et al., 2009). This is indicative of the subsurface condition of porosity. The drainage network order to a large extent depends on lithology, which provides an important indication of the percolation rate. Seventy three percent of the study area falls under low to moderate drainage density category. Thus, low drainage density was assigned for good ranking as high drainage density implies low groundwatwer potential in the study area.

3.5 Distance from structures

Linear structures, which are important for increasing the permeability of the bed rock are lineaments, faults, fractures, and joints (Fig. 6). O'Leary et al. (1976) defined a lineament as a mappable and simple or composite liner feature of a surface, whose parts are aligned in a rectilinear or slightly curvilinear relationship. These structural features are identified from the digital remote sensing data and distance to structure map is derived using the distance function. Areas close to structures develop a secondary porosity that will help them to percolate water better than those far from structures. Therefore, higher rank is given to areas proximal to geological structures. Generally, the folded structures in the form of synclines and anticlines are found in the study area. Syncline is found near Thana Panjahal in the western part, north of main boundary fault (Nag, 2005; Sander, 2007). This syncline is followed by anticlinal flexure exposing Dharmshala rocks within the core portion near Birla village. The synclinal axis is running nearly parallel to the main boundary fault.

The demarcation is more clear due to change in topography. This is also dipping towards north. Sudden changes in slope form saddle indication of thrust in the study area, which is clearly seen in remote sensing data as a deep trench extending E –W direction of the area. Roasted quartzite, crushing nature in upper Siwalik sand stone, depression in Sirmur tal (forming a big lake) also indicate thrust passing through the area. The lower Siwaliks are thrusted over the upper Siwaliks (Markanda fault) along Markanda and Bata river (flowing in a same line but both are 180^{o} apart to each other). This fault marks the southern boundary between lower Siwaliks. It runs eastwards and disappears over the alluvium deposits along Bata river in east and Marjanda in west. The differences in the levels as well as different geological unit on the both the banks of river are indication of fault. Near Dakpathar, the Bin river course follows the Markanda fault, which separates lower Siwaliks from middle Siwalik formation and joins with Main Boundary Fault (MBF). Number of transverse and cross faults is picked up from image interpretation of the study area. These faults are occurring the Pre Tertiaries and Tertiaries formation. Number of informational faults are observed in Siwalik group of rock. Major break in slope and variation dipping attitude were seen in lower Siwalik. Road section from Dhola Kuwan to Baila and other places show number of break in slope and sagging. Malgi village is a good example of these phenomena. Thrust is low angle reverse fault forming a wide zone known as Thrust Zone. One important thrust is available in the study area as follow: MBT also a low angle NW-SE to EW trending reverse fault, dipping towards N and NE. The Pre Tertiary rock like slate, phyllite and quartzite are moderately fractured and jointed. The lower Siwalik sndstone is also moderately fractured and shows criss cross jointing. The NS joint is prominent. The rocks of middle Siwaliks are poorly jointed.

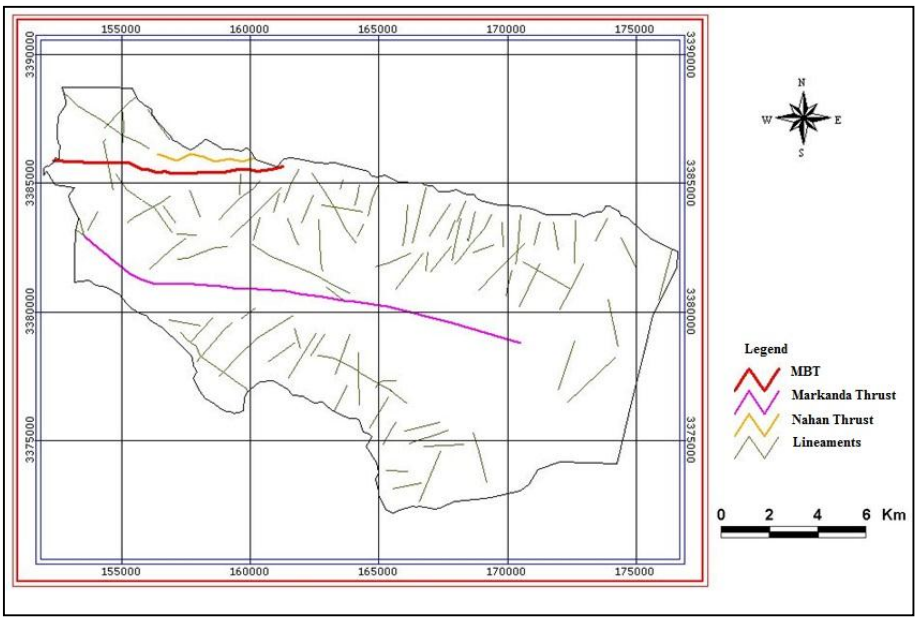

Figure 6: Lineament map

3.6 Land-use/land-cover

The land-use/land-cover map of the entire Bata basin was generated (Fig. 7) and derived classes is presented in Table 1. The effect of land cover to groundwater recharge is both negative and positive (Todd and Mays, 2005; Shaban et al., 2006; Chowdhury et al., 2009; Rawat and Manish, 2015). Trees may increase water loss by evapotranspitation or they may facilitate recharge by reducing runoff and by intercepting water and infiltrating its droplet slowly. For the identification and interpretation of the landuse pattern of area through image interpretation of remote sensing data, landcover classes were delineated. It includes standing crop, fallow land, dense forest, degraded forest, grass land, exposed rock, barren land and water body.

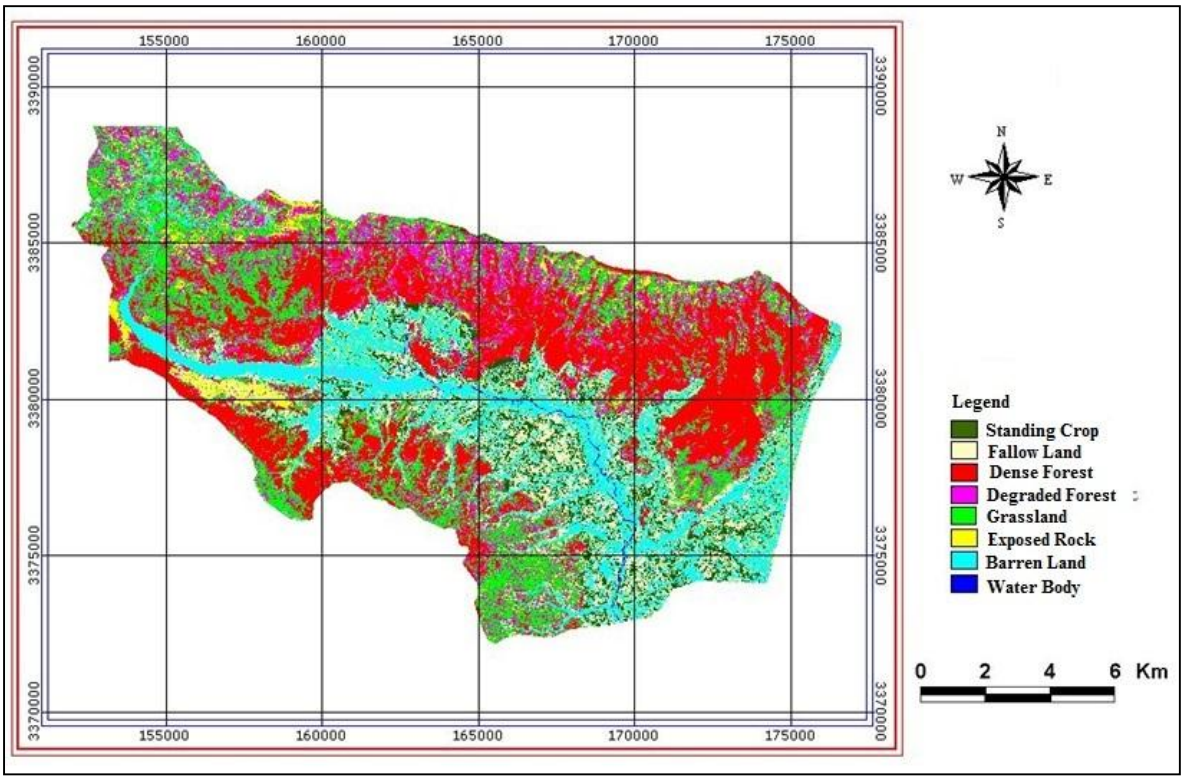

Figure 7: Land-use/land-cover map

3.7 Model validation

The groundwater potential map (Fig. 8) was generated on the basis of weights and ranks assigned to different parameters of the thematic layers in GIS, which was classified into groundwater potential zones based on the decision as very good (10.7% of the area), good (13.4% of the area), moderate (18.6% of the area), poor (32.4% of the area) and very poor (24.9% of the area). The validation of the model developed was done against the well inventory data, which reflects the actual groundwater potential zones prepared by the model to check the validity of the proposed model (Table 2).

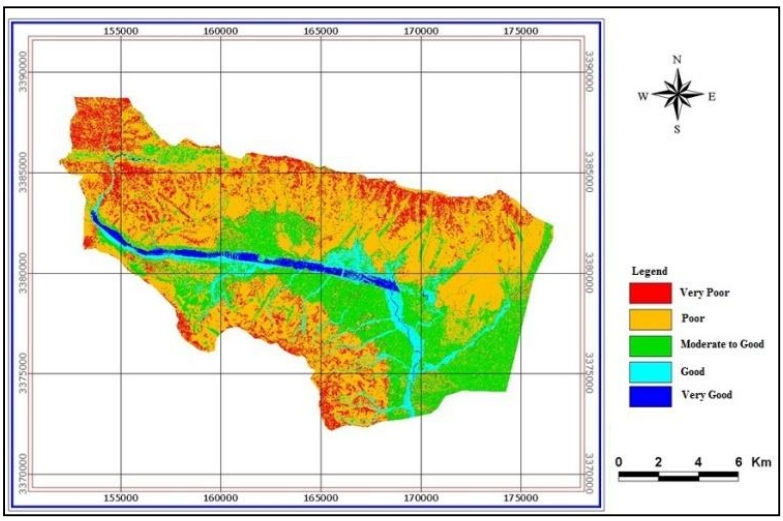

Figure 8: Groundwater potential zones of the study area

Table 2: Well inventory data of the study area

Sr. No.	Location (Village Name)	Depth of well (m)	Dia	Use
1	Teruwala	9.44	1.65	Domestic
2	Gondpur	9.16	2.39	Domestic
3	Jwalapur	25.96	2.9	Domestic
4	Naraingarh	36.1	2.84	Domestic
5	Kishankot	42.05	3	Domestic
6	Badrinagar	10.17	1.65	Domestic
7	Bhadripur	8.72	1.75	Domestic
8	Bain kuan	2.5	2.47	Domestic
9	Ganguwala	2.37	2.18	Domestic
10	Jamunawala	4.06	1.83	Domestic
11	Dhoka	1.89	1.85	Domestic
12	Gulabgarh	2.37	1.18	Irrigation
13	Ajiwala	4.67	1.89	Domestic
14	Khara	9.24	1.67	Domestic
15	Bhuppur	12.02	2.12	Domestic
16	Ganguwala	14.64	1.69	Domestic
17	Samsherpur	9.97	2.75	Domestic
18	Patiliyan	10.91	1.28	Domestic
19	Surajpur	7.83	1.76	Irrigation
20	Santokhgarh	4.22	1.31	Irrigation
21	Puuruwala	1.53	2	Irrigation
22	Johron	8.84	1.06	Domestic
23	Kiarda	7.19	2.12	Domestic
24	Misarwala	4.18	2.08	Domestic
25	Pipliwala	3.97	1.8	Domestic
26	Jagatpur	2.85	0.95	Domestic
27	Matak Majri	2.5	1.42	Domestic
28	Fatepur	2.38	1.97	Domestic
29	Kiratpur	1.56	1.62	Domestic
30	Nayagaon	9.7	2.08	Domestic
31	Sainwala	3.31	1.83	Irrigation
32	Tokion	4.69	1.7	Domestic
33	Dhaula Kuan	3.97	1.85	Irrigation
34	Bharapur	17.21	2.23	Irrigation
35	Rampur	10.48	2.1	Domestic
36	Majri	10.48	1.69	Domestic
37	Gunglo	3.5	1.44	Irrigation
38	Kolar	22.69	2.85	Domestic

4. Conclusion

Satellite imagery proved to be highly useful in terrain characterization i.e. in mapping of different groundwater potential zones. The groundwater potential zone map was validated by the coordinates of each well location, which were obtained by GPS and plotted in the data base. It was clearly shown that the well coordinates exactly match with the classified potential zones in the GIS environment. Excellent and good groundwater prospects zones mainly fall in the upper piedomant. The denudational hills, structural hills and residual hills mainly act as runoff zones. The final map prepared in the form of a prospect map would provide firsthand information to local authorities and planners about the areas to look for groundwater, followed by its suitable exploration. Based on the results of the study, concerned decision makers can formulate an efficient groundwater utilization plan for the study area so as to ensure long term sustainability of this vital resource.

Acknowledgements

First and foremost, I would like to thank to the School of Earth Sciences, College of Natural and Computational Sciences, Addis Ababa University, Addis Ababa, for providing lab facilities for research work. I wish to express my sincere thanks to the Indian Institute of Remote Sensing, Dehradun for provide data and research cooperation. The author would also like to thank anonymous reviewers for their valuable comments to the manuscript.

References

Avtar, R., C.K. Singh, S. Shashtri, A. Singh and S. Mukherjee (2010). Identification and analysis of groundwater potential zones in Ken-Betwa river linking area using remote sensing and geographic information system. Geocarto Int., 25: 379−396.

Burrough, P.A. (1986). Principles of geographic information system for land resources development. Oxford University Press, New York.

Choudhury, P.R. (1999). Integrated remote sensing and GIS techniques for groundwater studies in part of Betwa basin. Ph.D. Thesis (unpublished), Department of Earth Sciences, University of Roorkee, India.

Chowdhury, A., M.K. Jha, V.M. Chowdary and B.C. Mal (2009). Integrated remote sensing and GIS-based approach for assessing groundwater potential in West Medinipur district, West Bengal, India. Int. Jour. Remote Sensing, 30: 231−250.

Chowdhury, A., M.K. Jha and V.M. Chowdary (2010). Delineation of groundwater recharge zones and identification of artificial recharge sites in West Medinipur district, West Bengal, using RS, GIS and MCDM techniques. Env. Earth Sci., 59: 1209−1222.

Dar, I.A., K. Sankar and A. Dar Mithas (2010). Remote sensing technology and geographic information system modeling: An integrated approach towards the mapping of groundwater potential zones in Hardrock terrain, Mamundiyar basin. J. Hydrol., 394: 285– 295.

Dey, A.K. and A.C. Naithani (1988). Geological studies using remote sensing application in parts of Siwalik belt between Narayangarh and Paonta Sahib. Himachal Pradesh. Project Report, IIRS, Dehradun.

Devi and Wankhede (1995). Landform analysis related to environmental appraisal, slope stability and hydromorphogeological studies in part of Giri and Bata valley (Himachal Pradesh and Haryana). Project report, IIRS, Dehradun.

Dinesh Kumar, P.K., G. Gopinath and P. Seralathan (2007). Application of remote sensing and GIS for the demarcation of groundwater potential zones of a river basin in Kerala, southwest coast of India. Int. Jour. Remote Sensing, 28: 5583−5601.

El-Gammal, E.A., S.M. Salem and R.O. Greiling (2013). Applications of geomorphology, tectonics, geology and geophysical interpretation of, East Kom Ombo depression, Egypt, using Landsat images. Egyptian Journal of Remote Sensing and Space Sciences, 16:171–187.

Ibrahim-Bathis, K. and S.A. Ahmed (2016). Geospatial technology for delineating groundwater potential zones in Doddahalla watershed of Chitradurga district, India. The Egyptian Journal of Remote Sensing and Space Sciences, http://dx.doi.org/10.1016/j.ejrs.2016.06.002.

IMSD (1995). Integrated mission for sustainable development technical guidelines. National Remote Sensing Agency, Department of Space, Govt. of India.

Jugran, D.K. (2003). Geomorphic parameter for past Himalayan crustal deformation leading to geodynamic evolution and its effect on present instability in Trans Yamuna- Giri sector Paonta (H.P.) - A remote sensing and GIS based study. Dehradun. Report, IIRS, Dehradun.

Krishnamurthy, J. and G. Srinivas (1995). Role of geological and geomorphological factors in groundwater exploration – A study through remote sensing techniques. International Journal of Remote Sensing, 16: 2925−2618.

Murthy, K.S.R. (2000). Groundwater potential in a semi-arid region of Andhra Pradesh - A geographical information system approach. International Journal of Remote Sensing,21: 1867–1884.

Nag, S.K (2005). Application of lineament density and hydrogeomorphology to delineate groundwater potential zones of Baghmundi block in Prulia district, West Bengal. Jour. Indian Soc. Remote Sensing, 33: 521−529.

Nossin, J.J (1971). Outline of the geomorphology of the Doon valley, Northern U.P. India. Zeitschrift Fur Geomorphologie, Neue Folge, 12:18-50.

NRSA (1999). National rural drinking water mission methodology manual for preparation of groundwater prospects maps. National Remote Sensing Agency, Govt. of India, Hyderabad.

NRSA (2008). Groundwater prospect mapping using remote sensing and GIS, Rajiv Gandhi national drinking water mission project manual. National Remote Sensing Agency, Hyderabad.

O'Leary, D.W., J.D. Friedman and H.A. Poh (1976). Lineaments, linear, lineations: Some standards for old terms. Geol. Soc. Am. Bull., 87: 1463–1469.

Preeja, K.R., S. Joseph, J. Thomas and H. Vijith (2011). Identification of groundwater potential zones of a tropical river basin (Kerala, India) using remote sensing and GIS techniques. Jour. Indian Soc. Remote Sensing, 39: 83−94.

Rashid, M., M. Lone and S. Ahmed (2011). Integrating geospatial and ground geophysical information as guidelines for groundwater potential zones in hard rock terrains of south India. Environ. Monit. Assess., 184: 4829–4839.

Rawat, J.S. and Manish Kumar (2015). Monitoring land use/cover change using remote sensing and GIS techniques: A case study of Hawalbagh block, district Almora, Uttarakhand. India. Egypt. J. Remote Sens. Space Sci., 18: 77–84.

Rokade, V.M., P. Kundal and A.K. Joshi (2007). Groundwater potential modeling through remote sensing and GIS: A case study of Rajura taluka, Chandrapur district, Maharashtra. J Geol Soc India, 69: 943–948.

Saaty, T.L. (1980). Analytic hierarchy process; Planning, priority setting, resource caluculation. McGrow-Hill International Book company, New York. 1−287.

Sander, P. (2007). Lineaments in groundwater exploration: A review of applications and limitations. Hydrogeol. Jour., 15: 71−74.

Saraf, A.K. and P.R. Choudhury (1998). Integrated remote sensing and GIS for groundwater exploration and identification of artificial recharge sites. International Journal of Remote Sensing, 19, 1825–1841.

Sener, E., A. Davraz and M. Ozcelik (2005). An integration of GIS and remote Sensing in ground water Investigation: A case study in Burdur, Turkey. Hydrogeology Journal, 13: 826−834.

Senthil Kumar, G.R. and K. Shankar (2014). Assessment of groundwater potential zones using GIS. Front. Geosci., 2 (1):1–10.

Shaban, A., M. Khawlie and C. Abdallah (2006). Use of remote sensing and GIS to determine recharge potential zone: The case of Occidental Lebanon. Hydrogeology Journal, 14: 433–443.

Singh, A.K. and S.R. Prakash (2002). An integrated approach of remote sensing, geophysics and GIS to evaluation of groundwater potentiality of Ojhala sub-watershed, Mirjapur district, UP, India. In: Asian Conference on GIS, GPS, Aerial Photography and Remote Sensing, Bangkok-Thailand.

Sreedevi, P.D., S. Owais, H.H. Khan and S. Ahmed (2009). Morphometric analysis of a watershed of south India using SRTM data and GIS. Journal of Geological Society of India, 73:543–552.

Thomas, B.C., S.L. Kuriakose and S.K. Jaydev (2009). A method for groundwater prospect zonation in data poor areas using remote sensing and GIS: A case study in Kalikavu Panchayath of Malappuram district, Kerala, India. Int. Jour. Digital Earth, 2:155−170.

Todd, D.K (1980). Groundwater hydrology. 2nd ed., John Wiley & Sons. New York.

Todd, D.K. and L.W. Mays (2005). Groundwater hydrology. 3rd ed., Hoboken: John Wiley & Sons.

Tribe, A. (1991). Automated recognition of valley heads from digital elevation models. Earth Surf Process Landf., 16: 33–49.

Journal of Geomatics Vol 11 No. 1 April 2017

Effect of the global random distribution of data points on the estimated quality of datum transformation parameters: Simulation study

Raaed Mohamed Kamel Hassouna
Department of Civil Engineering, Faculty of Engineering in Shebin El-Kom, Menoufia University
Shebin El-Kom, 32511 Egypt
Email:raaedhassouna@gmail.com

(Received: Nov 08, 2016; in final form: Mar 25, 2017)

Abstract: In this study, the global random distribution of coordinate data points was investigated for its impact on the estimated quality of the geodetic datum transformation parameters. In particular, four data sample types with different spatial distribution characteristics were simulated within a global geographical window. The clustered, purely random, random grid and regular grid patterns were investigated. In order to support and generalize the results, these four data pattern types were simulated with four common global point densities. The results showed that for all the investigated point densities, the purely random data point configuration yielded the best estimated qualities for the predicted global datum transformation parameters.

Keywords: Point patterns, Random distribution, Geodetic datums, Datum transformation parameters

1. Introduction

Since the evolution of satellite geodesy, the determination of the optimal transformation parameters among geodetic datums has been a major task. Regionally, the estimation of transformation parameters between regional geodetic systems and global geocentric ones has become a need to globalize, densify and upgrade existing regional geodetic networks (El-Tokhey, 2000; Jekeli, 2006). Also, the mutual transformation parameters among the different regional datums have become a possible task (Twigg, 2000). Globally, one of the basic tasks of the various geodetic satellite missions is the determination, upgrade and refinement of the elements of the International Terrestrial Reference Frame (ITRF). This task is accomplished via the combinations of the GNSS, SLR, VLBI and DORIS satellite techniques. In the narrow sense, such refinement encounters the determination of the global datum transformation parameters between an old ITRF and a newer one (Altamimi et al., 2011).

Most common is Burša seven parameter model which accounts for three translation components, three rotation angles about the coordinate axes and a seventh scale factor parameter (Jekeli, 2006). Irrespective of whether the datum parameter estimation is a regional or a global task, two sets of 3D-Cartesian coordinates of some common data (or control) points must be known relative to both systems (Ghilani and Wolf, 2006). Such two sets of coordinates are input as observations into a combined (or mixed) least-squares adjustment procedure, where the seven transformation parameters are the unknowns to be estimated along with their uncertainties (Leick, 1990; Ghilani and Wolf, 2006).

The quality of the input observations, the density of the control points and their spatial distribution play important role on the quality of the parameters to be estimated (Altamimi et al., 2007). The quality and density of the globally gained point coordinates are continuously being improved and their impact is positively reflected on the quality of the estimated parameters (Altamimi et al., 2013).

However, the global coordinate data points are selected to be well distributed by visual inspection only. Spatial distribution of points and their impact on the quality of the target parameters have not been explicitly studied. Practical examples of spatial distribution models are the clustered, the purely random, the randomly displaced grid and the regular grid point configurations. Such point configurations can easily be simulated and analyzed over a pre-specified rectangular geographical window, based on the principles of stochastic geometry (Stoyan et al., 1987; Stoyan, 1998; Baddeley and Turner, 2005).

For local geographical windows, these four point pattern models were used to investigate the effect of data distribution on the quality of digital elevation models (Hassouna, 2013a) and on the quality of geoidal height prediction (Hassouna, 2013b). The results of the two studies implied that the randomness of data point configurations might be competitive to their regularity, in yielding better prediction qualities. In the second work, it was emphasized that the data distribution impact could vary according to the investigated geodetic task. So, it was recommended that the effect of data distribution should be separately studied for each task (Hassouna, 2013b).

Preliminary investigations have revealed that the spatial distribution variation of data point samples, within limited regional geographical windows like Egypt, would not significantly affect the quality of the target global transformation parameters. Whatever the point patterns, such limited windows would yield practically similar sparse global data coverage, thus resulting in negligible variations in the estimated qualities of the global parameters.

Thus, the objective of the current study is to investigate the effect of the global random distribution of the data points on the quality of the estimated datum transformation parameters. In particular, the aforementioned four point pattern types will be simulated to represent different sets of coordinate data points over a global window. This proposed simulation algorithm stands in analogy with the optimization of geodetic networks configurations before the collection of actual observations (Ashkenazi and Cross, 1972).

2. The simulated point configurations

In particular, four types of global point configurations were simulated, utilizing the software developed by Stoyan (1998). These are the Matérn-clustered pattern, the Poisson's purely random pattern, the random grid and the regular grid (Schmidt, 2011). The random displaced grid was simulated with a spatial standard deviation of 0.2 arc-degree (Stoyan, 1998). In order to support and generalize the results, all point pattern types were simulated with four numbers of global data points. Each type was generated with an average of 20, 80, 120 and 155 points. Such numbers of points were arbitrarily selected in order to verify the impact of data distributions on the quality of estimated parameters, taking into account the variation in global data density. Also, a global number of 120 or 155 points might be realistic for a set of ITRF stations.

In Hassouna (2013b), it was found that different realizations of the same point pattern type yielded practically the same spatial distribution characteristics. This agrees with the Ergodizity property of spatial point processes (Stoyan and Stoyan, 1992; Schmidt, 2011). So, in the current study, for a given global point density, only one point pattern type was simulated. Having geodetic latitudes and longitudes as horizontal curvilinear coordinates, these sixteen point configurations were realized within a rectangular global window bounded by ($-90° \le \varphi \le +90°$; $-180° \le \lambda \le 180°$). As illustrative examples, Figure (1) shows the four point pattern types with 120 points.

The clustered sample is irregular. In a purely random pattern, the point locations are spatially independent (Stoyan and Penttinen, 2000; Schmidt, 2011). Such sample is more regular than a clustered one. The randomly displaced grid is more uniform than the previous two types, whereas it is less regular than a grid pattern. However, it still exhibits slight randomness. Among all types, the regular grid pattern is the most uniform one. Statistically, both the clustered and regular grid patterns can be looked upon as exhibiting two opposite extreme systematic point arrangements (Ohser and Lorz, 1996).

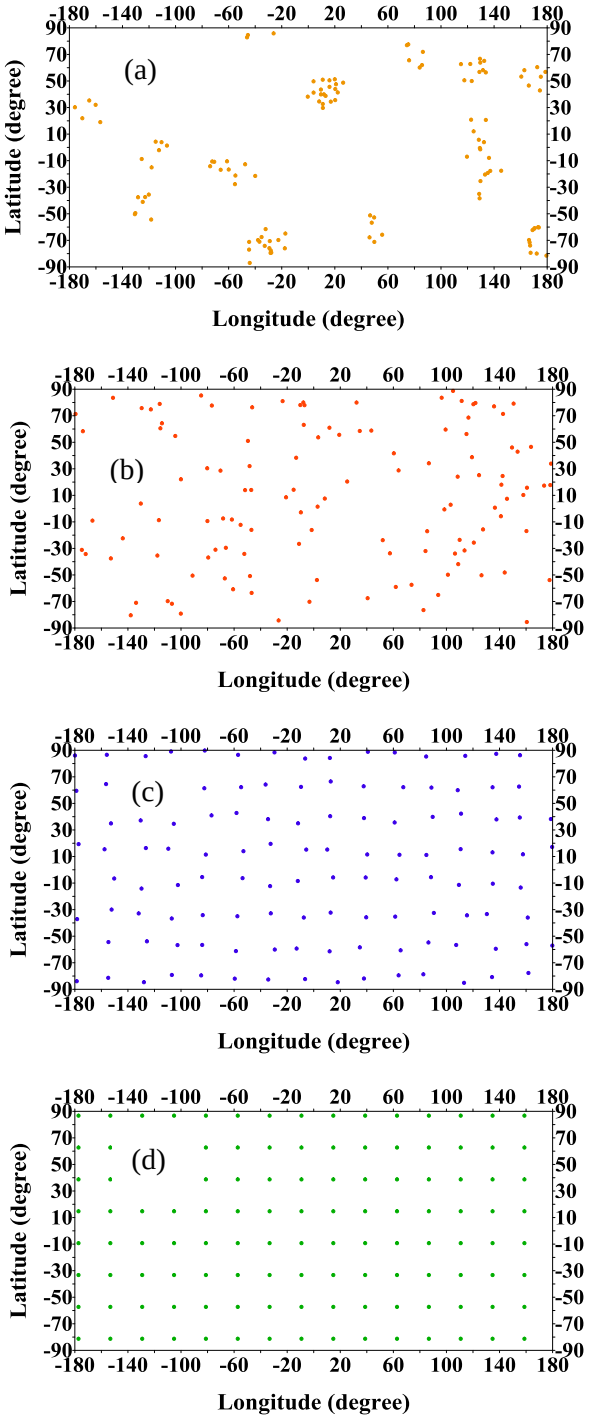

Figure 1: Illustrative point pattern types with 120 points (a) Clustered pattern (CT); (b) Purely random pattern (RN); (c) Random grid pattern (RG); and (d) Regular grid pattern (GR)

3. The simulated sets of noisy Cartesian coordinates

The above simulated sets of horizontal geodetic coordinates were assumed to be relative to the WGS-84 reference ellipsoid. In order to devote the current study to the effect of horizontal data distributions on the datum parameters quality, such simulated points were assigned zero ellipsoidal height values. The numerical significance of non-zero ellipsoidal heights will be clarified in Section (4). Thus, using the geodetic curvilinear coordinates (φ, λ, h=0) of the points of the

sixteen simulated configurations, the corresponding 3D-Cartesian ones were computed by (Jekeli, 2006)

$$\begin{bmatrix} X \\ Y \\ Z \end{bmatrix} = \begin{bmatrix} (R_n + h)\ \cos\varphi\ \ \cos\lambda \\ (R_n + h)\ \cos\varphi\ \ \sin\lambda \\ \left[\left(b^2/a^2\right)R_n + h\right]\ \sin\varphi \end{bmatrix}, \qquad (1)$$

where a and b are semi-major and semi-minor axis of the WGS-84 reference ellipsoid, respectively; and R_n is the prime-vertical radius of curvature at the point under consideration. For WGS-84, a = 6,378,137.0 and b = 6,356,752.3142 meters (Ghilani and Wolf, 2006).

The above computed sets of Cartesian coordinates were considered to represent start input coordinates, from which respective start sets of Cartesian coordinates were evaluated relative to another arbitrary coordinate system. The seven transformation parameters from the WGS-84 system to that arbitrary system were assigned the following adopted values

$$\text{Shift components} \equiv \begin{bmatrix} X_0 \\ Y_0 \\ Z_0 \end{bmatrix} = \begin{bmatrix} +150 \\ +115 \\ +7 \end{bmatrix} \text{ meter},$$

$$\text{Rotation angles} \equiv \begin{bmatrix} R_X \\ R_Y \\ R_Z \end{bmatrix} = \begin{bmatrix} +3 \\ +2 \\ +3 \end{bmatrix} \text{ arcsec.},$$

$$\text{Scale factor } S = 0.2 \text{ ppm}. \qquad (2)$$

The rotation angles about the coordinate axes are taken positive anti-clockwise. Hence, the sixteen sets of start point coordinates, which correspond to the second coordinate system, were assessed as follows (Jekeli, 2006)

$$\begin{bmatrix} x \\ y \\ z \end{bmatrix} = \begin{bmatrix} X_0 \\ Y_0 \\ Z_0 \end{bmatrix} + (1+S) \begin{pmatrix} 1 & R_Z & -R_Y \\ -R_Z & 1 & R_X \\ R_Y & -R_X & 1 \end{pmatrix} \begin{bmatrix} X \\ Y \\ Z \end{bmatrix}, \qquad (3)$$

where the small rotation angles are expressed in radian.

From Eq. (3), it is apparent that such adopted parameters (in Eq. 2) are consistent with both sets of Cartesian coordinates. Of course, any known regional or global datum parameters could be used instead, since all such datums are differentially similar.

It is worth mentioning that the transformed point configurations, as computed from Eq. (3), would practically show the same spatial distributions in terms of geodetic latitudes and longitudes, as those input to Eq. (1). This can be supported by the intuition that such two nearly aligned geodetic datums would yield systematic changes in the respective geodetic latitudes and longitudes, which are surely in range of arc-seconds.

As input simulated observations, both sets of the start Cartesian coordinates, in Eqs. (1) and (3) were assigned Gaussian normally distributed noises with a zero mean and a standard deviation of one meter (Press et al., 2001). Such unification of the simulated noise was thought to help in rendering the quality of the subsequently estimated datum parameters to the effect of data distribution, rather than to the relative quality of observations.

Then, for each of the sixteen "noisy" pairs of point configurations, a mixed least squares adjustment was performed, yielding the respective sets of seven transformation parameters along with their uncertainties.

4. The mixed least-squares adjustment model

The mixed least-squares adjustment functional model can be expressed as follows (Mikhail and Gordon, 1981)

$$F_{c,1}\left(\overline{P}_{u,1}\ ,\ \overline{L}_{n,1}\right) = 0, \qquad (4a)$$

where

$\overline{P}_{u,1}$ the vector of adjusted parameters,
$\overline{L}_{n,1}$ the vector of adjusted observations,
u the number of parameters,
n the number of observations,
c the number of condition equations among the adjusted parameters and observations.

Based on Eq. (3), for each coordinate data point common to both datums, the mathematical model in Eq. (4a) can be written as follows (El-Tokhey, 2000; Ghilani and Wolf, 2006)

$$\begin{bmatrix} \overline{X}_0 \\ \overline{Y}_0 \\ \overline{Z}_0 \end{bmatrix} + \left(1+\overline{S}\right) \begin{pmatrix} 1 & \overline{R}_Z & -\overline{R}_Y \\ -\overline{R}_Z & 1 & \overline{R}_X \\ R_Y & -\overline{R}_X & 1 \end{pmatrix} \begin{bmatrix} \overline{X} \\ \overline{Y} \\ \overline{Z} \end{bmatrix} - \begin{bmatrix} \overline{x} \\ \overline{y} \\ \overline{z} \end{bmatrix} = 0. \qquad (4b)$$

Thus, for a pair of point configurations having K points, the vectors of adjusted parameters and observations are given by

$$\bar{P}_{u,1}=\begin{bmatrix}\bar{X}_0\\ \bar{Y}_0\\ \bar{Z}_0\\ \\ \bar{R}_X\\ \bar{R}_Y\\ \bar{R}_Z\\ \\ \bar{S}\end{bmatrix}, \quad \bar{L}_{n,1}=\begin{bmatrix}\bar{X}_1\\ \bar{Y}_1\\ \bar{Z}_1\\ \\ \bar{x}_1\\ \bar{y}_1\\ z_1\\ \\ \cdots\\ \cdots\\ \\ \bar{X}_k\\ \bar{Y}_k\\ \bar{Z}_k\\ \\ \bar{x}_k\\ \bar{y}_k\\ z_k\end{bmatrix}. \quad (5)$$

Thus, u = 7, c = 3K and the degree freedom of the mixed adjustment process is given by

$$\begin{aligned} r &= c-u \\ &= 3K-7. \end{aligned} \quad (6)$$

The corresponding linearized form of the mixed adjustment algorithm was formulated as follows (Mikhail and Gordon, 1981)

$$A_{c,u}\ \delta_{u,1}+B_{c,n}\ V_{n,1}=W_{c,1}\ , \quad (7)$$

where

$A_{c,u}$ the design matrix, which carries the partial derivatives of the functional model (Eq. 4a) with respect to the parameters,

$\delta_{u,1}$ the vector of parameters corrections,

$B_{c,n}$ the coefficient matrix of condition equations, which contains the partial derivatives of the functional model (Eq. 4a) with respect to the observations,

$V_{n,1}$ the vector of observations residuals,

$W_{c,1}$ the vector of absolute terms.

While the partial derivatives in the matrix A are functions of the observations, those in B are expressed in terms of the approximate parameters (Ghilani and Wolf, 2006).

As stated in Section 3, the input observations were assigned equal noise standard errors. So, the least-squares adjustment algorithm was performed using equal weights. Thus, using an a priori reference variance of unity, the solution vector was computed as follows (Leick, 1990)

$$\delta=\left[A^T\left(BB^T\right)^{-1}A\right]^{-1}\left[A^T\left(BB^T\right)^{-1}W\right]. \quad (8)$$

Then, the observational residuals were assessed by

$$V=B^T\left(BB^T\right)^{-1}\left[A\,\delta-W\right]. \quad (9)$$

The seven datum parameters were initially assigned zero approximate values. The solution was improved, using the updated values of the observations and parameters, till the convergence of iterations. Denoting the approximate parameters of the last iteration as

$$\left[X_0^{\,a}\ Y_0^{\,a}\ Z_0^{\,a}\quad R_X^{\,a}\ R_Y^{\,a}\ R_Z^{\,a}\quad S^a\right]^T,$$

and the corresponding estimated corrections as

$$\left[\delta X_0\ \delta Y_0\ \delta Z_0\quad \delta R_X\ \delta R_Y\ \delta R_Z\quad \delta S\right]^T,$$

so, the estimated datum parameters were assessed as follows

$$\begin{bmatrix}\bar{X}_0\\ \bar{Y}_0\\ \bar{Z}_0\\ \\ \bar{R}_X\\ \bar{R}_Y\\ \bar{R}_Z\\ \\ \bar{S}\end{bmatrix}=\begin{bmatrix}X_0^{\,a}\\ Y_0^{\,a}\\ Z_0^{\,a}\\ \\ R_X^{\,a}\\ R_Y^{\,a}\\ R_Z^{\,a}\\ \\ S^a\end{bmatrix}+\begin{bmatrix}\delta X_0\\ \delta Y_0\\ \delta Z_0\\ \\ \delta R_X\\ \delta R_Y\\ \delta R_Z\\ \\ \delta S\end{bmatrix}. \quad (10)$$

And the reference variance was computed by

$$\hat{\sigma}^2_0=V^TV/r. \quad (11)$$

Finally, the covariance matrix of the estimated seven parameters was assessed as follows

$$\Sigma_{PP}=\hat{\sigma}^2_0\left[A^T\left(BB^T\right)^{-1}A\right]^{-1}. \quad (12)$$

Considering Eqs. (1), (4b) and (7), it could be sensed that even if the ellipsoidal heights were not ignored, they would have negligible numerical impact on the computed Cartesian coordinates. This numerical insignificance is reflected on the elements of the matrix A, and consequently, on the estimated covariance matrix (Eq. 12). Such thought could be verified by keeping in mind that those heights, even if they amounted to a few kilometers, are very small compared to R_n, which represents the principal maximal radius of curvature at

any point. Perhaps exceptions could arise for points that happen to have so large ellipsoidal heights and are located at the equator or at the poles.

In the current work, the above steps of the mixed least-squares procedure (Eq. 6 to 12) were performed using the DATUM software developed by Junkins (1998).

In Section 5, both the local and global precision criteria for the estimated seven parameters are explored and compared for all the investigated data point samples. As local measures of precision, the estimated standard errors of the parameters will be used. On the other hand, the traces of the estimated covariance matrices will be used as global precision measures (Blaha, 1971; Ashkenazi, 1974). For this purpose, it was necessary to have consistent sums for the diagonal elements with units of m^2. Using a mean Earth's radius of 6371 km, the standard errors of the rotation angles were converted to respective axes-displacement uncertainties on the Earth's surface in meter units as follows (Altamini et al., 2007)

$$\begin{bmatrix} \sigma_{\bar{R}_X} \\ \sigma_{\bar{R}_Y} \\ \sigma_{\bar{R}_Z} \end{bmatrix}_{meter} = \left(\frac{6371000}{206264.8}\right) \begin{bmatrix} \sigma_{\bar{R}_X} \\ \sigma_{\bar{R}_Y} \\ \sigma_{\bar{R}_Z} \end{bmatrix}_{arc\,sec.}, \quad (13)$$

and the estimated standard errors of the scale factors were expressed as radial errors by (Altamini et al., 2007)

$$\sigma_{\bar{S}\ meter} = \left(\frac{6371000}{10^6}\right) \sigma_{\bar{S}\ ppm}. \quad (14)$$

5. Results

Figure (2) plots the estimated reference variances which correspond to the four point pattern types with global number of points K= 20, 80 and 120. Figure (3) shows the respective estimated standard errors of the three datum shift components, while Figure (4) illustrates the estimated uncertainties of the three datum rotation angles. Also, Figure (5) plots the corresponding standard errors of the estimated scale factors.

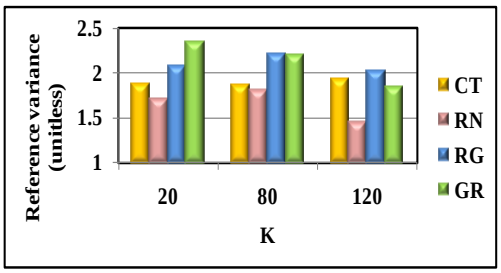

Figure 2: The estimated reference variances

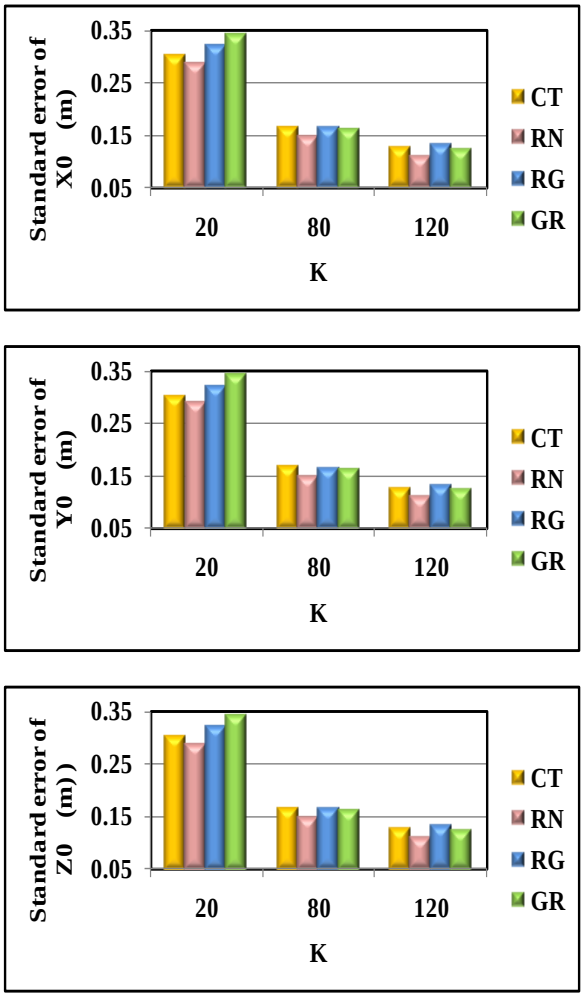

Figure 3: The estimated standard errors (top) of X_0 components, (middle) y_0 components; and (bottom) the Z_0 components

Figures (2 - 5) show that whatever the global data point density is, the pure random data point configuration resulted in minimal values of reference variances and optimal uncertainties of the estimated seven datum transformation parameters. Also, Figures (3 - 5) show significant differences among the uncertainties relevant to the pure random point sample type, and those corresponding to the other three configuration types. The significance of such differences can be directly sensed for the shift components. The significant differences among the uncertainties of the rotation angles and scale could be better sensed, if they are expressed in meter units on the Earth's surface and in the radial direction, respectively (Eqs. 13 and 14). Figure (3) shows that for a specific data configuration, the uncertainties of the shift components are nearly the same. This can be regarded to the fact that the mathematical model (in Eq. 4b) is marginally linear with respect to the shift parameters (Ghilani and Wolf, 2006).

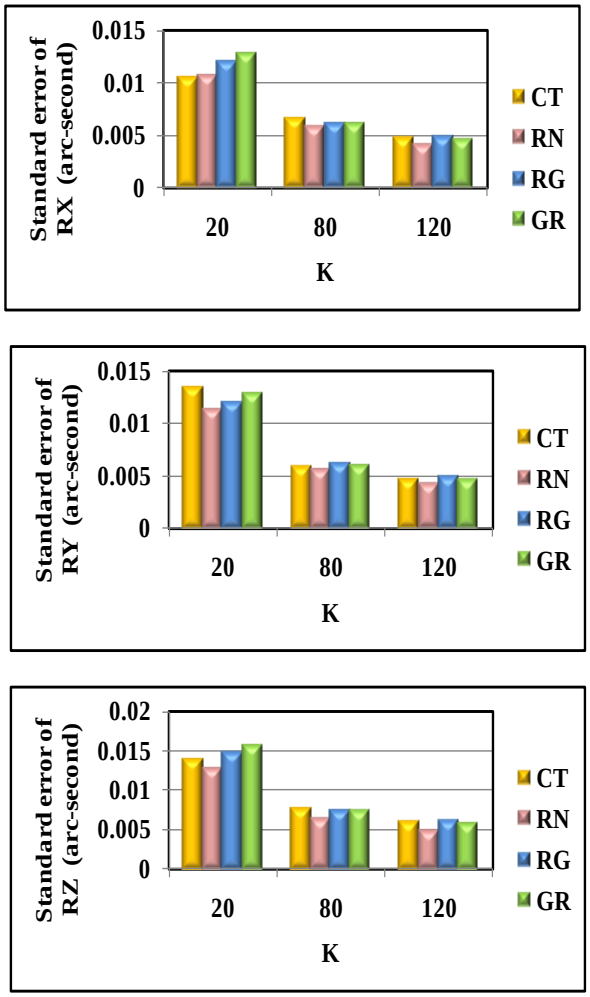

Figure 4: The estimated standard errors of (top) the R_x rotations; (middle) the R_y rotations; and (bottom) the R_Z rotations

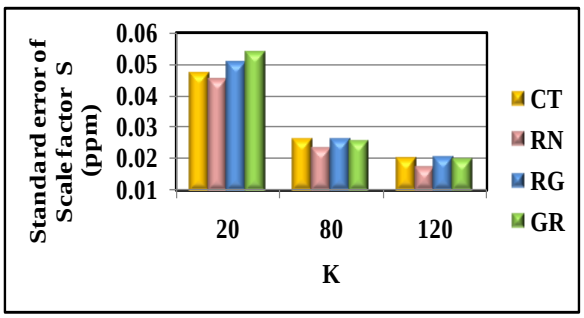

Figure 5: The estimated standard errors of the scale factors S

As the observations were assigned similar simulated noise, the minimal values of the variance factors imply respective optimal norms of the observational residuals that were produced by the adjustment process. In other words, the random point configurations yielded optimally filtered observational noise during the adjustment. On the other hand, the optimal standard errors pertaining to the random pattern type (Figures 3 - 5) imply respective minimal traces of the variance-covariance matrices (Eq. 12). This in turn means that the normal matrices relevant to the random point configurations are the most well conditioned ones, compared to those of the other data point patterns (Blaha, 1971; Ashkenazi, 1974). Such results imply that the random data point samples lead to optimal error propagation characteristics through the design matrix A. Namely, as denoted in Section 4, such A matrix depends on the observations which are point coordinates in the current investigation. Such optimal normal matrix conditioning must have been reflected on the respective estimated parameters (Eq. 10) and their uncertainties (Eq. 12).

Figures (6 - 9) plot similar comparisons, but only regarding the four point pattern types with K=155 points. Again, Figures (6 - 9) show that the random point samples yielded optimal variance factors and datum parameters uncertainties. Furthermore, the differences among the various quality measures are still significant.

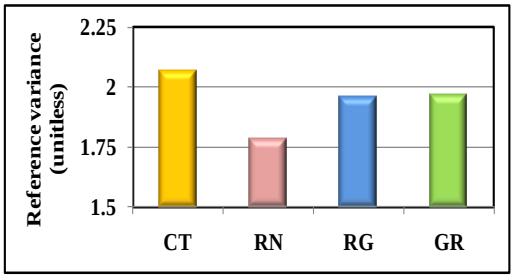

Figure 6: The estimated reference variances (K=155)

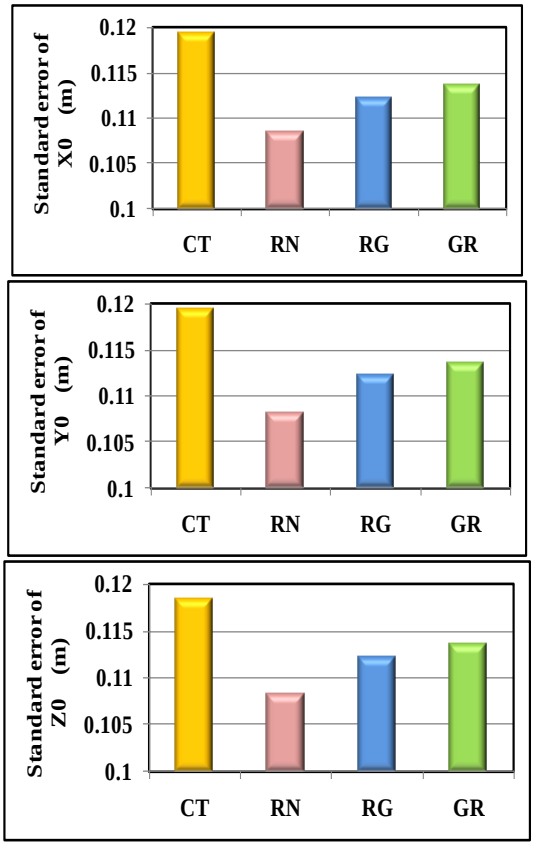

Figure 7: The estimated standard errors of (top) the X_0 components; (middle) the Y_0 components; and (bottom) the Z_0 components (K=155)

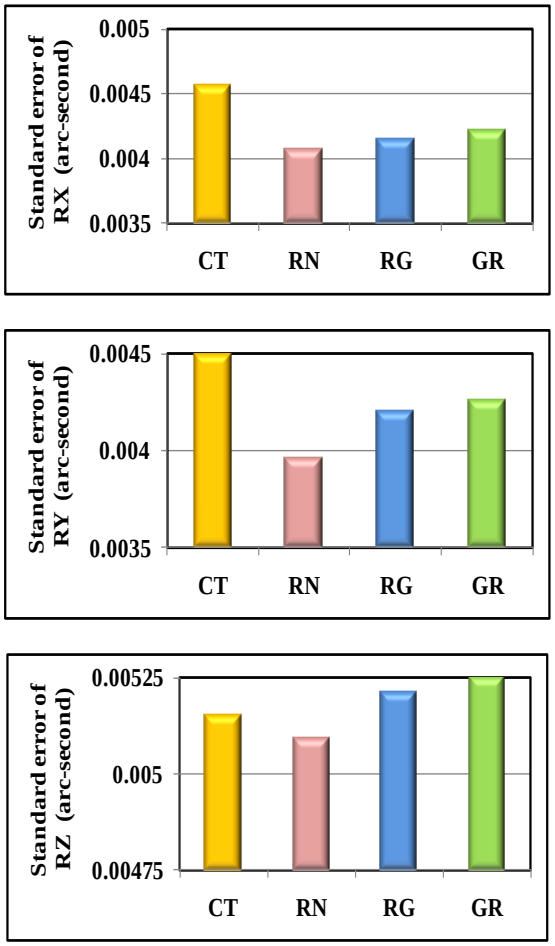

Figure 8: The estimated standard errors of the (top) R_x rotations; (middle) R_y rotations; and (bottom) R_Z rotations

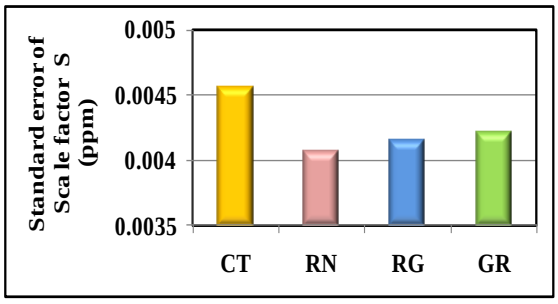

Figure 9: The estimated standard errors of the scale factors S (K=155)

Again, Figure (10) assures that, among the other three types, the purely random point configurations yielded the optimal global-wise precision for the estimated parameters. So, this final result supplements and is mutually related to the local-wise optimality of the purely random point samples in Figures (3 - 5) and Figures (7 - 9).

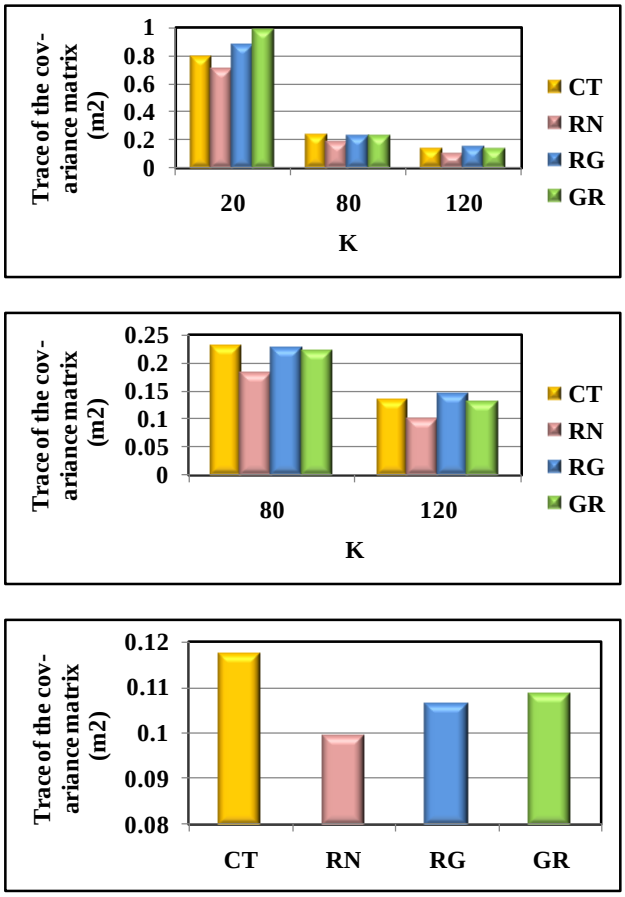

Figure 10: Comparison among the trace values of covariance matrix (top) for k = 20, 80 and 120; (middle) for k = 80 and 120; and (bottom) (K=155)

6. Discussions and recommendations

For the four investigated data point densities, the purely random coordinate data distribution proved to be the optimal one. This result was ascertained, based on both the local and global parameter precision criteria. Although the followed mixed adjustment procedure is originally regular, the minimal trace proximity of the random samples could stand in analogy with the free adjustment of geodetic networks (Blaha, 1971; Ashkenazi, 1974). So, among any other distributions of the data samples, the random point configurations could be considered as offering the optimal numerical stability of the normal matrix (Blaha, 1971). This was associated with mostly well conditioned normal matrices, which yielded optimal solutions and uncertainties for the respective estimated datum parameters.

Regarding the clustered (CT), nearly regular (RG) and regular (GR) configurations, the corresponding systematic arrangements of data points (Ohser and Lorz, 1996) could have worsen the condition number of the normal matrices, which negatively affected the estimated parameters qualities.

Hence, regarding the estimated parameters and their qualities, the purely random point patterns could be considered to have minimized the numerical problems, due to the arbitrary selection of a data distribution

pattern. In this sense, the qualities of the adjusted parameters might truly reflect the precision of the input observations.

Consider again the optionally adopted datum parameters (Eq. 2). The obtained results depict the major impact of the observational data on the estimated qualities of datum parameters. So, such results also assure that the same quality proportions could have been obtained, if another known or arbitrary set of parameters was adopted in the simulation process.

In comparison with the current realistic coordinate data noise and transformation parameters relevant to the successive ITRFs, the simulated input observational noise and the adopted magnitudes of the datum parameters are considerably large. Also, this holds true for the estimated quality measures (Altamimi et al., 2011). Such larger proportions were thought to help compare the variations of the parameter qualities with data distribution. Moreover, the investigation of actual ITRFs coordinate data distributions would surely yield significant differences among the output quality measures. Such quality differences, although might be much smaller, would be significant, compared to the nowadays strict ITRFs demands. For example, the adverse effect of a poor ITRF data coverage over the southern hemi-sphere, was apparent on the quality of the Z_0 parameter between ITRF2005 and ITRF2008 (Altamimi et al., 2011).

So, it is recommended to optimize the actual ITRF coordinate data distributions, regarding the estimated ITRF transformation parameters, their time rates and their uncertainties. Such data distribution optimization could be accomplished, leaning on the stochastic geometry approach, which was followed in the current study. It might be claimed that the investigated data distribution models might be only of theoretical benefit. However, based on the principles of stochastic geometry, there exist efficient computer modules that could statistically judge, whether a given proposed data pattern belongs to a specific spatial distribution model (e.g. Baddeley and Turner, 2005). Also, as the majority of the ITRFs stations are mostly continent- or nation-wise clustered (Altamimi et al., 2007 & 2011), such future outlook could be of benefit.

Regarding positioning by GNSS, it is well known that the quality of the estimated positions and position differences is highly dependent on the geometry of the tracked satellite constellation. Such geometry is often evaluated by the Dilution Of Precision (DOP) factors (Leick, 1990). Namely, the DOP factors are routinely used as an optimization criterion for the planning and post-processed solutions of the GNSS sessions. Again, a future work could be to try optimizing the GNSS observational sessions, leaning on specific spatial distribution models for the GNSS satellites. This is easy to achieve, based on the geocentric curvilinear coordinates of the GNSS satellites. So, using appropriate stochastic geometry modules, software packages could be designed and tested for the planning and post-processing of the GNSS observational sessions.

Finally, the current study could help optimizing local data configurations for country-level datum parameter estimation. However, in such case, the Molodensky-Badekas model might be used (Ng Boon Chye, 1992). This ten (7+3) parameter model accounts for the rotations and scale with respect to a central (average) origin that is close to the data points, and whose local 3D-coordinates represent the three additional parameters (Boon and Setan, 2007). In this manner, the problem of poor global coverage of the local data patterns, which was declared in Section 1, might be abridged.

7. Conclusions

Based on the current study, it can be concluded that the global density of the coordinate data points affects the absolute magnitudes of the estimated precisions of the datum parameters. However, the relative magnitudes of quality are dependent on the spatial distribution of the coordinated data samples. The current study could help optimizing local data configurations for country-level datum parameter estimation. The ten parameter model accounts for the rotations and scale with respect to a central (average) origin that is close to the data points, and whose local 3D-coordinates represent the three additional parameters. In this manner, the problem of poor global coverage of the local data patterns can be overcome considerably.

Aknowledgements

Two unknown reviewers are thanked for their critical and constructive review of the paper.

References

Altamimi, Z., X. Collilieux, J. Legrand, B. Garayt and C. Boucher (2007). ITRF2005: A new release of the International Terrestrial Reference Frame based on time series of station positions and Earth Orientation Parameters. Journal of Geophysical Research, 112 (B09401), 1-19.

Altamimi, Z., X. Collilieux and L. Métivier (2011). ITRF2008: An improved solution of the international terrestrial reference frame. Journal of Geodesy, 85, 457–473.

Altamimi, Z., X. Collilieux and L. Métivier (2013). Preliminary analysis in preparation for the ITRF2013. Geophysical Research Abstracts, 15, EGU2013-4671.

Ashkenazi, V. (1974). Criteria for optimization: A practical assessment of a free network adjustment. Bullettino di geodesia e scienze affini, 1(33), 77-91.

Ashkenazi, V. and P. Cross (1972). Strength analysis of Block VI of the European Triangulation. Bulletin Geodesique, (103).

Baddeley, A. and R. Turner (2005). spatstat: An R package for analyzing spatial point patterns. Journal of Statistical Software, 12 (6), 1- 42.

Blaha, G. (1971). Inner adjustment constraints with emphasis on range observations. Report No. 148, Department of Geodetic Science, Ohio State University.

Boon, P.S. and H. Setan (2007). 3D coordinate transformation using Molodensky-Badekas transformation model: MBT07. Proceedings of Joint International Symposium & Exhibition on Geoinformation/GNSS 2007 (ISG/GNSS2007). Johor Bharu, Johor, Malaysia, 5-7 November.

El-Tokhey, M. (2000). On the determination of consistent transformation parameters between GPS and the Egyptian geodetic reference systems. Paper presented at the Gravity, Geoid and Geodynamics (GGG2000), Banff, Alberta, Canada, July 31-August 5.

Ghilani, C. and P. Wolf (2006). Adjustment computations: Spatial data analysis. Fourth Ed., John Wiley & Sons, Inc.

Hassouna, R. (2013a). Assessing the role of point sample neighborhoods in digital elevation modeling. Engineering Research Journal, Faculty of Engineering, Menoufia University, Egypt, 36(4), 457-463.

Hassouna, R. (2013b). Models for assessing the spatial distribution of geodetic point patterns: Application to geoid prediction quality. Journal of Applied Geodesy, 7(2), 83-102.

Jekeli, C. (2006). Geometric reference systems in geodesy. Lecture Notes, Division of Geodesy and Geospatial Science, School of Earth Sciences, Ohio State University, December 2006.

Junkins, D. (1998). Program DATUM: Version 1.2 (98.09.24). Available at: http://www.geod.nrcan.gc.ca/ ~ craymer/ (accessed December 2010).

Leick, A. (1990). GPS satellite Ssurveying. John Wiley & Sons.

Mikhail, E. and G. Gordon (1981). Analysis and adjustment of survey measurements. Van Nostrand Reinhold, New York.

Ng Boon Chye (1992). Determination of three dimensional transformation parameters using Molodensky-Badekas model for coordinate transformation in Peninsular Malaysia. Kertas Projek Sarjana Muda, Universiti Teknologi Malaysia.

Ohser, J. and U. Lorz (1996). Quantitative gefüge analyse. Heft 276: Metallurgie und Werkstofftechnik, Freiberger Forschungshefte, Technische Universität Bergacademie Freiberg.

Press, W., S. Teukolsky, W. Vetterling and B. Flannery (2001). Numerical recipes in Fortran: The art of scientific computing. Second Ed., Cambridge University Press.

Schmidt, V. (2011). Räumliche statistik für punktprozesse und weitere Modelle der stochastischen geometrie, Institut für Stochastik, Universität Ulm, Germany.

Stoyan, D. (1998). Program STG 4.1. Available at: http://www.mathe.tu-freiberg.de/ (accessed July 2007).

Stoyan, D. and A. Penttinen (2000). Recent applications of point process methods in forestry statistics. Statistical Science, 15(1), 61-78.

Stoyan, D. and H. Stoyan (1992). Formen - Fraktale - Punktfelder: Methoden der Geometrie-Statistik. Akademie-Verlag, Berlin.

Stoyan, D., W.S. Kendall and J. Mecke (1987). Stochastic geometry and its applications. Akademie-Verlag, Berlin.

Twigg, D.R. (2000). OSGB36/WGS84 coordinate yransformations. Survey Review, 35(275), January, 292-306.

Journal of Geomatics Vol 11 No. 1 April 2017

Web-GIS based application for utility management system

Rajeshkumar J. Ajwaliya[1], Shashikant Patel[2] and Shashikant A. Sharma[2]
[1]Construction and Maintenance Group
[2]VEDAS Research Group, EPSA
Space Applications Centre-ISRO, Ahmedabad-380015.
Email: rjajwaliya@sac.isro.gov.in

(Received: May 18, 2016; in final form: Feb 02, 2017)

Abstract: Utility management processes are very complex, multidimensional and they require modification of traditional approaches. Managers and planners experience difficulty in data management and spatial data integration with traditional Management Information System (MIS). This paper presents a conceptual design model of a Geographic Information System (GIS) for a Web-based utility management system using open source technologies. As a case study, Web-GIS based Utility Management System (WGUMS) for six campuses of Space Applications Centre (SAC) viz., main campus, Bopal campus (technical and residential) and four residential housing colonies of center is presented. The developed web-GIS application contains physical information like campus boundary, buildings, roads, water supply lines, drainage lines, firefighting lines, pump house, wells, bore points, recharge wells, power substations, electrical light poles, solar light poles, nursery area and trees. The WGUMS is used to visualize and maintain utility assets in terms of database and operations, thus it has the potential to manage the scattered data into a single platform. Developed WGUMS is helpful in effective management of utility assets at SAC campus as well as residential area. WGUMS provides interactive Graphical User Interface (GUI) along with basic GIS functionalities over the web for users.

Keywords: GIS, Web-GIS, Open source, OGC, WMS, Utility management.

1. Introduction

Electricity distribution and water supply is the process of transporting electrical energy and water from the transmission point to the end user's points. Electricity and water are essential parts of everyday life that are often taken for granted. Like electricity and water, civilized society needs organized and well maintained other assets such as sewage lines, gardens and utility network. Using the GIS technology, complexities of utility network can be simplified and maintenance cost can be reduced to some extent. Geographic Information System (GIS) and web GIS technology can help resource managers in providing improved services. Traditional approaches are very complex to manage utility information, which are discussed later in 'characteristics of existing system' section, that upswings the need for the development of a Web-GIS based Utility Management System (WGUMS) system.

Today, the system of storing and sharing information is possible through the internet and World Wide Web (WWW). The internet technologies provide the facility to establish communication network between computers world-wide. Web services are modular, self-describing applications that can seamlessly interoperate directly across the internet. The development and availability of powerful GIS and visualization tools in conjunction with the internet have played an important role in the emergence of web-enabled management system. During the past decade, GIS has been widely used in various types of business, government and university projects. In order to utilize the available spatial datasets efficiently and effectively, web GIS has to play a significant role by providing information in decision making processes and it is not just in disseminating the spatial data (Yang et al., 2005). Web GIS is gaining popularity and it is an important tool to share and interoperate the heterogeneous spatial data. The web based applications consent a new forms of communication as well as information sharing. In essence, Web Services are able to package data without considering the specific application environment at the client end. Different systems can achieve seamless communication, data sharing and interoperation across platforms and languages based on Web Services framework.

Since the advancement of internet and geospatial technologies, various efforts have been made to generate information and utilization of these techniques for the well-being of society. Today in the advancement of Web technology, various management systems have been developed for utility mapping, power distribution, Earth data and Planetary data dissemination and archival. Web GIS is also important in decision making process such as urban planning process (Mansourian et al., 2011), Public Transport Management System, Emergency Response System (ERS), livestock information management system (Otieno and Nigigi, 2014; Baucic and Medak, 2015; Ranade and Mishra, 2015) which have been developed using various tools and technologies. The above mentioned applications highlight a variety of specific GIS applications within different management system.

Web Map Service (WMS) interface standard provides a simple HTTP interface for requesting geo-registered maps or images from geospatial database configured with PostgreSQL and PostGIS. Open Source technologies which follow the Open Geospatial Consortium (OGC) specifications are used in

application development e.g. Geo-Server, Open Layers, Tile Cache is an implementation of a WMS-C compliant server and can easily cache the data of WMS. It makes the response speed of WMS 10-100 times faster (Green and Bossomaier, 2002).

2. Objective

The paper aimed to design and develop a management system where information can be analyzed and managers can take the decisions on the basis of available information. Therefore, the key objective is to manage the information from different sources at center level using advanced methods and technologies which perform spatial analysis for enhanced administration and management. The study was intended to develop a WGUMS system at center level with interactive Graphical User Interface (GUI) along with GIS functionalities for utility management.

3. Study area

Premises of Space Applications Centre (SAC) is the study area. It has two functional office campuses (SAC-main Campus and SAC-Bopal Campus). Besides this, SAC owns four residential housing colonies and a residential area for Students/Guests constructed at Bopal village, within Ahmedabad, Gujarat India. System modules have been developed for both functional office campuses, four residential colonies along with Bopal residency.

SAC office campuses: SAC, spread over 83 acres, is one of the major centers of the Indian Space Research Organization (ISRO). SAC focuses on the design of space-borne instruments for ISRO missions and development and operationalization of applications of space technology for societal benefits. The applications cover communication, broadcasting, navigation, disaster monitoring, meteorology, oceanography, environment monitoring and natural resources survey. SAC-Bopal campus is spread over 14.7 acres land and is well equipped with pump house, LT/HT panels, light poles, fire line, nursery, bore wells, AC-plant etc.

Housing colonies: Vikramnagar housing colony is situated on Ambli - Bopal road, aproximately 2 km from SAC main campus. Antrixnagar housing colony is located behind the main campus over 7.6 acres land. Vastrapur housing colony has 288 quarters. Vastrapur housing colony is located at approximately 4 km east from the main campus over 13.84 acres land and well equipped with pump house, light poles, fire line, bore wells etc. Shastrinagar housing colony has 56 quarters. Shastrinagar colony is located at approximately 8 km east from the main campus over 0.63 acres land and is equipped with pump house, light poles, borewells etc.

Bopal residency: Bopal residency is at Bopal approximately 8 km west from the main campus over 11.92 acres land and well equipped with all utilities.

3.1 Characteristics of existing system

- All utilities information pertaining to the civil utility, electrical utility, mechanical equipment and nursery, which includes specification of pump houses, Sewage Treatment Plant (STP), lifts, buildings, roads, different features like water supply, sewage line, fire line, electric line, substations, High Tension (HT) / Low Tension (LT) distribution, street lighting and service connection of each quarters etc. are maintained by analogue methods.
- The data for water supply, firefighting, and drainage, details of buildings, roads, pump houses, wells, trees, electric cables and street light poles are maintained in separate map sheets. It is very difficult to update paper maps timely in traditional methods.
- In traditional system, the database are not managed and maintained in form of information where decision makers can extract information regarding buildings for plastering, painting, road maintenance, pump houses, wells locations, trees, electric cables, street light poles, substation equipment, LT panels, feeders and fault logging etc.
- Within the organization a desktop application has been developed for utility management system (Ajwaliya and Patel, 2014), where managers can manage spatial datasets using desktop application. The developed desktop application may not be available for general users to view their utility information.

The design and implementation of a WGUMS for SAC, Ahmedabad is to enable efficient network management by providing instant information access to all concerned engineers. This is essential to minimize time for locating any lines, buildings, power restoration and efficient planning for preventive maintenance. This paper demonstrates the use of open source GIS technologies and web services architecture for development of WGUMS. The interactive web user interface is built in using the ExtJS and the GeoExt frameworks with the OpenLayers libraries which are used as a main map client. Finally, a dynamic Styled Layer Descriptor (SLD), generated with a User-Friendly Desktop Internet GIS (uDig) open source software script is incorporated for creating interactive and user oriented maps.

Development of WGUMS is combination of various types of assets management which are essential in an organization as well as residential colony. The system contains electricity, drinking water supply, waste water line, sewage line, gardens, Diesel Generating (DG) set, Low Tension (LT) Panel and Sewage Treatment Plant (STP), along with office and residential buildings and many more. The beauty of the developed application is its ability to handle all assets on a single platform.

4. Tools and technology

The web based system is developed using various open source software and libraries, which are directly involved in web application, while many other desktop

GIS applications were used in preprocessing of spatial database and advanced analysis. uDig software is used for SLD (Styled Layer Descriptor) generation and editing. It is an open source (EPL and BSD) desktop application framework (http://udig.refrections.net/).

PostgreSQL is a database server for storage and transaction management. In the developed application, the open source database PostgreSQL with PostGIS extension could support spatial features very well. PostgreSQL is a powerful, open source object-relational database system. PostgreSQL tool can be downloaded from the web portal http://www.postgresql.org. PostGIS is a middleware between PostgreSQL and GIS engine. PostGIS libraries downloaded from the web "http://www.postgis.net/". GeoServer is an open source software server written in Java that allows users to share and edit geospatial data and is used for interoperability and publishing OGC web services. GeoServer forms a core component of the Geospatial Web (http://geoserver.org). Open Layers is an open source, client side JavaScript library for making interactive web maps, viewable in nearly any web browser. OpenLayers makes it easy to put a dynamic map in any web page. The open Layers libraries are archived from http://www.openlayers.org/ web portal. GeoExt is used for rich web mapping. GeoExt is built on top of the robust OpenLayers JavaScript mapping library and the rich graphical components of ExtJS. The core structure and the interface of the geoportal have been developed with the ExtJS framework. ExtJS is a cross-browser JavaScript library for building rich Internet applications. The Web user interface is built using the ExtJS and the GeoExt frameworks with the Open Layers as a main map client. GeoExt libraries archived from http://www.geoext.org web portal. The ExtJS is a popular JavaScript library used for building Web applications and ExtJS libraries are downloaded from http://www.snecha.com. A SLD is an XML-based mark-up language that allows user-defined symbolization of map layers. The SLD schema can be used for styling both vector and raster data, and the SLDs are used for map rendering by Web Map Services.

5. Framework

Figure 1 shows the framework of developed WGUMS application. It adopted three tier architecture i.e. application layer, service layer and data layer. The web server transmits the request and response at the client side; the web server deals with and distributes the request whereas database server provides data retrieval, storage, modification etc. Application server contains various models such as layer rendering, GIS functions etc.

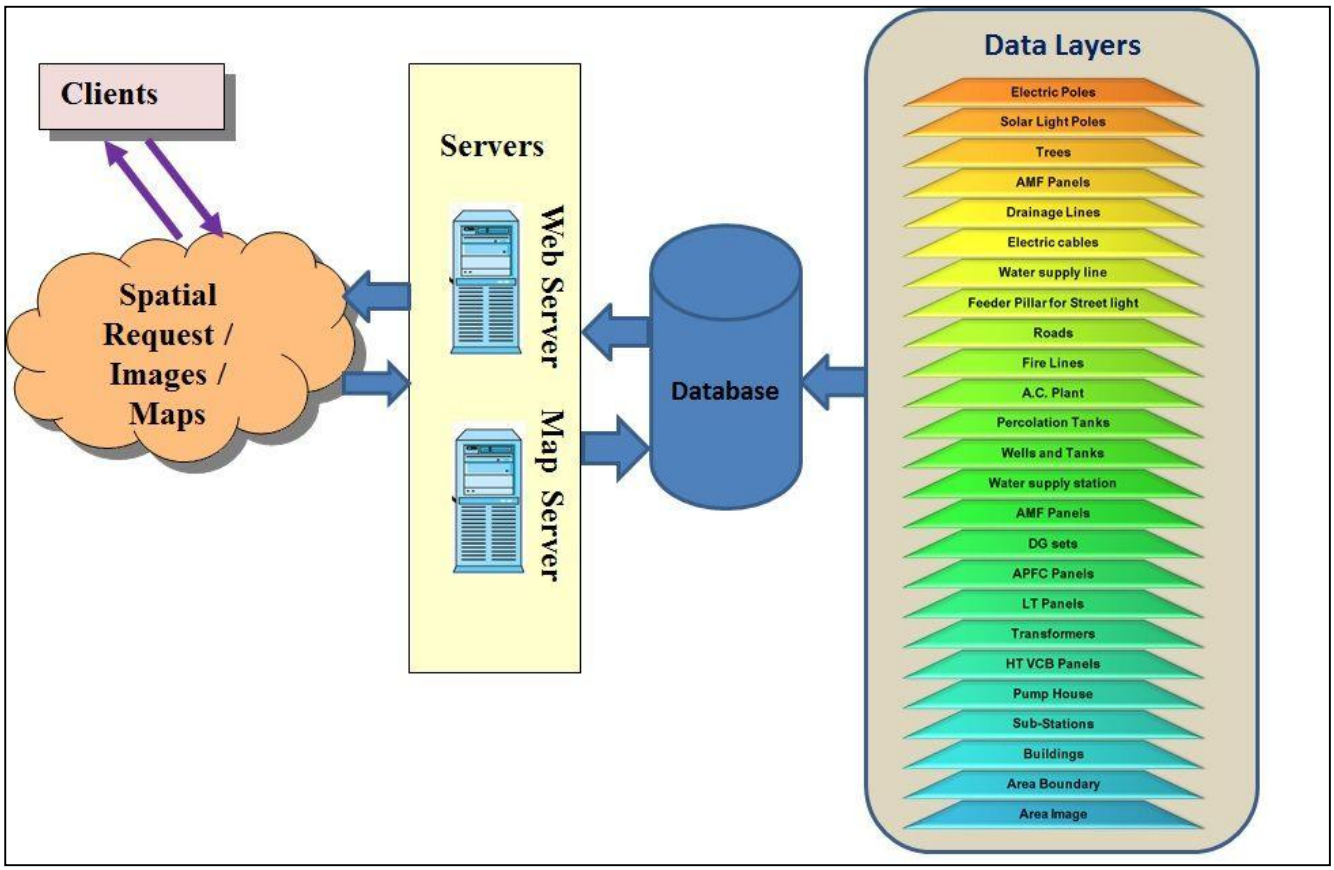

Figure 1: Basic framework

List of spatial layers integrated in WGUMS is described in Table 1 along with geometry of the layers and associated attributes. Table 2 describes the menus and sub-menus categorized in WGUMS and their associated information. The entire study area is categorized in three major parts namely office campus, housing colonies and

residential areas. Under each category information is classified in spatial (map and layers) and non-spatial (tables and photographs) datasets.

Table 1: Spatial layers and geometry type

Sr. No.	Layer Name	Data type / Geometry Type	Attributes
1	Electric Poles	Vector (Point)	ID, Name, Cable Size, Fitting, Type of Pole
2	Solar Light Poles	Vector (point)	ID., Layer, P-Max, Wattage-FF, IPM, ISC, VOC, EFF_M, EFF_C etc.
3	Trees	Vector (Point)	ID, Name
4	AMF Panels	Vector (Polygon)	ID, Name, ACB-Make, Make of R, Model Type
5	Drainage Lines	Vector (polyline)	ID, Diameter, Material etc.
6	Electric cables	Vector (polyline)	ID, Cable Size, Source, Destination, Sub-Station etc.
7	Water Supply Line	Vector (polyline)	ID, Diameter, Material etc.
8	Feeder Pillar for Street Lights	Vector(polygon)	ID, Wattage, Pole Type, Location, FPS-No, Fitting Type, Cable, etc.
9	Roads	Vector (polyline)	ID, Road type, Size, Source, Destination, Length, etc.
10	Fire Lines	Vector(polyline)	ID, Type, RPM, Pump-No., Model No., Make, Location, Installed etc.
11	A.C. Plant	Vector(polygon)	ID, Building-No, Layer, Name etc.
12	Percolation Tank	Vector(polygon)	ID, Depth, Name, Size etc.
13	Wells and tanks	Vector(polygon)	ID, Depth, Name, Size etc.
14	Water supply station	Vector(polygon)	ID, Name, Size, Type etc.
15	AMF panels	Vector(polygon)	ID, Name, Model Type, Make of R, ACB Make etc.
16	DG set	Vector(polygon)	ID, Name, Year of Make, Volts, Style, Sr. No., Speed, Phase, Make, Frequency etc.
17	APFC Panels	Vector(polygon)	ID, Name, Capacity, Relay Make, Relay Mode, Stages etc.
18	L T Panels	Vector(polygon)	ID, Cable Size, Capacity, Feeder No, Frame, Frequency, Name, etc.
19	Transformers	Vector(polygon)	ID, Name, Capacity, Frequency, HV-Amp., HV-Volts etc.
20	HT VCB Panels	Vector(polygon)	ID, Name, Type, Weight, Rated volt, current, Frequency etc.
21	Pump House	Vector (polygon)	ID, Building No., Discharge, Head, HP/KW, RPM etc.
22	Sub Stations	Vector (Polygon)	ID, Name, Location, Capacity, Make
23	Building	Vector (Polygon)	ID, Building No., Name etc.
24	Area Boundary	Vector (Polygon)	ID, Area, Perimeter etc.
25	Area Image	Raster (Geotiff)	RGB image for Visualization.

Table 2: WGUMS menu and description

Main Menu	Sub Menu-1	Sub Menu-2	Sub Menus-3	Details
Centres	Campus	SAC Main Campus	View Map	Layers Visualizations with Basic GIS functions for SAC Main Campus.
			Substation details	Sub-stations details in tabular form for visualization.
			AC-Plant Details	AC-Plant details in tabular form.
			Building Details	Information about buildings in tabular form.
		Bopal Campus	View Map	Layers visualization with information in map window along with GIS functions.
			Single Line Diagrams	Visualization of Single Line Diagrams (constructed and proposed buildings).
	Housing Colonies	Vikramnagar	View Map	All layers overlay and visualization of Vikramnagar colony in map window along with GIS functions.
			LT Panels	Complete LT-Panels list with all information in tabular form, installed in Vikramnagar colony.
			STP	Sewage Treatment Plant details in table form.
			Pump House	All information in Tabular form and picture form can be visualize for vikramnagar colony.
			Fire Fighting Lines	
			Building Details	
			Maintenance	
			Single Line Diagrams	
			Service connection	
		Antrixnagar	View Map	Layers visualization with information in map window along with GIS functions for Antrixnagar colony.
			Pump Details	Pump houses details available in a table form.
		Vastrapur	View Map	Layers visualization with information in map window along with GIS functions for Vastrapur colony.
			Single Line Diagram	Single Line Diagrams of Electric supply in Vastrapur colony.
			Photographs	Recent Photographs of Buildings, Gate, office, School etc.
		Shastrinagar	View Map	Layers Visualizations with Basic GIS functions for shastrinagar colony.
			Service Connections	Service connections details available in tabular form.
	Residential Area	Bopal Residential	View Map	All layers overlay of Bopal residential in map window for visualization along with GIS functions.

6. Application

6.1. The web application framework

Figure 2 illustrates architecture of the developed application, where user can send data request from a web browser as HTML/JavaScript and they can get response from server in HTML/ JavaScript client node. Web server Apache is handling the request from client and the same is passed to Geo-server which is used as map server; from map server, request has been responded to the client in form of spatial data or query results in tabular form.

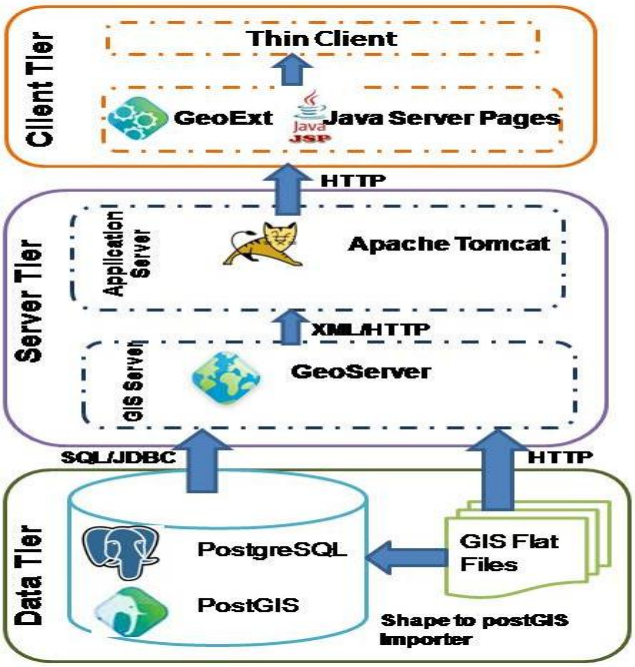

Figure 2: Service architecture and data sharing

6.2. Implementation

Based on the architecture of developed web application, the spatial data management and visualization system was completed in this section. First, the original data were standardized into datasets by unifying the coordinate system and file format using desktop GIS software. The data were collected from different sources, for example, maintenance data in the form of Microsoft Excel (MS-Excel) file; linear features and polygon features from CAD (Computer Aided Design) files; electric poles and feeder's locations collected from Mobile Global Positioning System (GPS) device. Figure 3 describes flow chart depicting preprocessing of the database for application.

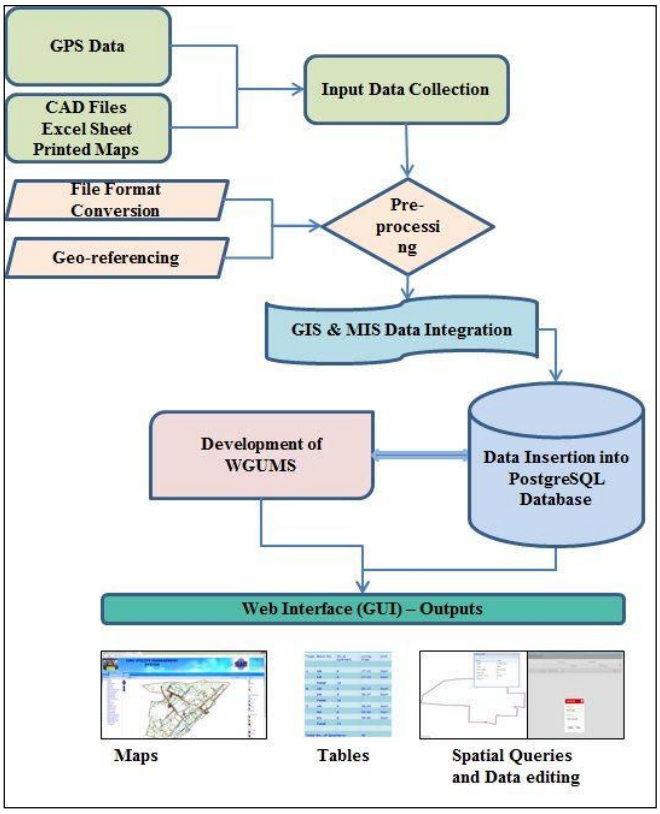

Figure 3: Pre-processing and implementation flow chart

The database preparation and metadata standardization of spatial data has been carried out in following steps:

- GPS Point Collection: First step is to collect GPS locations survey of bore point, poles and tree; this involves the database preparation of utility assets, followed by the preparation of GIS base map.
- Digitization: Second step is the digitization of utility assets which were not included in digital maps such as lines, building, substations, feeders, wells, and poles from geo-registered paper maps. Vector layers were imported from CAD file and converted into shape file format, spatial referencing with base map has been performed in converted shape files. Subsequently, geo-referenced database schema has been defined for each vector layer. All required attribute information incorporated with vector layers using join operations along with spread sheets.
- Pre-processed spatial data imported into Post-GIS database.
- Eventually, a Web GIS application developed using open source GIS technology.

The spatial database description has been categorized into three levels; datasets, layers and maps. Dataset has been prepared as discussed above. A layer is referred as a dataset that completed specific style conversion and can be visualized in map window (Yin and Feng, 2009). Map is a combination of one or more layers with specific style specification where the information can be extracted using visual interpretation.

7. Use case model and diagrams

Web GIS system presented in this paper is used by two classes of users: web GIS users and web GIS portal administrators. General relationship between user classes represents ability of a user to play multiple roles. Web GIS users are the most general class with the visualization and rendering functionality available along with basic GIS functions. Web GIS users can access the system through a web GIS portal for viewing maps and querying geographic features. Authorized web GIS portal administrators have access to all functions of their developed GIS applications. Finally, the portal administrator is responsible for defining content that will be available to web users. An important feature of developed web GIS portal is the ability of an integration of spatial information with MIS dataset. The characteristic of WGUMS is defined in two levels of information integration. First is display level integration that consist map composition formed by overlays of various layers and their SLD definition. Second level is database update and basic GIS functionality integration.

Use case diagram is used to describe the relationships among the functionalities and their controllers. These diagrams represent the use case view of a system. A use case represents a particular functionality of a system. These controllers are known as actors. Figure 4 describes the role of administrator, where administrator can extract information from various sources viz., CAD files, field data, and spread sheets and administrator can manage to insert and update the database. Figure 4 illustrates the use case diagram, where administrator plays an actor for spatial and non-spatial data management and backup restore activities for the system.

Figure 5 describes the use case diagram for map visualization and overlay of layers. User can view maps of utilities along with associated attribute information using 'http' web link (e.g. Vikramnagar residential colony, SAC campus, Bopal Campus, Shastrinagar colony, Antrixnagar colony, Bopal residential area, Vastrapur residential colony). User can visit map page via click on "View Map" link on home page and also can mark desired layers as visible over map area.

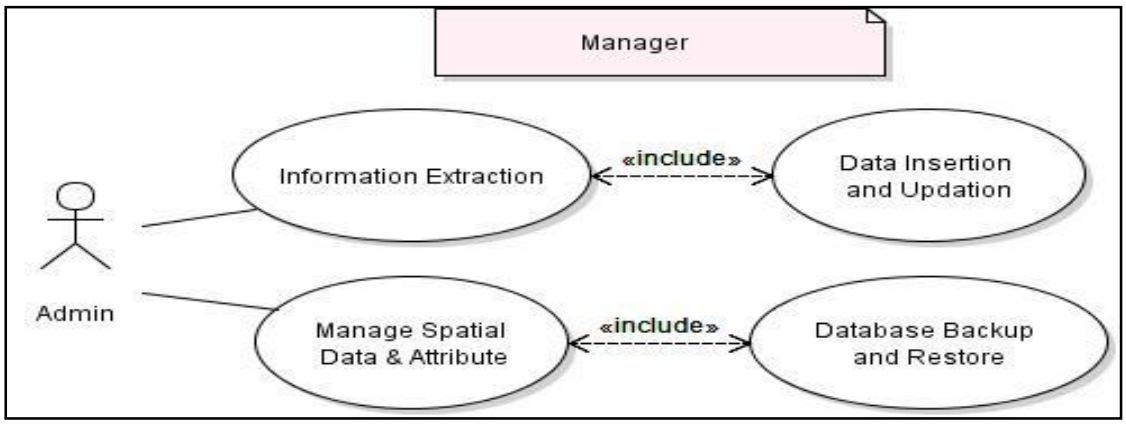

Figure 4: Use case-1 for data insertion and management

Basic GIS functionalities are provided in the System to render layers within the map area. Figure 6 illustrates the Use case-3 diagram where, user can zoom-in, zoom-out, pan layer on map area. Full extent is the functionality to render all active layers with common bonding box over map area. Measurement functionality has been incorporated for features over map area (length

measurement for line feature, area measurement for polygon feature etc.). Zoom to particular feature function provides the functionality to search that feature over map and render map to specific feature.

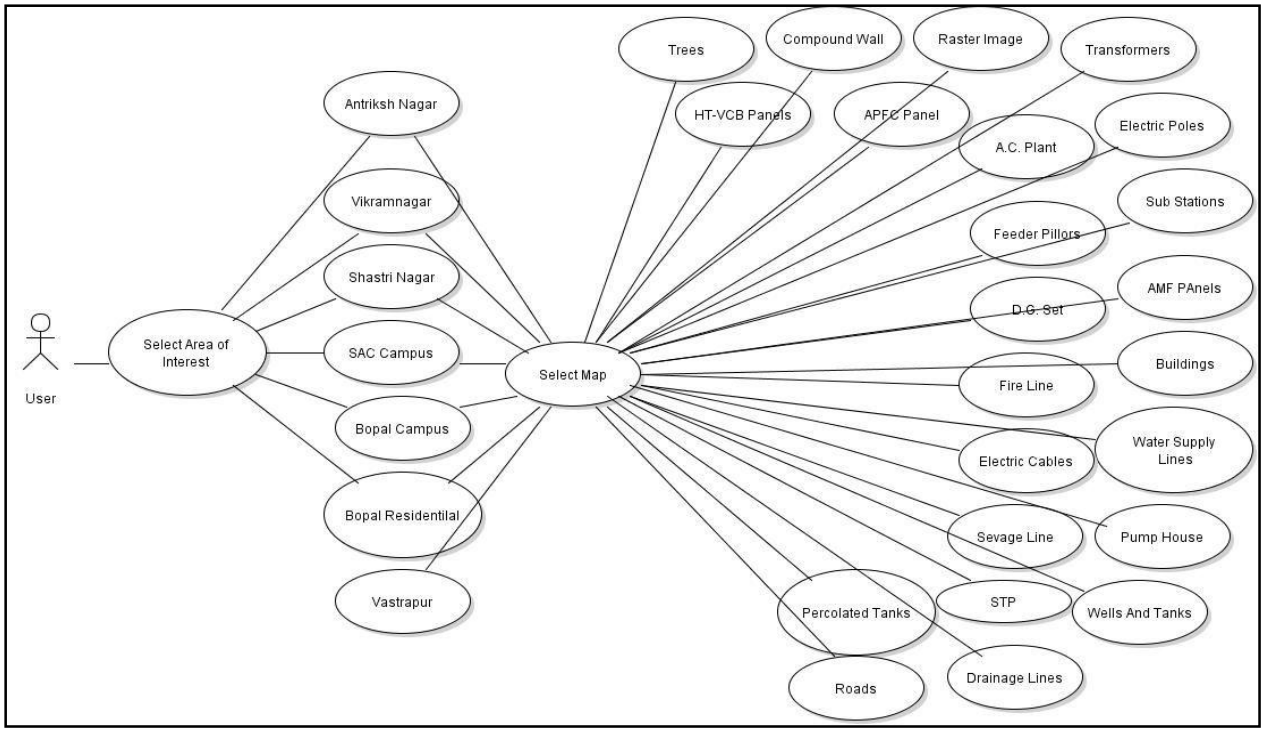

Figure 5: Use case-2 for map visualization

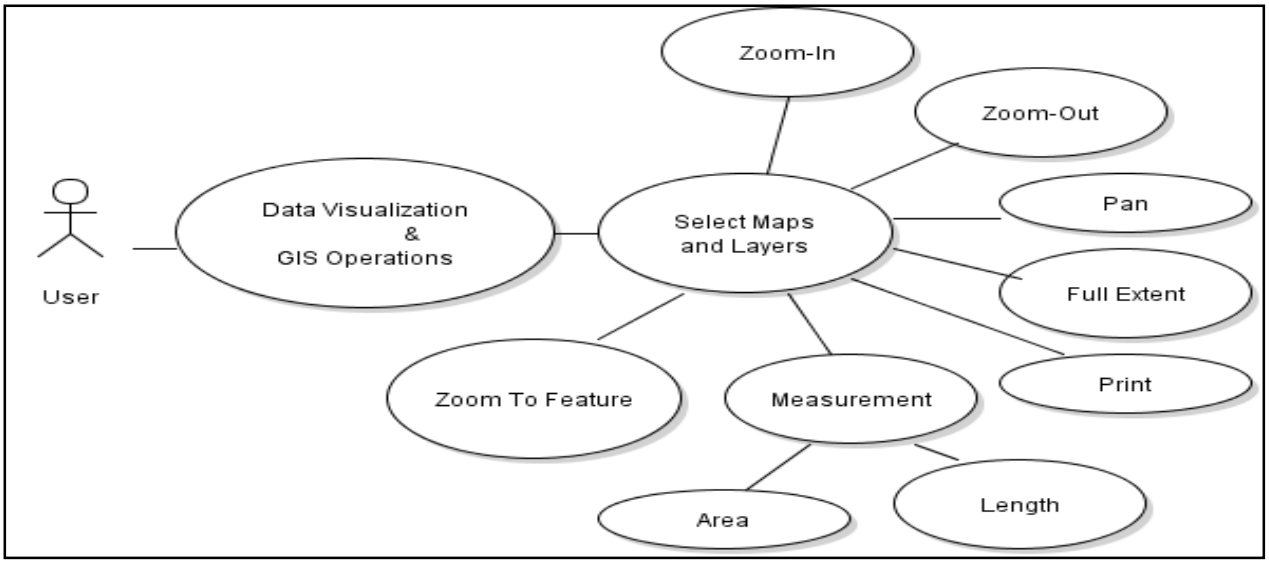

Figure 6: Use case-3 for map visualization and GIS operations

Performance of the map pages in WGUMS is governed by on hardware configuration and network connectivity, with present configuration home page response is 1.36 seconds minimum response time, 3.21 seconds maximum time and 2.96 seconds is average time.

The developed WGUMS application may provide a wide range of data for various types of analysis to enable routine maintenance and management. Strength of GIS is integrating data and preparing it for analysis or modeling apart from tying together data from various sources which makes it an important tool for planning and decision making. WGUMS is able to display legend of all layers displayed on the map. This legend is represented by the symbol of each layer with color and the name of the layers in the legend list. System displays coordinate of the current mouse position. User can see co-ordinate only when the mouse pointer is inside the map area. If the mouse pointer moves beyond the map area the system will not display the coordinate. User can measure length of cable, roads, water supply line, firefighting lines, drainage lines from one place and other place in entire SAC-ISRO centre. User can query

any layer of the GIS map to get the attribute data for a particular feature of that layer. User has to click on any feature of a particular layer to get the attribute of that feature.

Developed system provides facility for viewing of maintenance schedule, HT distribution and substation layout, as shown in Figure 7 to 10. Figure 11 shows maintenance schedule menu for the themes in the WGUMS and figure 12 represents maintenance schedule in tabular form under WGUMS.

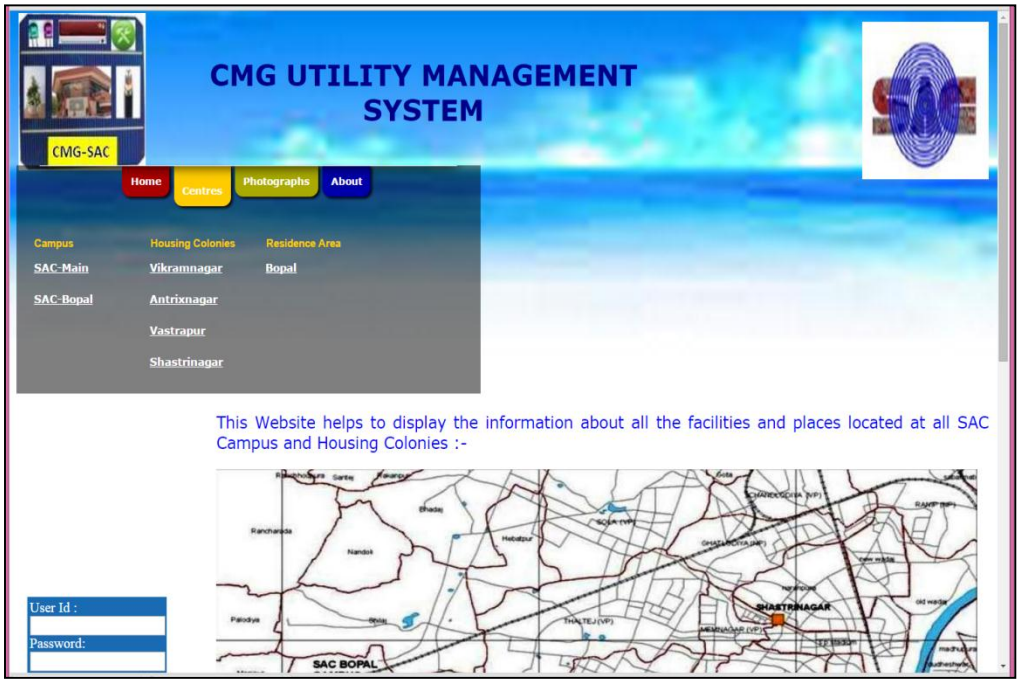

Figure 7: WGUMS home page

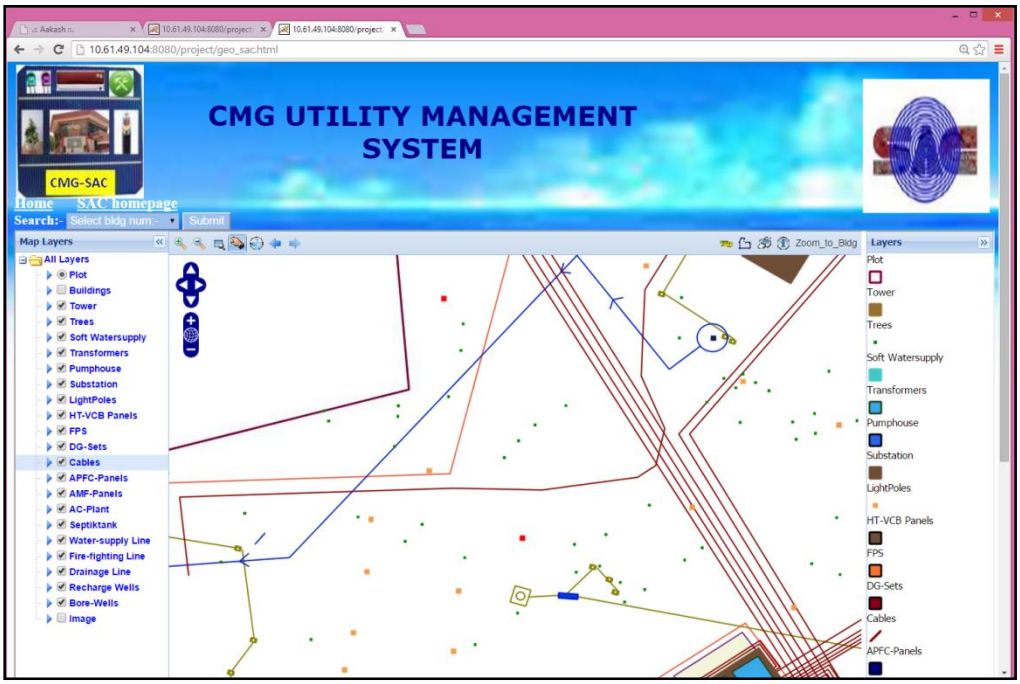

Figure 8: SAC campus-sub stations with panels and cable

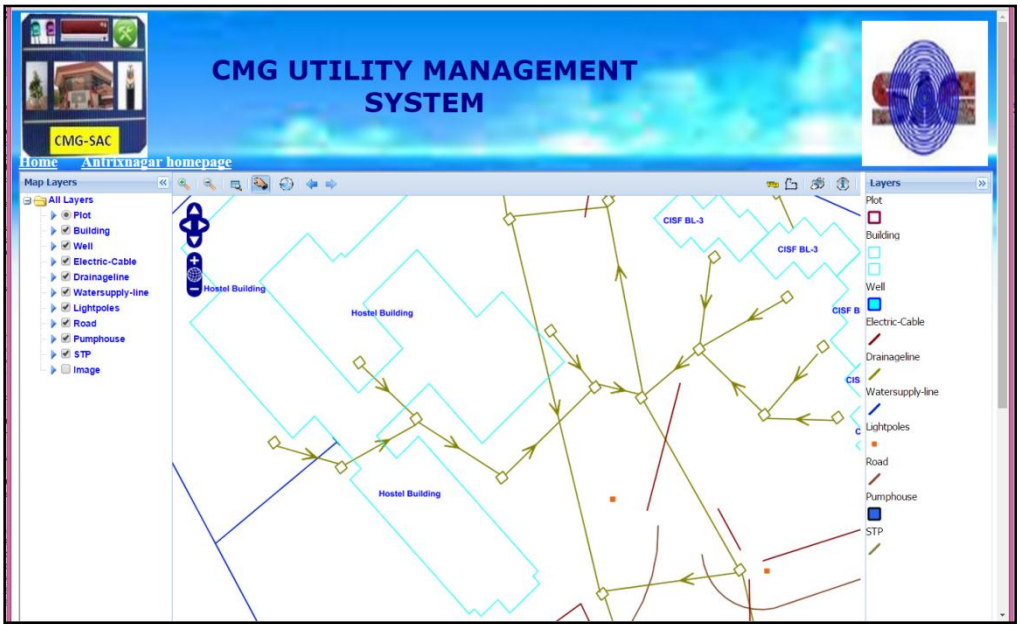

Figure 9: Antrixnagar residential colony with different utilities

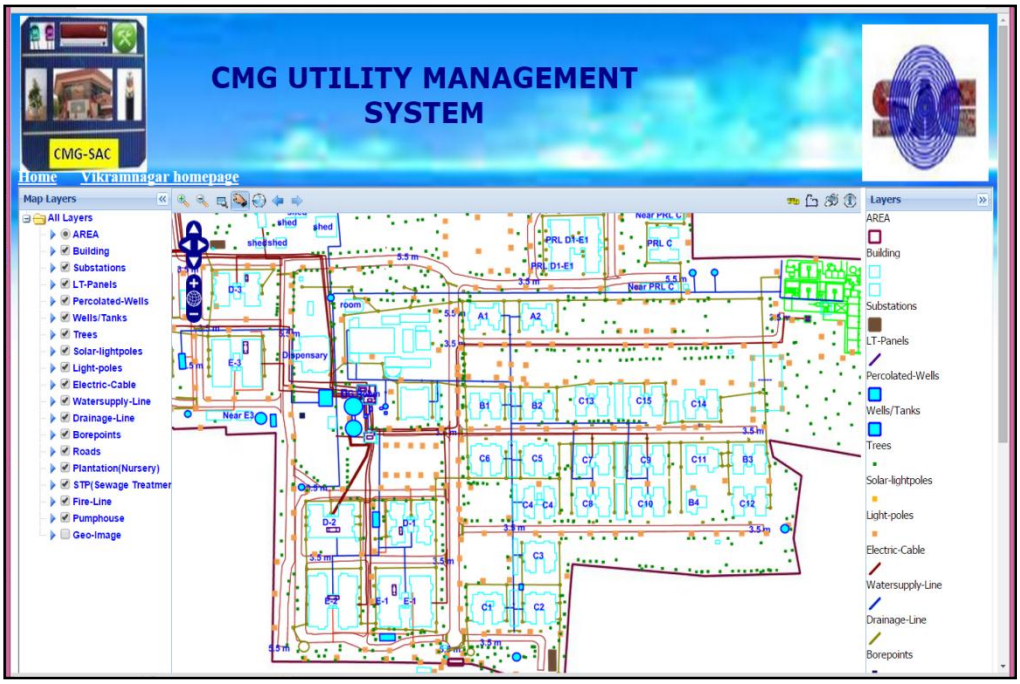

Figure 10: Vikramnagar residential colony with different utilities

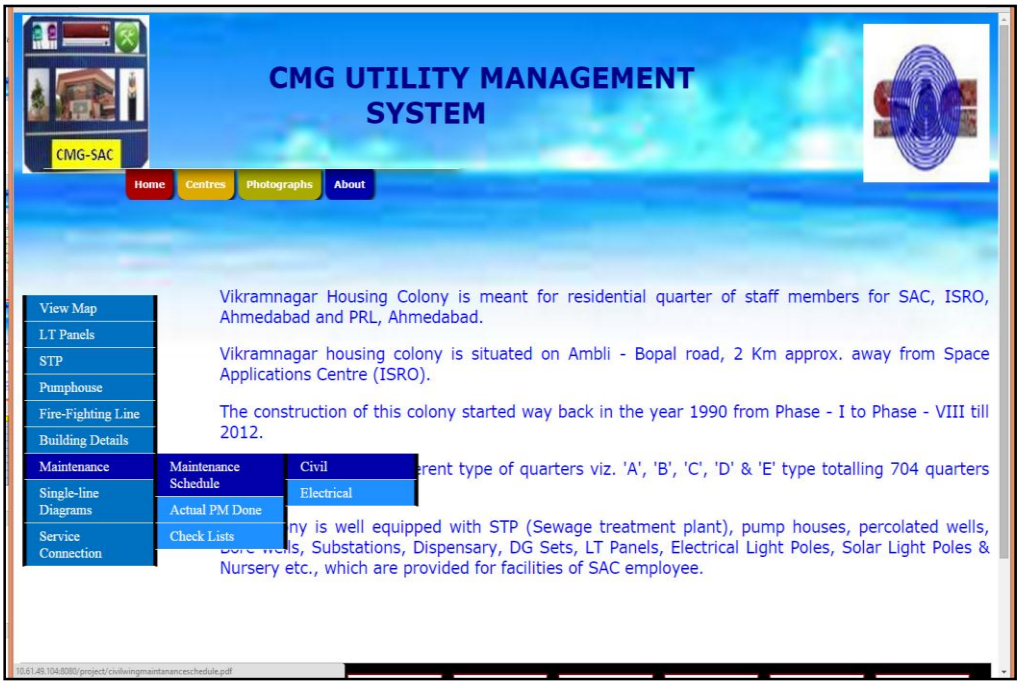

Figure 11: Maintenance schedule for Vikramnagar housing colony

CIVIL WING MAINTANANCE SCHEDUAL AT VIKRAMNAGAR DOS HOUSING COLONY.

	MAINTANANCE ITEMS	FREQUINCY OF MAINTANANCE
➲	Painting of Quartres	After every three years
➲	Plastring of Internal walls	As and when required, depends on conditions of wall
➲	Plastering of External wall	As and when required, depends on conditions of wall
➲	Painting dooors/windows	After every three years
➲	Painting [white wash]	Yearly
➲	Periodic cleaning of water tank	Half Yearly
➲	Terrace cleaning	Quarterly
➲	Sewage lines Cleaning	Yearly
➲	Grass cutting	As and when required, depends on conditions

Figure 12: Report of maintenance schedule for Vikramnagar housing colony

Conclusion

WGUMS will help in identifying pipe lines, electrical lines, sewage lines, buildings, parking areas and gardens etc. for better understanding and identification. From the present development authors can conclude that this is an attempt to develop a WGUMS for spatial planning in the field of utility management, however still there are scopes for future advancement in the system capability by adding some advanced functions and modules in account to lodge user's complaint, further, Administrator or managers can track the registered complaint whether it is attended by concern technician and regularly updated. This paper provided a practical web GIS framework combined with latest web services technology and open source projects. Based on this solution, and spatial data services were developed to access and publish spatial data. The spatial data management and visualization system was developed to provide a new solution for the public to share geospatial data on the web. The WGUMS is developed for visualization and analysis of electrical assets, pipeline,

sewage lines, trees and gardens. The developed system contains the facility to interactive visualization spatial data and in-situ data.

This WGUMS application has been deployed in intranet, to facilitate user from SAC for map visualization from different locations and managers or planners can view and manage from anywhere within the Centre. The software is useful for planning, maintenance, and improvement of information standard and decision making processes, still there is scope for future advancement in the system capability by adding some analytical modules in account to decision making process for utility management.

Acknowledgement

The authors would like to thank Shri Tapan Misra, Director, Space Applications Centre, Dr. Rajkumar, Deputy Director, EPSA, SAC and Dr. Markand Oza, Head, CGDD, for their kind support. The authors would like to express their thanks to Ms. Shweta Mishra, Scientist, SAC for her kind support in technical implementation. The authors also gratefully acknowledge Shri S.S. Chadar, Group Head, CMG, SAC and Shri Rakesh Jain, Head Maintenance Division, CMG, SAC for their kind support and suggestions. The authors would like to express their thanks to Architecture Division, CMG, SAC for providing the updated drawings related to utilities and also for their kind support.

References

Ajwaliya, R.J. and S. Patel(2014). Design and development of GIS based utility management system at DOS housing colony, Vikramnagar, Ahmedabad. International Journal of Engineering Research and Applications, ISSN:2248-9622, Vol.4, Issue 9 (Version 6), 56-73.

Baucic, M. and Medak, D. (2015). Web GIS for airport emergency response - UML model. Promet – Traffic & Transportation, Vol. 27, 2015, No. 2, 155-164.

ExtJs: http://www.snecha.com/.

Geoext: http://www.geoext.org/.

Geoserver: http://geoserver.org/.

Green, D. and Bossomaier, T. (2002). Online GIS and spatial metadata. London: Taylor & Francis, 2002. ISBN:0748409548.

Mansourian, A., Taleai, M. and Fasihi, A. (2011). A web-based spatial decision support system to enhance public participation in urban planning processes. Journal of Spatial Science, Vol. 56, No. 2, December 2011, 269–282 (doi:10.1080/14498596.2011.623347).

Openlayers: http://www.openlayers.org/.

Otieno, E.O. and Ngigi, M.M. (2014). Web based public transport management system: A prototype PSV tracking system for Nairobi city. International Journal of Science and Research (IJSR). Volume 3 Issue 6, 922-926. (online): 2319-7064.

PostGIS: http://www.postgis.net/.

Postgresql: http://www.postgresql.org/.

Ranade, P. and Mishra, A. (2015). Web-GIS based livestock information management system (WGLIMS): Review of Indian scenario. Int. Journal of Applied Sciences and Engineering Research, Vol. 4, Issue 2, 2015. DOI: 10.6080. ijaser.04020. ISSN:2277-9442.

Udig: http://udig.refrections.net/.

Yang, C., Wong, D.W., Yang, R. Kafatos, M. and Li, Q. (2005). Performance-improving techniques in web-based GIS. International Journal of Geographical Information Science. Vol.19 No. 3, March 2005, 319–342. ISSN (Print): 1365-8816. DOI: 10.1080/13658810412331280202.

Yin, F. and Feng, M (2009). A WebGIS Framework for Vector Geospatial Data Sharing Based on Open Source Projects. Proceedings of the 2009 International Symposium on Web Information Systems and Applications (WISA'09), Nanchang, P. R. China, May 22-24, 2009, 124-127. ISBN 978-952-5726-00-8 (Print).

Journal of Geomatics Vol 11 No. 1 April 2017

Land use and land cover changes and their impacts in Pampa river basin in Kerala: A remote sensing based analysis

N.A. Mayaja[1] and C.V. Srinivasa[2]
[1]Dept. of Civil Engineering, Atria Institute of Technology, Bangalore
[2]Dept. of Civil Engineering, Global Academy of Technology, Bangalore
Email: mayaja@hotmail.com

(Received: Aug 20, 2016; in final form: Mar 20, 2017)

Abstract: Increased rate of urbanization along with other human intervention factors have been cited as major challenges faced by river basins, which ultimately change the basin ecology and end up in serious natural havocs like floods and droughts. As far as a river basin is concerned, the spatio-temporal changes in land use have direct influence on its hydrological realm. Deforestation and conversion of waterlogged wetlands into built-up areas directly affect the characteristics of the basin and natural water flow regimes and the obvious consequence is flood. Analyzing the spatial and temporal variations in land use and land cover (LULC) of river basin provides meaningful insight to these issues. The state of Kerala in general, and the Travancore- the central region in particular, is well known for high level of growth in terms of socio –economic factors, literacy, health care etc. The extensive socio-economic changes have led to increased rate of infrastructure and building construction and profuse landscape changes in this region during the last decade. Consequently, the basin characteristics of Pampa river - flowing through the heart of this region – has succumbed to terrific variations. Recurring flood and drought has become a predominant feature of this river, which is the lifeline of the region. In this context, this study attempts to evaluate the LULC changes that have taken place in Pampa river basin during the last three decades by employing the remote sensing based digital images for the period from 1985 to 2012. From the results derived by analyzing satellite images, the possible human intervention factors have been identified and discussed. The transformations in the land use pattern of Pampa river basin revealed in this study are 'strong negative changes', aggravating the havocs now being experienced due to recurring flood and drought situations.

Keywords: LULC changes, Pampa river basin, Land use transformations

1. Introduction

Analyzing the spatial and temporal changes in land use and land cover (LULC) is one of the diagnostic methods to understand the problems persisting in a river basin. Rapid growth of urbanization along with other increasing human intervention factors have been identified as major reasons of land use changes and land conversions, which ultimately poses serious havocs like flood and drought. As far as a river basin is concerned, the spatio-temporal changes in land use in the basin have a direct influence on its hydrological realm. Currently fresh water resources in several parts of the globe are facing severe crisis due to unsustainable river utilization. Deforestation and conversion of waterlogged wetlands into built-up areas directly affect the characteristics of the basin and natural water flow regimes, and the obvious impacts are flood and drought.

The state of Kerala in general and the Travancore region (the mid-region of the State) in particular is well known for high level of growth, in terms of socio-economic, literacy and health care factors. River Pampa, which used to be a rich and sustainable source of water throughout the seasons, was known to be the lifeline of the Travancore region. However, the extensive socio-economic changes that Kerala has undergone in the past few decades resulted in an apparent increase in the rate of infrastructure and building construction in this region. Profuse landscape changes in this region have happened during the last few decades. The river basin experiences alternating cycles of recurring flood and drought. In the years 1993 and 1994 the region underwent acute water scarcity and the water level in the river Pampa hit rock bottom that the world famous Aranmula boat race was ruined. Similar dry spells occurred in 2003 and 2016 when the boat race had to be cancelled. A good number of villages and densely populated regions on the banks of this river also face the ravage of frequent severe floods. According to a research conducted by Swaminathan Research Foundation, the intensity, frequency and severity of floods in the region are increasing (M. S. Swaminathan Research Foundation, 2007). In July 2007, Alappuzha district in the Pampa basin witnessed the worst flood in sixteen years. Around 1,34,000 people were evacuated from the region. In the year 2008, within three months six incidents of floods occurred. In 2009 on the first day of the monsoon floods, 10553 persons including 2134 children were evacuated. In Pathanamthitta district (which occupies a major share of the Pampa basin) alone, the death toll was six and crop loss was worth Rs 5.64 crores. In this context, this study attempts to evaluate the changes in LULC in Pampa river basin during 1985 to 2012 and deliberate on the possible impacts of human intervention factors on the flood occurring in this river basin.

Numerous recent studies have successfully employed remote sensing based LULC analysis to identify the watershed and river basin characteristics in India. A land use based study on the Khanpara watershed area of

Assam-Meghalaya region was done by Santanu and Tivari (Sarma and Saikia, 2012). Roy *et al.* (2008), in a significant work, developed a satellite-based methodology for evaluating the forest ecosystem. Samarakoon (2004) employed satellite based land use images for flood mitigation studies of Dhaka city. In a study by Bhaskaran and Baijulal (2008), land use changes in a limited portion of the Pampa river basin were examined through satellite images.

2. Land use pattern of the study area

Pampa river encompasses a basin area of approximately 2235 km^2 spread over four districts of the state of Kerala, viz., Idukki, Pathanamthitta, Kottayam and Alappuzha. The study is done only on the part of the basin which exclusively belongs to the Pampa river. The area lying to the western side of Veeyapuram (i.e., lower Kuttanad and parts of upper Kuttanad, covering an area of nearly 455 km^2) is not included in this study since it is drained jointly by Pampa, Achancoil, Manimala and Meenachil rivers and has unique geological and ecological characteristics. Hence, a total area of around 1780 km^2 comes under the purview of this study. A map of study region is provided as Fig. 1. As per the census 2011, the total population in the above four districts is about 6.40 million (Census of India, 2011). The area extends over thick tropical forests, wasteland, built up (urbanized and semi-urbanized) settlements, few water bodies and a rich agricultural bowl called Kuttanad.

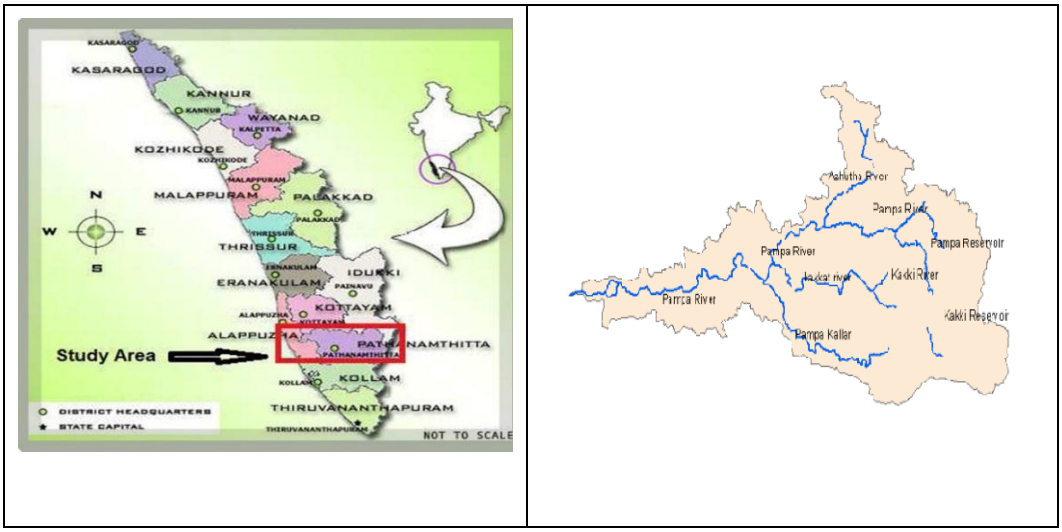

Figure 1: Pampa river basin - the study area

The land use pattern of this river basin is unique and diverse. Physiographically, the 2235 km^2 of river basin terrain has three natural regions namely, lowland (about 229 km^2), midland (about 933 km^2), and highland (about 1073 km^2) (Fig.2). The high land consists of high altitude areas of thick forests whereas midland consists of region of cash crops like rubber and tea. The low land is basically providing agrarian crops like rice, paddy and coconut. The undulating topography, vibrant climate and vivacious hydrology of this river basin are unique and provide multitudes of lively micro ecosystems. Though the official statistics does not highlight any significant changes in the forest cover and cropping pattern, many recent researches brought out that the utilization pattern of pampa river basin has been substantially altered by human interventions.

Physiographic units, altitudes and areas

Unit	Altitude (m)	Area (km^2)	Area (%)
Lowland	0 – 7.5	228.86	10.24
Midland	7.5 – 75	933.34	41.76
Highland	> 75 m	1072.80	48.00

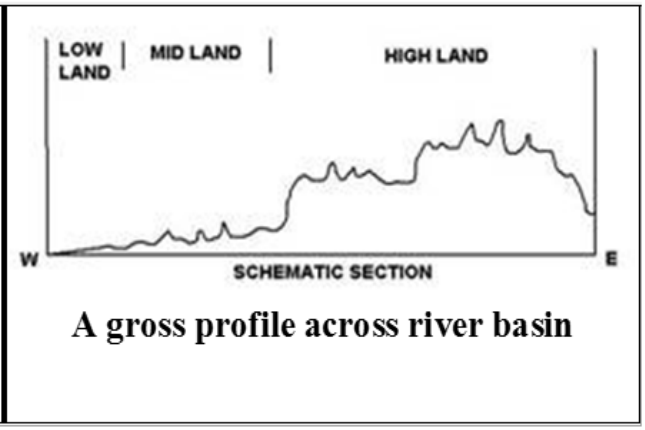

Figure 2: Physiographic pattern of river basin (Source: Kerala State of Environment report)

3. Methodology

Remote Sensing (RS) and Geographic Information System (GIS) have been widely applied to understand the LULC changes and are considered to be a powerful tool to document the spatio-temporal changes of an area for the purpose of conservation and management of natural habitats. The multispectral images obtained from recent satellites provide satisfactory spectral resolution, which in turn offers a reliable means to diagnose LULC changes. The satellite images were obtained from ISRO and belong to the following satellites. Year 1985 – Landsat: Year 1995-IRS-1C: Year 2005 Resourcesat-1: Year 2012 Resourcesat- 2. Landsat Thematic Mapper data for 1985 has a ground resolution of 30 m. LISS - III sensor data (having ground resolution of 23.5 m) have been utilized for the years 1995, 2005 and 2012 in this study. In order to avoid the image processing errors due to seasonal variations, images pertaining to the month of April, which is a peak summer period, were considered. The basin area was delineated using the relevant Survey of India (SOI) topographic maps. Pre-processing of the images has been carried out using software *Erdas Imagine*. Supervised classification was done in the spatial analyst extension of Arc *GIS* under multivariate tool set. Maximum likelihood classification method was adopted for this.

In this study, the classification of the study basin area of 1780 km^2 has been carried out for six main categories viz: forest land, agriculture land, built up area, wasteland, grass land and water bodies.

4. Results of image analysis

Land use changes in the river basin of Pampa during the years 1985, 1995, 2005 and 2012 have been mapped. The selection of data for the above years was predominantly decided by the availability of clear, cloud free satellite images of this region. A summary of results of analysis is shown in table 1. The land use map pertaining to the years 1985 and 2012 corresponding to each category are provided in figure 3 for comparison.

Table 1: Summary of results of LULC mapping

LULC category	Area occupied (km^2) in the year			
	1985	**1995**	**2005**	**2012**
Built up area	16.90	31.30	38.50	70
Forest	1167	1156	1146	1114
Agriculture	520.80	512.60	515.10	507
Wasteland	12.60	13.40	14.10	23.40
Grass land	25.10	29.10	28.70	28
Water bodies & other class	37.60	37.40	37.60	37.60
Total	1780	1780	1780	1780

The above results clearly testify significant changes in the pattern of land use in this river basin over the period of study.

4.1 Built up area

During the period of study, significant increase has been observed in the built up area in this river basin. A total built up area of about 16.9 km^2 in the year 1985 has increased to 70 km^2 by the year 2012. The increase in built up area (314%), corroborates with the change in urbanization depicted in the map-to-map comparison of this study. The increase has predominantly happened in the downstream regions, that too at regions which are in very close proximity of the river. These regions are already densely populated and undergoing a high rate of urbanization (7.64% decennial growth, 2011 Census). Various studies have indicated that this rapid urbanization is on account of the fast changing socio-economic transition structure of this region [NIU, KSUDP]. The phenomenal increase in the built up area of the river basin is one of the factors contributing to the flood havoc of this region.

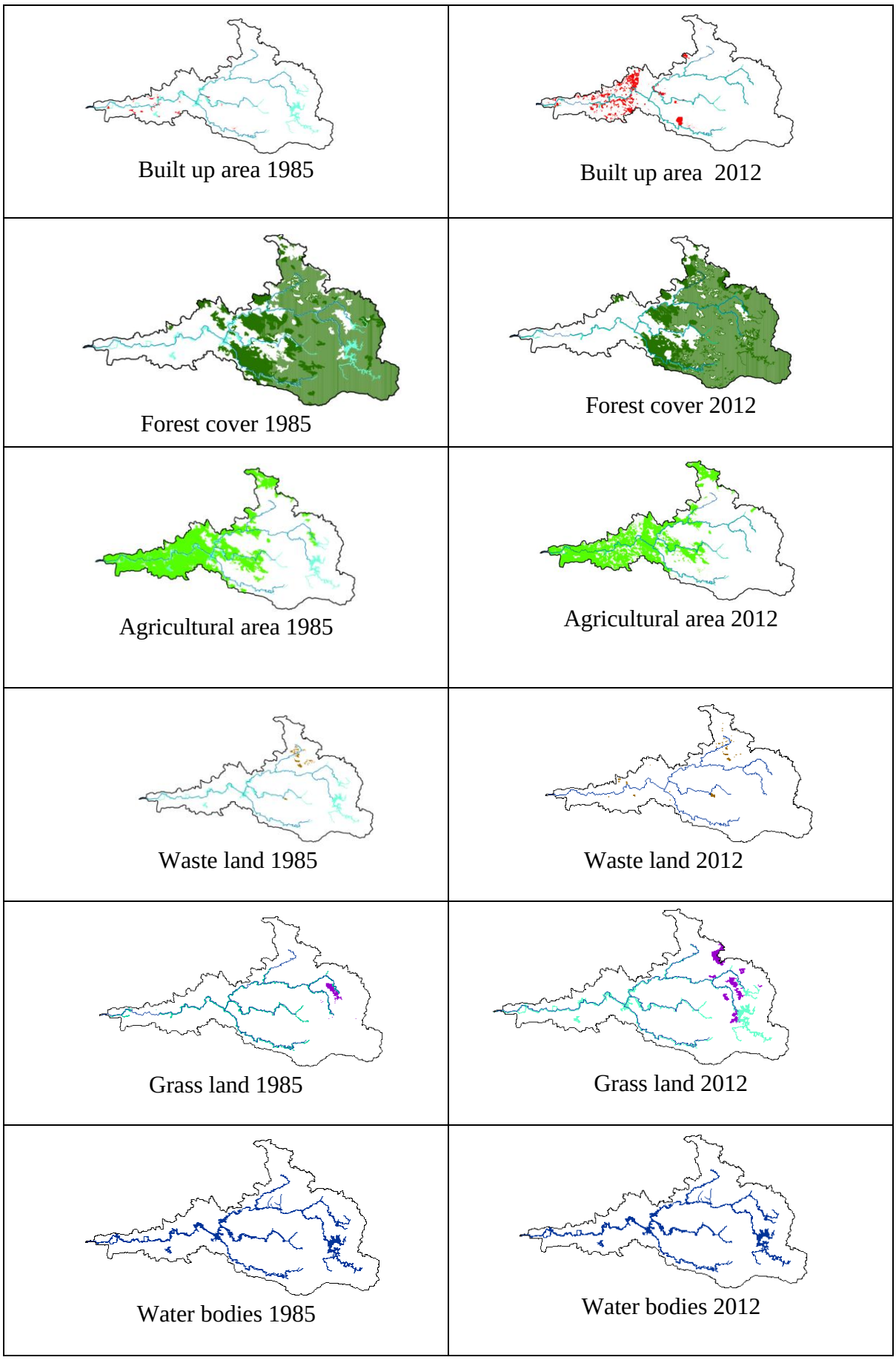

Figures 3: Comparison of land utilization in 1985 (left) and 2012 (right)

4.2 Forest cover

About 40% of the basin area is covered under forest. While a major share of this is on account of the notified tropical monsoon forest, in the image classification, thick forest plantation also forms under the category 'forest'. While the forest cover in the year 1985 was approximately 1167 km^2, the same has dwindled to 1114 km^2 by the year 2012, involving a reduction of about 4.5%. This amounts to an annual shrinkage of forest cover of the region by about 0.2%. Though a few official statistics indicate that the forest area of Kerala as 'reasonably stable', it is a well-known fact that the forest cover in the pampa river basin is depleting on account of various reasons. The main reasons for the forest cover shrinkage are the deforestation - both legal and illegal-, encroachments, irrational expansion plans of the pilgrimage areas like Sabarimala, and above all the absence of an effective preservation policy. In fact, if the coverage on account of thick green plantation corps could be segregated, the actual rate of forest cover depletion would be much more.

4.3 Agriculture area

The results show that the total agricultural area has come down by 3% over the period of study. The main agricultural production of rice, coconut etc is limited to the downstream and middle regions of the basin. A few studies have identified that this slowdown of agriculture dynamism in central Travancore region are mainly on account of various socio-economic factors and 'political climate' non-conducive for labour oriented agriculture activities (Economic Review, 2007; KSCSTE). However, though marginally, the change in pattern of basin utilization from agrarian to non-agrarian applications adds to the flood related issues of the region, apart from making the state of Kerala more import dependant on food.

4.4 Wasteland

Wastelands are lands that cannot be put to productive use. They include barren and rocky lands, degraded forests, scrub lands, abandoned quarries, lands subjected to excessive erosion, which are deprived of complete topsoil etc. Wasteland may also be formed due to salinity and infertility of the soil used by poor land practices. An area of 12.6 km^2 has been mapped in 1985 as waste land where as this has substantially increased to 23.4 km^2 by the year 2012 indicating about 85% increase. It can be seen that the wasteland during 1990s was sparsely distributed in the upstream alone, whereas by the year 2012 it has substantially spread to the rich down stream river basin also. This is evidently on account of the human intervention factors like indiscriminate sand mining, excavating fertile soil for clay mining etc and poor land practices that resulted in excessive soil erosion. The shrinkage of river and alterations of the river ecology also aggravates the flood features of this river.

4.5 Grassland

The grasslands in the Pampa river basin, popularly known as 'Plumed' are located in the upstream region of the basin, surrounding the holy shrine 'Sabarimala'. With a marginal increase during the year 1985-95, this has slightly dwindled by the year 2012. This is mainly on account of the human intervention by the pilgrims, by using this grassland as trekking pathway to the Sabarimala temple. The projections for the year 2020 and 2025 also shows that if the same trend continues, the grassland area may remain more or less unaltered.

4.6 Water bodies

This class includes lakes, tanks and similar water collections near the basin. This class remained more or less unchanged throughout the period of analysis. As a total transformation of the LULC of the river basin will have impacts on the water bodies also, it is necessary to carefully preserve this region to ensure the sustained health of the basin.

4.7 Significance of results

The most significant observations in this study are the exponential increase in the built up area (314%), quick transition of fertile land to waste land (85%) reduction in agriculture land (3%) and marginal decrease in the forest cover (4.5%). It was observed that during period 1985 to 1995 the agricultural pockets of Elanthoor, Ranni Pazhavangadi and Chengannur villages have been converted to built up land. This conversion further increased during the decade 1995 to 2005 when Kadapra, more parts of Chengannur and Ranni Angadi which were agriculture – predominant villages became urbanized and forest land in Thannithode village was also transformed to a built up hub. The period 2005 – 2012 witnessed the distribution of built up land further downstream to convert agricultural lands in the villages Niranam, Kadapra, Pandanad, Kuttoor, Koipram, Aranmula, Kidangoor, Mezhuvely etc. During this period, parts of the Pampa river was also encroached in the villages of Ranni, Athikkayam and Vadasserikkara. The rapid increase in the built up area bears a significant impact in the basin ecology, especially in aggravating the flood havoc in Pampa river basin. This many fold increase in infrastructure and built up area in the close proximity of the river channel blocks the natural flood plain and there by the flood water levels in the remaining areas increase substantially. Massive and irrational infrastructure realizations is quite apparent all around the villages and towns in this river basin. This is mainly due to the absence of an infrastructure policy, scientifically taking care of the river basin and its ecology.

Further, major increase in wasteland area indicates the alarming level of human intervention. It was observed that in the decade 1985 – 1995 wasteland spread in the forests of Kumily while the same phenomenon occurred in the forests of Peruvanthanam in the decade 1995 – 2005. The period 2005 – 2012 witnessed spread of wasteland throughout the basin. In this period the agricultural lands in the villages of Elappara, Vechoochira, Naranamoozhi, Ranni Perunad, Ranni, Mylapra, Naranganam, Ayiroor and Aranmula and the forest lands in Peermade, Peruvanthanam, Mundakkayam, Seethathode, Chittar and Aruvapulam were converted to wasteland. The mathematical model

showing the 'best fit' for this variation is a 'MMF function', which also is a steady growth function. Though moderate in mathematical terms, this transition of fertile river basin to waste land is a matter of serious concern. The silt formation (consequent to sand mining), unauthorized settlements in basins (called 'Purambokku'), drying of rivulets, formation of scrub lands etc. contribute to increase in rapid transition of fertile land to wasteland regions, which will aggravate the flood.

The reduction in agriculture area is a clear indication of the slowdown in the agrarian dynamism of this region. The rich agricultural bowl is quickly transiting towards non-cropping barren fields or housing settlements. This is in corroboration with a few studies which showed that the crop efficiency and cropping pattern itself of this region is fast changing. Such a transition, that too of an agriculture-predominant region is certainly an indication of a strong negative change. Though marginally, the reduction in forest cover also is another factor aggravating the intensity of flood havocs. Natural tropical forest act as an effective sponge for reducing the quick rain water run off and prevents flash floods. Further, forest cover in the river basin prevents soil erosion altering the river contours. Many studies have shown that forest cover is an effective stabilizing factor to control unlimited run offs. The annual reduction in forest cover in the river basin, will aggravate flood incidents.

5. Conclusion

The radical variations in the land use pattern of Pampa river basin revealed strong negative changes, directly affecting the basin ecology and aggravating the flood and drought situation of this river basin. The exorbitant increase in built up area, fast transition of fertile land to wastelands, increased deforestation, changing agrarian crop intensity etc calls for an urgent need for a diligent policy formulation to protect the river and basin. Also, there should be a conscious urban planning policy to cap the rate of urbanization in the river flood plain. Perhaps the only prescription is an urgent comprehensive policy planning with diligent implementation.

References

Bhaskaran Baijulal and P. Prateesh (2008). Land use change in upper catchment of Pampa river basin – A GIS based approach. Journal Eco-chronicle, vol.3, No.2. June 2008, pp: 127-130.

Census of India (2011). Provisional population totals – website http://census india.gov.in.

Economic Review (2007). Publication by State Planning Board, Government of Kerala.

KSCSTE. Kerala State Council for Science, Technology & Environment, Government of Kerala- Various reports- Website: www.kscste.kerala.gov.in/

KSUDP. Kerala Sustainable Urban Development Project, Government of Kerala. Report- Website http://ksudp.org.

M. S. Swaminathan Research Foundation (2007). Measures to mitigate Agrarian distress in Alappuzha and Kuttanad wetland ecosystem: A study report. Website. www.kuttanadupackage.in.

NUI. National Institute of Urban affairs, New Delhi. Various study reports - Website: www.niua.org.

Roy, P.S., V. Bhanumurthy, C.S. Murthy and T. Chand Kiran (2008). Space for disaster management: Lessons and perspectives. Journal of South Asia disaster studies. 1(1): 157-177

Samarakoon, L. (2004). Land use planning for flood mitigation of Dhaka city using remote sensing and GIS. ISTS-2004 n-22: 1-5.

Sarma, Santanu and Trivani Saikia (2012) Prioritization of subwatersheds in Khanapara-Bornihat area of Assam-Meghalaya (India) based on land use and slope analysis using remote sensing and GIS. Journal of Indian Society of Remote sensing. Sep.2012.40 (3): 435-446.

Journal of Geomatics Vol 11 No. 1 April 2017

Assessment of urban land cover classification using Wishart and Support Vector Machine (SVM) based on different decomposition parameters of fully-polarimetric SAR

LamyaaGamal El-deenTaha
Aviation and Aerial Photography Division, National Authority of Remote Sensing and Space Science, Cairo, Egypt
Email: Lamyaa@narss.sci.eg

(Received: Dec 20, 2016; in final form: Mar 20, 2017)

Abstract: Urban land cover mapping is one of the most important remote sensing applications. In this research, various polarimetric SAR parameters derived from fully-polarimetric SAR were explored for urban land cover mapping. The optimization of features is an important step for improving classification accuracy. First, radiometric correction of RADARSAT-2 Single Look Complex (SLC) product data has been performed using PolSARpro5. Two speckle filters (refined Lee and sigma Lee) were selected to be tested in RADARSAT-2 for elimination of noise and smoothing of the SAR images. It was found that sigma Lee filter is better than refined Lee filter with kernel size 5*5. Secondly, geometric correction was performed. The RADARSAT-2 was primarily geometrically corrected using ASF map ready tool in PolSARpro5 software for geocoding. Then second order polynomial based on fifteen well-distributed DGPS points was performed using ENVI 5 software. After that polarimetric decomposition parameters of RADARSAT-2 fully polarimetric SAR image was extracted from polarimetric decomposition techniques like Cloude-Pottier and Yamaguchi 4 components. Preprocessing of RADARSAT-2 data was achieved using PolSARpro5. In the present paper two classification methods, namely, Wishart and Support Vector Machine (SVM), were used for classification based on Cloude-Pottier and Yamaguchi's decompositions and combination of both decompositions. Three processing schemes were proposed based on decomposition parameters and were fed to Wishart and SVM algorithms. A comparison between these three schemes has been carried out and their usefulness in classifying urban land cover type was explored. It was found that SVM is better than Wishart classifier for classification of fully polarimetric synthetic aperture radar data. When applying the classification scheme based on each theorem separately, Yamaguchi's 4 components decomposition gave higher classification accuracy than ''H/A/α' components. The 7 parameter combination gives superior results than applying each theorem separately. Results show that SVM method discriminated each class better than Wishart supervised classification method did, especially for identifying the urban area. In the Wishart supervised classification based on 7parameters, the user's accuracy of the built-up area is very poor (54.73 %). In SVM classification based on 7 parameters, the user's accuracy of the built-up area was much higher (78.03 %).

Keywords: Polarimetric SAR; RADARSAT-2; Multi-polarization; full polarimetric; microwave-polarimetric decomposition; polarimetric classification algorithm; quadpol; Wishart supervised classification; SVM

1. Introduction

Polarimetric Synthetic Aperture Radar (SAR) is a very important source of information for Earth observation. Polarimetric SAR sensors, in comparison to single channel SAR sensors, have the advantage of a more complete description of objects' scattering behavior (Dabboor, 2011). A substantial amount of research has been carried out showing that fully polarimetric SAR systems are better in discriminating different land covers than single or dual polarimetric SAR data (Mishra and Singh, 2011). It is well known that the classification of different objects, as well as different terrain characteristics, with single channel SAR images can carry a significant amount of error (misclassification) even when operating after multilooking.

One of the main applications of Polarimetric SAR (POLSAR) is the segmentation of different land cover types. However, segmentation of SAR data was always a difficult task due to the presence of speckle noise (Pellizzeri, 2003; Dabboor, 2011). A variety of papers demonstrate how to improve information extraction from SAR images (Sabour et al., 2007).

A precise identification of the borders between built-up and non-built-up areas is particularly interesting for many applications like the study of risks, the study of the population density and the monitoring of urban growth, which is a key issue in many developing countries, where urban growth is an increasing and often uncontrolled phenomenon (Pellizzeri, 2003).

Polarimetric SAR data is available from different sensors for different frequencies like RADARSAT-2, ALOS_PALSAR and TerrSAR-X, RISAT-1 (Moreira et al., 2013). RADARSAT-2 is an active microwave sensor operating at C-band frequencies, to achieve land observations in cloudy conditions. The SAR may transmit and receive waves with vertical and horizontal linear polarization (Sakshaug, 2013; Wiseman et al., 2014). Four different modes are usually considered: HH, horizontally polarized emitted, horizontally polarized received and similarly for HV horizontally polarized emitted, vertically polarized received, VV vertically polarized emitted, vertically polarized received and VH vertically polarized emitted, horizontally polarized received. A fully polarimetric SAR system has all 4 channels HH, HV, VH and VV (Zyl and Kim, 2011).

It is possible to show that the same scene has a different behavior at different polarizations. Therefore, when data of different polarizations about the same scene are available, the information content about the observed region can be increased by fusing the multipolarization information (Dabboor et al., 2011). Recent research work indicates that polarimetric data provide significantly more information than conventional or multi-polarized images, particularly due to the additional phase information. Traditional pixel-based classification methods yield poor results when applied to SAR imagery because of the presence of the speckle and limited spectral information in SAR data (Qi et al., 2010). Therefore, polarimetric classification algorithms evolved. Many classification techniques for PolSAR data have been studied. The classification of PolSAR data itself is not good therefore polarimetric decomposition is made. The input parameters for PolSAR classification are SAR observables obtained by decomposition methods. Many methods for decomposition have been proposed (Qi et al., 2010) and classification methods based on the decomposition results were also used by some researchers.

The research objective is to evaluate two classifications techniques (Wishart and Support Vector Machine (SVM)) based on decomposition parameters or combination of decompositions for urban land cover classification, to assess Ismailia Governorate from RADARSAT 2. The other goal is to find the most favourable subset of polarimetric features derived from the decomposition theorems. The features are evaluated on the basis of an accuracy measure of a classification.

2. Study area and data set

The study area is located at Ismailia Governorate with an area of approximately 625km^2. Various land cover categories exist in the selected area, e.g., vegetation, urban area, roads, desert, power lines and water (lake). The study area has considered flat terrain.

The following data sources are available for the study area:

- Fully polarimetric data RADARSAT-2 (C band) acquired on 25 Nov 2014 with a 8m spatial resolution–Ismailia was used. The fully polarimetric image was composed by the HH, HV, VH and VV polarizations, each in Single Look Complex (SLC) format, Based on the reciprocity theorem, the VH polarization was not considered since it is equal to the HV polarization.
- Fifteen well-distributed differential ground control points (GPS) and twenty well-distributed differential GPS check points that were observed with accuracy ±10 cm in x, y and z.

Figure 1 depicts RADARSAT 2 image. Table 1 summarizes characteristics of RADARSAT 2 image.

Table 1: Characterstics of RADARSAT 2 image

System parameters	Values
Incidence Angle Near Range	19.6 degree
Incidence Angle Far Range	21.6 degree
Swath width	25 km
Range resolution	11 m
Azimuth resolution	9 m
Noise equivalent sigma zero	Better than 30 dB

3. Methodology

3.1. Data extraction and importing

The quad-pol data set used is C-band RADARSAT- 2 data. The data set was extracted and imported to PolSAR pro version 5. Scattering matrix was transformed to covariance matrix, the window size selected for covariance matrix generation is 3 x 3 then the covariance matrix was transformed to coherence matrix, the window size selected for coherence matrix generation is 3 x 3.

3.2. Speckle filtering

Speckle is a kind of noise usually appears as bright or dark dots in an image (Sakshaug, 2013). Speckle in the radar image is often a problem and should be reduced before the image is used for further quantitative analysis. Many speckle suppression techniques, such as median, Lee-sigma, Gamma-map, local-region and Frost (Lee et al., 1994), can be used to reduce the speckle noise. It is important to identify a suitable filtering method and suitable moving kernel size based on certain criteria. In general, the following factors are used to identify the best filtering method: (1) speckle reduction, (2) edge sharpness preservation, (3) line and point target contrast preservation, (4) retention of texture information, and (5) computational efficiency (Lu et al., 2011). Figure 2 depicts image after filtering with sigma Lee.

In this research refined Lee and sigma Lee filters were applied to the available data. A comparative analysis based on visual interpretation of the filtered images indicated that sigma Lee filter with kernel size 5 x 5 is better than refined Lee filter.

3.3 Geometric correction

The RADARSAT-2 was primarily geometrically corrected using ASF map ready tool in PolSARpro5 software for geocoding tool. Then RADARSAT-2 was registered using second order polynomial based on fifteen well-distributed DGPS points observed within 10 cm accuracy and the image was resampled to pixel size of 8 m using the nearest neighbor technique. The resulted RMSE of control points was 0.46 pixel. Rectification was validated using an independent set of twenty well distributed DGPS. The resulted RMSE of check points was 0.49 pixel. This step was performed in ENVI 5. Fig. 3 depicts Pauli RGB.

Figure 1: RADARSAT 2 image.

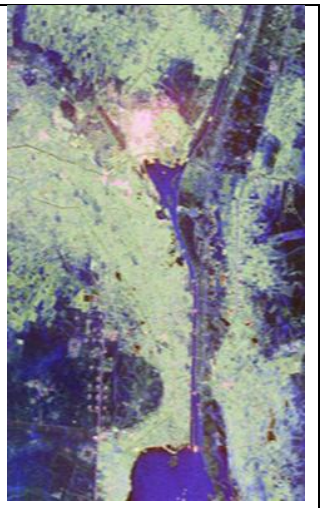

Figure 2: Image after filtering with sigma Lee.

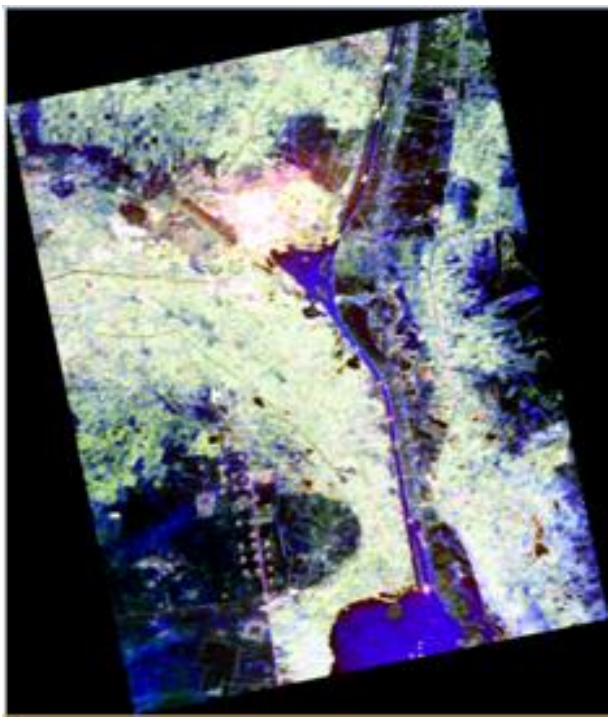

Figure 3: Pauli RGB ($|HH-VV|$ as red, $|HV|$ as green and $|HH+VV|$ as blue)

3.4. Polarimetric decomposition

Polarimetric decomposition theorems break polarimetric SAR measurements into components that describe the scattering behaviour of the target (Sakshaug, 2013) to provide a way for interpretation. The objective of target decomposition theory is to express the average scattering mechanism as the sum of independent elements to associate a physical mechanism with each component (Dabboor, 2011; Mishra and Singh 2011).

The polarimetric decomposition theorems project the matrices that describe the backscattering, on to a set of basis matrices and express the backscatter as a linear sum of the basis matrices multiplied with corresponding coefficients (Sakshaug, 2013).

There are many target decomposition techniques available to decompose the data. In this research polarimetric decomposition has been performed by different techniques namely Cloude-Pottier (Entropy – Anisotropy – Mean scattering angle or H-A-α) and Yamaguchi decomposition for understanding polarization-specific scattering behavior of the land use / land cover (LULC) classes. PolSARPro5.0 software was used to implement the H/A/Alpha decomposition, Yamaguchi decomposition and Freeman decomposition. Three processing schemes, namely H/A/α decomposition, Yamaguchi decomposition and a combination of both were attempted.

3.4.1 Cloude-Pottier (The ‘‘H/A/α’’) polarimetric decomposition: Cloude-Pottier decomposition is incoherent decomposition method based on the eigen vector / eigen value analysis of the coherency matrix T (Dabboor, 2011). It is also called eigen vector – eigen value based decomposition (Qi et al., 2010). The ‘‘H/A/α’’ decomposition theorem is the basis for the design of the proposed processing scheme for polarimetric SAR images. Entropy (H) is the measure of randomness of scattering. Anisotropy (A) can be defined as the normalized difference between the appearance probabilities of the second and third scattering components (eigen value). From a practical point of view, the anisotropy can be employed as a source of discrimination only when entropy is greater than 0.7 because for lower entropies, the second and third eigen values are highly affected by noise. Consequently, the anisotropy is also very noisy. The parameter α is an indicator of type of scattering and is called scattering mechanism (Mishra and Singh, 2011). Figure 4 depicts polarimetric decomposition main parameters H, A and α.

3.5 Fully-polarimetric SAR classification

The choice of the classification algorithm is critical to success and each supervised classification approach has associated pros and cons (McNairn et al., 2009). The Wishart supervised classification and SVM were conducted by using the PolSARPro5.0 software based on the selected polarimetric decomposition parameters and combination of different decomposition parameters. The classification maps resulted from the three schemes of the Wishart supervised classification and SVM were produced as the comparison.

First, a processing scheme that jointly exploits the three parameter (H, α and A) to form a multichannel image in a single classification process was implemented. Secondly, a processing scheme that jointly exploits the Yamaguchi 4 parameter (single, double, volume and helix) to form a multichannel image in a single classification process was implemented. Thirdly, processing scheme that jointly exploits the seven parameters images entropy (H), alpha (α), anisotropy (A) and Yamaguchi (single, double, volume and helix)

to form a multichannel image in a single classification process was implemented.

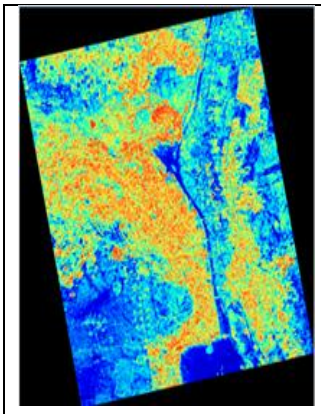

Figure 4 (a): Entropy

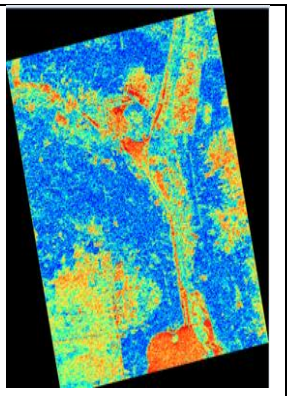

Figure 4 (b) : Anisotropy

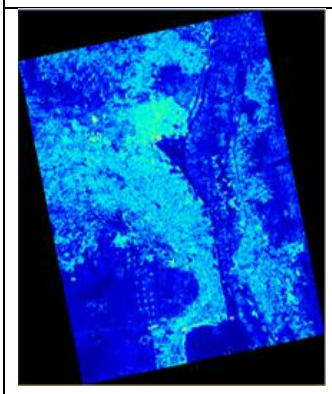

Figure 4 (c) : Alpha

Figure 4: Polarimetric decomposition main parameters: H, A and α.

Next, both classifiers are trained by using training data (sample data) that extracted from the three processing schemes (30 samples per class) for each scheme). Signatures were evaluated. Meanwhile, a total of 6 classes features (urban, road, desert, water, vegetation, power lines) were extracted for different classifications. Test samples for these classes were collected to generate confusion matrices, Kappa coefficient of agreement, overall accuracy in order to evaluate the classifications. Finally, land cover classification was performed using the Wishart supervised classification and SVM for all three schemes.

The LULC classification results of RADARSAT-2 data based on different decomposition and combination of decompositions were compared for both classifiers. Also an evaluation of the accuracy improvements in the detection of urban features was performed.

3.5.1 Supervised Wishart classifiers: The availability of the Wishart classifier in polarimetric tools has led to their widespread use among those performing PolSAR classification. The Wishart algorithm is a maximum-likelihood classifier in which a distance measure is established between each pixel's coherency matrix and the respective cluster means in an iterative process (Atwood et al., 2012), the Wishart classification involved only the T matrix elements especially dedicated to SAR data as it accounts for the Wishart distribution observed due to the presence of speckle noise (Lardeux et al., 2014).

The presented supervised algorithm, is a maximum likelihood classifier based on the complex Wishart distribution for the polarimetric coherency matrix, given by:

$$P\left(\langle[T]\rangle / [T_m]\right) = \frac{L^{Lp}\left|\langle[T]\rangle\right|^{L-p} e^{-L\,Tr\left([T_m]^{-1}\langle[T]\rangle\right)}}{\pi^{\frac{p(p-1)}{2}}\Gamma(L)\ldots\Gamma(L-p+1)\left|[T_m]\right|^{L}} \quad (1)$$

Each class is characterized by its own coherency matrix $[T_m]$ which is estimated using training samples from the m^{th} class ω_m. According to the Bayes maximum likelihood classification procedure, an averaged coherency matrix $\langle[T]\rangle$ is assigned to the class ω_m, if :

$$[T] \in [T_m] \quad if \quad d_m([T]) < d_j([T]) \quad \forall j \neq m \quad (2)$$

$$d_m([T]) = LTr\left([T_m]^{-1}[T]\right) + L\,ln\left(|[T_m]|\right) - ln\left(P([T_m])\right) + K \quad (3)$$

This relation shows that if the number of look (L) increases, the a priori probability $P([T_m])$ of the class ω_m does not play a significant role for the classification. It is generally assumed that without a priori knowledge, the different $P([T_m])$ are equal, in which case the distance measure is not a function of the number of look (L). Usually, to implement the classification, the classified pixel by pixel. These different training sets have to be selected in advance. For each pixel, represented by the averaged coherency matrix $\langle[T]\rangle$, the distance is computed for each class, and the class associated to the minimum distance is assigned to the pixel. During the procedure, each feature coherency matrix $[T_m]$ is iteratively updated from the initial estimate. The algorithm of this iterative procedure, similar to the k-mean method, is given as follows

1 : Provide an initial $[T_m](0)$ as an initial guess for each class (k=0)
2 : Classify the whole image using the distance measure procedure
3 : Compute $[T_m](k+1)$ for each class using the classified pixels of step 2
4 : Return to step 2, until a termination criterion

defined by the user is met (Pottier et al., 2004).

3.5.2 Support Vector Machine (SVM) algorithm: SVM is a modern machine learning method that offers improved generalization performance and can model complex nonlinear boundaries through the use of adapted kernel functions (Li et al., 2011), particularly in the case of extracting feature vectors from fully polarimetric SAR data. Figure 5 illustrates the classification map using SVM utilizing from 7 polarimetric decomposition as features. Table 2 shows the overall accuracy and Kappa coefficient of Wishart and SVM classifiers.

SVM method distinguished each class better than Wishart supervised classification did, especially for identifying the built up area. In the Wishart supervised classification based on 7 parameters, the user's accuracy of the built-up area is very poor (54.73 %). In SVM classification based on 7 parameters, however, the user's accuracy of the built-up area was much higher (78.03 %).

Figure 6 depicts User's accuracy % of Wishart classifier. Figure 7 depicts the Kappa coefficient of Wishart and SVM classifiers.
coherency matrix [T_m] is estimated using pixels within different selected areas of the m^{th} class and data is then

Table 2: The overall accuracy and Kappa coefficient of Wishart and SVM classifiers

Polarimetric features	Wishart overall accuracy (%)	SVM classifier overall accuracy (%)	Kappa coefficient of Wishart	Kappa coefficient of SVM
H/A/α decomposition	66.27	89.08	0.62	0. 89
Yamaguchi's 4 component	78.53	99.08	0.79	0.95

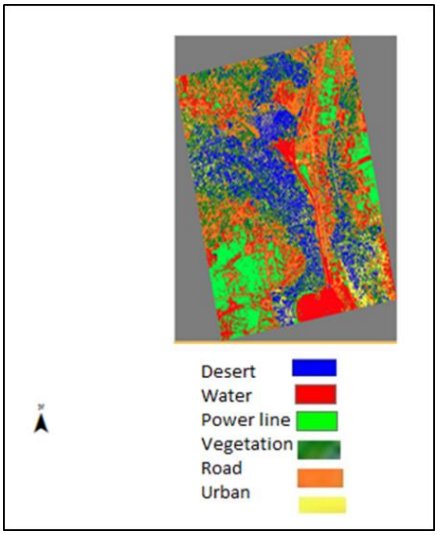

Figure 5: The classification map using SVM utilizing from 7 polarimetric features.

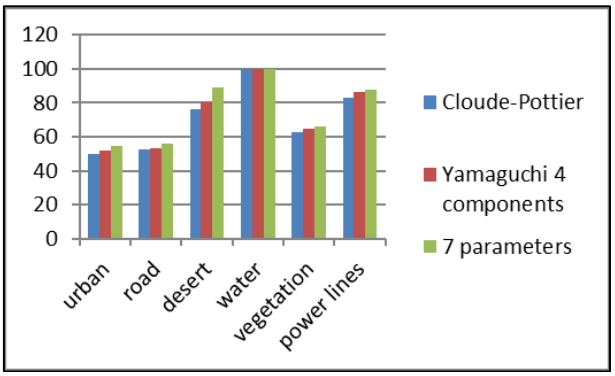

Figure 6: User's accuracy % of Wishart classifier

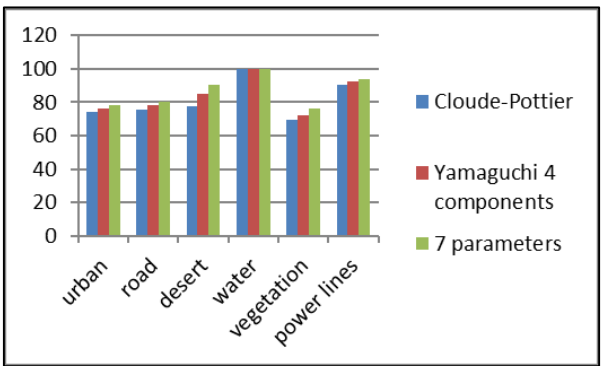

Figure 7: User's accuracy % of SVM classifier.

4. Results and discussions

The LULC classification results of fully-polarimetric RADARSAT-2 data using Wishart and SVM classifiers based on different decomposition and combination of decompositions were compared. The features are evaluated on the basis of an accuracy measure of a classification. Also an evaluation of the accuracy improvements in the detection of urban features was performed. PolSARPro 5 and ENVI5.1softwares were used for processing of the data sets.

First, sigma Lee and refined Lee filters were applied to the fully-polarimetric RADARSAT -2 image to reduce the noise and enhance the image quality. After speckle reduction SAR was georeferenced to a UTM coordinate system. As the study area presents an almost flat topography, a second order polynomial transformation and nearest neighbour resampling were used to create the output images with 8 m ground resolution. The root mean square error of the polynomial transformation was less than half a pixel. Check points were measured on the geometrically corrected image. The root mean square error of the check points was less than half a pixel.

Total of 7 PolSAR features (parameters) are extracted from the RADARSAT-2 full polarimetric data by the PolSARpro program. The optimization of features is an important step for improving accuracy. Three

processing schemes were proposed based on decomposition parameters and were fed to Wishart and SVM algorithms. The classification maps using the three schemes of the Wishart supervised and SVM classifications were produced as the comparison.

By comparing the overall accuracy and kappa index of the Wishart and SVM classifiers, based on Table 2 and from figures 6 and 7, it is clear that different classification accuracies are derived when different PolSAR features are input to the Wishart and SVM classifiers. SVM based approaches for classification of polarimetric synthetic aperture radar data is better than Wishart classifier. One can attribute this to the fact that Wishart algorithm is a maximum-likelihood classifier which mean Wishart algorithm is per pixel classifier (traditional or hard classifier). On the other hand, SVM classifier is a subpixel classifier (soft classifier). The 7-parameters combination gives superior results compared to the other decompositions. Yamaguchi's 4 components is better than H/A/α decomposition. Figure 8 depicts flowchart of urban land cover classification.

In the classification result with the Wishart (approach 1 - H/A/α decomposition), an overall accuracy of 66.27 % percent was achieved. The following compares other approaches with approach 1, so as to determine whether insertion of other information's will improve the classification accuracy. The overall classification accuracy of approach 2, which used the Yamaguchi's 4 components, is 78.53 %, a slight improvement was achieved compared to approach 1. Approach 3 clearly outperforms approach 1. The overall accuracy of 78.99 % was achieved, an improvement of 12.27 %. The combination of 7 parameters improved the classification accuracies of most LULC classes. Approach 3 has the best performance among all the approaches examined.

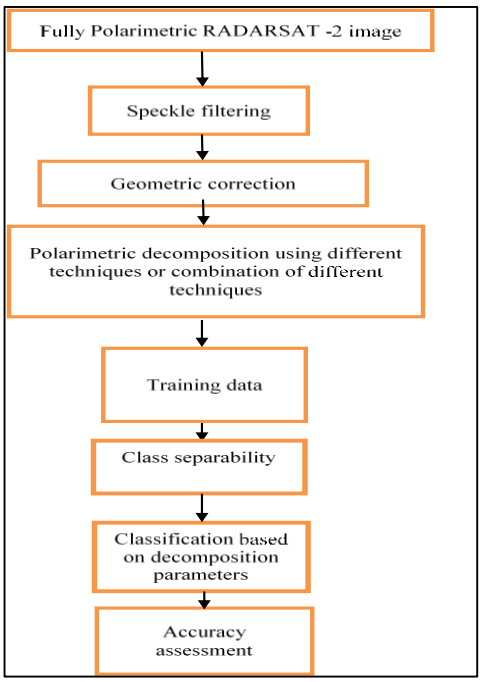

Figure 8: Flowchart of urban land cover classification

In the classification result with the SVM (approach 1 - H/A/α decomposition), an overall accuracy of 89.08% percent was achieved. The following compares other approaches with approach 1, so as to determine whether insertion of other information's will improve the classification accuracy. The overall classification accuracy of approach 2, which used the Yamaguchi's 4 components, is 99.08 % percent, an improvement was achieved compared to approach 1. Approach 3 clearly outperforms Approach 1. The overall accuracy of 99.67 % percent was achieved, an improvement of 10.59 %. The combination of 7 parameters improved the classification accuracies of most LULC classes. Approach 3 has the best performance among all the approaches examined.

Based on figures 6 and 7, it is clear that SVM method discriminate each class better than the Wishart supervised classification did, especially for identifying the urban area.

5. Conclusion and recommendations

In this study, RADARSAT-2 full PolSAR has been used to extract two decomposition techniques (Cloude-Pottier and Yamaguchi 4 components) and combination of decomposition parameters for urban land cover classification. Experimental results show a better performance of SVM based approaches compared to Wishart based approaches for classification of polarimetric synthetic aperture radar. When applying the decomposition theorems separately, Yamaguchi's 4 component decomposition theorem gave the higher accuracy. The 7-parameters combination gives superior results compared to H/A/α decomposition or Yamaguchi's 4 components.

ACKNOWLEDGEMENT

The author thanks NARSS for giving the data. The editing and comments of the reviewers is gratefully appreciated.

REFERENCES

Atwood, D.K., D. Small and R. Gens (2012). Improving PolSAR land cover classification with radiometric correction of the coherency matrix. IEEE Journal of Selced Topics in Applied Earth Observations and Remote Sensing, vol. 5, no. 3, 848 – 856.

Dabboor, M. (2011). New segmentation algorithms for dual and full polarimetric SAR Data. Ph.D. thesis, Department of Geomatics Engineering, Schulich School of Engineering, University of Calgary URL: http://www.geomatics.ucalgary.ca/graduatetheses.

Dabboor, M., V. Karathanassi and A. Braun (2011). Multi-level segmentation methodology for dual-polarized SAR data. International Journal of Applied Earth Observation and Geoinformation 13, 376-385

Han, Y. and Y. Shao (2010). Full polarimetric SAR classification based on Yamaguchi decomposition model and scattering parameters. IEEE International conference on Progress informatics and computing.

Lardeux, C., P. Frison, J.P. Rudant, J.C. Souyris, C. Tison and B. Stoll (2014). Classification of fully polarimetric SAR data for land use cartography. The International Archives of the Photogrammetry, Remote Sensing and Spatial Information Sciences, Volume XL-8, 2014

Lee, J.-S., M.R. Grunesm, E. Pottier and L.F. Famil (2005). Automated terrain classification using polarimetric synthetic aperture radar remote sensing. Remote Sensing NRL Review, 203 – 205.

Li, X., H. Guo, Z. Sun and G. Shen (2011). Urban impervious surfaces estimation from RADARSAT-2 polarimetric data using SVM method. PIERS Online, Vol. 7, No. 7, 671-676.

Lu, D., G. Li, E. Moran, L. Dutra and M. Batistella (2011). A comparison of multisensor integration methods for land cover classification in the Brazilian amazon. GIScience & Remote Sensing, 2011, 48, No. 3, p. 345–370. DOI: 10.2747/1548-1603.48.3.345.

McNairn, H., C. Champagne, J. Shang, D. Holmstrom and G. Reichert (2009). Integration of optical and Synthetic Aperture Radar (SAR) imagery for delivering operational annual crop inventories. ISPRS Journal of Photogrammetry and Remote Sensing 64 (2009) 434_449

Mishra, P. and D. Singh (2011). Land cover classification of PALSAR images by knowledge based decision tree classifier and supervised classifiers based on SAR observables. Progress in Electromagnetics Research B, Vol. 30, 47-70.

Moreira, A., P. Prats-Iraola, M. Younis, G. Krieger, I. Hajnsek and K.P. Papathanassiou (2013). A tutorial on synthetic aperture radar. IEEE Geoscience and remote sensing magazine, March 2013, 6-43.

Pellizzeri, T.M. (2003). Classification of polarimetric SAR images of suburban areas using joint annealed segmentation and ‘‘H/A/a’’ polarimetric decomposition. ISPRS Journal of Photogrammetry & Remote Sensing 58 (2003) 55– 70

Pottier, E., J. S. Lee, L. Ferro – Famil (2004). Advanced concepts in polarimetry – Part 2 (Polarimetric Target Classification). Ottawa, Canada, 21-22 October 2004, and published in RTO-EN-SET-081.

Sabour, S.M.T., P. Lohmann and U. Soergel (2007). Monitoring agricultural activities using ASAR ENVISAT data. Proc. ‘Envisat Symposium 2007’, Montreux, Switzerland 23–27 April 2007 (ESA SP-636, July 2007), 6p.

Sakshaug, S.E. (2013). Evaluation of polarimetric SAR decomposition methods for tropical forest analysis. Master Thesis in Energy, Climate and Environment, University of Tromso, UIT June 2013.

Qi, Z., A.G. Yeh, X. Li and Z. Lin (2010). Land use and land cover classification using RADARSAT-2 polarimetric SAR image. ISPRS TC VII Symposium – 100 Years ISPRS, Vienna, Austria, July 5–7, 2010, IAPRS, Vol. XXXVIII, Part 7A.

Wiseman, G., H. McNairn, S. Homayouni and J. Shang (2014). RADARSAT-2 polarimetric SAR response to crop biomass for agricultural Production monitoring. IEEE Journal of Selected Topics in Applied Earth Observations and Remote Sensing, Vol. 7, No. 11, November 2014

Zyl, A.V. and Y. Kim (2011). Synthetic aperture radar polarimetry. Wiley Publication.

Journal of Geomatics Vol 11 No. 1 April 2017

Estimation of change in glacier ice thickness using ICESat laser altimetry data

Ritesh Agrawal[1], Gunjan Rastogi[1] and Ajai[2]
[1]Space Applications Centre (SAC/ISRO), Ahmedabad-380015, Gujarat, India
[2] ES-CSIR, Space Applications Centre (SAC/ISRO), Ahmedabad-380015, Gujarat, India
Email ritesh_agrawal@sac.isro.gov.in

(Received: Jan 16, 2017; in final form: Apr 20, 2017)

Abstract: Himalaya have the highest concentration of glaciers outside the polar regions and thus hold one of the most important natural resources in the form of frozen water. Himalayan glaciers also act as sensitive indicators of climate change. In view of above one needs to study and monitor the status of these glaciers. Present study deals with estimation of elevation change in the selected glaciers of the Himalaya using ICESat/GLAS data for the period 2003 to 2009. One glacier from Ganga basin and three glaciers from Indus basin have been taken for present study. ICESat data of the similar period have been analyzed using near-repeat track projection approach with the help of reference Digital Elevation Model (DEM). Average ice thickness change for the Gangotri glacier has been found to be +0.24 m/year while in Indus Basin, average rate of ice thickness change has been found to be +0.02 m/year, +0.44 m/year and -1.02 m/year for Siachin, Baltoro and Drenmarg glacier, respectively.

Keywords: ICESat, Himalaya, Glacier thickness

1. Introduction

Surface elevation and its variation remains an important parameter for studying the global environment and climate change. Till date a large number of earth observation satellites have been launched to retrieve surface elevation data. Satellite radar altimetry have been used for estimation of surface elevation and its change detection since late 1970s (Robin, 1966; Zwally et al., 1989, Wingham et al., 1998; Johannessen et al., 2005). Due to limitation of large footprint size, the satellite radar altimetry is mainly suitable to the region of low relief glaciers and ice sheets in cryosphere studies. Estimation of surface ice thickness change over high relief glaciers, requires high resolution altimetry datasets. In last few years, altimeters like Ice, Cloud and land Elevation Satellite (ICESat) laser altimeter (Zwally et al., 2002) have been providing high resolution elevation data sets. Cryosat-2 radar altimeter (Wingham et al., 2006) also provides high resolution datasets by employing advanced SAR interferometric altimeter techniques that are comparable to maps (Sauber et al., 2005; Muskett et al., 2008; Nuth et al., 2010).

ICESat, launched by NASA in January 2003, had the prime objective of estimating ice-elevation changes in Polar regions. Laser altimeter named Geoscience Laser Altimeter System (GLAS) on board ICESat with a high resolution footprint of 70m and along-track spacing of 170m provided elevation data. During 2003 to 2009 a large amount of data has been acquired by three laser sensors of GLAS. However, the utility of ICESat/GLAS data covered more aspects other than its main objective (Berthier et al., 2007; Kropacek et at., 2014; Kaab et al., 2015).

Glaciers, among the best indicators of terrestrial climate change, contribute importantly to water resources in many mountainous regions of the world. Himalayan glaciers cover an area of 71,182km2 (Arun et al., 2013) and monitoring changes in their thickness is a key issue as the melting of glaciers in central Asia may significantly contribute to sea level rise (Arun et al., 2013). In addition, runoff generated by the melting of the glaciers in the Himalaya is an important source of water for the people living in the plains. Given the size and remoteness of glaciers in Himalayas, in-situ measurements are sparse and thus satellite remote sensing is a viable alternative for comprehensive and frequent monitoring of this important resource (Berthier et al., 2006; Kasturirangan et Al., 2011; Bahuguna et al., 2014). The most commonly used technique for estimation of glacier ice thickness change is based on the subtraction of the two-time frame DEMs generated from satellite photogrammetry or interferometry (Gardelle et al., 2012).

Himalayan glaciers, however, generally have rougher surfaces and steeper regional slopes than the ice sheets for which ICESat was optimized (Sauber et al., 2005). Elevation changes (or ice thickness changes) over glaciers from satellite altimetry is computed directly using elevation difference at crossover points between ascending and descending satellite passes. This method gives coarse sampling for computation of elevation changes (Brenner et al., 2007). In this paper, an attempt has been made to explore the potential of repeat track ICESat to derive glacier elevation changes (glacier ice thickness change) for four glaciers; three in Indus basin (Siachin, Baltoro and Drenmarg) and one in the Ganga basin (Gangotri) of the Himalayan region.

2. Study area

Three glaciers from Indus basin, namely, Siachin, Drenmarg and Baltoro and one from Ganga basin (Gangotri), have been taken in this study. These four glaciers have been selected since GLAS/ICESat repeat track data was available over these glaciers. In addition, these four glaciers are among the largest glaciers in the

Indus and Ganga basin of the Himalaya. The glacier information and their attribute information is taken by the glacier inventory generated at Space Applications Centre (Arun et al., 2013) Figure 1 a and b shows the location of these four glaciers.

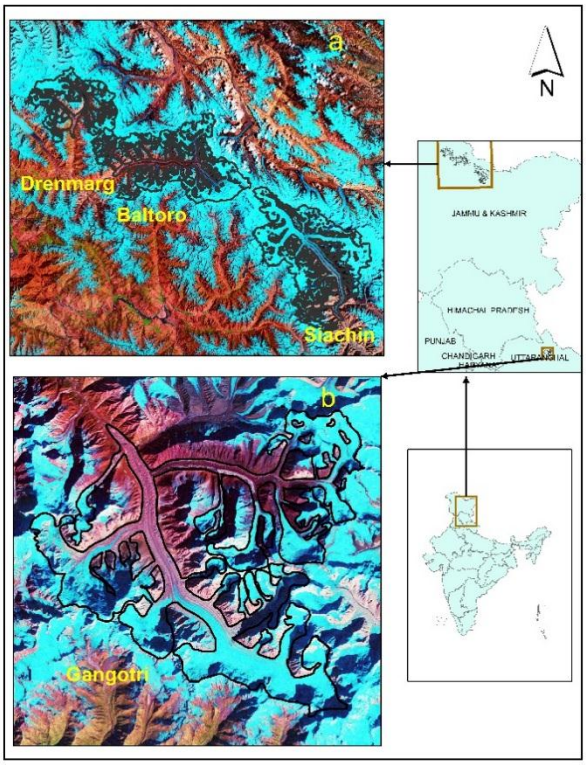

Figure 1: False Color Composite of Landsat TM image showing location of glacier a) Three glaciers (Drenmarg, Baltoro, Siachin in Indus basin) b) Gangotri glacier in Ganga basin of Himalayan region

- **Gangotri glacier**, one of the largest glaciers in the central Himalaya, is located in Uttarkashi district, Uttarakhand state of India. This valley type glacier is the source of a major river system Ganga in northern India. The glacier has an estimated ice volume of about 27 km3 (about 27 km long and 1 km wide). The orientation of the glacier is towards NW (North West).
- **Siachin glacier,** located in the eastern Karakoram range in the Himalayan mountains, is the longest glacier in the Karakoram and second-longest among the world's mountain glaciers. It lies between Saltoro ridge immediately to the west and the main Karakoram range to the east. Including all tributary glaciers, the Siachin glacier system covers about 700 km2 area and 1.3 to 3.2 km wide. The orientation of the glacier is towards SE (South East).
- **Baltoro glacier,** located in the Karakoram range, is the origin of Shigar river which is a tributary of the Indus river. The glacier is about 57.6 km long and 1.7 to 3 km wide with orientation towards SW (South West).
- **Drenmarg glacier** is located in the eastern Karakoram range in the Himalayan mountains. The glacier altitude varies from 5,467 m to 3,769 m above mean sea level. The glacier covers an area of 413.5 km2. It is about 25.31 km long with orientation toward SE (South East) and 0.8 to 1.5 km wide.

3. Data used

3.1 ICESat/GLAS

ICESat has an onboard laser altimeter system to collect surface elevations all over the globe with high precision. Since 2003 to the end of its operation in 2009, GLAS has been operating for three annual observation campaigns, each of approximately 35 days. This instrument combines a 3 cm precision 1064-nm laser altimeter with a laser pointing angle determination system (Sirota et al., 2005) and it is used to measure the Earth's surface and it also measure the backscattering profile from thicker clouds, while those at 532-nm use photon-counting detectors and measure the height distributions of optically thin clouds and aerosol layers. A GPS receiver on the spacecraft provides data for determining the spacecraft position, and also the absolute time reference for the instrument measurements and altimetry clock (Abshire et al., 2005). It retrieves surface elevations within 70 m diameter footprints and along track spacing of 170 m. GLAS elevation accuracy is reported to be 15 cm over flat terrain (Zwally et al., 2002). Average error of 20 cm has been reported in estimating glacier ice thickness change in the Alps / Himalaya (Kropacek et al., 2014; Kaab et al., 2015; Kaab et al., 2012). In this study GLA06 product of ICESat has been used between 2003 and 2009 available from the National Snow and Ice Data Centre, (http://nsidc.org/data/icesat) in geographical co-ordinate system with WGS-84 datum (Zwally et al., 2008).

3.2 Digital Elevation Model (DEM)

CartoDEM and SRTM DEM have been used to project ICESat repeat tracks onto common locations and to extrapolate elevation changes to unmeasured locations. The thickness change has been computed by projecting the secondary track to reference track by using both SRTM DEM and CartoDEM.

3.2.1 Carto DEM : Cartosat-1 Digital Elevation Model (CartoDEM) is a National DEM developed by the Indian Space Research Organization (ISRO), derived from the Cartosat-1. Cartosat-1 has a pair of Panchromatic cameras having an along track stereoscopic capability to acquire two images simultaneously, one forward looking (Fore) at +26 degrees and another rear looking (Aft) -5 degrees with a base-to-height ratio of about 0.63. Its Absolute planimetric accuracy is 15 m and absolute vertical accuracy is 8 m and having 5 m relative vertical accuracy (Muralikrishnan et al., 2011). Cartosat derived DEM in the hilly terrain of Chamoli and Shimla districts of the Himalaya were validated (Agrawal et al., 2006) and reported the relative vertical accuracy of the DEM to be about 5 m. CartoDEM v1 data, available through Bhuvan portal (bhuvan.nrsc.gov.in) of NRSC in geographical projection and WGS-84 datum, were used.

3.2.2 SRTM DEM : The SRTM (Shuttle RADAR Topographic Mission) was the first mission using space-borne single pass interferometric SAR which was flown in 11 February 2000. The goal of the mission was to survey the Earth surface and to generate a homogeneous elevation data set of the world with a grid spacing of 3arcsec available from USGS (earthexplorer.usgs.gov). The digital topographic map products were expected to meet the Interferometric Terrain Height Data (ITHD)-2 specifications sampling with 16 m absolute vertical height accuracy, 10 m relative vertical height accuracy and 20 m absolute horizontal accuracy (Bamler, 1999). The horizontal datum is the World Geodetic System 1984 in geographical projection system. The vertical datum is mean sea level as defined by the Earth Gravitational Model (EGM-96) geoid. Most of the users commonly ignore the original vertical datum and use SRTM data as referenced to the WGS84 ellipsoid as geoid models (Markus, 2005). The problems can be resolved by use of the WGS-84 orthometric height correction calculated from EGM-96 to convert it in ellipsoidal height (Agrawal R et.al 2006).

4. Methodology

Researchers have used mainly three approaches for estimation of the elevation change using ICESat altimetry (Moholdt et al., 2010a). The first approach, which computes elevation changes at crossover points, has very high accuracy. Elevations at crossover points are linearly interpolated from the two closest footprints within 200 m in each track (Brenner et al., 2007). The main drawback of this approach is that the sampling is too coarse. The second approach uses a DEM to correct for the surface slope between the center points of overlapping footprints (Slobbe et al., 2008). This approach takes care of the slope-induced errors; however, it is constrained by the data availability for comparison. It is difficult to compare repeat track ICESat profiles due to the relatively large cross track separation between repeat profiles. In view of the limitations of the first two approaches, the third approach has been used in this study which utilizes near repeat ICESat tracks having small (up to 200 m) cross-track separation (Moholdt et al., 2010a) shown in figures 2 and 3.

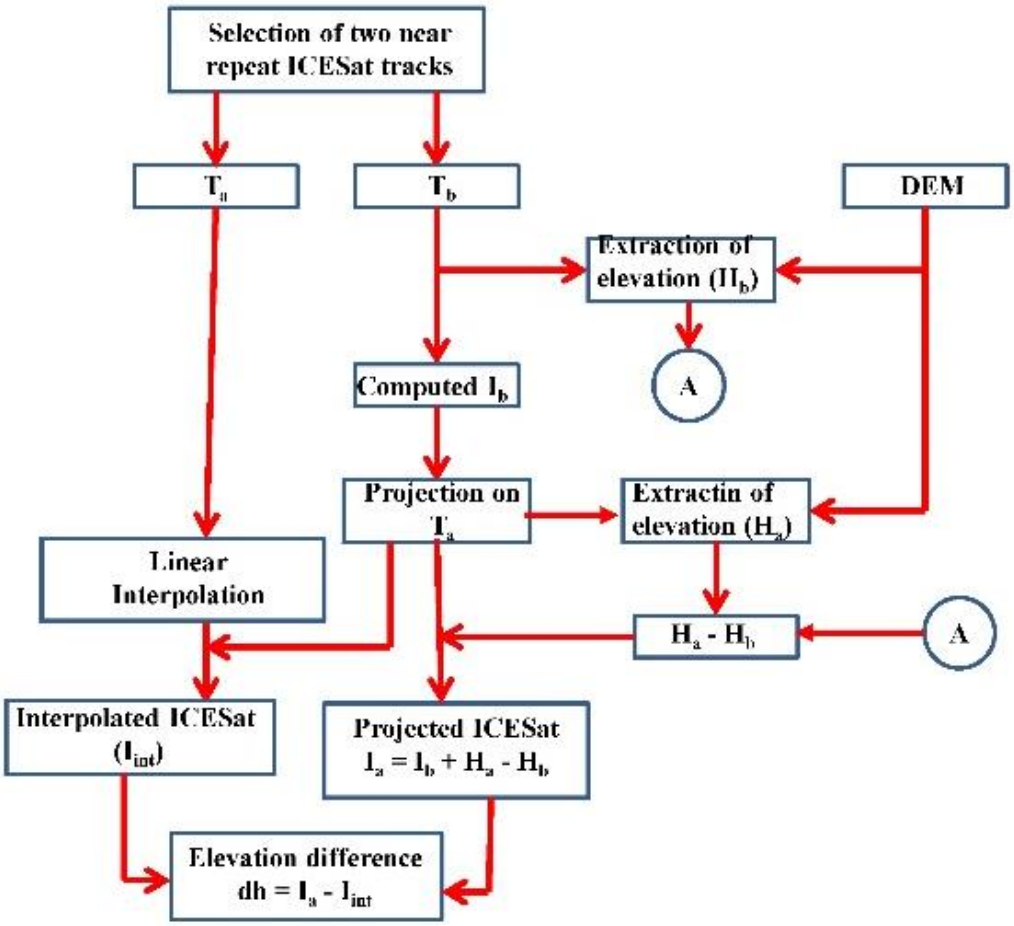

Figure 2: Flowchart showing the near repeat track methodology for elevation change estimation.

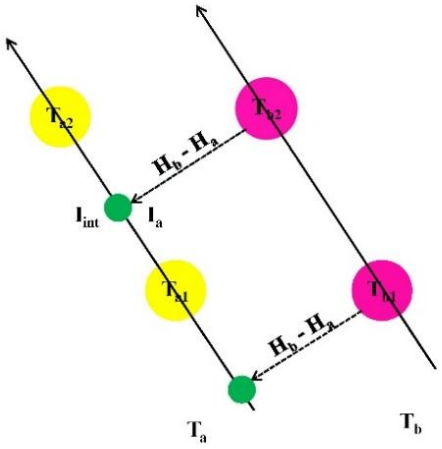

Figure 3: Projection of near repeat tracks on common locations using DEMs. Green dots represent projected location, Pink dots represent secondary track and Yellow dots represent reference track

In this approach, two near repeat ICESat tracks (T_a and T_b) pertaining to different years and same month have been taken for computing the glacier ice thickness change. For every pair of ICESat repeat tracks, one track is considered as the reference track and other one as secondary track. The track T_a which is older in time sequence, is chosen as the reference track. The secondary track is projected on the reference track and surface elevation change at these two locations can be estimated by the change in elevation values of these locations using DEM. The elevation information H_a and H_b have been extracted from the DEM at the ICESat footprints on track T_a and T_b, respectively. The difference ($H_a - H_b$) of this elevation information (H_a & H_b) is represented as the unmeasured topography between the near repeat tracks. Here the utility of DEM implies along-track interpolation to restrict the DEM slope correction to the cross-track distance between two repeat-tracks (Moholdt et al., 2010b). Now each footprint on track T_b is projected perpendicularly on track T_a using CartoDEM or SRTM DEM. The ICESat elevation on the projected points (I_a) over reference track (I_a) can be computed as in equation (1).

$$I_a = I_b + H_a - H_b \qquad (1)$$

At the same projected points on the reference track T_a, ICESat elevation (I_{int}) is estimated through linearly interpolating the neighboring footprints (T_{a1} and T_{a2}) along the track. The elevation difference at the projected points (dh) is the change in the elevation between the projected (I_a) and interpolated ICESat elevation (I_{int}) and it can be computed as in equation (2):

$$dh = I_a - I_{int} \qquad (2)$$

where,

dh= elevation difference of two different periods;

I_a = ICESat elevation at projected location on track T_a;

I_{int}= interpolated ICESat elevation on track T_a

I_b= ICESat elevation on track T_b;

H_a= extracted elevation from DEM on track T_a;

H_b= extracted elevation from DEM on track T_b.

5. Results and discussion

The ICESat altimetry data of near repeat tracks (T_a and T_b) have been used to estimate the surface elevation changes in the glaciers and thus change in glacier ice thickness. In this study, track T_a is considered as the reference track and track T_b as secondary track. The mean elevation changes and mean track separation, computed from the repeat passes of the ICESat for the four selected glaciers, are given in Table 1. Different tracks over Gangotri glacier show the variations in the thinning / thickening rate in the range of 0.01 to 0.71 m/year by utilizing CartoDEM for projecting secondary track over the reference track. Similar ice thickness changes (-0.20 to 0.84 m/year) have been observed while using SRTM DEM.

There has been significant positive change in the ice thickness (0.71 m/year) for Gangotri glacier during the period 2005-07. However, ice thickness change during the period of 2004-08 has been found to be negligible (Table 1).

For Siachin glacier, mean separation between the ICESat near repeat tracks (T_a and T_b) has been found to be 14.5 m. The mean thicking rate during 2004-09 has been found to be 0.23 m/year and 0.27 m/year by using CartoDEM and SRTM respectively. The positive ice thickness change (thickening) has been observed during the period 2004-09. There has been a very small negative ice thickness change during the period 2003-05 (Table 1).

For Baltoro glacier, the near repeat track has a temporal separation of six years (2003-09). The mean ice thickness change (thickening) during this period have been found as 0.44 m/year and 0.66 m/year using CartoDEM and SRTM respectively for projecting secondary track over the reference track.

The mean ice thickness change in the case of Drenmarg glacier, during the period (2003-07) are found to be -1.02 m/year and -1.05 m/year using CartoDEM and SRTM respectively. Figure 4 shows the average annual rate of ice thickness change along the ICESat reference track for all the four glaciers. It is observed that the thinning / thickening rate computed using SRTM and CartoDEM are almost similar.

Table 1: Mean elevation change along the ICESat tracks of Gangotri, Siachin, Baltoro and Drenmarg glacier

S. No.	Glacier name	ICESat Tracks		Mean Track Separation (m)	Elevation change rate (m/year)	
		Track T_a (Ref.)	Track T_b		Carto-DEM	SRTM
1.	Gangotri	Mar-04	Mar-08	273.77	0.01 ± 2.83	-0.20 ± 2.85
		Mar-05	Apr-07	34.67	0.71 ± 3.24	0.84 ± 4.25
		Feb-04	Feb-08	15.06	0.02 ± 2.54	0.04 ± 2.39
2.	Siachin	Oct-04	Oct-09	5.14	0.23 ± 0.60	0.27 ± 0.56
		Oct-03	Oct-05	24.03	-0.19 ± 1.70	-0.38 ± 0.95
3.	Baltoro	Oct-03	Oct-09	277.95	0.44 ± 1.27	0.66 ± 1.20
4.	Drenmarg	Oct-03	Oct-07	182.68	-1.02 ± 2.21	-1.05 ± 2.64

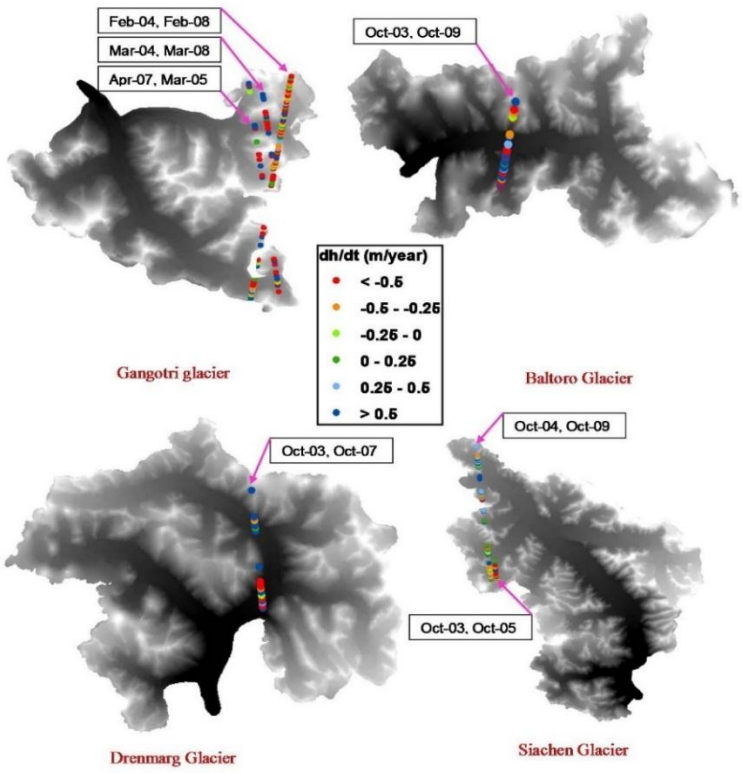

Figure 4: The Elevation change rate along ICESat tracks for Siachin, Gangotri, Baltoro and Drenmarg glaciers of the Himalayan region.

6. Conclusion

In this study four large glaciers of the Himalaya have been taken up for the estimation of ice thickness change using ICESat altimetry data and DEMs (CartoDEM and SRTM). ICESat laser altimetry has proved to be a highly valuable dataset for computing elevation / thickness changes and thus mass change for larger glaciers with mountainous topography. In this study the near repeat track approach has been used to compute ice thickness changes by estimating unmeasured variation in local topography with the consideration of reference DEM. This approach takes care of the slope induced error but the relative error in the DEM may play an important role for change detection. To minimize the relative inaccuracies in DEM the near repeat track separation should have minimum value. To get the better accuracy it is important to use the near repeat datasets which is closer as much as possible with the utilization of the DEM having better relative accuracies in the mountainous regions.

For Gangotri glacier, ice thickness change has been found to be negligible during the period 2004-08. Positive thickness changes (thickening) have been observed for the Siachin and Baltoro glaciers during the period 2004-09 and 2003-09 respectively. Negative thickness change (thinning) at the rate of about 1 m/year has been observed for the Drenmarg glacier during the period 2003-07. Similar values of thickness change have been found while using CartoDEM and SRTM DEM for projecting the secondary tracks over the reference tracks. This procedure can be used for estimation of glacier surface elevation (or ice thickness) change for large number of glaciers in the Himalayan region with the availability of data from future ICESat-2 mission, which will have close coverage with close spacing and dense point coverage using six laser beam configuration.

References

Abshire, J., X. Sun, H. Riris, J. Sirota, J. McGarry, S. Palm, D. Yi and P. Liiva (2005). Geoscience Laser Altimeter System (GLAS) on the ICESat mission: On-orbit measurement performance. Geophysical Research Letters, 32, L21S02 doi:10.1029/2005GL024028

Agrawal, R., N. Ahmed, P. Jayaprasad, A. Mahtab, A Kumar, S.K. Pathan and Ajai, (2006). Comparative evaluation of various algorithms for drainage extraction using cartosat-1 stereo data. Asia Pacific Remote Sensing Symposium, International society for optics and Photonics, 64110X-64110X-11,

Agrawal R, Mahtab A, Jayaprasad P, Pathan S K and Ajai, 2006. "Validating SRTM Dem with Differential GPS Measurements – A Case Study with Different Terrains" ISPRS International Symposium on Geospatial Database for Sustainable Development, September 27-30, Goa.

Arun, S., S. Sushil, K. Anil and Ajai, (2013). Glacier Inventory in Indus, Ganga and Brahmaputra basins of the Himalaya. National Academy of Science Letters, 36(5):497–505

Bahuguna. I.M., B.P. Rathore, B. Rupal, S. Milap, D. Sunil, S.S. Randhawa, K. Kireet, R. Shakil, R.D. Shah, R.K. Ganjoo and Ajai (2014). Are the Himalayan glaciers retreating? Current Science, 106(7), 1008-1013

Bamler, R. (1999). The SRTM mission – A worldwide 30 m resolution DEM from SAR interferometry in 11 days. In. D. Fritsch, R. Spiller (Eds.), Photogrammetric Week ´99, WichmannVerlag, Heidelberg, Germany, 145-154.

Berthier, E., Y. Arnaud, K. Rajesh, A. Sarfarz, P. Wagnon and P. Chevallier (2007). Remote sensing estimates of glacier mass balance in the Himachal Pradesh (western Himalaya, India). Remote Sensing of Environment, 108 (3), 327-338

Berthier, E., Y. Arnaud, C. Vincent and F. Remy (2006). Biases of SRTM in high-mountain areas: Implications for the monitoring of glacier volume changes. Geophysical. Research. Letters, 32(8), L08502. doi:10.1029/2006GL025862.

Brenner, A., J. DiMarzio and H.J. Zwally (2007). Precision and accuracy of satellite radar and laser altimeter data over the continental ice sheets. IEEE Transaction on Geoscience and Remote Sensing, 45(2), 321–331

Gardelle, J., E. Berthier and Y. Arnaud (2012). Slight mass gain of Karakoram glaciers in the early twenty-first century. Nature Geoscience 5(5), 322-325

Johannessen, O.M., K. Khvorostovsky, M.W. Miles and L.P. Bobylev (2005). Recent ice sheet growth in the interior of Greenland. Science, 310(5750), 1013−1016

Kaab, A., E. Barthier, C. Nuth, J. Gardelle and Y. Arnoud (2012). Contrasting patterns of early twenty first century glacier mass change in the Himalayas. Nature, Vol 488 issue, 7412, 495- 498.

Kaab, A., D. Treichler, C. Nuth and E. Berthier (2015). Contending estimates of 2003 – 2008 mass balance over Pamir- Karakoram- Himalaya. The Cryosphere, 9, 557-564.

Kasturirangan, K., R.R. Navalgund and Ajai (2011). Observed changes in the Himalayan - Tibetian glaciers. In "fate of Mountain in the Anthropocene". Pontifical Academy of Science, Vatuican. WWW.pas.va/content/dam/accademia/pdf/sv118/sv118-kasturiranaga.pdf

Kropacek, J., N. Neckel and B. Andreas (2014). Estimation of mass balance of the Grosser Aletschgletsher, Swiss Alps from ICESat laser altimetry data and digital elevation models. Remote Sensing, Vol 6, 5614- 5632

Markus, N., (2005). SRTM and VMAP0 data in OGR and GRASS. GRASS-News Vol. 3, 2-6.

Moholdt, G., J. Hagen, T. Eiken and T. Schuler (2010). Geometric changes and mass balance of the Austfonna ice cap, Svalbard. The Cryosphere, 4(1), 21−34

Moholdt, G., C. Nuth, J.O. Hagen and J. Kohler (2010).

Recent elevation changes of Svalbard glaciers derived from ICESat laser altimetry. Remote Sensing of Environment, 114(11), 2756−2767

Muralikrishnan, S., B. Narender, S. Reddy and A. Pillai (2011). Evaluation of Indian national DEM from Cartosat-1 Data. Summary Report (Ver.1).

Muskett, R.R., C.S. Lingle, J. Sauber, B.T. Rebus and W.V. Tangborn (2008), Acceleration of surface lowering on the tidewater glaciers of Icy Bay, Alaska, USA from InSAR DEMs and ICESat altimetry. Earth and Planetary Science Letters, 265(3-4), 345−359

Nuth, C., G. Moholdt, J. Kohler, J, Hagen and A. Kaab (2010). Svalbard glacier elevation changes and contribution to sea level rise. Journal of Geophysical Research, 115, F01008 doi:10.1029/2008JF001223.

Robin, G., (1966) Mapping the Antarctic ice sheets by satellite Altimeters. Canadian Journal of Earth Science, 3(6), 893-901

Sauber, J., B. Molnia, C. Carabajal, S. Luthcke and R. Muskett (2005). Ice elevations and surface change on the Malaspina glacier, Alaska. Geophysical Research Letters, 32, L23S01, doi:10.1029/2005GL023943

Sirota, J.M., S. Bae, P. Millar, D. Mostofi, C. Webb, B. Schutz and S. Luthcke (2005). The transmitter pointing determination in the geoscience Laser altimeter system. *Geophysical Research Letters, 32*, L22S11, doi:10.1029/2005GL024005.

Slobbe, D., R. Lindenbergh and P. Ditmar (2008). Estimation of volume change rates of Greenland's ice sheet from ICESat data using overlapping footprints. Remote Sensing of Environment, 112(12), 4204−4213

Wingham, D.J., C.R. Francis, S. Baker, C. Bouzanac, D. Brockley, R. Cullen, P.C. Thierry, S.W. Laxon, U. Mallow, C. Mavrocordatoy, L. Phalippou, G. Ratio, L. Rey, F. Rostan, P. Viau and D.W. Wallis (2006). CryoSat: A mission to determine the fluctuations in Earth's land and marine ice fields. Advance in Space Research, 37(4), 841−871

Wingham, D.J., A.J. Ridout, R. Scharroo, R.J. Arthern and C.K. Shum (1998). Antarctic elevation change from 1992 to 1996. Science, 282(5388), 456−458

Zwally, H.J., A.C. Brenner, J.A. Major, R.A. Bindschadler and J.G. Marsh (1989). Growth of the Greenland ice sheet: measurement. Science, 246(4937), 1587−1589

Zwally, H.J., B. Schutz, W. Abdalati, J. Abshire, C. Bentley, A. Brenne, J. Bufton, J. Dezio, D. Hancock, D. Harding, T. Herring, B. Minster, K. Quinn, S. Palm, J. Spinhirne and R. Thomas (2002). ICESat's laser measurements of polar ice, atmosphere, ocean, and land. Journal of Geodynamics, 34(3-4), 405−445

Zwally, H.J., R. Schutz, C. Bentley, J. Bufton, T. Herring, B. Minster, J. Spinhirne and R. Thomas (2008). GLAS/ICESat L1B global elevation data. V028, 20 February 2003 to 21 March 2008. Boulder. CO: National Snow and Ice Data Centre Digital media.

Journal of Geomatics Vol 11 No. 1 April 2017

Review Article

A survey of modern classification techniques in remote sensing for improved image classification

Mahmoud Salah
Department of Surveying Engineering, Shoubra Faculty of Engineering, Benha University, Egypt
Email: mahmoud.goma@feng.bu.edu.eg

(Received: Dec 13, 2016; in final form: Apr 13, 2017)

Abstract: Land Use and Land Cover (LULC) maps are the most important products of remote sensing which can be managed through a process called image classification. This paper reviews the major advanced classification approaches such as Artificial Neural Network (ANN), Classification Trees (CTs) and Support Vector machines (SVMs). This work compares performance of conventionally vis-à-vis recent classification techniques on satellite data. In addition, there are several issues requiring consideration in respect of the classification of remotely sensed data: 1) how to select the proper size of training samples? 2) how to set up the classifier parameters? and 3) how to combine classifiers in an efficient way? The objective of this paper is to answer these questions based on an intensive literature review. This review suggests that effective use of multiple features of remotely sensed data and the selection of a suitable classification method are pivotal for improving classification accuracy. More research, however, is needed to identify and reduce uncertainties in the image-processing to improve classification accuracy.

Keywords: Remote sensing, Image classification, Summary of reviews

1. Introduction

Till today, there is a need to produce regional Land Use and Land Cover (LULC) maps for a variety of applications such as landscape planning, change detection, disaster monitoring, resource management, site suitability analysis and ecological studies (Jensen, 2005). Remotely sensed images provide quantitative and qualitative information that reduces complexity and time of field work and can be used for producing LULC maps through a process called image classification (Chaichoke et al., 2011). Image classification is the process of extracting valuable information from massive satellite imagery by categorizing the image pixel values into meaningful categories or land cover classes. In the context of remote sensing, pixel is the ground area corresponding to one number of a digital image data set. The idea behind image classification is that different features on the earth's surface have a different spectral reflectance (Lillesand and Keifer, 2004).

With the advances of high resolution (HR) and very-high resolution (VHR) remotely sensed imagery such as IKONOS, QuickBird and World View, modern classification techniques are recently gaining the interest of the researchers. Comprehensive review of image classification techniques is required. Lu and Weng (2007) examined current practices, problems and prospects of image classification and summarized major advances in classification algorithms. Recently, Kumar and Singh (2013) reviewed digital image processing techniques for feature extraction from HR satellite imagery. Kamavisdar et al. (2013) have provided a brief theoretical knowledge about different image classification algorithms. Abburu and Golla (2015) summarized the various reviews on satellite image classification methods and techniques. Prasad et al. (2015) summarized the widely used advanced classification techniques that are used to improve classification accuracy. They considered various remote sensing features including spectral, spatial, multi temporal, multi sensor information, as well as ancillary data. Minu and Bindhu (2016) analyzed different supervised classification algorithms, post classification techniques and spectral contextual classification. The present review provides a comparative study on the efficiency, advantages and limitations of these techniques.

The motivation behind this review is to help the analyst, especially those who are new to the field of remote sensing, to select the most suitable classification approach in order to successfully classify a remotely sensed satellite imagery to produce a LULC map. In this review, recent advances in classification algorithms are considered such as Artificial Neural Network (ANN), Classification Trees (CTs) and Support Vector machines (SVMs). On the other hand, the most common problems associated with them have been discussed.

2. Remote-sensing classification process

According to Lu and Weng (2007), the major steps of image classification may include:

- Choice of a suitable classification system;
- Design image classes such as urban, agriculture, water areas, etc;
- Conduct field surveys and collect ground information;
- Image preprocessing for the enhancement of geometric and radiometric qualities of satellite imagery;
- Feature extraction and selection;
- Selection of training samples;
- Image classification;

- Post-processing: filtering, and classification decorating; and
- Accuracy assessment: compare classification results with ground truth data.

3. Selection of remotely sensed data

Remotely sensed data varies in spatial, spectral, temporal and radiometric resolutions. In order to get a better image classification, the most suitable sensor data should be selected. The characteristics of remotely sensed data are summarized by Lefsky and Cohen (2003). Many factors should be considered while selecting suitable sensor data such as scale, availability, characteristics, cost, time constraints and analyst's experience in using selected imagery. At a local level, HR data such as IKONOS and SPOT 5 data are the most useful data. At a regional scale, medium spatial resolution data such as Landsat TM/ETM+ and Terra ASTER are the most commonly used data. At a global scale, coarse spatial resolution data such as AVHRR, MODIS and SPOT Vegetation are needed (Lu and Weng, 2007). In general, spatial resolution is the most important factor that affects classification details and influences the selection of a classification algorithm as shown in table 1.

Table 1: Relation between spatial resolution and classification approach (Prasad et al., 2015).

High resolution	- Objects are made up of several pixels.
	- Object-based classification is superior to traditional pixel-based one.
Medium/low resolution	- Pixels and objects are similar in scale.
	- Both pixel-based and object-based image classifications perform well.

4. Data Preprocessing

It is necessary to check the quality of the remotely sensed data before stepping to classification stage. Image preprocessing includes restoration of bad lines; geometric rectification; radiometric calibration; and atmospheric and topographic corrections. If single data source is applied in classification, atmospheric corrections may not be required. If the study area includes rugged or mountainous regions, a topographic correction becomes necessary (Hale and Rock, 2003). A wide range of correction techniques are presented in Hadjimitsis et al. (2004). The detailed description of such corrections is beyond the scope of this review.

5. Feature extraction and selection

An effective use of features or attributes as input data for a classification procedure can improve the classification accuracy. A wide variety of variables are available which includes spectrum signature, vegetation indices, transformed images, textual information, height texture or surface roughness, multitemporal images, multisensor images, ancillary data (for non-spectral geographical information) and shape and size of objects. The selection of the most useful set of attributes for a classification process is necessary in order to reduce dimensionality of datasets without scarifying accuracy. On the other hand, it is necessary to compensate for some common problems associated with HR data such as shadows and the spectral variability within the same land-cover class (Lu and Weng, 2007). Many techniques can be applied for feature extraction which include principle component analysis (PCA), minimum noise fraction (MNF), transform discriminant analysis (TDA), decision boundary (DP), feature extraction (FE), non-parametric weighted feature extraction (NPWFE), wavelet transform (WT) and spectral mixture analysis (SMA). Table 2 summarizes the research efforts to improve the classification accuracy by applying such features in the classification process (Prasad et al., 2015):

Table 2: Using multiple features for improving classification accuracy

Method	Features	References
Ancillary data	DEM - land use - soil maps	(Maselliet al., 2000) (Baban and Yusof, 2001)
	Road density - road coverage - census data	(Zhang et al., 2002) (Epstein et al., 2002)
Stratification	Topography - census data - shape index of the Patches	(Bronge, 1999) (Helmer et al., 2000)
Post classification processing	Housing density - contextual correction	(Groom et al., 1996)
	Co-occurrence matrix - polygon and rectangular mode filters - expert system – knowledge based	(Zhang, 1999) (Stefanov et al., 2001) (Salah, 2014)
multisource data	Spectral – texture - ancillary	(Tso and Mather, 1999) (Trinder et al., 2010)

6. Selection of training samples

A better classification can be achieved only by considering a suitable classification algorithm with sufficient number of training samples. Training samples are often prepared by fieldwork or from other data sources such as aerial photographs and satellite imagery of fine spatial resolution based on single pixel, seed or polygon. In case of coarse resolution data, the selection of training samples is often tedious as it contains large regions of mixed pixels. Mixed pixels are due to existence of different classes in the same pixel. The purpose of generating training samples is to assemble a set of statistics that describe the spectral response patterns for each land cover class to be classified in the image (Lillesand and Kiefer, 2004). These training samples will be used later to train the algorithm. In case of parametric classifiers, for a fixed sample size, as the dimensionality of the data increases beyond a limit, the precision of the model parameter become lower (Hughes phenomenon). In this regard, it might be difficult to have a significant number of training pixels, and consequently parametric classifiers are not adequate to integrate ancillary data (Caetano, 2009). According to Kavzoglu and Mather (2003), the training sample sizes should range between [30 * Ni *(Ni + 1)] and [60 * Ni *(Ni + 1)] depending on the difficulty of the problem under consideration, where Ni is the number of input features or layers.

7. Classification approaches

There is a variety of classification techniques that have been developed and widely used to produce LULC maps. Satellite image classification methods can be broadly classified into three categories 1) unsupervised 2) supervised and 3) hybrid (Abburu and Golla, 2015). All three methods have their own advantages and disadvantages.

Unsupervised classification technique uses clustering mechanisms to group satellite image pixels into unlabeled classes/clusters. The analyst identifies the number of classes/clusters to generate and which bands to use. Based on this information, the image classification algorithm generates classes/clusters. In order to produce well classified satellite image, the analyst manually identifies each cluster labels a land cover class. It is often the case that multiple clusters represent a single land cover class. The analyst merges clusters into a single land cover class. The unsupervised classification technique is commonly used when no training sample sites exist. There are two most frequent clustering methods used for unsupervised classification, namely, K-means and Iterative Self-Organizing Data Analysis Technique (ISODATA). These two methods rely purely on pixel-based statistics and incorporate no prior knowledge of the characteristics of the themes under investigation.

On the other hand, supervised classification is a method in which the analyst defines small representative samples for each land cover class called training sample. In supervised classification, the analyst must be familiar with the area covered by the satellite image and the spectral properties of the land cover classes. Accuracy of the classification results highly depends on the samples taken for training. The image classification algorithm uses the training samples to identify the land cover classes in the entire image. The common supervised classification algorithms are minimum distance (MD), Mahalanobis distance (MhD), parallelepiped (PP), maximum likelihood classifier (MXL), K-nearest neighbor (KNN), SVMs, and spectral angle mapper (SAM) (Jawak et al., 2015). Figure 1 shows the major steps in the two major types of image classification (Al-doski et al., 2013):

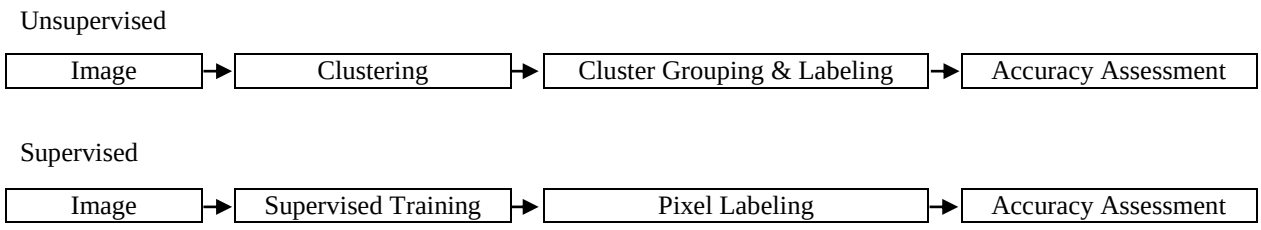

Figure 1: The major steps of supervised and unsupervised image classification

Supervised and unsupervised classifications can be used as alternative approaches, but are often combined to form a hybrid system using more than one methods. On the other hand, when using new generation of images, characterized by a higher spatial and spectral resolution, it is still difficult to obtain satisfactory results by using supervised and unsupervised techniques alone. More specifically, a wide variety of classification categories is available. For the sake of convenience, this review categorized classification approaches as shown in table 3.

Table 3: A taxonomy of image classification methods (Kamavisdar et al., 2013)

Criteria	Categories	Characteristics	Example
Training Sample	Supervised	- Use training sets to classify pixels of unknown identity.	- MD - PP - MXL
	Unsupervised	- Divides pixels into number of classes based on natural groupings. - No prior knowledge is required.	- K-means - ISODATA
Assumptions on Data distribution	Parametric	- Based on assumption of Gaussian distribution. - Mean vector and covariance matrix are generated from training samples.	- MXL
	Non-Parametric	- No prior assumptions about data distribution.	- ANN - SVMs - CTs - Expert system - Knowledge based
Number of Outputs	Hard (crisp)	- Each pixel shows membership to single class.	- MXL - MD - ANN - CTs - SVMs
	Soft (fuzzy)	- Each pixel exhibits partial class membership. - Produces more accurate result. - Ability to deal with mixed pixels.	- MXL - ANN - Fuzzy C-means (FCM)
Pixel Information	Per-pixel classifier (PP)	- Pixel by pixel classification. - Generates signatures by using the spectra of all training pixels. - Low accuracy because of the impact of mixed pixel problem. - Salt and pepper phenomenon.	- MXL - ANN - SVMs - MD
	Sub-pixel classifiers	- Provides membership of each pixel to each class. - Has the capability to handle the mixed pixel problem. - Suitable for medium and coarse spatial resolutions. - Difficult to access accuracy.	- SMA - Fuzzy classifiers
	Per-field	- Averages out the noise by using land parcels as individual units. - Integrates vector and raster data. - Difficult to handle the dichotomy between vector and raster data. - Suitable for fine spatial resolutions	- GIS-based approaches
	Object-oriented (OO)	- Pixels are grouped into objects of different shape and scale (segmentation) and then classification is performed on the basis of objects. - Additional information such as object texture, shape and relations to adjacent regions can be used. - Perfect especially for HR imagery. - Over- and under-segmentation may reduce the classification accuracy.	e-Cognition software
Spatial Information	Spectral	- Based on pure spectral information	- MXL - MD - ANN
	Contextual	- Spatial measurements related to the neighborhoods	- Markov random field
Multiple classifiers	Hybrid Systems	- combine the advantages of multiple classifiers	- Voting rules - Bayesian formalism - Evidential reasoning - Multiple ANN

8. Selection of suitable classification method

8.1 Classic classifiers

In addition to the aforementioned categories, this work has further categorized classifiers as classic and advanced classifiers. Most classic classifiers are based on assumptions of data distribution. The performance of such classifiers depends largely on the accuracy of the estimated model parameters. Classic classifiers suffer from the curse dimensionality of new satellite imagery (Hughes phenomenon). As a result, it might be difficult to select a significant number of training samples. Another drawback of the classic classifiers is the difficulty of combining spectral data with ancillary data (Wilkinson, 2005). Classic classifiers include ISODATA, K-Means, KNN, MD, MhD, PP, MXL and SAM. They are not discussed, since the readers can find them in many textbooks (Lillesand and Keifer, 2004). MXL, however, is the most widely used statistical supervised classifiers. This classifier is based on the Bayesian theory of probability and uses an array of patterns and a covariance matrix from a Gaussian distribution sample set. MXL allocates pixels to appropriate classes based on probability values of the pixels and has been adapted as an indicator of sub-pixel proportions. While using the MXL algorithm, several issues must be taken into consideration: 1) sufficient ground truth data should be sampled to allow accurate estimation of the mean vector and the variance-covariance matrix; 2) the inverse matrix of the variance-covariance matrix becomes unstable in the case of high correlation between two image bands; and 3) when the population is not normally distribution, the MXL algorithm cannot be applied (Kussul et al., 2006). Table 4 summarises the advantages and disadvantages of classic classifiers (Richards, 2013).

Table 4: Advantages and disadvantages of classic classifiers

Classifier	Advantages	Disadvantages
ISODATA	fast and simple to process	- Needs several parameters
K-Means	- Fast and simple to process	- Could be influenced by: the number and position of the initial cluster centers specified by the analyst, the geometric properties of the data, and clustering parameters
KNN	- Simple to process	- Computationally expensive when the training dataset is large
MD	- Fast and simple to process	- Considers only mean value
MhD	- Fast and simple to process	- Considers only mean value
PP	- Fast and simple to process	- Overlap may reduce the accuracy of the results
MXL	- Sub-pixel classifier	- Time consuming - insufficient ground truth data and/or correlated bands can affect the results - Cannot be applied when the dataset is not normally distribution

8.2 Advanced classification algorithms

The improvement in the spatial resolution and quality of remotely-sensed data does not guarantee more accurate feature extraction. The image classification techniques used are a very important factor for better accuracy (Robert et al., 2010). The advanced classification algorithms such as ANN, SVMs and CTs algorithms are highly applied for image classification and have commonly outperformed conventional classifiers in their performance. They are especially suitable for the incorporation of non-spectral data into the classification process. A brief description of each classifier is provided below. Readers who wish to have a detailed description of a specific classifier can refer to cited references.

8.2.1 Artificial Neural Networks (ANN) ANN is a form of artificial intelligence that simulates some functions of the human brain to associate the correct meaningful labels to image pixels. ANN-based classification uses nonparametric approach and hence it is easy to incorporate supplementary data in the classification process in order to improve classification accuracy (Abburu and Golla, 2015). An ANN consists of a series of layers, each containing a set of processing units called neurons. All neurons on a given layer are linked by weighted connections to all neurons on the previous and subsequent layers. During the training phase, the ANN learns about the regularities present in the training data and then constructs rules that can be extended to the unknown data (Foody, 1999). ANN algorithms are extremely efficient when the classification process is not a simple one. A well trained network is capable of classifying highly complex data.

There are several ANN algorithms that can be used to classify remotely sensed images which include:

8.2.1.1 Multi-layer perceptron (MLP): MLP is the most widely used type of ANN. It is a feed-forward ANN model that maps input data sets onto a set of appropriate outputs (Rosenblatt, 1962). MLP has three primary layers: input layer; output layer; and one or more hidden layers with each layer connected to the next one as shown in figure 2. Each layer is composed of a user-defined number of neurons. Input layer neurons represent the input variables while output layer neurons represent the classes specified by input training samples. In this regard, there is one input neuron for each input variable and one output layer neuron for each class. MLP utilizes a supervised learning technique called back-propagation for training the network. Mathematically this can be expressed as:

$$y = \varphi(\sum_{i=1}^{n} w_i x_i + b) = \varphi(w^T x + b) \quad (1)$$

where w refers to the vector of weights, x is the vector of inputs, b is the bias and φ is the activation function. The activation function is normally selected to be the sigmoid 1/ (1+e-x). This function has proved to model nonlinear mappings well (Cybenko, 1989). MLP interprets the weights and activation functions of the neurons. Input and hidden layer neurons are randomly weighted and each pixel in the training data is assigned probability to an output neuron based on maximum activation. Each solution is compared with the previous one, and the solution that results in the lowest error is retained. The process continues until acceptable testing error for the partition of input variables into the specified output classes is reached. The trained network is then used to classify the remaining dataset based on the level of output neuron activation produced by a given pixel (Foody, 1995). The main difficulty with MLP is that it requires a complete retraining of the whole network. This may modify or even erase previous learning, and lead to longer training time even for small size dataset (Liu et al., 2004). In order to improve the MLP performance without costs large computation time, Kavzoglu and Mather (2003) have suggested a set of parameter values for MLP classifiers as shown in table 5 where N is the number of classes.

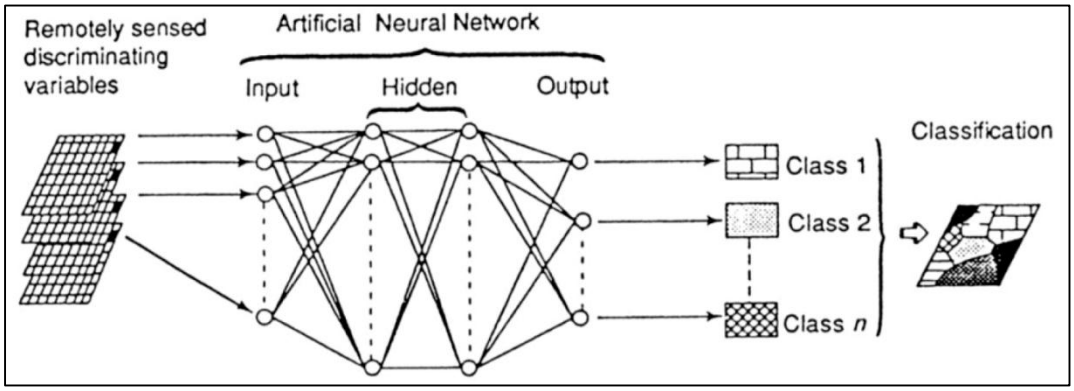

Figure 2: A typical MLP with back-propagation (Foody, 1999)

Table 5: The basic architecture to start MLP classifier

Number of hidden layers/nodes	Between $2N_i$ to $3N_i$
Learning rate	0.01- 0.001
Momentum factor	0.5
Sigmoid constant	1
RMSE	0.0001
Number of iterations	10000
Accuracy rate percent	100%

8.2.1.2 Fuzzy ArtMap classification: Fuzzy ArtMap performs classification based on Adaptive Resonance Theory (ART) (Carpenter et al., 1991). Fuzzy ArtMap is a clustering approach that operates on vectors with fuzzy inputs (real numbers between 0 and 1) and incorporates an incremental learning method to learn continuously without forgetting previous learned states (Oliveira et al., 2007). It adopts only the weights of the neurons encoding the class that best matches the input pattern. In this regard, it can solve large scale problems through a few training epochs. On the other hand, it is sensitive to noise and outliers that may lead to increased misclassified pixels. Fuzzy ArtMap consists of four layers of neurons: input (F1), category (F2), map field and output. Five parameters should be specified for the Fuzzy ArtMap as shown in table 6 (Li et al., 2012):

Table 6: The proposed parameters to start Fuzzy ArtMap classifier

Choice parameter α	A small positive constant
Learning rate parameters β1 in ARTa	$0 \leq \beta 1 \leq 1$
Learning rate parameters β2 in ARTb	$0 \leq \beta 2 \leq 1$
Vigilance parameters ρ1 in ARTa	Normally set very close to 1
Vigilance parameters ρ2 in ARTb	Normally set very close to 1

The ρ1 and ρ2 are the most important parameters and control the process during learning and operational phases of the network. Map field and category layer weights are learned adaptively during the process. Each input layer (F1) observation (pixel) is assigned to a category layer (F2) neuron based on its spectral data characteristics. If no F2 neuron meets the similarity threshold of a given F1 observation, a new F2 Neuron is created in order to partition subsets of a degree of homogeneity defined by the user through a vigilance parameter (Tso and Mather, 2009).

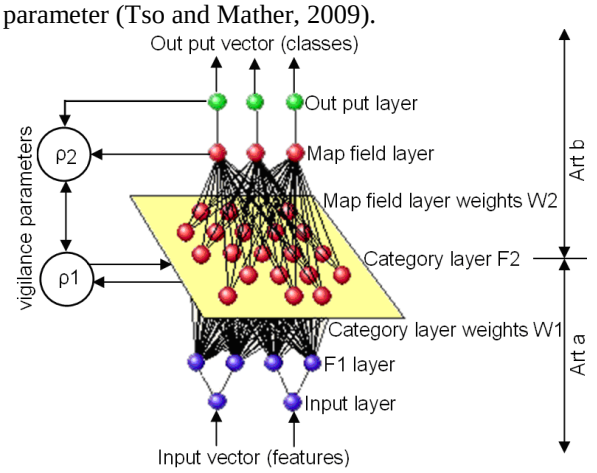

Figure 3: Fuzzy ArtMap architecture (Eastman, 2006)

8.2.1.3 Self-Organized feature Map (SOM) : SOM is a neural network algorithm composed of a single layer of neurons as shown in figure 4 (Kohonen, 1990). The input layer represents the input feature vector and thus has neurons for each measurement dimension. For the output layer of an SOM, a 15 x 15 array of neurons has been recommended by Hugo et al. (2007). Small networks of neurons may result in some unrepresented classes in the final labeled network. On the other hand, large arrays of neurons lead to improved overall classification accuracy. Synaptic weights that connect output layer neuron to all neurons in the input layer are randomly initialized and subsequently organized by systematic sampling of the input data. The organization process progressively adjusts the weights based on data characteristics such that neurons with similar weights spatially cluster in the neuron layer.

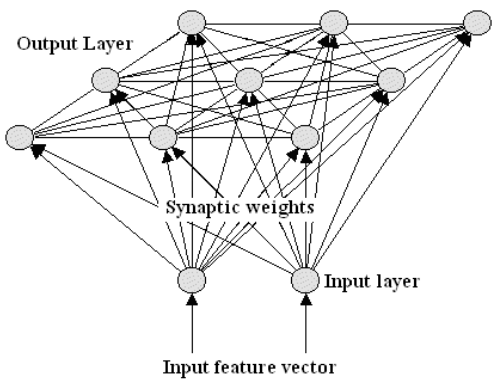

Figure 4: Example of a SOM with a 2 neurons input layer and 3x3 neurons output layer

During the training phase, each neuron with a positive activity within the neighborhood of the winning neuron participates in the learning process. A winning processing element is determined for each input vector based on the similarity between the input vector and the weight vector (Jen-Hon and Din-Chang, 2000). Let X= (x1, x2, x3…, xn) be a vector of reflectance for a single pixel input to the SOM. First, synaptic weights between the output and input neurons are randomly assigned (0-1). The distances between a weight vector and an input feature vector are then calculated, and the neuron in the output layer with the minimum distance to the input feature vector, winner neuron, is then determined. The weight of the winner and its neighbors within a radius γ are then altered (while those outside were left unaltered) according to a learning rate αt.

SOM supervised classification has two training phases: 1) unsupervised classification phase in which competitive learning and lateral interaction lead to a regional organization of neuron weights (topology); and 2) refinement of the decision boundaries between classes based on the training samples using a learning vector quantization (LVQ) algorithm (Nasrabadi and Feng, 1988). Each pixel is then assigned a class of the most similar neuron or neurons in weight (minimum Euclidian distance) to the pixel vector of reflectance. Unlike MLP or Fuzzy ArtMap, SOM acknowledges relationships between classes (i.e., feature map neurons), which allows for the discrimination of multimodal classes. On the other hand, the system normally yields many unclassified pixels (Qiu and Jensen, 2004). In order to improve the classification accuracy without costs large computation time, Vesanto et al. (2000) has suggested a set of parameter values for an SOM classifier as shown in table 7.

Table 7: The proposed parameters to start SOM classifier.

Course tuning parameters				**Fine tuning parameters**		
Output neurons	Initial γ	Min. α	Max. α	Min. δ^t	Max. δ^t	Fine tuning epoch
225 (15*15)	25	0.5	1	0.0001	0.0005	50

8.2.1.4 Radial Basis Function Network (RBFN) : RBFN is a non-linear neural network classifier that consists of an n-dimensional input vector, a layer of RBF neurons and an output layer with one node per category or class of data. An RBFN performs classification by measuring the similarity of input to training data. Each RBFN neuron stores a prototype, one example from the training set. A fairly straight forward approach for making an intelligent selection of prototypes is to perform k-Means clustering on the training set and to use the cluster centers as the prototypes. Each neuron computes the Euclidean distance between the input and its prototype and outputs a value, called activation value, between 0 and 1 which is a measure of similarity. If the input is equal to the prototype, then the output of that RBF neuron will be 1.

As the distance between the input and prototype grows, the response falls off exponentially towards 0. Each output node computes a sort of score for the associated category. The score is computed by taking a weighted sum of the activation values from every RBF neuron, and multiplies the neuron's activation by this weight before adding it to the total response. Typically, a classification decision is made by assigning the input to the category with the highest score.

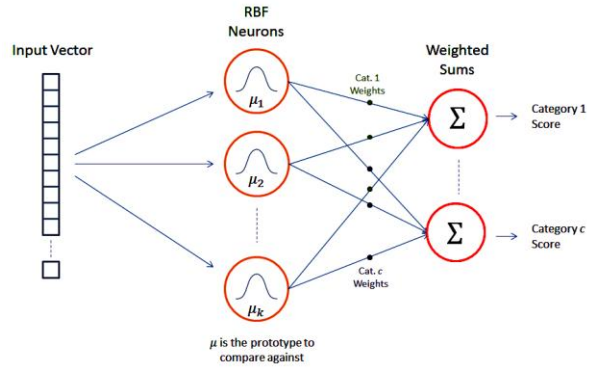

Figure 5: RBF Network Architecture

There is a variety of similarity functions, but the commonly used one is based on the Gaussian. Equation 2 represents a Gaussian with a one-dimensional input, where x is the input, μ is the mean, and σ is the standard deviation. The RBF neuron activation function is slightly different as shown in equation 3. The training process for an RBFN consists of selecting three sets of parameters: the prototypes (μ); β coefficient for each of the RBF neurons; and the matrix of output weights between the RBF neurons and the output nodes. In order to improve the classification accuracy, Hwang and Bang (1997) suggested setting the parameters μ and β to 1.05 and 5 respectively.

$$f(x) = \frac{1}{\sigma\sqrt{2\pi}} e^{-\frac{(x-\mu)^2}{2\sigma^2}} \quad (2)$$

$$\varphi(x) = e^{-\beta\|x-\mu\|^2} \quad (3)$$

8.2.2 Classification trees (CTs) : The theory of CT was introduced by Breiman et al. (1984). CT is a non-parametric, iterative and progressive method of pattern recognition based on hierarchical rule approach. A CT consists of the following elements: the root node (the starting node); the non-terminal nodes (between the root node and all other internodes); and the terminal node (that represents the group of pixels that are assigned to the same class as shown in figure 6. It predicts class membership by recursively partitioning a dataset into homogeneous subsets using a variety of binary splitting rules (Tso and Mather, 2009). These rules are derived from training data using statistical methods and based on the 'impurity'. If all pixels contained by a given node belong to the same category, the node is pure and the impurity is 0. If the logical condition at a given node is fulfilled, the left branch is chosen; otherwise the branch to the right is followed. The process continues until the node becomes pure and is assigned as a terminal node.

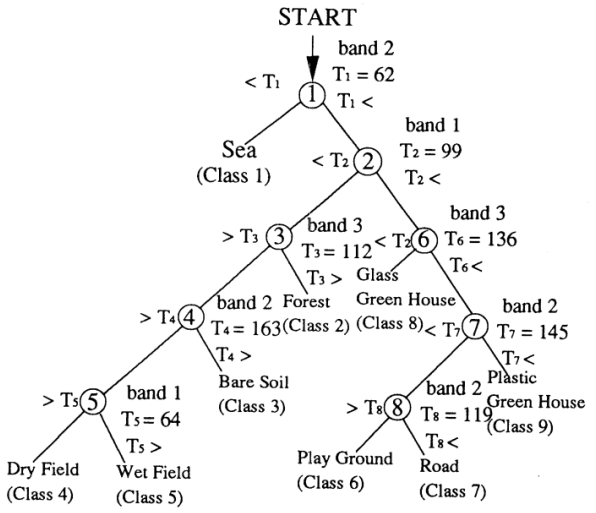

Figure 6: Classification tree. The numbers indicate the variables and their values that are used as thresholds for each node condition.

The most widely used splitting rules are: 1) the Entropy; the Gain Ratio or Information Gain (IG); and the Gini models. Entropy measures the homogeneity and aims to decrease the entropy until a pure terminal node, has zero entropy, is reached (Shannon, 1949). IG is a measure of reduction in Entropy that would result from splitting node N using rule T (Quinlan, 1987). By calculating IG(T) for each variable, the variable that achieves the highest IG will be chosen to split the data at that node. One drawback of this approach is that the variables with relatively high variances are generally selected. This would lead to a bias towards a large number of splits. In order to overcome this problem, the IG(T) can be adjusted by the entropy of the partitioning. The Gini index measures the impurity of the node and separates the largest homogeneous group from the remaining training data (Breiman et al., 1984). The Gini index of all parts is summed for each split rule. The split rule with the maximum reduction in impurity, minimum Gini index, is selected.

When the CT characterizes too much details or noise in the training data, an over-fitting process may occurs and reduces classification accuracy. Pruning normally results in small and more effective trees by up to 25% and avoids such fitting process. Among the proposed pruning methods, the 10-fold cross validation process has proved to be a robust method and does not require any independent dataset to assess the performance of the splitting model. The pruned tree is normally resulted in the best classification accuracy. More details about the cross-validation process are given by Sherrod (2008).

8.2.3 Support Vector Machines (SVMs) : SVMs are one of the more recent developments in the field of machine learning and based on the principles of

statistical learning theory (Vapnik, 1979). Mountrakis et al. (2011) summarized results from over 100 articles using the SVMs algorithm. In conclusion, SVMs have proved to be superior to most other image classification algorithms in terms of classification accuracy. SVMs as binary classifier delineate two classes by fitting an optimal separating hyperplane to the training data in the multidimensional feature space to maximize the margin between them. In figure 7, m is the distance between H1 and H2, and H is the optimum separation plane. For a binary classification problem in n-dimensional feature space, xi is a training set of l samples, i=1,2,…,l, with their corresponding class labels yi {1, -1}. The optimum separation plane is defined by equation 4, where x is a point on the hyperplane, w is an n-dimensional vector perpendicular to the hyperplane, and b is the distance of the closest point on the hyperplane to the origin. Equation 5 and equation 6 can be combined into equation 7. SVMs attempt to find a hyperplane, equation 4, with minimum ||w||2 that is subject to constraint 7.

$$w.x + b = 0 \quad (4)$$

$$w.x_i + b \le -1, \quad for\ class\ 0 \quad (5)$$

$$w.x_i + b \ge -1, \quad for\ class\ 1 \quad (6)$$

$$y_i\left[(w.x_i) + b\right] - 1 \ge 0 \quad \forall i \quad (7)$$

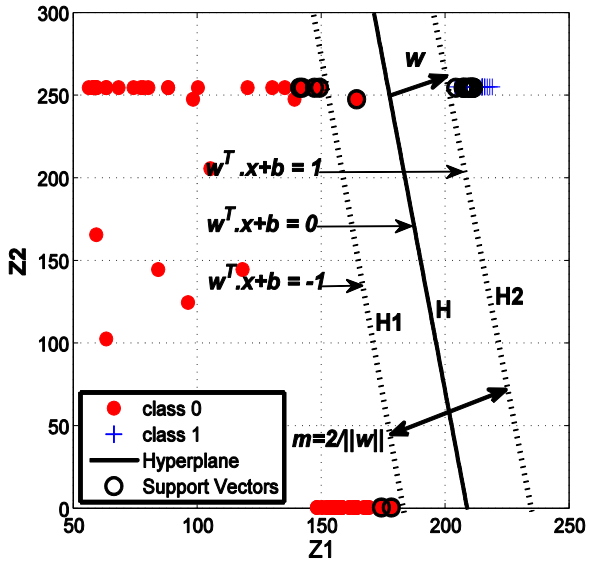

Figure 7: Optimum separation plane in the (Z1, Z2) space

Four kernel functions (functions used to project the data from input space into feature space) are available for SVMs: Gaussian Radius Basis Function (RBF); Linear; Polynomial; and Sigmoid (Quadratic). In remote sensing applications the Gaussian radial basis function (RBF) kernel has proved to be effective with reasonable processing times (Van der Linden et al., 2009). Two parameters should be specified while using RBF kernels: C, the penalty parameter that controls the trade-off between the maximization of the margin between the training data vectors and the decision boundary plus the penalization of training errors, and γ, the width of the kernel function. The problem is that C and γ depend on the data range and distribution and they differ from one classification problem to another. The most common used way to optimize the C and γ parameters is a grid-search using a 10-fold cross-validation error as a measure of quality. This method can prevent the overfitting problem and results in better accuracy (Hsu et al., 2009).

In order to solve for the binary classification problem that exists with SVMs and to handle the multi-class problems in remote sensing applications, two approaches are commonly used: the One-Against-All (1AA); One-Against-One (1A1). Anthony et al. (2007) have reported that the resulting classification accuracy from 1AA is not significantly different from 1A1 approach. However, the 1A1 technique results in a larger number of binary SVMs and then in subsequently intensive computations than the 1AA technique. The original output of a SVM represents the distances of each pixel to the optimal separating hyperplane, referred to as rule images. All positive (+1) and negative (-1) votes for a specific class are summed and the final class membership of a certain pixel is derived by a simple majority voting.

8.2.4 Fuzzy Classifiers : Fuzzy classifiers express the fuzzy set membership of each pixel in each class. The fuzzy set membership is calculated based on standardized Euclidean distance from the mean of the signature, using a specific algorithm. The underlying logic is that the mean of a signature represents the ideal point for the class, where fuzzy set membership is 1. When distance increases, fuzzy set membership decreases, until it reaches the user-defined distance where fuzzy set membership decreases to 0. The FCM clustering algorithm (Bezdec, 1981) is the most representative fuzzy classification algorithms since it is suitable for tasks dealing with overlapping clustering. The classification is performed with an iterative optimization of minimizing a fuzzy objective function (Jm) defined as equation 8.

$$J_m = \sum_{i=1}^{c}\sum_{k=1}^{n}(\mu_{ik})^m d^2(x_k, V_i) \quad (8)$$

where
c = number of clusters
n = number of pixels
μik= membership value of ith cluster of kth pixel
m = fuzziness for each fuzzy membership.
xk= vector of kth pixel
Vi= center vector of ith cluster
d2(xk,Vi) = Euclidean distance between xkand Vi

The membership (μik) is estimated by the distance between kth pixel and center of ith cluster, and is constrained as follows:

$$\begin{cases} 0 \le \mu_{ik} \le 1 & \text{for all } i,k \\ \sum_{i=1}^{c}\mu_{ik} = 1 & \text{for all } k \\ 0 < \sum_{k=1}^{n}\mu_{ik} < n & \text{for all } i \end{cases} \quad (9)$$

The center of cluster (Vi) and the membership value (μik) could be calculated by equations 10 and 11, respectively.

$$V_i = \frac{\sum_{k=1}^{n}(\mu_{ik})^m x_k}{\sum_{k=1}^{n}(\mu_{ik})^m}, 1 \le i \le c \quad (10)$$

$$\mu_{ik} = \left[\sum_{j=1}^{c}\left(\frac{d(x_k,V_i)}{d(x_k,V_j)}\right)^{\frac{2}{m-1}}\right]^{-1}, 1 \le i \le c, 1 \le k \le n \quad (11)$$

Therefore, Jm can be minimized by iteration through equations 10 and 11. The first step of the iteration is to initialize a fixed c, a fuzziness parameter (m), a threshold ε of convergence, and an initial center for each cluster, then computing μik and Vi using equations 10 and 11 respectively. The iteration is terminated when the change in Vi between two iterations is smaller than ε. Finally, each pixel is classified into a combination of memberships of clusters.

Table 8: Comparison of modern classification techniques (Kamavisdar et al., 2013)

Method	Advantages	Disadvantages
ANN	- Non-parametric classifiers. - High computation rate of very large datasets - Efficiently handles noisy inputs	- It is difficult to understand how the result was achieved. - The training process is slow. - Problem of over fitting. - Difficult to select the type network architecture. - Dependent on user-defined parameters.
CTs	- Non-parametric classifiers - Does not require an extensive design and training. - Easy to understand the classification process. - Accurate and computational efficiency is good. - Easy to integrate multi-source data.	- Calculation becomes complex when various outcomes are correlated.
SVMs	- Non-parametric classifiers - Provides a good generalization. - The problem of over fitting is controlled. - Computational efficiency is good. - perform well with minimum training set size and high-dimensional data - Often outperform other classifiers.	- Training is time consuming. - Difficult to understand its structure. - Dependent on user-defined parameters. - Determination of optimal parameters is not easy.
Fuzzy Classifiers	- Efficiently handle overlapping data. - Minimize computation time and reduces memory requirements.	- Without priori knowledge output is not good

For a specific dataset, it is often difficult to identify the classifier with the best performance due to the lack of a guideline for selection on hand. Moreover, the analyst has to make many decisions and choices through image classification process. Many researchers have compared unsupervised, supervised and hybrid classification techniques. Table 9 provides summary of different researchers' conclusion and the situation in which each classifier is most useful. The researchers' opinion about the best classification method is not consistent. Many more suggestions on the selection of classifiers can be found in Foody et al. (2007)

Table 9: performance evaluation of various classification methods against different datasets

Researcher	Classifier	Datasets	Best Performance
Pal and Mather (2005)	- SVMs - MXL - ANN	- Landsat 7 ETM+ - Hyperspectral data	SVMs
Oliveira et al. (2007)	- MXL - CTs - MLP - SOM - ArtMap	- Landsat (ETM+)	ArtMap
Lippitt et al. (2008)	- SOM - MLP - ArtMap - CTs	- Landsat7 (ETM+)	CTs
Li et al. (2012)	- MXL - CTA - ArtMap - KNN	- Landsat 5 TM - ALOS PALSAR (L-band HH and HV)	ArtMap
Maryam et al. (2014)	- SVMs - MXL - MD - PP	- Landsat7 ETM+	SVMs
Shaker et al. -2012	- Contextual - MXL - MD	- SPOT	MXL
Mannan et al. (1998)	- ArtMap - MXL - MLP	- IRS-1B	ArtMap
Gil et al. -2011	- SVMs - ANN - MXL	- IKONOS	SVMs
Du et al. (2012)	- MLP - ANN - CTs - MXL - SVMs - ArtMap	- QuickBird - Spectral/textural features	SVMs
Doma et al. (2015)	- PP - MD - MXL - ANN - SVMs	- Quick bird	SVMs
Hamedianfar et al. (2014)	- OO/fuzzy - SVM	- World View-2 (WV-2)	OO/fuzzy
Camps-Valls et al. (2003)	- SVMs - ANN	- hyperspectral data (128 bands)	SVMs
Trinder et al. (2010)	- SVMs - SOM - CTs	- Aerial Images - LiDAR data	SVMs

9. Hybrid Classifiers

Different classifiers resulted in different classes for the same test area. No single classifier can performs the best for all classes. Many of the classification algorithms are complementary. Analyses of the results reported in Kanellopoulos et al. (1997) have confirmed the complementary information of neural and statistical algorithms. These classifiers result in uncorrelated classification errors and hence higher classification accuracies can be obtained by combining them. In the hybrid classifiers-based approach, the classifiers should use independent feature set and/or be trained on separate sets of training data. Two strategies exist for combining classifiers: 1) Classifier Ensembles (CE); and 2) Multiple Classifier Systems (MCS) as shown in figure 8.

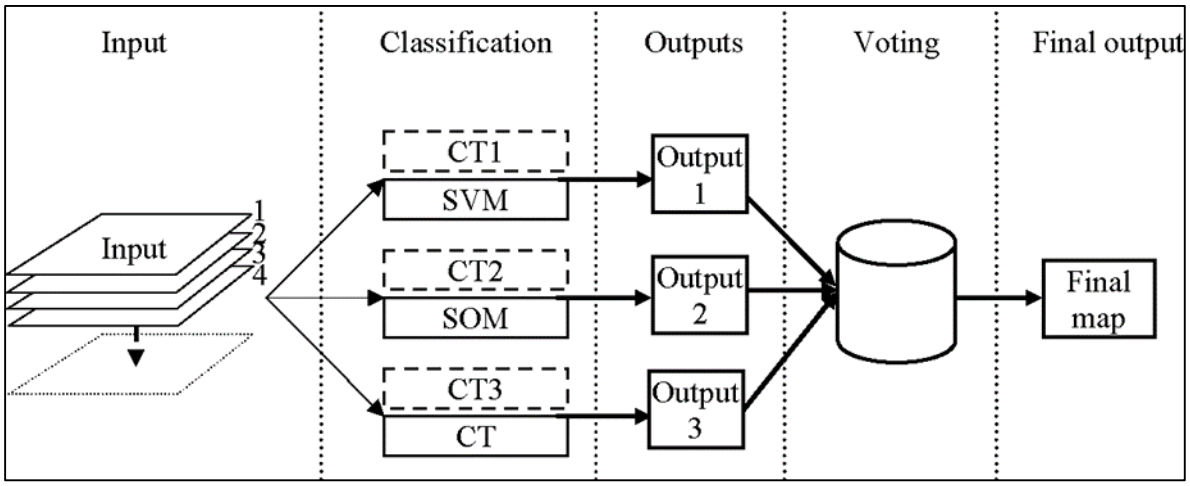

Figure 8: Classifier Ensemble (dashed) versus Multiple Classifier Systems (solid) (Waske, 2007, modified)

If the classification results are similar, the combination process would not improve the classification accuracy. Therefore, diversity is an important requirement for the success of hybrid systems (Chandra and Yao, 2006). Diversity measures are rarely used and compared for remote sensing image classification which includes: Kappa statistics (Congalton and Mead, 1983); double fault (Giacinto and Roli, 2001); agreement measure (Michail et al., 2002); similarity, non-inferiority, difference (Foody, 2009); weighted count of errors and correct results (WCEC) (Aksela and Laaksonen, 2006), entropy (Kuncheva and Whitaker, 2003); and Disagreement-accuracy measure (Du et al., 2012). The results obtained by Du et al. (2012) indicate that the combination selected by Disagreement accuracy measure outperform the ones selected by other diversity measures in terms of overall accuracy.

9.1. Classifier Ensembles

Classifier ensembles are based on the combination of a variety of the same algorithm. By training the so-called base classifier on modified training data, a set of independent classifiers can be obtained. Normally, a voting scheme is applied to combine the results. The widely applied strategies for generating classifier ensembles include: 1) resampling of the training data, such as bagging or boosting; and 2) resampling of the input features, such as random feature selection (Waske, 2007).

9.1.1. Bagging (bootstrap aggregating) or Boosting :

Bagging (Breiman, 1996) and boosting (Freund and Schapire, 1997) have been proposed to combine classifiers. The performance of such algorithms is limited by the high level of ambiguities among classes which may result in poor classification accuracy (Yu-Chang and Kun-Shan, 2009). In bagging, n samples are selected randomly from a training set with k bags, created iteratively, and each bag is classified by vote to predict its class. Some training instances will occur multiple times in a bag, while others may not appear at all. After that, each bag is used to train a classifier. These classifiers are then combined. Such a method is not very sensitive to noise in the data. On the other hand, boosting is based on multiple learning iterations. At each iteration, instances that are incorrectly classified are given a higher weight in the next iteration. By doing so, the classifier is forced to concentrate on instances that were not correctly classified in earlier iterations. At the end, all of the trained classifiers are combined.

Bagging has proved to reduce the variance of the classification, while Boosting reduces both the variance and the bias of the classification. In this regard, Boosting can produce more accurate classification results than Bagging (Du et al., 2012). However, Boosting is computationally more demanding than other simpler algorithms, while the lack of robustness to noise is another shortcoming (Benediktsson et al., 2007). In addition, there is a great variety of approaches drawn upon the basic idea of Bagging and Boosting such as: Wagging (Bauer and Kohavi, 1999), Random Forest (Breiman, 2001), Random Subspace (Ho, 1998), Logistic Boosting (Collins et al., 2002), MultiBoost (Webb, 2000), Rotation Forest (Rodriguez and Kuncheva, 2009), and Rotboost (Zhang and Zhang, 2008).

9.1.2. Random Feature Selection (RFS) : Another approach for generating independent classifiers is the modification of the input feature space, by a random selection of features. This approach has proved to be superior to bagging and boosting, since the method normally selects a subset of the available input features without replacement. The number of selected features within the subset is user-defined, and is usually set to the square root of the number of input features. The computational cost is lighter than bagging and boosting because it is only based on subsets of input data. Because of that this method can handle high-dimensional data sets. On the other hand, the correlation between the classifiers is decreased, and the obtained classification accuracy is improved (Gislason et al. 2006).

9.2. Multiple Classifier Systems (MCS)

In contrast to the classifier ensembles, MCS are based on the combination of different classifier algorithms and hence the individual advantages of each method can be combined. In terms of combination style, three categories can be applied: 1) Concatenation combination (the classification result generated by a classifier is used as the input into the next classifier until a result is obtained through the final classifier in the chain); 2) Parallel combination (multiple classifiers are designed independently and their outputs are combined according to certain strategies; and 3) Hierarchical combination (combines both concatenation and parallel combination) (Ranawana and Palade, 2006). According to the classifiers outputs, MCS in a parallel combination can be further divided into three levels: abstract level (each classifier outputs a unique label); rank level (classes are ranked based on decreasing likelihood); and measurement level (Based on probability values) (Ruta and Gabrys, 2000). But however, this review will be focused on the widely used parallel MCS combination. Some of the widely and successfully applied MCS approaches are:

9.2.1. Maximum Rule (MR) : MR is a simple method for combining probabilities provided by multiple classifiers. It interprets each class membership as a vote for one of the k classes. For each individual classifier, the class that receives the highest class membership is taken as the class label for that classifier. After that, the class labels from the N classifiers are compared again and the class that receives the highest class membership is taken as the final classification as in equation 12. is the class membership of a pixel to belong to a class Ck given by classifier fi, and PMR is the probability based on MR. The major problem of maximum rule is that all the classifiers have the same authority regardless of their reliability (Foody et al., 2007).

$$P_{MR} = \max\left[\max\ pp(C_k \mid f_i)\right] \qquad (12)$$

9.2.2. Weighted Sum (WS) : First, the class membership at the output of each classifier is weighted according to the classifiers' reliability (accuracy) for each class ($0 \leq \alpha ci \leq 1$). After that and for each class, the class memberships at the output of all classifiers are summed together. Finally, the class that receives the maximum sum is taken as the final class label as in equation 13. PWS is the probability based on the weighted sum, αci is the weight of each classifier, ppi: is the class membership value obtained for the ith classifier and N is the Number of classifiers (Le et al., 2007).

$$P_{WS} = \sum_{i=1}^{N} \alpha_{ci}\ pp_i \qquad (13)$$

9.2.3. Fuzzy Majority Voting (FMV) : The idea is to give some semantics or meaning to the weights so that the values for the weights can be provided directly. In the following, the semantics based on fuzzy linguistic quantifiers for the weights are used (Zadeh, 1983). First, the membership function of relative quantifiers can be defined as in equation 14 (Herrera and Verdegay, 1996). The parameters a, b [0, 1] and ppi is the class membership of pixel i. Then, Yager (1988) proposed to compute the weights based on the linguistic quantifier represented by Q as in equation 15.

$$Q_{P_i} = \begin{cases} 0 & if\ \ pp_i < a \\ \dfrac{pp_i - a}{b - a} & if\ \ a \leq pp_i \leq b \\ 1 & if\ \ pp_i > b \end{cases} \qquad (14)$$

$$w_{P_i} = Q_{P_i}\left(\frac{i}{N}\right) - Q_{P_i}\left(\frac{i-1}{N}\right),\ for\ i = 1, ..., N \qquad (15)$$

Q_{P_i} is the membership functions of relative quantifiers, i is the order of the classifier after ranking for all classifiers in a descending order and N is the total number of classifiers. A relative quantifier 'at least half' with the parameter pair (0, 0.5) is normally applied for the membership function Q in equation 14. Then, depending on the total number of classifiers N, and from equation 15 the corresponding weighting vector W = [w1, ….., wR] can be obtained. The final combined probability can be calculated as in equation 16, with is the weight based on linguistic quantifier, ppi is the Markovian probability of pixel i and k is the number of classes.

$$P_{FMV} = \arg\max_{k}\left[\sum_{i=1}^{N} w_{p_i}\ pp_i\right] \qquad (16)$$

9.2.4. Dempster-Shafer Theory (DST) : The theory of evidence was introduced by Shafer (1976) for combination of different measures of evidence. It is a generalization of the Bayesian framework and permits the characterization of uncertainty and ignorance. Consider a classification problem where the input data are to be classified into n classes Cj ∈ θ, θ is referred to as the frame of discernment. The power set of θ is denoted by 2θ (the set of all subsets of θ). A probability mass m (A) is assigned to every class A∈2θ by a classifier such that m (Ø) = 0, $0 \leq$ m (A) ≤ 1, and Σ m

(A) =1, and Ø denotes the empty set. m (A) can be interpreted as the amount of belief that is assigned exactly to A and not to any of its subsets. Imprecision of knowledge can be handled by assigning a non-zero probability mass to the union of two or more classes Cj. The support Sup (A) of a class A∈2θ is the sum of all masses assigned to that class. The plausibility Pls (A) sums up all probability masses not assigned to the complementary hypothesis Ā of A with A∩ Ā =Ø and A Ā = θ:

$$Sup(A) = \sum_{B \subseteq A} m(B); \qquad Pls(A) = \sum_{A \cap B \neq \phi} m(B) = 1 - Sup(\bar{A}) \tag{17}$$

Sup (A) is also called dubiety. It represents the degree to which the evidence contradicts a proposition. If k classes are available, probability masses mi (Bj) have to be defined for all these classes i with $1 \leq i \leq z$ and Bj 2θ.

From these probability masses, a combined probability mass can be computed for each class A 2θ as follow:

$$m(A) = \frac{\sum_{B_1 \cap B_2 \cap \ldots . B_z = A} \left[\prod_{1 \leq i \leq z} m_i(B_j) \right]}{1 - \sum_{B_1 \cap B_2 \cap \ldots . B_z = \phi} \left[\prod_{1 \leq i \leq z} m_i(B_j) \right]} \tag{18}$$

As soon as the combined probability masses m (A) are determined, both Sup (A) and Pls (A) can be computed. The accepted hypothesis Ca ∈ θ is determined according to a decision rule (the class of maximum plausibility or the class of maximum support). It is worth mentioning that the combination rule given by equation 18 assumes that the belief functions to be combined are independent. Many researchers have compared MCS. Table 10 provides summary of different researchers' conclusion and the situation in which each MCS is most useful.

Table 10: Performance evaluation of different MCSs

Researcher	Classifier	Datasets	MCS	Best Performance
Ebeir et al. (2001)	- ANN - CTs	- HR satellite imagery. - Spectral, spatial and contextual information.	- Bagging	- Bagging
Briem et al. (2002)	- MD - MXL - CTs	- SAR data. - Topographical data.	- Bagging - Bagging	- Boosting
Kumar et al. (2002)	- MXL	- Hyperspectral data	- Hierarchical fusion	- Hierarchical fusion
Waske and Benediktsson (2007)	- SVMs	- SAR data. - multispectral imagery	- CE/SVM	- CE/SVM
Ceamanos et al. (2010)	- SVMs	- Hyperspectral data	- CE/SVM	- CE/SVM
Trinder et al. (2010)	- SVMs - SOM - CTs	- Aerial Images - LiDAR data	- MR - WS - FMV - DST	- DST
Du et al. (2012)	- MLP - CTs - MD - SVMs - SAM - ArtMap	- QuickBird - OMISII - Landsat ETM+	- BPT - FMV - DST - CE/SVM	- BPT
	- MLP (Base classifier) - CTs	- QuickBird - OMISII	- Bagging - Boosting	- Boosting
	- MLP - SVMs - ArtMap - CTs	- QuickBird - Landsat ETM+	- MR - WS - FMV - DST -	- FMV
Ko et al. (2014)	- RFS - KNN - SVMs	- LiDAR data	- average voting	- average voting
Salah (2014)	- PB SVMs - OO SVMs	- IKONOS	- BPT	- BPT

10. Post classification processing

Post classification techniques can eliminate the short comings associated with classification algorithms such as unclassified or misclassified pixels, and hence improve the classification accuracy (Lu and Weng, 2007). The commonly used post classification techniques include: majority filter (MF); probability label relaxation (PLR); and cellular automata (CA) (Espinola et al., 2008). The MF reclassifies the center pixel when it is not a member of the majority class. It improves the overall accuracy of classification but merges some land cover classes together. The PLR is an iterative technique which considers the probabilities of the neighboring pixels for updating the probability of the center pixel. The PLR technique provides higher accuracy than the MF method, but it requires lot of computation. The approach of CA consists of regular grid of cells. Each cell is associated with a particular state from a set of possible states. The CA reassigns a class of the pixel according to the class of the neighboring pixels and based on a set of defined rules. In terms of accuracy, the CA approach has proved to be better than other two filters (Minu and Bindhu, 2016). On the other hand, ancillary data can be integrated after image classification. This can be done through very specific strategies such as: expert systems, rule based systems; and knowledge base systems.

11. Classification of accuracy assessment

Many sources of errors can affect the classification results which include: classification error, error from registration, and poor quality of training (Powell et al., 2004). These errors generate uncertainties (where is the error?) at different stages in the classification process which may influence the classification accuracy, as well as the estimated area of land-cover classes Posterior probabilities are an indicator of the uncertainty in making a particular class allocation. Accuracy assessment allows analyst to evaluate the utility of the resulted thematic map for the intended applications. In order to assess the classification accuracy, the classification results can be compared against the reference data. DeFries and Chan (2000) suggested the use of multiple criteria to evaluate the performance of algorithms. These criteria include classification accuracy, computational resources, stability, and robustness to noise in the training data. Classification accuracy is the most important criteria to evaluate the classification performance. The most common used methods for accuracy assessment are:

11.1 Overall Classification Accuracy

The overall accuracy is the most widely used approach for the evaluation of the classification results and can be calculated by equation 19:

$$\mathrm{OCA} = \frac{\mathrm{NCP}}{\mathrm{NRP}} \qquad (19)$$

Where OCA is the overall classification accuracy; NCP is the total number of correctly classified pixels (along the diagonal of the error matrix) and NRP is the total number of reference pixels. The error matrix is a simple cross tabulation of the resulted class label against the observed one in the reference data. Since the OCA is a global measure the performance of the classifier should also be evaluated by determining some other criteria as shown below.

11.2 Kappa Index of Agreement (KIA)

The Kappa Index of Agreement (KIA) is a statistical measure adapted for accuracy assessment in remote sensing fields by Congalton and Mead (1983). KIA tests two images, if their differences are due to chance or real disagreement. It is often used to check for accuracy of classified satellite images versus some real ground-truth data as in equation 20. For the per-category-Kappa, equation 21 was introduced by Rosenfield and Fitzpatrick-Lins (1986):

$$k = \frac{N\sum_{i=1}^{r} X_{ii} - \sum_{i=1}^{r}(X_{i+} * X_{+i})}{N^2 - \sum_{i=1}^{r}(X_{i+} * X_{+i})} \qquad (20)$$

r: number of row in the error matrix.
xii : number of combinations along the diagonal.
xi+ : total observations in row i.
x+i : total observations in column i.
N : total number of cells.

$$k_i = \frac{P_{ii} - P_{i+}P_{+i}}{P_{i+} - P_{i+}P_{+i}} \qquad (21)$$

pii : proportion of units agreeing in row i / column i
pi+ : proportion of units for expected chance agreement in row i
p+i : proportion of units for expected chance agreement in column i

11.3 Omission and Commission Errors

Unlike OCA, commission and omission errors clearly show whether the proposed classifier improves or deteriorates the results for each individual class compared to the reference data (Congalton, 1991).

$$CE_I = \frac{A_1 + A_2 + A_3}{R_1} \qquad (22)$$

$$OE_I = \frac{B_1 + B_2 + B_3}{R_1} \qquad (23)$$

CEI and OEI are commission and omission errors of class increased; A1, A2 and A3 are the numbers of incorrectly identified pixels of class increased associated with classes decreased, background and unchanged; R1 is the total number of pixels of the class increased as observed in the reference data; B1, B2 and B3 are the numbers of unrecognized pixels that should have identified as belonging to the class increased. The same is applicable for the class decreased.

12. Commercial software

The availability of classification software is one of the most important factors that must be taken into account when selecting a classification method for use. Various image processing software packages make it possible to enhance, analyze, interpret and extract meaningful information from remotely sensed data. Table 11 lists the most common used image processing packages along with the available classification approaches. This table is intended to be highly useful for those wishing to select the most appropriate software for the problem under investigation.

Table 11: Classification techniques available in the commonly used commercial software

IDRISI	ENVI	Erdas Imagine	ILWIS
- ISODATA	- ISODATA	- ISODATA	- PP
- K-means	- K-means	- MD	- MD
- PP	- CTs	- MXL	- MhD
- MD	- SVM	- MhD	- MXL
- MhD	- PP	- Expert Classifier	
- MXL	- MD		
- Fisher LDA	- MhD		
- KNN	- MXL		
- CTs	- SAM		
- MLP	- RBF		
- SOM			
- Fuzzy ArtMap			
- RBF			
- Bayesian probability			
- Fuzzy set			
- Linear Spectral Unmixing			

13. Summary and discussion

The most suitable classification algorithm is based on the spatial resolution of the used satellite imagery. In the case of HR data such as IKONOS, SPOT 5 HRG and World View-2, per-field and object-oriented classifiers may outperform the per-pixel ones. On the other hand, the integration of spectral and texture information can reduce the problem of shadow and the wide spectral variation within the land-cover classes. In the case of medium and coarse spatial resolution, sub-pixel classifiers have proved to be more useful than per-pixel classifiers because of the mixed pixels problem. In this case, the loss of spatial information makes spectral information more important than spatial one. Furthermore, ancillary data can be integrated with spectral data for improved classification results.

The optimum training sample size varies from one classifier to another. Selection of proper size of samples are important factors which governs the classification accuracy. All classifiers are shared in the same behavior of after certain size of training sample, the classification accuracy showed downward trend with the increasing size of training data. In the case of limited number of training samples, SVM and maximum likelihood have proved to be the best choice. When multisource data are used, parametric classifiers such as MXL are typically not appropriate for image classification. Advanced non-parametric classifiers, such as ANN, SVMs and CTs can be more suitable.

There are several ANN approaches that can be used to classify remotely sensed images which include: MLP; SOM; and Fuzzy ArtMap. Fuzzy ArtMap has proved to be the most efficient algorithms, followed by the MLP. SOM produced the lowest classification accuracy in the majority of articles. All these algorithms depend mainly on the operators experience in setting up their parameters in order to reach the optimal performance. MLP requires a complete retraining of the whole network. This may lead to long training time, even for small size test areas. Fuzzy ArtMap, on the other hand, can solve large scale problems through a few training epochs. The only defect with Fuzzy ArtMap is that it is sensitive to noise and outliers that may decrease the classification accuracy. Unlike MLP and Fuzzy ArtMap, SOM allows for the discrimination of multimodal classes. On the other hand, SOM normally yields many unclassified pixels.

In case of CTs, the Entropy splitting algorithm has proved to be a preferable algorithm for image classification. On the other hand, the 10-fold cross validation process has proved to be an accurate method. As well, CT derived from a given test area could be successfully transferred to another area provide the remotely sensed images having the same sensor characteristics and the LULC are similar. In general,

SVMs outperform other classifiers in terms of classification accuracy. SVMs show a balance between errors of the classes. In some cases, the RBF kernel would be the best choice. However, a grid search with a 10-fold cross validation has to be applied to search for the RBF kernel parameters, C and γ for the SVM classifier.

Different classifiers offer complementary information about the data to be classified. One classifier might be more efficient at detecting a specific class, while another classifier is more efficient for another specific one. Combining classifiers in an efficient way can improve classification accuracy than any single classifier, even the best one. Neural and statistical classifiers result in uncorrelated classification errors and hence higher classification accuracies can be obtained by combining them. It is worth mentioning that adding more classifiers to the system does not guarantee improvements in the performance. However, diversity is an important requirement for the success of hybrid systems. The combination selected by Disagreement accuracy measure usually outperforms the ones selected by other diversity measures. Two approaches exist for combining classifiers: 1) CE; and 2) MCS. Classifier ensembles are based on the combination of a variety of the same algorithm. On the other hand, MCS are based on the combination of different classification algorithms. Most of the existing MCSs suffer one or more shortcomings such as: high ambiguities between classes; high sensitivity to noise in the data; and high computational load. D-S combination, as a MCS, has proved to be superior to other hybrid systems in terms of classification accuracy.

14. Conclusion

Image classification has made great progress over the past few decades in the development and use of advanced classification algorithms. This review gives a brief guide about different classification techniques and lists the advantages and disadvantages of each. It is concentrated extensively on recent classification algorithms such as ANN, SVMs and CTs. These classification approaches have significantly improved the accuracy of the results in the case of HR satellite imagery. This paper helps researchers in selecting a suitable classification algorithm for a specific task, optimization of the classifiers and selecting the optimal classifiers for constructing MCS. Most of the MCS can enhance classification accuracy, but the performances are affected by different factors such as the selected base classifiers and the combination strategy. Diversity measures can play a vital rule in selecting the base classifiers for a MCS.

References

Abburu, S. and S. Golla (2015). Satellite image classification methods and techniques: A review. International Journal of Computer Applications, 119 (8): 20-25.

Aksela, M. and J. Laaksonen (2006). Using diversity of errors for selecting members of a committee classifier. Pattern Recognition, 2006(39): 608–623.

Al-doski, J., S. Mansor and H. Shafri (2013). Image classification in remote sensing. Journal of Environment and Earth Science, (3)10: 141-148.

Anthony, G., H. Gregg and M. Tshilidzi (2007). Image classification using SVMs: One-against-one Vs one-against-all. Proceedings of the 28th Asian Conference on Remote Sensing ARCS, Learning (cs.LG); Artificial Intelligence (cs.AI); Computer Vision and Pattern Recognition (cs.CV) , Kuala Lumpur, Malaysia, 12-16 November 2007.

Baban, S.M.J. and K.W. Yusof (2001). Mapping land use/cover distribution on a mountainous tropical island using remote sensing and GIS. International Journal of Remote Sensing, 22(10): 1909–1918.

Bauer, E. and R. Kohavi (1999). An empirical comparison of voting classification algorithms: Bagging, boosting, and variants. Machine Learning, 36(1): 105–139.

Benediktsson, J.A., J. Chanussot and M. Fauvel (2007). Multiple classifier systems in remote sensing: From basics to recent developments. MCS 2007, LNCS 4472, (M. Haindl, J. Kittler, and F. Roli, editors), Springer Verlag, Berlin 2007: 501-512.

Bezdec, J.C. (1981). Pattern Recognition with Fuzzy Objective Function Algorithms, Plenum Press, New York.

Breiman, L. (1996). Bagging predictors. Machine Learning, 24(2):123–140.

Breiman, L. (2001). Random forest. Machine Learning, 45(1): 5–32.

Breiman, L., J.H. Friedman, R.A. Olshen and C.J. Stone (Ed.) (1984). Classification and regression trees. 358 p (New York: Chapman & Hall).

Briem, G., J. Benediktsson and J. Sveinsson (2002). Multiple classifiers applied to multisource remote sensing data. IEEE Transactions on Geoscience and Remote Sensing, 40 (10): 2291–2299.

Bronge, L.B. (1999). Mapping boreal vegetation using Landsat TM and topographic map data in a stratified approach. Canadian Journal of Remote Sensing, 25(5): 460–474.

Caetano, M. (2009). Image classification. An ESA Advanced Training Course on Land Remote Sensing, 28 June-03 July 2009 in Prague, Czech Republic.

Camps-Valls, G., L. Gomez-Chova, J. Calpe-Maravilla, E. Soria-Olivas, J.D. Martin Guerrero and J. Moreno (2003). Support vector machines for crop classification

using hyperspectral data. Proceedings of ibPRIA, Mallorca, Spain, 4-6 June 2003: 134-141.

Carpenter G.A., S. Crossberg and J.H. Reynolds (1991). ARTMAP: Supervised real time learning and classification of nonstationary data by a self-organizing neural network. Neural Networks, 4(5): 565-588.

Ceamanos, X., B. Waske, J.A. Benediktsson, J. Chanussot, M. Fauvel and J.R. Sveinsson (2010). A classifier ensemble based on fusion of support vector machines for classifying hyperspectral data. International Journal of Image and Data Fusion, 1 (4): 293–307.

Chaichoke, V., P. Supawee, V. Tanasak and K.S. Andrew (2011). A Normalized Difference Vegetation Index (NDVI) time-series of idle agriculture lands: A preliminary study. Engineering Journal, 15(1): 9-16.

Chandra, A. and X. Yao (2006). Evolving hybrid ensembles of learning machines for better generalisation. Neurocomputing, 69(7-9): 686–700.

Collins, M., R.E. Schapire and Y. Singer (2002). Logistic regression, Adaboost and Bregman distances. Machine Learning, 48(1): 31–44.

Congalton, R.G. and R.A. Mead (1983). A quantitative method to test for consistency and correctness in photointerpretation. Photogrammetric Engineering and Remote Sensing, 49(1): 69 – 74.

Congalton, R.G. (1991). A review of assessing the accuracy of classifications of remotely sensed data. Remote Sensing of Environment, 37(1): 35–46.

Cybenko, G. (1989) Approximation by superpositions of a sigmoidal function. Mathematics of Control, Signals, and Systems, 2(4): 303–314.

Defries, R.S. and J.C. Chan (2000). Multiple criteria for evaluating machine learning algorithms for land cover classification from satellite data. Remote Sensing of Environment, 74(3):503–515.

Doma, M.L., M.S. Gomaa and R.A. Amer, R.A. (2015) Sensitivity of pixel-based classifiers to training sample size in case of high resolution satellite imagery. Journal of Geomatics, 9(2): 53-58.

Du, P., J. Xia, W. Zhang, K. Tan, Y. Liu and S. Liu (2012). Multiple classifier system for remote sensing image classification: A review. Sensors, 12(4): 4764-4792.

Eastman, J.R. (2006). Idrisi Andes: Tutorial. Clark Labs. Clark University, Worcester.

Ebeir, L.D., P.A.L. Atinne and I.S. Teen (2001). Remote sensing classification of spectral, spatial and contextual data using multiple classifier systems. Proceedings of the 8th ECS and Image Analysis, September 4-7, Bordeaux, France, 584–589.

Epstein, J., K. Payne and E. Kramer (2002). Techniques for mapping suburban sprawl. Photogrammetric Engineering and Remote Sensing, 63(9): 913–918.

Espinola, M., R. Ayala, S. Leguizamon and M. Menenti (2008). Classification of satellite images using the cellular automata approach. Proceedings of the 1st WSKS, CCIS, 19: 521-526.

Foody, G.M. (1995). Land-cover classification by an artificial neural network with ancillary information. International Journal of Geographical Information Systems, 9(5): 527–542.

Foody, G.M. (1999). Image classification with a neural network: From completely crisp to fully-fuzzy situations. In P.M. Atkinson and N.J. Tate (eds), Advances in Remote Sensing and GIS analysis, Chichester: Wiley&Son.

Foody, G.M. (2009). Classification accuracy comparison: Hypothesis tests and the use of confidence intervals in evaluations of difference, equivalence and non-inferiority. Remote Sensing of Environment, 113(8), 1658–1663.

Foody, G.M., D.S. Boyd and C. Sanchez-Hernandez (2007). Mapping a specific class with an ensemble of classifiers. International Journal of Remote Sensing, 28(8): 1733–1746.

Freund, Y. and R.E. Schapire (1997). A decision-theoretic generalization of online learning and application to boosting. Journal of Computer and System Science, 55(1): 119-139.

Giacinto, G. and F. Roli (2001). Design of effective neural network ensembles for image classification. Image and Vision Computing, 19(9-10): 697–705.

Gil, A., Q. Yu, A. Lobo, P. Lourenço, L. Silva and H. Calado (2011). Assessing the effectiveness of high resolution satellite imagery for vegetation mapping in Small islands protected areas. Journal of Coastal Research, 64(2011): 1663-1667.

Gislason, P.O., J.A. Benediktsson and J.R. Sveinsson (2006). Random forests for land cover classification. Pattern Recognition Letters, 27(4): 294-300.

Groom, G.B., R.M. Fuller and A.R. Jones (1996). Contextual correction: Techniques for improving land cover mapping from remotely sensed images. International Journal of Remote Sensing, 17(1): 69–89.

Hadjimitsis, D.G., C.R.I. Clayton and V.S. Hope (2004). An assessment of the effectiveness of atmospheric correction algorithms through the remote sensing of some reservoirs. International Journal of Remote Sensing, 25(18): 3651–3674.

Hale, S.R. and B.N. Rock (2003). Impacts of topographic normalization on land-cover classification accuracy. Photogrammetric Engineering and Remote Sensing, 69(7): 785–792.

Hamedianfar, A., H.Z. Mohd Shafri, S. Mansor and N. Ahmad (2014). Detailed urban object-based classifications from WorldView-2 imagery and LiDAR data: Supervised vs. fuzzy rule-based. FIG Congress 2014, Engaging the Challenges—Enhancing the Relevance, Kuala Lumpur, 16-21 June 2014.

Helmer, E.H., S. Brown and W.B. Cohen (2000). Mapping montane tropical forest successional stage and land use with multi-date Landsat imagery. International Journal of Remote Sensing, 21(11): 2163–2183.

Herrera, F. and J.L. Verdegay (1996). A linguistic decision process in group decision making. Group Decision Negotiation, 5(2): 165-176.

Ho, T.K. (1998) The random subspace method for constructing decision forests. IEEE Transactions on Pattern Analysis and Machine Intelligence, 20(8): 832–844.

Hsu, C.W., C.C. Chang and C.J. Lin (2009). A practical guide to support vector classification. Department of Computer Science, National Taiwan University, http://www.csie.ntu.edu.tw/~cjlin/papers/guide/guide.pdf (Accessed 7 September 2016).

Hugo, C., L. Capao, B. Fernando and C. Mario (2007). MERIS based land cover classification with self-organizing maps: Preliminary results. In Proceedings of the 2nd EARSeL SIG Workshop on Land Use & Land Cover (unpaginated CD-ROM), 28 – 30 September 2006, Bonn, Germany.

Hwang, Y.S. and S.Y. Bang (1997). An efficient method to construct a radial basis function neural network classifier. Neural Networks, 10(8): 1495-1503.

Jawak, S., P. Devliyal and A. Luis (2015). A comprehensive review on pixel oriented and object oriented methods for information extraction from remotely sensed satellite images with a special emphasis on cryospheric applications. Advances in Remote Sensing, 4(3): 177-195.

Jen-Hon, L. and T. Din-Chang (2000). Self-organizing feature map for multi-spectral spot land cover classification. GIS development.net, AARS, ACRS 2000.

Jensen, J. (2005). Introductory Digital Image Processing, Third Edition, Prentice Hall, 526 p.

Kamavisdar, P., S. Saluja and S. Agrawal (2013). A survey on image classification approaches and techniques. International Journal of Advanced Research in Computer and Communication Engineering, 2(1): 1005-1008.

Kanellopoulos, I., G. Wilkinson, F. Roli and J. Austin (editors) (1997). Neurocomputation in remote sensing data analysis. Springer, Berlin.

Kavzoglu, T. and P.M. Mather (2003). The use of back propagating artificial neural networks in land cover classification. International Journal of Remote Sensing, 24(3): 4907- 4938.

Ko, C., G. Sohn, T. Remmel and J. Miller (2014). Hybrid ensemble classification of tree genera using airborne LiDAR data. Remote Sensing, 6 (x): 11225-11243.

Kohonen, T. (1990) The self-organizing map. Proceedings of the IEEE, 78: 1464-80.

Kumar, M. and R.K. Singh (2013). Digital image processing of remotely sensed satellite images for information extraction. Conference on Advances in Communication and Control Systems (CAC2S 2013), Atlantis Press, pp. 406-410.

Kumar, S., J. Ghosh and M.M. Crawford (2002). Hierarchical fusion of multiple classifiers for hyperspectral data analysis. Pattern Analysis and Applications, 5: 210–220.

Kuncheva, L.I. and C.J. Whitaker (2003). Measures of diversity in classifier ensembles and their relationship with the ensemble accuracy. Machine Learning, 51(2): 181–207.

Kussul, N., S. Skakun and O. Kussul (2006). Comparative analysis of neural networks and statistical approaches to remote sensing image classification. Computing, 5(2): 93-99.

Le, A.C., V.N. Huynh, A. Shimazu and Y. Nakamori (2007). Combining classifiers for word sense disambiguation based on Dempster-Shafer theory and OWA operators. Data and Knowledge Engineering, 63 (2): 381-396.

Lefsky, M.A. and W.B. Cohen (2003). Selection of remotely sensed data. In M.A. Wulder and S.E. Franklin (Eds), Remote Sensing of Forest Environments: Concepts and case studies, 13– 46 (Boston: Kluwer Academic Publishers).

Li, G., D. Lu, E. Moran and S. Sant'Anna (2012). Comparative analysis of classification algorithms and multiple sensor data for land use/land cover classification in the Brazilian Amazon. Journal of Applied Remote Sensing 6(1): 11 pages.

Lillesand, T. and R. Kiefer (2004). Remote Sensing and Image Interpretation. Fourth Edition, John Willey & Sons, Inc., New York.

Lippitt, C., J. Rogan, Z. Li, J. Eastman and T. Jones (2008). Mapping selective logging in mixed deciduous forest: A comparison of machine learning algorithms.

Photogrammetric Engineering and Remote Sensing, 74(10): 1201–1211.

Liu, W., K. Seto, E. Wu, S. Gopal and C. Woodcock (2004). ARTMMAP: A neural network approach to subpixel classification. IEEE Transactions on Geoscience and Remote Sensing, 42(9): 1976–1983.

Mannan B., J. Roy and A.K. Ray (1998). Fuzzy ArtMap supervised classification of multi-spectral remotely-sensed images. International Journal of Remote Sensing, 19(4): 767-774.

Maryam, N., M.Z. Vahid and H. Mehdi (2014). Comparing different classifications of satellite imagery in forest mapping (Case Study: Zagros Forests in Iran). International Research Journal of Applied and Basic Sciences, 8(7): 1407-1415.

Maselli, F., A. Rodolfi, L. Bottai, S. Romanelli and C. Conese (2000). Classification of Mediterranean vegetation by TM and ancillary data for the evaluation of fire risk. International Journal of Remote Sensing, 21(17): 3303–3313.

Michail, P., J.A. Benediktsson and K. Ioannis (2002). The effect of classifier agreement on the accuracy of the combined classifier in decision level fusion. IEEE Transactions on Geoscience and Remote Sensing, 39(11): 2539–2546.

Minu, N.S. and J.S. Bindhu (2016). Supervised techniques and approaches for satellite image classification. International Journal of Computer Applications, 134(16): 0975 – 8887.

Mountrakis, G., J. Im and C. Ogole (2011). Support vector machines in remote sensing: A review. ISPRS Journal of Photogrammetry and Remote Sensing, 66(3): 247-259.

Nasrabadi, N.M. and Y. Feng (1988). Vector quantization of images based upon the Kohonen self-organizing feature maps. Proceedings of the IEEE International Conference on Neural Networks (ICNN-88), 24-27 July 1988, San Diego, California, 101-108.

Oliveira, L., T. Oliveira, L. Carvalho, W. Lacerda, S. Campos and A. Martinhago (2007). Comparison of machine learning algorithms for mapping the phytophysiognomies of the Brazilian Cerrado. IX Brazilian Symposium on GeoInformatics, Campos do Jordão, Brazil, November 25-28, 2007, INPE, 195-205.

Pal, M. and P. Mather (2005). Support vector machines for classification in remote sensing. International Journal of Remote Sensing, 26(5): 1007-1011.

Powell, R.L., N. Matzke, C. De Souza Jr, M. Clark, I. Numata, L.L. Hess and D.A. Roberts (2004). Sources of error in accuracy assessment of thematic land-cover maps in the Brazilian Amazon. Remote Sensing of Environment, 90(2): 221–234.

Prasad, S., T. Savithri and I. Murali Krishna (2015). Techniques in image classification; A survey. Global Journal of Researches in Engineering: Electrical and electronics Engineering, 16(6): 17-32.

Qiu, F. and J.R. Jensen (2004). Opening the black box of neutral networks for remote sensing image classification. International Journal of Remote Sensing, 25(9): 1749–1768.

Quinlan, J.R. (1987). Simplifying decision trees. International Journal of Man-Machine Studies, 27(3): 227–248.

Ranawana, R. and V. Palade (2006). Multi-classifier systems: Review and a roadmap for developers. International Journal of Hybrid Intelligent Systems, 3(1): 35–61.

Richards, J.A. (2013). Remote sensing digital image analysis. Springer-Verlag, Berlin, 5th Ed. 496 p.

Rodriguez, J.J. and L.I. Kuncheva (2009). Rotation forest: A new classifier ensemble method. IEEE Transactions on Pattern Analysis and Machine Intelligence, 28(10): 1619–1630.

Rosenblatt, F. (1962). Principles of neurodynamics: Perceptrons and the theory of brain mechanisms. Spartan Books, Washington DC, 1962.

Rosenfield, G.H. and K. Fitzpatrick-Lins (1986). A coefficient of agreement as a measure of thematic classification accuracy. Photogrammetric Engineering and Remote Sensing, 52(2): 223 – 227.

Ruta, D. and B. Gabrys (2007). An overview of classifier fusion methods. Computing and Information Systems, 2000(7): 1–10.

Salah, M. (2014). Combining pixel-based and object-oriented support vector machines using Bayesian probability theory. ISPRS Annals of the Photogrammetry, Remote Sensing and Spatial Information Sciences, Volume II-7, 2014 ISPRS Technical Commission VII Symposium, 29 September – 2 October 2014, Istanbul, Turkey.

Shafer, G. (1976). A mathematical theory of evidence. Princeton University Press.

Shaker, A., W.Y. Yan and N. El-Ashmawy (2012). Panchromatic satellite image classification for flood hazard assessment. Journal of Applied Research and Technology, 10 (x): 902-911.

Shannon, C.E. (Ed.) (1949). The mathematical theory of communication. (Urbana, IL: University of Illinois Press).

Sherrod, P.H. (2008). DTREG tutorial home page. Available online at:

http://www.dtreg.com/crossvalidation.htm (Accessed 7 September 2016).

Stefanov, W.L., M.S. Ramsey and P.R. Christensen (2001). Monitoring urban land cover change: An expert system approach to land cover classification of semiarid to arid urban centers. Remote Sensing of Environment, 77(2): 173–185.

Trinder, J., M. Salah, A. Shaker, M. Hamed and A. Elsagheer (2010). Combining statistical and neural classifiers using Dempster-Shafer theory of evidence for improved building detection. 15th ARSPC, Alice Springs, Australia, 13- 17 September 2010.

Tso, B. and P.M. Mather (2009). Classification methods for remotely sensed data. 2nd Ed. Chapter 2-3, Taylor and Francis Group, America.

Tso, B.C.K. and P.M. Mather (1999). Classification of multisource remote sensing imagery using a genetic algorithm and Markov random fields. IEEE Transactions on Geoscience and Remote Sensing, 37(3): 1255–1260.

Van der Linden, S., A. Rabe, A. Okujeni and P. Hostert (2009). Image SVM classification. application manual: imageSVM version 2, Humboldt-Universität zu Berlin, Germany.

Vapnik, V. (1979). Estimation of dependences based on empirical data [in Russian]. Nauka, Moscow, 1979. (English translation: Springer Verlag, New York, 1982).

Vesanto, J., J. Himberg, E. Alhoniemi and J. Parhankangas (2000). SOM toolbox for Matlab. Technical Report A57, Helsinki University of Technology, Neural Networks Research Centre, Espoo, Finland.

Waske, B. (2007). Classifying multisensor remote sensing data: Concepts, algorithms and applications. PhD thesis, Bonn University, Germany.

Waske, B. and J.A. Benediktsson (2007). Fusion of support vector machines for classification of multisensory data. IEEE Transactions on Geoscience and Remote Sensing, 45(12): 3858–3866.

Webb, G.I. (2009). Multiboosting: A technique for combining boosting and wagging. Machine Learning, 40(2): 159–196.

Wilkinson, G.G. (2005). Results and implications of a study of fifteen years of satellite image classification experiments. IEEE Transaction on Geosciences and Remote Sensing, 43(3): 433-440.

Yager, R.R. (1988). On ordered weighted averaging aggregation operators in multicriteria decision making. IEEE Transactions on Systems, Man, and Cybernetics, 18(1): 183-190.

Yu-Chang, T. and C. Kun-Shan (2009). An adaptive thresholding multiple classifiers system for remote sensing image classification. Photogrammetry Engineering and Remote Sensing, 75(6): 679-687.

Zadeh, L.A. (1983). A computational approach to fuzzy quantifiers in natural languages. Computers and Mathematics with Applications, 9(1): 149-184.

Zhang, C., and J. Zhang (2008). RotBoost: A technique for combining rotation forest and AdaBoost. Pattern Recognition Letters, 29(10): 1524–1536.

Zhang, Q., J. Wang, X. Peng, P. Gong and P. Shi (2002). Urban built-up land change detection with road density and spectral information from multitemporal Landsat TM data. International Journal of Remote Sensing, 23(15): 3057–3078.

Zhang, Y. (1999). Optimization of building detection in satellite images by combining multispectral classification and texture filtering. ISPRS Journal of Photogrammetry and Remote Sensing, 54(1): 50– 60.

Journal of Geomatics Vol 11 No. 1 April 2017

National Geomatics Award for Excellence

This award has been instituted to recognize outstanding and conspicuously important contribution in promoting geomatics technology and applications at the country level. The contributions should have made major impact on the use of this technology for national development.
Areas of contribution considered for the award are:

1. Geographical Information System
2. Global Positioning System
3. Photogrammetry
4. Digital Cartography
5. Applications of Geomatics

The award shall consist of Rs. 50,000/- in cash, a medal and citation.

Eligibility

Any citizen of India, engaged in activities related to geomatics technology and its applications is eligible for this award. The prize is awarded on the basis of work primarily done in India.

The age limit for awardees is 45 years or above as on June 30 of the year of award.

Selection

A duly constituted Award Committee will evaluate all nominations received. The committee shall consist of eminent experts in the field of geo-spatial technology, to be identified by the Executive Council, ISG. The committee shall forward selected name/s to ISG – EC for approval and announcement. Apart from those persons, whose nominations have been received, the Committee may consider any person or persons who, in their opinion, have made outstanding contributions to development of geo-spatial technology and applications.

The award can be withheld in any year if, in the opinion of the committee, no candidate is found suitable in that particular year.

Presentation of the Award

The award shall be presented during the Annual Convention of ISG. Local Hospitality shall be taken care by ISG & Air fare (low cost) may be reimbursed if awardees request for it.

How to make Nomination

The nominations can be proposed by Head of a major research institute/ centre; Vice-Chancellor of a university; Secretary of Government Scientific Departments; President of a National Academy, President, Indian Society of Geomatics / Indian Society of Remote Sensing / Indian National Cartographic Association / ISG fellow or two life members of the society with more than 10 year old membership.

A candidate once nominated would be considered for a total period of two years. Nomination should be sent in the prescribed format to Secretary, ISG.

The last date for receiving nominations shall be September 31 or otherwise extended.

Format for nomination of Geomatics Award for Excellence

1. Name of the Nominee
2. Postal Address
3. Academic Background (Bachelor degree onwards)
4. Field of Specialisation
5. Important positions held (in chronological order)
6. Professional Experience including foreign assignments.
7. Important Awards / Honours
8. Important Publications/Patents: (A set of ten most important publications to be enclosed with this form)
9. Contributions of Nominee based on which the nomination is sent (in 1000 words, also provide a statement
   in 50 words which may be used for citation.):
10. Other Relevant Information:

Proposer:

Signature
Name
Address
Phone/ Fax
E-mail
Life Membership No. (in case of ISG Member):

Place & Date

Endorsed by (in case nomination is by 2 ISG Life members)

Signature
Name
Address
Phone/ Fax
E-mail
Life Membership No. (in case of ISG Member):

Place & Date
(The proposer should give a brief citation of the nominee's work)

NATIONAL GEOMATICS AWARD

Indian Society of Geomatics has instituted two National Geomatics Awards to be given each year for (a) Original and significant contribution in Geomatics technology, (b) Innovative application(s) in the field of Geomatics. Each award comprises a medal, a citation and a sum of Rs. 25,000/-.

The guidelines for the award are as under

Areas of contribution considered for the award (both technology and applications)

1. Geographical Information System
2. Global Positioning System
3. Photogrammetry
4. Digital Cartography
5. Remote Sensing

Eligibility

Any citizen of India engaged in scientific work in any of the above-mentioned areas of research is eligible for the award.

The awards are to be given for the work largely carried out in India.

- First award will be given for original contribution in the field of Geomatics technology supported by publications in a refereed journal of repute.
- Second award will be given for carrying out innovative application(s). Supported by publications in rear reviewed Journals of repute.
- The contribution for the first award should have been accepted by peers through citation of the work.
- Work based on the applications of existing technologies will not be considered for the first award.
- The work should have made impact on the overall development of Geomatics.

How to Send Nomination

Nominations should be sent in the prescribed format, completed in all aspects to the Secretary, Indian Society of Geomatics, Space Applications Centre Campus, Ahmedabad 380 015 by August 31, 2017.

Selection Process

An expert committee, consisting of at least three members, constituted by the Executive Council of the Indian Society of Geomatics, will scrutinize the nominations and recommend the awardees' names to the Executive Council. The Council will decide on the award based on the recommendations.

Journal of Geomatics Vol 11 No. 1 April 2017

FORMAT FOR AWARD NOMINATION

1. Name of the Candidate:
2. Present Position:
3. Positions held earlier (chronological order):
4. Academic qualifications (Bachelor's degree onwards):
5. Names of at least three Indian Scientists/Technologist in the area as possible referees *:
6. Brief write up on the work (500 words) for which award is claimed:
7. Publication(s) on the above work (reprint(s) to be enclosed):
8. List of other publications of the candidate:
9. Citation of the work for which award is claimed:
10. Impact of the work (for which award is claimed) on the development in the field of Geomatics (500 words):
11. Whether the work has already won any award? If so, give details:

The Applications in the above format (five copies) should be submitted (by Registered Post or Speed Post) to

The Secretary, Indian Society of Geomatics,
Space Applications Centre Campus,
Ahmedabad-380015

so as to reach by September 31, 2017.

*ISG is, however, not bound to accept these names and can refer the nomination to other experts/peers

INDIAN SOCIETY OF GEOMATICS FELLOWS

Shri Pramod P. Kale, Pune
Dr George Joseph, Ahmedabad
Dr A.K.S. Gopalan, Hyderabad
Dr Prithvish Nag, Varanasi
Dr Baldev Sahai, Ahmedabad
Shri A.R. Dasgupta, Ahmedabad
Dr R.R. Navalgund, Bengaluru
Shri Rajesh Mathur, New Delhi
Dr Ajai, Ahmedabad
Prof P. Venkatachalam, Mumbai
Prof SM Ramasamy, Tiruchirapalli
Dr Ashok Kaushal, Pune

INDIAN SOCIETY OF GEOMATICS - PATRON MEMBERS

P-1 Director, Space Applications Centre (ISRO), Jodhpur Tekra Satellite Road, Ahmedabad - 380 015
P-2 Settlement Commissioner, The Settlement Commissioner & Director of Land Records-Gujarat, Block No. 13, Floor 2, Old Sachivalay, Sector-10, Gandhinagar – 382 010
P-3 Commissioner, Mumbai Metropolitan Region Development Authority, Bandra-Kurla Complex, Bandra East, Mumbai - 400 051
P-4 Commissioner, land Records & Settlements Office, MP, Gwalior - 474 007
P-5 Director General, Centre for Development of Advanced Computing (C-DAC), Pune University Campus, Ganesh Khind, Pune - 411 007
P-6 Chairman, Indian Space Research Organization (ISRO), ISRO H.Q., Antariksha Bhavan, New BEL Road, Bengaluru 560 231
P-7 Director General, Forest Survey of India, Kaulagarh Road, P.O. I.P.E., Dehra Dun – 248 195
P-8 Commissioner, Vadodara Municipal Corporation, M.S. University, Vadodara - 390 002
P-9 Director, Centre for Environmental Planning and Technology (CEPT), Navarangpura, Ahmedabad - 380 009
P-10 Managing Director, ESRI INDIA, NIIT GIS Ltd., 8, Balaji Estate, Sudarshan Munjal Marg, Kalkaji, New Delhi - 110 019
P-11 Director, Gujarat Water Supply and Sewerage Board (GWSSB), Jalseva Bhavan, Sector – 10A, Gandhinagar - 382 010
P-12 Director, National Atlas & Thematic Mapping Organization (NATMO), Salt Lake, Kolkata - 700 064
P-13 Director of Operations, GIS Services, Genesys International Corporation Ltd., 73-A, SDF-III, SEEPZ, Andheri (E), Mumbai - 400 096
P-14 Managing Director, Speck Systems Limited, B-49, Electronics Complex, Kushiaguda, Hyderabad - 500 062
P-15 Director, Institute of Remote Sensing (IRS), Anna University, Sardar Patel Road, Chennai - 600 025
P-16 Managing Director, Tri-Geo Image Systems Ltd., 813 Nagarjuna Hills, PunjaGutta, Hyderabad - 500 082
P-17 Managing Director, Scanpoint Graphics Ltd., B/h Town Hall, Ashram Road, Ahmedabad - 380 006
P-18 Secretary General, Institute for Sustainable Development Research Studies (ISDRS), 7, Manav Ashram Colony, Goplapura Mod, Tonk Road, Jaipur - 302 018
P-19 Commandant, Defense institute for GeoSpatial Information & Training (DIGIT), Nr. Army HQs Camp, Rao Tula Ram Marg, Cantt., New Delhi - 110 010
P-20 Vice President, New Rolta India Ltd., Rolta Bhavan, 22nd Street, MIDC-Marol, Andheri East, Mumbai - 400 093
P-21 Director, National Remote Sensing Centre (NRSC), Deptt. of Space, Govt. of India, Balanagar, Hyderabad - 500 037
P-22 Managing Director, ERDAS India Ltd., Plot No. 7, Type-I, IE Kukatpalli, Hyderabad - 500 072
P-23 Senior Manager, Larsen & Toubro Limited, Library and Documentation Centre ECC Constr. Gp., P.B. No. 979, Mount Poonamallee Road, Manapakkam, Chennai - 600 089.
P-24 Director, North Eastern Space Applications Centre (NE-SAC), Department of Space, Umiam, Meghalaya 793 103
P-25 Progamme Coordinator, GSDG, Centre for Development of Advanced Computing (C-DAC), Pune University Campus, Pune – 411 007
P-26 Chief Executive, Jishnu Ocean Technologies, PL-6A, Bldg. No. 6/15, Sector – 1, Khanda Colony, New Panvel (W), Navi Mumbai – 410 206
P-27 Director General, A.P. State Remote Sensing Applications Centre (APSRAC), 8th Floor, "B" Block, Swarnajayanthi Complex, Ameerpet, Hyderabad- 500 038
P-28 Director, Advanced Data Processing Res. Institute (ADRIN), 203, Akbar Road, Tarbund, Manovikas Nagar P.O., Secunderabad –500 009
P-29 Managing Director, LEICA Geosystems Geospatial Imaging Pvt. (I) Ltd., 3, Enkay Square, 448a Udyog Vihar, Phase-5, Gurgoan- 122 016
P-30 Director, Defense Terrain Research Limited (DTRL), Ministry of Defense, Govt. of India, Defense Research & Development Organisation, Metacafe House, New Delhi – 110 054
P-31 Chairman, OGC India Forum, E/701, Gokul Residency, Thakur Village, Kandivali (E), Mumbai – 400 101
P-32 Managing Director, ML Infomap Pvt. Ltd., 124-A, Katwaria Sarai, New Delhi – 110 016
P-33 Director, Rolta India Limited, Rolta Tower, "A", Rolta Technology Park, MIDC, Andheri (E), Mumbai – 400 093
P-34 Director, State Remote Sensing Applications Centre, Aizawl – 796 012, Mizoram

Instructions for Authors

The journal covers all aspects of Geomatics – geodata acquisition, pre-processing, processing, analysis and publishing. Broadly this implies inclusion of areas like GIS, GPS, Photogrammetry, Cartography, Remote Sensing, Surveying, Spatial Data Infrastructure and Technology including hardware, software, algorithm, model and applications. It endeavours to provide an international forum for rapid publication of developments in the field – both in technology and applications.

A manuscript for publication must be based on original research work done by the author(s). It should not have been published in part or full in any type of publication nor should it be under consideration for publication in any periodical. Unsolicited review papers will not be published.

The Editorial Board or the Indian Society of Geomatics is not responsible for the opinions expressed by the authors.

Language

The language of the Journal will be English (Indian). However, manuscripts in English (US) and English (British) are also acceptable from authors from countries located outside India.

Manuscript Format

Each paper should have a title, name(s) of author(s), and affiliation of each of the authors with complete mailing address, e-mail address, an abstract, four to six keywords, and the text. The text should include introduction/background, research method, results, discussion, followed by acknowledgements and references. The main text should be divided in sections. Section headings should be concise and numbered in sequence, using a decimal system for subsections. Figures, images and their captions should be inserted at appropriate points of the text. Figures, images and tables should fit in two column format of the journal. If absolutely necessary, figures, images and tables can spread across the two columns. Figures and images, however, should not exceed half a page in height. A title should be provided for each Table, Image and Figure. All figures and images should be in 600 dpi resolution and sized as per column/margin width. Authors must ensure that diagrams/figures should not lose easy readability upon reduction to column size. The SI (metric) units and international quantities should be used throughout the paper. In case measurements are given in any other system, equivalent measurements in SI (metric) units should be indicated in brackets.

Use MS Word with English (UK/US) or English (Indian) dictionary. The page size should be A4 paper, with 2 cm margin on all sides. Title, authors and affiliation should be centred. Abstract should be justified across margins. The manuscript text should be in two columns of 8.2 cm each with a gutter of 6mm between them. Use only Times New Roman fonts. Title should be 12 points bold. Authors and affiliation should be 9 points. All other text including headings should be 10 points. Heading numbering scheme should be decimal e.g. 1, 1.1, 1.2.3, etc. Headings should be in bold.

Normally length of a published paper should be about 6-10 pages in A4 size including figures. Use of illustrations in colour should be restricted and resorted to only where it is absolutely necessary and not for enhancing the look of the paper. If the number of colour illustrations exceeds five, authors' institution may be asked to reimburse the extra cost involved, which at current rates is about Rs. 2500 per coloured figure/diagram/plate/illustration.

Submission of Manuscript

Submissions should be in electronic form via email. The manuscript may be sent by email to drajai1953@gmail.com. In exceptional cases hard copy submission in camera ready form may be allowed with the prior permission of the Chief Editor. Submission in any other form will be returned to the author. To speed up the review process, authors are advised to provide a list of three probable reviewers with their institutional address and e-mail IDs.

Guidelines for Citing References

Names of all cited publications should be given in full. No abbreviations should be used. Following procedure is to be adopted.

Journal Publications

Bahuguna, I.M. and A.V. Kulkarni (2005). Application of digital elevation model and orthoimages derived from IRS-1C Pan stereo data in monitoring variations in glacial dimensions, Journal of the Indian Society of Remote Sensing, 33(1), 107- 112. (to be referred to in the text as Bahuguna and Kulkarni (2005) or if more than two sets of authors are to be referred to, as (Bahuguna and Kulkarni, 2005; Jain et al., 1994)) When more than two authors are to be referred to, use Jain et al. (1994). However, in References, all authors are to be mentioned.

Publication in a Book

Misra, V.N. (1984). Climate, a factor in the rise and fall of the Indus Civilization – Evidence from Rajasthan and Beyond in Frontiers of the Indus Civilization (B.B. Lal and S.P. Gupta: Chief Editors) Books and Books, New Delhi, pp. 461-489

Papers Published in Seminar/ Symposium Proceedings

Jain, A., A.R. Shirish, M. Das, K. Das, M.C. Porwal, and P.S. Roy (1994). Remote Sensing and Geographic Information System – An approach for the assessment of biotic interference in the forest ecosystem. Proceedings. 15th Asian Conference on Remote Sensing, Bangalore, November 17-23, 1994, pp. 65-72.

Books

Possehl, Gregory L. (1999). Indus Age: The beginnings. Oxford and IBH Publishing Corporation, New Delhi.

Reviewing

Each paper will be reviewed by three peers. Papers forwarded by members of the Editorial or Advisory Boards along with their comments would get processed faster and may be reviewed by two referees only.

Sample format for Authors is available in downloadable form at ISG website: www.isgindia.org/JOG/Sample_format.doc

Copyright

The copyright of the paper selected for publication will rest with the Indian Society of Geomatics. Corresponding author shall be required to sign a copyright assignment form, on behalf of all authors, once the paper is selected for publication. Authors are, however, at liberty to use this material elsewhere after obtaining permission from the Indian Society of Geomatics.

If the authors have used any copyright material in their manuscript, it is understood that they have obtained permission from the owner of the copyright material and they should convey the same along with the manuscript to the Chief Editor.

Certificate of Original Work

The authors will also provide a certificate that the paper is an original work, not published or being considered for publication elsewhere.

In the event the certificate turns out to be false, the Journal shall ban the author(s) from publishing in the Journal for a period of five years and inform the same to all other related publications.

Reprints

Authors will be allowed to download the (PDF) of their paper from ISG Website www.isgindia.org, No hard copy reprints will be provided.

Journal of Geomatics

Advertisement Rates

	1 Issue	4 Issues
Back Cover Page in colour	**Rs. 25,000**	**Rs. 80,000**
Inside Cover Page in colour	**Rs. 20,000**	**Rs. 64,000**
Full Page inside in colour	**Rs. 15,000**	**Rs. 48,000**
Full Page inside in B/W	**Rs. 10,000**	**Rs. 32,000**

Advertisement Details

Mechanical Details
Double Spread/Center Spread (42 x 29.7) cm
Full page bleed (21 x 29.7) cm
Full page non-bleed (19 x 27.7) cm

Art Requirements

Negatives: Art must be right reading, emulsion, down. Film must be supplied in one piece per color, each identified by color. Camera-ready art is accepted for black & White adds; however, film is preferred. Electronic Files are also accepted.

Electronic File Requirements: All material must be received before ad close dates.

Software: Adobe illustrator 9.0 (saved as EPS). Adobe Photoshop CS (saved as EPS or TIFF). Please convert higher versions down. If you can only supply an IBM format, the file must be in viewable EPS or TIFF format with fonts embedded as that format.

Colour Ads: Colour separations must be provided, right reading, emulsion down. Please note that files using RGB or Pantone colours (PMS) must be converted to CMYK before we receive files.

To,
The Secretary, Indian Society of Geomatics
6202, Space Applications Centre (ISRO)
AHMEDABAD – 380 015. INDIA

Sir,

I want to become a Member/ Life Member/ Sustaining Member/ Patron Member/ Foreign Member/ Student Member of the Indian Society of Geomatics, Ahmedabad for the year _____. Membership fee of Rs. _____ /- is being sent to you by Cash/ DD/ Cheque. (In case of DD/ Cheque No._____dated_____drawn on Bank
_____ . I **agree to abide by the Constitution of the Society.**

Date:

Place: **Signature**

- Name: Mr/Ms/Mrs/Dr_____
- Address: _____

_____PIN: _____

Phone: _____ Fax: _____Email:

_____ • Date of Birth

_____

•Qualifications_____

- Specialisation: _____
- Designation: _____ Organisation. _____
- Membership in other Societies: _____
- Mailing Address: _____

_____PIN: _____

Proposed by:
(Member's Name and No)
Signature of Proposer

For Office Use: A/P/L Member No.		Receipt No.		Date:	

Indian Society of Geomatics (ISG), Room No. 6202 Space Applications Centre (ISRO), Ahmedabad-380015, Gujarat. Url: www.isgindia.org Phone: +91-79 26916202
Email: secretary@isgindia.org or sasharma@sac.isro.gov.in Fax +91-79-26916287

MEMBERSHIP FEES

Sr. No.	Membership	Life/Patron Membership fees		Annual Subscription
	Category	₹ Indian	US $ Foreign	₹ Indian
1.	Annual Member	10	---	300
2.	Life Member a) Admitted below 45 years of age	2500	250	
	b) Admitted after 45 years of age	2000	200	
3.	Sustaining Member	---	---	2000
4.	Patron Member	50000	3000	---
5.	Student Member	10	---	100

MEMBERSHIP GUIDELINES

- Subscription for Life Membership is also accepted in two equal instalments payable within duration of three months, if so desired by the applicant. In such a case, please specify that payment will be in instalments and also the probable date for the second instalment (within three months of the first instalment).
- A Member of the Society should countersign application of membership as proposer.
- Subscription in DD or Cheque should be made out in the name of **'Indian Society of Geomatics'** and payable at Ahmedabad.
- Direct deposit in ISG A/Cs must include bank fee RS. 25/- for cash payment.
- Financial year of the Society is from April 1 to March 31.
- For further details, contact Secretary, Indian Society of Geomatics at the address given above.
- ISG has chapters already established at the following places. Ahmedabad, Ajmer, Bhagalpur, Bhopal, Chennai, Dehradun, Delhi, Hissar, Hyderabad, Jaipur, Ludhiana, Mangalore, Mumbai, Mysore, Pune, Shillong, Trichi, Srinagar, Vadodara, Vallabh Vidya Nagar, Visakhapatnam and Trivandrum. Applicants for membership have the option to contact Secretary/Chairman of the local chapter for enrolment. Details can be found at the website of the Society: www.isgindia.org.
- Journal of the Society will be sent to Life Members by softcopy only.

Indian Society of Geomatics (ISG), Room No. 6202 Space Applications Centre (ISRO), Ahmedabad-380015, Gujarat. Url: www.isgindia.org Phone: +91-79 26916202
Email: secretary@isgindia.org or sasharma@sac.isro.gov.in Fax +91-79-26916287

Geomatics Revealed

IGiS

Integrated GIS & IP Software

VERSION 2.0

MAKE IN INDIA

National Awards on Technology
By The Former President of India,
Dr. A. P. J. Abdul Kalam

Launch of IGiS Version 2.0
By Padam Shri AS Kiran Kumar, Chairman, ISRO and
Shri Tapan Mishra, DIRECTOR, SAC, ISRO.

What's new in IGiS

IGiS Version 2.0 is full of enhancements which you'll appreciate every day. New advanced GIS/IP and SAR modules are vital now a days. New COM Based Architecture makes you even more productive. The more you do with IGiS Version 2.0, the more you'll wonder how you ever did without it.

Enhancements in IGiS Version 2.0

- Advanced GIS / Image Processing
- Microwave SAR Analysis
- Meteorological Analysis
- COM Based Scalable Architecture
- New Ribbon Bar GUI
- Python Customization
- OGC Standards

Product Development Partner

इसरो isro
Government of India | Department of Space
Indian Space Research Organisation - (ISRO)

SGL Scanpoint Geomatics Ltd.
www.scanpointgeomatics.com

Scanpoint Geomatics Ltd.
Corporate Office : 12, Abhishree Corporate Park, Iskcon - Ambli Road, Ahmedabad - 380 058. Gujrat (India)
[P] +91 2717 297096-98 [F] +91 2717 297039 [E] info@scanpointgeomatics.com [W] www.scanpointgeomatics.com

INDIAN SPACE RESEARCH ORGANISATION
GOVERNMENT OF INDIA

A Smart Destination For Geospatial Solutions

National Remote Sensing Centre
Hyderabad, India
www.nrsc.gov.in
www.bhuvan.nrsc.gov.in
data@nrsc.gov.in

nrsc

इसरो isro

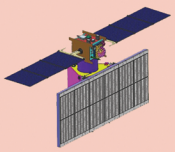

Only Organization in the Country to Acquire & Supply Satellite Data to Users

Aerial Acquisition for Specific User Demands & Disaster Management Support

Open Data & Value Added Products Dissemination Through Bhuvan

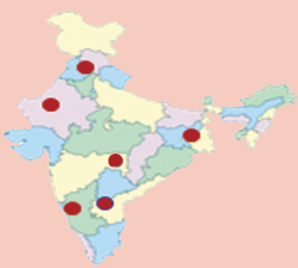

Region Specific Solutions

Capacity Building in Remote Sensing Applications